

Syracuse University

## SURFACE at Syracuse University

---

Dissertations - ALL

SURFACE at Syracuse University

---

5-12-2024

# MULTI-SCALE ANALYSIS OF THE STRUCTURE-MECHANICS RELATIONSHIP OF MYCELIUM-BASED BIO-COMPOSITES

Libin Yang  
*Syracuse University*

Follow this and additional works at: <https://surface.syr.edu/etd>



Part of the [Civil Engineering Commons](#)

---

### Recommended Citation

Yang, Libin, "MULTI-SCALE ANALYSIS OF THE STRUCTURE-MECHANICS RELATIONSHIP OF MYCELIUM-BASED BIO-COMPOSITES" (2024). *Dissertations - ALL*. 1957.  
<https://surface.syr.edu/etd/1957>

This Dissertation is brought to you for free and open access by the SURFACE at Syracuse University at SURFACE at Syracuse University. It has been accepted for inclusion in Dissertations - ALL by an authorized administrator of SURFACE at Syracuse University. For more information, please contact [surface@syr.edu](mailto:surface@syr.edu).

## **Abstract**

The construction industry faces significant challenges due to the environmental impact of traditional materials like steel and concrete, whose production is energy-intensive and contributes to environmental pollution. This issue is exacerbated by the growing global demand for construction materials, driven by an increasing population. Concurrently, the agricultural and wood industrial sectors produce vast byproducts, such as straw, husk, coir, sawdust, and wood chips. They are often considered as wastes and disposed of through methods like burning. Such a reckless treatment releases greenhouse gases that further lead to environmental degradation.

Mycelium, the vegetative part of fungi, presents a natural, promising solution to treat these wastes due to its energy-efficient growth, minimal byproduct generation, and broad application range. Integrating mycelium with organic substrates such as agricultural waste makes it possible to create lightweight and biodegradable materials. These mycelium-based composites offer numerous advantages, including sustainability, non-toxicity, and the ability to be composted at the end of their lifecycle, thus contributing to a circular economy.

This dissertation explores the potential of mycelium-based bio-composite materials for future development into a class of promising insulation materials. Central to the dissertation is integrating mycelium with organic substrates, such as agricultural waste, to create bio-composites with multifunctional features (e.g., mechanical solidity and thermal insulation) obtained through lab treatments after growth. This

approach presents a method to repurpose agrarian byproducts and reduce waste. The study meticulously examines the applicability of these bio-composites in the inner layer of the structure (insulation layer), assessing their potential use in various contexts.

The dissertation is structured to methodically address these research goals, starting with a comprehensive literature review of mycelium and its potential applications. Subsequent chapters detail experimental investigations into mycelium-based materials' physical and mechanical properties, exploring species selection, substrate composition, and environmental conditions that influence mycelium growth and material performance. The study emphasizes the importance of continued research and development in this area while acknowledging the current limitations in strength, stiffness, hardness, flexibility, toughness, and durability compared to conventional construction materials.

This dissertation contributes to the field of insulation materials by studying mycelium-based bio-composites. It highlights the potential of these materials to address some environmental challenges and offer a viable path toward more sustainable practices in the long term. The findings underscore the need for ongoing exploration and innovation in material science to meet the demands of a growing population while preserving environmental integrity.

MULTI-SCALE ANALYSIS OF THE STRUCTURE-MECHANICS  
RELATIONSHIP OF MYCELIUM-BASED BIO-COMPOSITES

by

Libin Yang

B.S., Renai College of Tianjin University, 2015

M.S., Syracuse University, 2019

Dissertation

Submitted in partial fulfillment of the requirements for the degree of  
Doctor of Philosophy in Civil Engineering.

Syracuse University

June 2024

Copyright © Libin Yang 2024  
All Rights Reserve

## **Acknowledgments**

I would love to express my sincere gratitude to all the individuals who have been a constant pillar of support and have guided and encouraged me throughout my journey in the Ph.D. program.

Firstly, I would like to extend my deepest gratitude to my advisor and mentor, Dr. Zhao Qin, without whose support this would not have been possible. Under his tutelage, I was able to move ahead swiftly with my research and learn a lot along the way. His patience and encouragement have been invaluable to me throughout this process.

I would also like to express my heartfelt thanks to the members of my oral committee, Dr. Daekwon Park, Dr. Eric Lui, Dr. Yilei Shi, and Dr. Teng Zhang, for investing their time and providing invaluable feedback. I would also like to show my appreciation for Mr. Nicholas Clarke for his unwavering support throughout my time at Syracuse University.

My thanks go out to all my friends and lab mates who were by my side, encouraging me every step of the way. I want to thank Ruohan Xu for contributing to building the green tent, Gargi De helped to perform the flammability and contact angle test, and Jaejun Lee, Yu-Han Wu, and Dr. Zhiting Tian, all from Cornell University for helping with testing the thermal conductivity.

I am grateful to the Department of Civil and Environmental Engineering, Syracuse University, for offering me a Teaching Assistantship.

My time at Syracuse University was truly memorable, and those memories will stay with me always. I'd also like to extend my most profound appreciation and love to my parents for their constant love and steadfast support.

## **Table of Content**

**Abstract** ----- i

**Acknowledgments**----- v

**List of Figures** ----- xi

**List of Tables**-----xxii

**CHAPTER 1. INTRODUCTION** ----- 1

**1. Introduction**----- 2

**1.1 Background**----- 2

**1.2 The potential to advance knowledge and broad impact**----- 6

**1.3 Objectives and Scope** ----- 8

**1.4 Organization of Chapters**----- 10

**CHAPTER 2. MATERIAL FUNCTION OF MYCELIUM-BASED BIO-COMPOSITE:**

**A REVIEW**----- 13

**2.1 Introduction** ----- 14

**2.2 Mycelium Fabrication Environment**----- 18

**2.2.1 Substrate Types**----- 18

**2.2.2 Humidity and Temperature for Mycelium Growth and Its Water Content** 20

**2.2.3 Fabrication Process**----- 23

**2.3 Multiscale Structure of Mycelium** ----- 24

<b>2.3.1 Fungal Species</b>	24
<b>2.3.2 Structural Features of Mycelium at Different Scales</b>	26
<b>2.3.2.1 Protein</b>	29
<b>2.3.2.2 Glucans</b>	31
<b>2.3.2.3 Chitin</b>	31
<b>2.4 Material Functions</b>	35
<b>2.4.1 Mechanical Properties</b>	35
<b>2.4.2 Biomedical Application</b>	46
<b>2.4.3 Other Engineering Applications</b>	47
<b>2.5 Modeling and Simulation</b>	48
<b>2.6 Discussion and Conclusion</b>	51
<b>CHAPTER 3. DESIGN AND BUILD A GREEN TENT ENVIRONMENT FOR GROWING AND CHARACTERIZING MYCELIUM GROWTH</b>	56
<b>3.1 Introduction</b>	57
<b>3.2. Green Tent Design</b>	59
<b>3.2.1 Circuit Design for Sensing, Storing Data and Device Control</b>	59
<b>3.2.2 Electric device for heat and humidity generation</b>	60
<b>3.3 Experimental Method and Procedures</b>	61
<b>3.3.1 Preparation of Agar Plate for Mycelium Growth</b>	61

**3.4 Results and Discussion ----- 63**

**CHAPTER 4. EXPLORING THE RELATIONSHIP BETWEEN AGAR**

**CONCENTRATION AND MYCELIUM GROWTH RATES IN FUNGI ----- 71**

**4.1 Introduction ----- 72**

**4.2 Experimental Method and Procedures ----- 77**

**4.2.1 Agar Plate Preparation ----- 77**

**4.2.2 Mycelium Species and Sample Preparation ----- 78**

**4.2.3 Time Lapse Photography Preparation ----- 78**

**4.2.4 Characterization of Agar Gel Stiffness ----- 80**

**4.2.5 Imaging with a Scanned Electronic Microscope (SEM) ----- 84**

**4.2.6 Monte Carlo Simulation of Mycelium Growth ----- 85**

**4.3 Results and Discussion ----- 87**

**CHAPTER 5. MYCELIUM-BASED WOOD COMPOSITES FOR LIGHT WEIGHT**

**AND HIGH STRENGTH BY EXPERIMENT AND MACHINE LEARNING 102**

**5.1 Introduction ----- 103**

**5.2 Experimental Method and Procedures ----- 107**

**5.2.1 The General Information of Experiment----- 107**

**5.2.2 Preparation of Mechanical Samples----- 107**

**5.2.3 Mold Design ----- 109**

<b>5.2.4 Heat-Press Procedure</b>	110
<b>5.2.5 Tensile Test and Density Measurement</b>	112
<b>5.2.6 K-means Clustering before Machine Learning</b>	112
<b>5.2.7 K-means Clustering for Scanning the Promising Processing Conditions</b>	113
<b>5.3 Result and Discussion</b>	114
<b>5.3.1 Wood Composites Samples from Different Substrates</b>	114
<b>5.3.2 Mechanics of Mycelium-Based Composites</b>	116
<b>5.3.3 Design Toward the Specific Mechanics of Mycelium-Based Composites</b>	128
<b>5.3.4 Supervised Machine Learning for Predicting the Specific Mechanics of Mycelium-Based Composites</b>	131
<b>CHAPTER 6. DEVELOPMENT AND EVALUATION OF MYCELIUM-BASED BIO-COMPOSITE INSULATION: A SUSTAINABLE ALTERNATIVE TO CONVENTIONAL BUILDING MATERIALS</b>	141
<b>6.1 Introduction</b>	142
<b>6.2 Experimental Method and Procedures</b>	145
<b>6.2.1 Flammability test</b>	145
<b>6.2.2 Surface flammability analysis</b>	146
<b>6.2.3 Contact angle measurements</b>	146
<b>6.2.4 Surface wettability analysis</b>	147
<b>6.2.5 Laser Flash Analysis</b>	147

<b>6.2.6 Differential Scanning Calorimetry</b>	-----	148
<b>6.2.7 Thermal Conductivity Calculation</b>	-----	148
<b>6.2.8 Dog bone samples preparation</b>	-----	149
<b>6.2.9 Mycelium based bio composite bricks preparation</b>	-----	152
<b>6.2.10 Compression Test</b>	-----	154
<b>6.3 Results and Discussion</b>	-----	155
<b>6.3.1 Surface Flammability</b>	-----	155
<b>6.3.2 Surface Wettability</b>	-----	156
<b>6.3.3 Mycelium membrane thermal conductivity</b>	-----	158
<b>6.3.4 Tensile test results</b>	-----	162
<b>6.3.5 Compression test results</b>	-----	167
<b>CHAPTER 7. CONCLUSION AND RECOMMENDATIONS</b>	-----	171
<b>7.1 Summary and Conclusion</b>	-----	172
<b>7.2 Recommendations for Further Study</b>	-----	175
<b>References</b>	-----	179
<b>Current Vita</b>	-----	224

## List of Figures

- Figure 2-1.**The mycelium study, including its multiscale structure, material function, and how environmental factors define these characteristics. It is essential to reveal their relationships by using experiments combined with modeling and simulation methods (the finite element modeling [17] and mycelium-based structures [23] are reused under a Creative Commons Attribution License)..... 15
- Figure 2-2.** A snapshot of the mycelium-based foam (left) [52] (reused under a Creative Commons Attribution License) and a schematic of the mycelium-based sandwich composite (right). ..... 17
- Figure 2-3.** The amount of water loss percentage compared to the original weight. Inserted figure (LEFT): the natural mycelium fiber from the skin of king oyster mushroom. Inserted figure (RIGHT): baked 30 min of mycelium fiber from the skin of a king oyster mushroom. It is shown that the natural fibers represent tubes with naturally bent overall conformation. In contrast, the dry ones become a flat ribbon curved up in the radial direction with a straight overall conformation, suggesting the more significant bending stiffness of the fiber. ....22
- Figure 2-4.** The main fungal species used for fabricating mycelium composites in the literature of the current review. Structural features of mycelium at different scales. (Not specified: the references do not state the fungi species they use. Other: the fungi species except than the other 6 species and occupy a small amount in the study).....26
- Figure 2-5.** Multiscale structure of the mycelium. From the bottom left, the figure shows the molecular formula of chitin and chitosan, followed by two figures showing the structure of the single mycelium and mycelium cell wall and the SEM image of the mycelium network, as

well as two figures showing the wet and dry mycelium samples in the culturing disk. The last figure at the right-up corner shows the cultured king oyster mushroom. We can use different research methods to study the structure-function relationship of the mycelium network at different scale levels, as noted at the axis of the plot (The AFM figure is reproduced under a creative commons attribution license) [23].....28

**Figure 2-6.** The molecular structure of  $\alpha$  chitin (left) and  $\beta$  chitin (right). Each atom is colored according to its type, with red for oxygen, cyan for carbon, blue for nitrogen, and white for hydrogen.....35

**Figure 2-7.** Tensile tests of *P. eryngii* samples after low-temperature baking (A). Snapshots of *P. eryngii* mushroom and the location where we obtain the skin and core samples (B). Snapshot of the Instron machine for tensile test (C). The natural *P. eryngii* (without baking and water loss) near the skin (LEFT) and core (RIGHT) samples before (UPPER) and after (lower) the tensile test (D–G). Stress-strain curve of different baking time of samples near the skin, with baking time of 0, 30, 40, and 50 min, respectively (H–K). Stress–strain curve of different baking times of samples near the core, with baking time of 0, 30, 40, and 50 min, respectively (L). Critical stress of *P. eryngii* mushrooms as a function of baking time for samples at skin and core (M). Critical strain of *P. eryngii* mushrooms as a function of baking time for samples at skin and core.....45

**Figure 3-1.** (A). Green tent appearance, a schematic of Arduino connection, a 3D circuit board, a placement chart of the system overview 60

**Figure 3-2.** A schematic information flow chart from the sensor to Arduino and controllers. ....61

**Figure 3-3.** The general process of the agar substrate preparation and mycelium sample preparation. ....63

**Figure 3-4.** The plot of the **A.** Temperature, **B.** Humidity, and **C.** CO<sub>2</sub> history for the consequent 8 hours.....64

**Figure 3-5.** **A.** Picture of dried petri dish before and after taking the samples and SEM pictures for 6 different positions **B.** Diameter measurement histograms for each position.....67

**Figure 3-6.** Distribution of two groups data (diameter of mycelium fiber on agar versus wood surface), the ANOVA test suggests that the mycelium diameters of the two groups are equivalent.....69

**Figure 3-7.** **A.** The freeze-dryer sample of mycelium grown alone on agar plates and hardwood. **B.** Diameter measurement histograms for each sample. **C.** Distribution of two groups of data (diameter of mycelium fiber on agar versus wood surface).....70

**Figure 4-1.** Mycelium growth schematic and digital microscope image. Agar substrate is prepared with different agar concentration to tune the substrate stiffness ( $E$ ). It fully covers the bottom of the petri dish. A small agar cube fully loaded with mycelium is placed at the center as the initiation point of the network. Timelapse images are taken during the growth of mycelium and analyzed to obtain the occupied area ( $A$ ) as a function of time ( $T$ ). We repeat the test on different substrates to investigate how substrate stiffness affects mycelium growth rate ( $v$ ). The right-down images are obtained from Hirox digital microscope. They show the microstructure of *G. lucidum* mycelium after growing for three days and dyed (blue color dye) before taking the image. The clamp connection and the branching structures are circled and highlighted. 76

**Figure 4-2.** The general process of making the mycelium agar plate (SEM images and mycelium diameter distribution is next to each species) and setting the shelf for time-lapse photography.....80

**Figure 4-3.** The time-lapse photograph for all four species' **A.** *P. eryngii* **B.** *G. lucidum* **C.** *T. versicolor* **D.** *F. velutipes* growth on the 45g/L agar plate within 15 days. ....80

**Figure 4-4.** **A.** The indentation test of the agar plate is on the INSTRON machine, and the schematic drawing shows the details of the dimensions of the indenter and sample. **B.** The average Young's modulus for 11 types of agar concentration results. ....82

**Figure 4-5.** The indentation test curve ( $F - \delta$ ) for all the different agar concentration samples. ....82

**Figure 4-6.** The flowchart of Metropolis-Hastings Monte Carlo algorithm for mycelium growth from a single point to a complex network. ....87

**Figure 4- 7.** **A.** The schematic figures of mycelium growth on different days, and the *G. lucidum* mycelium grows in the Petri dish until fully colonized. **B.** The images taken during the growth of *G. lucidum* at different time. The red dash lines are used to compute the occupied area. **C.** The growth curve (solid line) and exponential fitting curve (dotted line) of *P. eryngii* growth on the 20 g/L agar plate. ....90

**Figure 4-8.** The growth curve (solid line) and exponential fitting curve (dotted line) of **A.** *P. eryngii* (repeating test #1, #2, #3), **B.** *G. lucidum* (repeating test #1, #2, #3), **C.** *T. versicolor*, and **D.** *F. velutipes*.....91

**Figure 4-9.**  $v - E$  relationship obtained from three batches of experimental repeats for individual substrate stiffness and different mycelium species: **A.** *P. eryngii*, **B.** *G. lucidum*.

Error bars are given for the standard deviation of the substrate stiffness with same agar concentration (horizontal) and the standard deviation of  $v$  obtained from the repeating growing tests on the substrates of the same agar concentration (vertical). The exponential decaying curve fitting function is obtained for all the test results for *P. eryngii* is  $v = 21.61 - 34.45e^{-E11.2}$  ( $R^2 = 0.618$ ), and that for *G. lucidum* is  $v = 2045 - 2013e^{-E92000}$  ( $R^2 = 0.041$ ). It is noted that each data point in the plots is obtained from an individual growth experiment. (detailed growth and fitting curves are summarized in **Fig. 4-8**). The plot of the growth rate that based on the agar stiffness for the *C. T. versicolor* and *F. velutipes* as the comparison group. ....94

**Figure 4-10. A.** The HPP260ECO MEMMERT constant climate chamber is used to culture the mycelium. **B.** The *P. eryngii* and *G. lucidum* growth pictures within seven days. **C.** The growth curve (solid line) and exponential fitting curve (dotted line) of *P. eryngii* and *G. lucidum*.....95

**Figure 4- 11. A.** The schematic of the sample for imaging the cross-section of the mycelium agar plate preparation for SEM. **B.** The sample of mycelium growth on the soft agar plate with the sputter coating. The SEM shows the unique structure of the mycelium, which is a clamp connection, and the mycelium is growing vertically into the agar plate. **C.** The sample of mycelium growth on the rigid agar plate with the sputter coating. The SEM shows the unique structure of the mycelium, which is a clamp connection, and the mycelium only grows horizontally on the agar plate surface. **D.** The schematic of mycelium growth on the soft and rigid agar plate. On the soft agar plate, the mycelium growth shape is a 3D structure of a semicircle. On the rigid agar plate, the mycelium only grows a layer on the agar plate. ....96

**Figure 4- 12. A.** The area-time relationship obtained from the Monte Carlo simulation of mycelium growth with (for soft substrate) and without (for rigid substrate) penetration. **B.** Simulation snapshots taken during the mycelium growth on without (I, II, III, and IV) and with (i, ii, iii, and iv) penetrating substrate as indicated on the *A-T* curves as given in panel **A**. The inserted Figures show the structural difference of the mycelium grow on different substrates. The blue stars correspond to the initially randomly distributed nutrition points, the green network is for the mycelium, and the blue block is for the clamp connection within the mycelium fiber for the potential growth and branching point. ....99

**Figure 5-1.** Multiscale structure of the mycelium in our study. From the bottom left, the figure shows the SEM image of the mycelium network and mycelium's unique structure (i.e., thin straight fiber with clamp connection), as well as the two figures of the wet mycelium sample's growth on day 3 and day 7 in the culturing disk. The schematics show the general process of preparation, including growth of mycelium in petri dish, jars, move the incubated mycelium on the rye from the jar to the larger substrate and heat press for samples for mechanical tests. 106

**Figure 5-2. A.** Mold design drawing (left) and model(right) **B.** Three different materials: stalk (S), stalk with mycelium (SM), and hardwood mixed with coffee grounds with mycelium (HCM) (from left to right.) ..... 109

**Figure 5-3.** Processing of mycelium-based wood composites and their microstructural features. **A.** The general process of the experiment. The dog bone samples shown in the Figure are made with three different materials based on the 80 centigrade and 6.75 MPa pressure combined with five different baking times, which are 1 hour, 2 hours, 4 hours, 8

hours, and 16 hours. (material → mix with water → mushy material → heat press machine → test samples → Instron machine → broken samples) **B.** The SEM image of mycelium-based bio-composite material at room temperature dried for a month (left) and after the heat-pressing of 90 °C, baking time 16 hours, and 20.27 MPa pressure (right)..... 111

**Figure 5-4.** The last cluster's mean value which based on the different k values. Stalk (S); Stalk with mycelium (SM); Hardwood with coffee grounds with mycelium (HCM). ..... 114

**Figure 5-5.** The stress-strain curve for dog bone samples tests the composites made of the pure stalk, stalk with mycelium, and hardwood mixed with coffee grounds and mycelium grown in it. Tests are based on samples prepared under 90 °C with different pressure (6.75, 13.51, and 20.27 MPa) and baking time (1, 2, 4, 8, 16 hours.)..... 117

**Figure 5-6.** The stress-strain curve for dog bone samples tests the composites made of the **A.** Stalk (S) **B.** Stalk with mycelium (SM), and **C.** Hardwood, coffee grounds and mycelium grown. Tests are based on samples prepared under 80 and 100 °C with different pressure and baking time. (Different color in the stress-strain curve means the different baking times, which are 1 hour-red, 2 hours-yellow, 4 hours-green, 8 hours-blue, 16 hours-black.)..... 118

**Figure 5-7.** The SEM imaging of the mycelium (left: the mycelium-based bio-composite under 100 °C press for 16 hours, right: the unique structure, which is the clamp connection of mycelium fiber.)..... 119

**Figure 5-8.** Ashby plots for specific mechanical properties of different wood composites. **A.** specific ultimate strength and Young’s modulus normalized by density, showing these two mechanical properties of the wood composite are well aligned, that largely agrees with the other cellular materials (e.g., foams, cork, bone, wood) [297]; **B.** specific modulus of

toughness and Young's modulus normalized by density, showing the toughness of the composites are highly dispersed and weakly determined by the Young's modulus. .... 129

**Figure 5-9.** The general process of data clustering and the tri-layered neural networks classification method for making predictions beyond experimental tests. .... 132

**Figure 5-10.** The confusion matrix of each response by the prediction (**A:** training, **B:** testing)..... 134

**Figure 5-11.** 3D scatter plots for the processing conditions of randomly generated 100,000 imaginary samples made of different raw materials (S, SM and HCM), with the points corresponding to the highest specific mechanical properties ( $\sigma U/\rho$ ,  $E/\rho$  and  $UT/\rho$ ) highlighted by a red color. .... 135

**Figure 5-12.** 3D scatter plots based on the treatment conditions and the color bar based on random 100,000 data specific mechanical properties. Stalk (S); Stalk with mycelium (SM); Hardwood with coffee grounds with mycelium (HCM). .... 135

**Figure 5-13.** Histograms and the error bar for the treatment conditions of the cluster correspond to the high specific mechanical properties (colorful bars), in comparison to the direct experimental observations (black bars) as summarized in **Table 5-6**. A. Stalk (S); B. Stalk with mycelium (SM); C. Hardwood with coffee grounds with mycelium (HCM). .... 138

**Figure 6-1.** We illustrate the application and effectiveness of Mycelium-based coconut panels as sustainable insulation materials in building construction. The left part of the figure shows that using agricultural waste (coir) combined with mycelium (*Ganoderma Lucidum*) generates mycelium-based bio-composite materials. It can provide excellent thermal and acoustic insulation, water and fire resistance, and sustainability. The diagrams on the right

compare the thermal resistance (R-value) contributions of various components within masonry and timber frame constructions, emphasizing the significant impact of the insulation layer. Additionally, the pie charts delineate energy consumption patterns in buildings, underscoring the potential of improved insulation for energy savings in areas like space heating and water heating. 145

**Figure 6-2. A.** The experimental setup with the spectrometer is used for thermal conductivity measurements. **B.** Comparative visual of untreated mycelium membrane and graphite-coated mycelium membrane. **C.** Cross-sectional microscopy image of the mycelium membrane... 149

**Figure 6-3.** The general process of making the dog bone shape samples. Preparing the rye mycelium culture first, then inoculating it with the composite material to make the mycelium-based bio-composite bag for making the food bone shape samples. The dog bone samples shown in the figure are made with coir and oak wood with wheat as the nutrition based on different treatment conditions (material/mixed with water / mushy material / heat-press machine/test samples / Instron machine / broken samples). ..... 152

**Figure 6-4.** The general process of preparing the mycelium-based bio-composite brick. We use two different mycelia inoculated coir, rye mycelium culture and liquid mycelium culture, and two different molds, which are 1 larger square mold and a 5 X 5 small square mold. ... 154

**Figure 6-5. A.** Comparative analysis of fire resistance properties among different materials, represented in terms of area burnt and depth penetrated. The graph illustrates experimental results for three material categories: mycelium composite, cellulose, and EPS foam. The blue bars indicate the total area burnt during the test, while the orange bars represent the depth to which the fire penetrated each material. Insets show close-up images of each material post-

burn, highlighting the physical impact of fire exposure. **B.** Contact angle tests on three different material samples. The top row displays the initial interaction of water droplets with each material—left to right: mycelium composite, cellulose, and EPS foam. The lower row images capture the droplet profiles at rest, demonstrating the contact angles of the surfaces. These images illustrate the varying hydrophobic properties of each material, with the mycelium composite and EPS foam showing significant water resistance compared to the more absorbent cellulose.....157

**Figure 6-6.** Graphical representation of the experimental data showing: **A.** thermal diffusivity ( $\alpha$ ), **B.** mycelium membranes density ( $\rho t$ ), **C.** heat capacity ( $C$ ), and **D.** thermal conductivity ( $K$ ) of various mycelium species. ....160

**Figure 6-7. A.** Stress-strain curves for various dog bone shape samples under different treatment conditions. The treatments include the original specific ultimate stress (OS), the original specific toughness (OT) with a baking time increase and decrease of 50% (t+50 and t-50), and pressure increase and decrease of 50% (p+50 and p-50). Showing how the different treatment conditions affect the mechanical behavior of the materials. **B.** Stress-strain curves for mycelium-based bio-composite bricks that are prepared by inoculating coir by using rye mycelium culture and 2 different amounts of nutrition concentrations in the larger square mold for 2 weeks. (L: larger mold, R: rye mycelium culture, S: low nutrition concentration, and L: high nutrition concentration). **C.** Stress-strain curves for mycelium-based bio-composite bricks that are prepared by inoculating coir using rye mycelium culture and a concentration of nutrition in the small square mold for 4 months. (S: small mold, R: rye mycelium culture, L: high nutrition concentration, and L: longest growth time). **D.** Stress-

strain curves for mycelium-based bio-composite bricks that are prepared by inoculating coir by using 2 different mycelium cultures and 2 different amounts of nutrition concentrations in the small square mold for 1 week. (S: small mold, R: rye mycelium culture, L: liquid mycelium culture, S: low nutrition concentration, and L: high nutrition concentration). B, C, and D show how the different growth periods, forming mold shape, mycelium culture source, and nutrition concentration affect the mechanical behavior of the materials. .... 166

**Figure 6-8.** Comparison of mechanical properties under different treatment conditions. **A.** shows the specific ultimate strength ( $\sigma t/\rho$ ), specific Young's modulus ( $Et/\rho$ ), and specific toughness ( $Ut/\rho$ ) for dog bone shape samples based on various treatments labeled OS, OT, and combinations with  $t \pm 50$  and  $p \pm 50$  suffix. Error bars are given for the standard deviation of each mechanical property. The highlighted sections in red indicate the maximum average results. **B.** shows the 0.2% yield strength ( $\sigma c$ ), elastic modulus ( $Ec$ ), and toughness ( $Uc$ ) for the mycelium-based bio-composite bricks based on different processing methods labeled SLS, SLL, SRS, SRL, LRS, LRL, and SLLL. Error bars are given for the standard deviation of each mechanical property. The highlighted sections in red indicate the maximum average results..... 167

**Figure 7-1.** Future study directions for mycelium materials and mycelium-based bio-composites focus on their applications in packaging, textiles, and filtration media. It also highlights the importance of investigating the effects of light, CO<sub>2</sub> levels, different mycelium species, and substrate types on mycelium growth and its mechanical properties. 178

## List of Tables

<b>Table 2-1.</b> Advantages and disadvantages of chitosan from crustacean shells and fungi. ....	32
<b>Table 2-2.</b> The mechanical properties of mycelium-based composites. MBF = mycelium-based foam; MBSC = mycelium-based sandwich composite.....	36
<b>Table 2-3.</b> Summary of main properties of mycelium film by Haneef et al [23]. ....	41
<b>Table 2-4.</b> Summary of main properties of mycelium film by César et al [168]. ....	41
<b>Table 2- 5.</b> The main mechanical properties result of different conditions of <i>P. eryngii</i> . ....	45
<b>Table 3- 1.</b> The mean value and standard deviation (SD) of the temperature, humidity, and CO <sub>2</sub> .	64
<b>Table 3- 2.</b> The mean and standard deviation of the histogram curve fitting for 6 different positions.....	67
<b>Table 3- 3.</b> The mean and standard deviation of the histogram curve fitting for mycelium growth on the agar and hardwood.....	70
<b>Table 4- 1.</b> All the parameters for use to calculate the shear modulus and Young's Modulus, and the average Young's Modulus results for 11 agar concentration samples. These results were obtained by testing with a cylindrical indenter of 10 mm diameter, sample height of 10 mm and sample diameter of 76.2 mm, corresponding to the geometry factor $\kappa=1.947$ . The Poisson's ratio of the hydrogel is assumed to be incompressible as $\nu=0.5$ .	83
<b>Table 5-1.</b> Mechanical properties and density are obtained from each tested stalk (S) sample.	120
<b>Table 5-2.</b> Mechanical properties and density are obtained from each tested stalk with mycelium (SM) sample.....	122

**Table 5-3.** Mechanical properties and density are obtained from each tested hardwood with coffee grounds with mycelium (HCM) sample..... 125

**Table 5-4.** The maximum ultimate strength and other physical properties of a sample made of each raw material ..... 127

**Table 5-5.** The treatment conditions (i.e., Time (*H*), Pressure (*P*), Temperature(*T*)) of each raw material to achieve the maximum specific mechanical properties ..... 130

**Table 5-6.** The range and mean value of treatment conditions that shows the maximum mechanical properties of each material by the prediction ..... 136

**Table 6-1.** Compares the thermal resistance (R-value), thickness, and specific thermal resistance of different pure mycelium materials (P.E., G.L., T.V., F.V., P.O., G.S.) and conventional construction materials (Basswood, Plywood, Drywall, EPS board). The R-value is presented in both metric ( $m^2 \cdot K/W$ ) and imperial ( $ft^2 \cdot ^\circ F \cdot h/BTU$ ) units. Specific thermal resistance is given in metric ( $m \cdot K/W$ ) and imperial ( $inch \cdot K/W$ ) units, demonstrating the effectiveness of each material in providing thermal insulation. 160

**Table 6-2.** Mechanical properties and density are obtained from each tested sample. .... 164

**Table 6-3.** Mechanical properties are obtained from each tested sample..... 169

## **CHAPTER 1. INTRODUCTION**

## **1. Introduction**

### **1.1 Background**

A brief analysis of world population statistics highlights a steady increase in the human population, rising from 7.4 billion in 2013 to 8.1 billion in 2023 [1]. The population growth implies increased pressure on available social amenities such as housing. As the demand for housing increases exponentially, these further strains the construction industry and the production of conventional materials such as cement, steel, aluminum, and wood [2], [3]. The production of traditional construction materials consumes significant energy. For instance, the calcination process employed in cement manufacture requires a temperature of up to 1450 °C and releases about 0.85 tons of CO<sub>2</sub> per 1 ton of cement produced [4]. It pollutes our environment that can be measured and tracked by embodied carbon, limiting their massive production and usage [2], [5]. For steel, the embodied carbon typically ranges between 1.2 to 2.1 tons of CO<sub>2</sub> per ton of steel produced. The embodied carbon is approximately 0.1 tons of CO<sub>2</sub> per cubic meter of concrete, mainly due to the cement content, which significantly contributes to emissions [6].

At the same time, the rapidly increasing global population leads to increasing annual consumption of agricultural products, which generates more byproducts (e.g., rice husks, cotton stalks, and straw), with most of them being tracked as purely agricultural wastes largely discarded or burned, generating carbon dioxide, atmospheric particulate matters, and other greenhouse gases [5], [7], [8]. They have been partly used as the additive to fertilizers, animal bedding, and low-quality building materials for infrastructures (e.g., brick elements

and green concrete for low-rise buildings, insulation materials particleboards for non-structural applications) and fillings for road construction (e.g., The local bitumen road that contains rice hull ash can bear a higher load and have water resistance) [8].

In recent years, mycelium has attracted increased attention in academic and commercial research due to its energy-efficient growth, absence of byproducts, and wide range of potential applications [9], [10], [11], [12], [13], [14]. Mycelium refers to the dense, thread-like vegetative part of fungi. It is essentially a network of branching hyphae, which are tiny filamentous structures [15], [16], [17]. Mycelium plays a critical role in the fungal life cycle, allowing fungi to absorb nutrients from their surroundings [18]. Beyond the functional role in the fungal kingdom, mycelium has a broader ecological significance. It decomposes organic matter (e.g. leaves, wood, roots, food scraps, agricultural waste, and compostable materials), turning dead plant material into rich soil and playing a pivotal role in the earth's carbon cycle [19], [20]. The critical component in the mycelium that allows it to decompose organic matter is its enzymes. Mycelium produces a variety of extracellular enzymes, such as cellulases, ligninases, and proteases, which break down complex organic compounds like cellulose, lignin, and proteins into simpler molecules that can be absorbed and utilized by the fungus [21], [22], [23]. The interconnectedness of mycelial networks also fosters communication between plants [24], [25].

Mycelium-based bio-composite materials are a groundbreaking innovation in the realm of sustainable materials. These bio-composites are formed by integrating mycelium with organic

substrates, such as agricultural waste or sawdust. Over time, the mycelium grows through this substrate, breaking it down and binding it together, resulting in a strong, lightweight, and biodegradable material [26], [27], [28]. The process is akin to a natural form of 3D printing, where the mycelium weaves intricate patterns, forming sheets or blocks of material.

Mycelium-based materials offer a myriad of advantages. Firstly, they are sustainable.

Cultivated from organic waste and fungi, they divert waste from landfills and reduce the need for petroleum-based products [29]. Furthermore, they can be composted at the end of their life cycle, returning nutrients to the soil [30]. Additionally, mycelium composites are non-toxic and devoid of harmful chemicals often found in conventional building and packaging materials [31], [32], [33], [34]. From an industrial perspective, they can be grown with minimal energy input and in a short time frame, making the production process efficient and scalable [35].

The potential applications for mycelium-based bio-composites are vast. The construction industry explores them as insulating materials, acoustic panels, and structural components by treatment such as dehydrating, heat pressing, and coating after growth [10], [36], [37], [38].

Their natural resistance to mold and fire makes them particularly attractive for building purposes. In product design, these bio-composites have been utilized in crafting furniture, packaging, and even art installations [39], [40], [41]. The flexibility in the post-growth process allows for creating varied textures, densities, and forms, catering to specific needs.

As global awareness about environmental sustainability grows, the demand for eco-friendly alternatives like mycelium-based materials is set to increase. Their versatility and green

credentials position them as a promising solution to several environmental challenges. With continued research and development, the scale of production and variety of applications can expand, further integrating mycelium-based bio-composites into mainstream industries and everyday life.

It is crucial to understand the structure-process-function relationship to facilitate the design of functional bio composite materials. While multiscale physical modeling can reveal the structure-function relationship, the process-function relationship is complex. Usually, it involves multi-physical interactions that become too complicated to simulate accurately. Machine learning can play a pivotal role in this context by analyzing large datasets generated from experiments to identify patterns and predict the outcomes of different processing conditions. For instance, in the production of mycelium-based bio-composites, the choice of substrate and the environmental conditions during growth (such as temperature and humidity) significantly influence the material properties like mechanical strength and thermal conductivity. Machine learning algorithms can optimize these variables to enhance the performance of the bio-composites. This approach has been successfully employed to improve mycelium-based materials' density, compressive strength, and overall durability, making them more suitable for applications in construction and other industries [42], [43]. Such advanced methodologies not only streamline the development process but also enable fine-tuning bio-composites for specific applications, ensuring that the materials meet the desired functional requirements while maintaining sustainability and cost-effectiveness.

## **1.2 The potential to advance knowledge and broad impact**

This thesis shows several advantages over Medium Density Fiberboard (MDF), plywood, and other mycelium-based composites. One of the primary benefits is the environmentally friendly nature of mycelium-based composites. Unlike MDF and plywood, which require synthetic adhesives that can release harmful formaldehyde and are derived from non-renewable petroleum resources, mycelium-based composites use natural mycelium as a binding agent, both renewable and biodegradable. Additionally, the production process of mycelium-based composites is more energy-efficient compared to the high-energy requirements of manufacturing MDF and plywood. Mycelium growth only requires basic environmental controls, such as maintaining appropriate humidity and temperature. It does not need the high-temperature processes associated with synthetic adhesives and wood fiber bonding.

Another significant advantage is mechanical properties. The mycelium composites developed in this research exhibit enhanced compressive and tensile strengths. This is achieved by integrating machine learning models to predict material performance under various environmental and processing conditions. This technological approach allows for more precise optimization of the growth process, ensuring consistent quality and performance of the mycelium-based composites. Such predictive modeling is not commonly found in producing traditional MDF, plywood, or other mycelium-based materials. Moreover, the resistance of mycelium-based composites to water and fire, as discussed in the thesis, offers a substantial advantage over traditional materials, which often require additional chemical

treatments to achieve similar properties. This inherent resistance enhances the safety and longevity of the materials in construction applications, primarily used as insulation materials, reducing the need for harmful chemical additives and further contributing to environmental sustainability.

Compared to other mycelium-based composites, the methods outlined in this thesis provide a more controlled and scalable approach to production. By optimizing the growth conditions and processing method, this research ensures more consistent quality and performance of the final composite materials. The mycelium-based composites discussed in this thesis offer a sustainable alternative to MDF and plywood and push the boundaries of what mycelium-based materials can achieve regarding functionality and environmental impact. The combination of low energy consumption, biodegradability, and enhanced mechanical properties positions these composites as a competitive material for various applications in construction.

In this dissertation, we prepared three types of samples to investigate various stages of mycelium-based materials: Mycelium Agar Plate, Mycelium-Based Bio-Composite Brick, and Heat Press Dog Bone Shape Samples. The mycelium agar plate samples study the growth behavior and structural properties of different mycelium species under controlled environmental conditions, providing foundational insights into the factors that influence mycelium development. The mycelium-based bio-composite brick samples are developed to evaluate the potential of mycelium-based materials as sustainable and functional construction

components. Focusing on their mechanical, thermal, and fire-resistant properties. These bricks demonstrated the practical applicability of mycelium composites in building envelopes, highlighting their environmental benefits and performance capabilities. The heat press dog, bone shape samples, are created to assess the mechanical performance of mycelium-based composites under tensile stress, aiming to increase the material mechanical properties using different treatment conditions. This comprehensive approach allowed for tests of mycelium-based materials across various scales and conditions, ultimately contributing to the advancement of sustainable material science.

### **1.3 Objectives and Scope**

The thesis addresses the construction industry's significant challenges, particularly the environmental impact of conventional insulation materials such as fiberglass, mineral wool, polystyrene, polyurethane, and polyisocyanurate. While these materials are fundamental to constructing the building wall, their production is highly energy-intensive and contributes significantly to environmental pollution through elevated levels of embodied carbon. The escalating demand for building construction driven by global population growth further exacerbates the issue, placing additional pressure on the environment and resource sustainability.

To address these concerns, the thesis focuses on the potential of mycelium-based bio-composite materials as viable insulation materials. Mycelium, the vegetative part of fungi, emerges as a promising solution due to its energy-efficient growth, negligible byproduct

generation, and suitability for various applications. The thesis emphasizes the innovative application of mycelium in creating bio-composites by amalgamating it with organic substrates, such as agricultural waste. This approach presents a sustainable material option and reduces waste by repurposing agrarian byproducts.

The dissertation's objectives and scope revolve around leveraging mycelium's unique properties to develop materials for insulation in the construction sector. The thesis aims to assess the applicability of mycelium-based materials in contexts such as thermal insulation and acoustic panels. This endeavor is motivated by the urgent need for materials that meet the industry's requirements for sustainability and performance without compromising on these critical aspects.

The dissertation is structured into chapters that methodically address these research goals. It begins with a literature review on mycelium, examining its growth factors and potential uses. The following chapters detail experimental investigations into the physical and mechanical properties of mycelium-based materials, exploring aspects such as species selection, substrate composition, and environmental conditions that affect mycelium growth and the performance of the resulting materials. The thesis underscores the promise of mycelium-based bio-composites as sustainable materials in insulation material, highlighting the critical need for ongoing exploration and development to confront environmental challenges and foster more sustainable construction through material innovations. Details of the organization of the chapters are given below.

## 1.4 Organization of Chapters

Chapter 1, introduces the background information and the objectives of the current research work.

Chapter 2, summarizes the literature reviews of the mycelium fabrication environment, the multiscale structure of mycelium, and the material functions. The effect factors of mycelium growth, such as mycelium species, substrate, humidity, and temperature, and the application of mycelium-based bio-composite materials in different areas, including construction, manufacturing, agriculture, and biomedical. Moreover, this chapter addresses the fresh king oyster mushrooms (*Pleurotus eryngii*) water content and mechanical tests. To better understand the material's physical property and mechanical properties of the mushroom species. It can give us an overall understanding of the material before designing the experiment.

Chapter 3, we built a green tent to better understand the mycelium growth period and environmental conditions. We used the Arduino to detect and control the humidity, temperature, and CO<sub>2</sub> levels for growing the mycelium-based bio composite materials. To understand how different substrates will affect the mycelium diameter. We used hardwood and agar substrate to grow the *P. eryngii* mycelium and studied the mycelium diameter distribution.

Chapter 4, from the small-scale study, we focus on the mycelium growth effect factor on the agar. There are thousands of species of mycelium around the world. It is essential to use the suitable species to do the study. We use 4 different species of mycelium, which are king oyster mushroom (*Pleurotus eryngii*), red reishi (*Ganoderma lucidum*), turkey tail (*Trametes versicolor*), and velvet shank (*Flammulina velutipes*) to grow on different stiffnesses of the agar plate to not only find out how the stiffness will affect the mycelium growth but also to find out which species are growing fast, which allows us to study the mycelium on a larger scale that is mass produce the mycelium-based bio-composite material.

Chapter 5, based on the results from Chapter 3, we selected *P. eryngii* as the primary study subject. We obtained the king oyster mushroom mycelium-based bio-composite from the online store. We use it to gain wood composites and integrate experiments and machine learning for better mechanical properties. By forming a secondary fibrous network, we grow mycelium *P. eryngii* on stalk fibers as a natural adhesive. Also, we build machine learning models based on experimental tests to predict the material functions for any treatment conditions.

Chapter 6, we investigate the potential of mycelium-based bio-composites as sustainable insulation materials in building construction. We highlight the environmental impact of conventional insulation materials and compare their properties with mycelium composites derived from *Ganoderma Lucidum* and coconut coir. We make mycelium-based bio composite bricks to test the mechanical, thermal, fire resistance, and hydrophobic characteristics, demonstrating its advantages, including good mechanical properties and

comparable thermal and water resistance performance. To emphasize the potential of mycelium composites to reduce greenhouse gas emissions and support sustainable building practices.

Chapter 7, summarizes the current study's findings, presents conclusions, and identifies issues that need further investigation.

**CHAPTER 2. MATERIAL FUNCTION OF MYCELIUM-BASED BIO-COMPOSITE:  
A REVIEW**

## 2.1 Introduction

In recent years, mycelium gains more interest in academics and commerce studies because of its low energy consumption in growth, zero-byproduct, and broad potential application [9], [10], [11], [14] (**Figure 2-1**). Mycelium is the vegetative part of a fungus, consisting of a network of fine white filaments of 1–30  $\mu\text{m}$  in diameter, which spreads out from a single spore into every corner of the substrate [15], [17]. Each mycelium filament is composed of multiple layers that vary in chemical composition, including proteins, glucans, and chitin [23]. The substrate composed of organic matter provides nutrition for the growth of the mycelium network. In nature, these organic matters come from the remains of organisms such as plants and animals and their waste products in the environment [44], [45]. Their elemental composition includes cellulose, tannin, cutin, and lignin, along with other various proteins, lipids, and carbohydrates [46]. The general procedure used to grow the mycelium composite is similar to the standard protocol of raising mushrooms, which includes 1) inoculate the culturing dish with mushroom spores and sufficient nutrients and water. The incubation time for the mycelium to completely cover the dish is about 7–14 days 2) Prepare the sterilized growing substrate composed of various organic matters (e.g., brown rice, roasted buckwheat, wheat, and straw) and transfer a small piece of mycelium sample cut from the culturing dish into the growing substrate for further incubation. 3) When the substrate is full of mycelium, it is dried at a high temperature for several hours to inactivate the hyphae and stop the growth process before gaining the mycelium composite. Humidity and temperature are two important factors that can affect mycelium growth during the second stage. High humidity (relatively humidity 98%) and warm room temperature (24–25°) with fresh air provide an excellent

environment for growing mycelium [47].

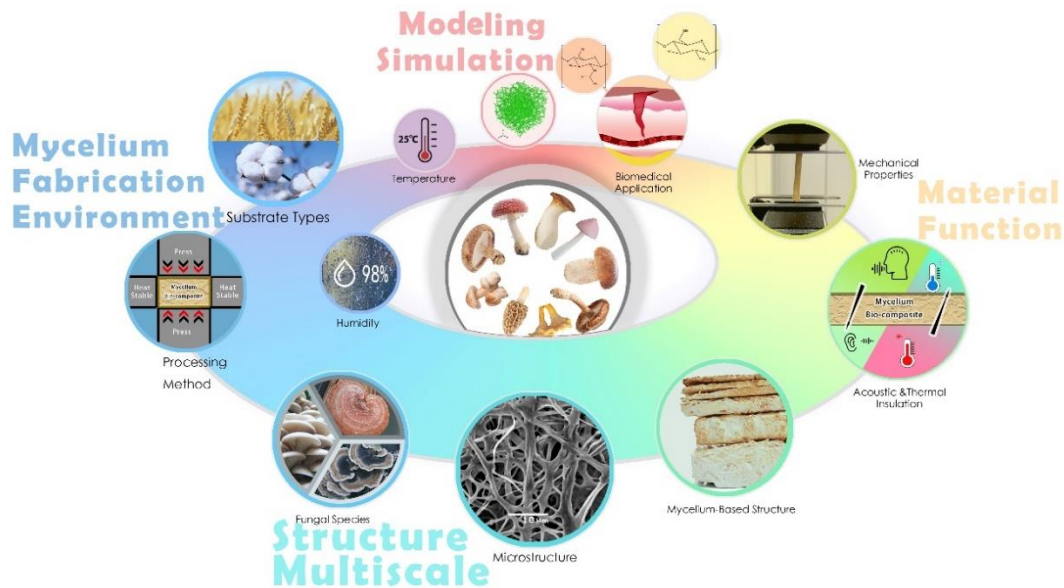


**Figure 2-1.** The mycelium study, including its multiscale structure, material function, and how environmental factors define these characteristics. It is essential to reveal their relationships by using experiments combined with modeling and simulation methods (the finite element modeling [17] and mycelium-based structures [23] are reused under a Creative Commons Attribution License).

The mycelium-based material can reach specific structures and material functions by controlling the substrate and processing method. Mycelium combines with organic matter generated from agricultural and industrial wastes to form the bio-composite that can be used to produce low-value materials (e.g., gap filling, packaging) and high-value composite materials for structural applications [9], [10], [11], [17], [23], [48]. Unlike metal alloy or polymer composite that require energy or complex equipment to melt the raw material and mix different parts, one can uniformly mix various components in the form of small pieces to

form the substrate before growing mycelium, which naturally binds and integrates the elements during its growth. Different substrates can achieve specific functions by growing mycelium composites (e.g., structural support, fire resistance, and acoustic insulation). For example, by adding rice husks and glass fines to the substrates, one can significantly increase the fire resistance of the mycelium bio-composite because it can release a lot of char and silica ash to tolerate high temperature during the burning [48], [49]. In addition, mycelium bio-composite can be used as an acoustic insulation material with an outstanding capability of noise absorption. By testing different mycelium bio-composite panels using various substrates, even the worst-performing samples have over 70–75% acoustic absorption at 1,000 Hz. The substrate composed of 50% switchgrass and 50% sorghum leads to the composite of highest acoustic absorption, which can make acoustic panels with economic advantage and capability of biodegradation once exposed to nature [10].

Two different mycelium-based composite materials have been studied and produced for construction: mycelium-based foam (MBF) and mycelium-based sandwich composites (MBSC) are shown in **Figure 2-2** [36]. MBF is made by growing fungi homogeneously in agricultural wastes in small pieces [50]. As the mycelium network grows, it produces fibers that bind these pieces together to form a porous material [29], [51], [52]. MBSC adds natural fiber fabric (e.g., jute, hemp, and cellulose) as the top and bottom layers aside from the central core as the agricultural wastes combined with mycelium form a sandwich structure of higher bending rigidity [29]. Both MBF and MBSC as the “mycelium bricks” or “panels” have shown mechanical strength, are lightweight, and have environmental advantages in

packing, building insulation, and interior design in comparison to expanded polystyrene (EPS) foams [9], [11], [36], [48].

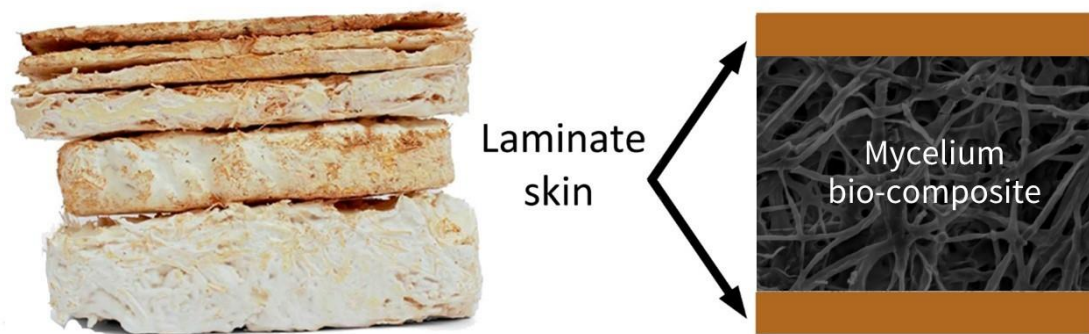


**Figure 2-2.** A snapshot of the mycelium-based foam (left) [52] (reused under a Creative Commons Attribution License) and a schematic of the mycelium-based sandwich composite (right).

As one of the main building blocks of mycelium, chitin is a natural polymer abundantly found in both fungal cell walls and exoskeletons of crustaceans [53]. It has been applied to biomedical applications [53], [54], [55], [56]. Chitin and its derivative chitosan are both long linear macromolecules that can be used to make fibers for wound dressing by electrospinning [55], [56], [57], [58], which is a fiber production method that uses the force from an electric field to draw charged polymer chains from solutions to form a continuous fiber as a bundle of aligned chains [59]. Chitin has been used to produce nonwoven cloths and gels to cover a wound and interact with the open tissue for healing, making it necessary to look into their multiscale structures at the interface with biological tissues [60], [61], [62]. Both crustacean chitin and fungal chitin are applied in wound-dressing research, but there are significant

differences in the structure, properties, and processing between them [53], [63]. Both need to be extracted from the compound, as crustacean chitin often binds with sclerotized proteins and minerals, while fungal chitin binds to other polysaccharides (e.g., glucans) [64]. Highly purified crustacean-derived chitin and chitosan have been used more widely. Still, less research has been done on fungi-derived chitin, even though the extraction process of fungal chitin is more straightforward [53], [65], [66], [67]. Also, fungi-derived chitin has advantages in quantity and availability, as the growth of mycelium is not subjected to seasonal and regional restrictions as for that of crustaceans [65], [66].

## **2.2 Mycelium Fabrication Environment**

### **2.2.1 Substrate Types**

The feedstock materials employed in producing Mycelium-Based Composites derive from three primary sources: agricultural by-products, industrial waste, and post-consumer waste. In terms of their chemical composition, these substrates can be categorized into three main groups: annual plants, softwood, and hardwood. The typical constituents of bulk substrates encompass a variety of elements, including wood chips or sawdust, finely shredded straw (derived from crops such as wheat and rice), chopped corncobs, recycled paper, husks or meals from nuts and seeds, coffee pulp or grounds, and the residual grains from the brewing process [42], [68], [69], [70], [71], [72], [73], [74], [75], [76], [77], [78], [79], [80], [81], [82], [83], [84], [85], [86]. An ideal substrate should exhibit an optimal balance of nitrogen and carbohydrates to facilitate rapid fungal mycelium growth. Comparative analyses of diverse substrates are frequently conducted in scientific investigations, and they can also be blended

in varying proportions to create custom mixtures.

All of the raw materials are classified as lignocellulosic materials. Their composition typically consists of cellulose (30-50%), lignin (15-30%), hemicelluloses (25-35%), along with non-structural components such as pectins, waxes, pigments, tannins, lipids, and minerals [87], [88], [89], [90]. The specific composition of these materials is contingent upon their origin and plant species [91], [92], [93]. Cellulose, a natural polymer, is the predominant structural component in all plant fibers [94]. The cellulose macromolecule is characterized by its linear chains of glucose moieties, conjoined through  $\beta$ -1,4 glycosidic bonds, giving rise to the repeated units of D-anhydro glucose ( $C_6H_{11}O_5$ ) [95]. These chains subsequently associate into microfibril aggregates, imparting the material's characteristic mechanical properties of strength, rigidity, and resilience [96]. Hemicelluloses, on the other hand, are polysaccharides linked together in relatively short, branched chains. They are closely associated with cellulose microfibrils, forming a matrix surrounding cellulose [97], [98]. Hemicelluloses exhibit high hydrophilicity and lower molecular weights compared to cellulose [95].

Lignin is a complex aromatic hydrocarbon polymer with a three-dimensional polymer characterized by an amorphous structure and a high molecular weight [99]. It is less polar than cellulose and acts as a chemical adhesive within and between plant fibers [100]. Lignin serves primarily as a structural component, enhancing the strength and rigidity of cell walls. Additionally, it facilitates the transport of water and solutes through the plant's vascular system and acts as a physical barrier against invasions by phytopathogens and environmental

stresses [101]. Lignin consists of three fundamental phenylpropanoic monomers known as monolignols: p-coumaryl, coniferyl, and sinapyl alcohols [102]. The quantity of lignin varies depending on the source of the lignocellulosic material, and the proportion of different monolignols and chemical bonds within the lignin structure is also contingent upon the specific type of lignocellulosic biomass, differing between softwoods (gymnosperm), hardwoods (angiosperm), and grasses. The lignin in softwood contains only a guaiacyl aromatic nucleus. In contrast, the lignin in hardwood comprises guaiacyl and syringyl aromatic nuclei in various proportions depending on the wood species [103]. Grass lignin is characterized by guaiacyl, syringyl, and hydroxyphenyl units [104].

### **2.2.2 Humidity and Temperature for Mycelium Growth and Its Water Content**

The temperature and humidity are important factors that can affect mycelium growth. The best temperature for growing mycelium is room temperature (24–25°C) [47]. Moreover, growing mycelium should stay in a relatively high humidity environment. Therefore, humidifiers or sprinkler systems are usually used for mycelium growth. For example, [29] et al. created a high humidity environment (up to 98% relative humidity) for the respiration of mycelium fungi by using a semi-permeable polypropylene bag, which provides a high humidity environment and a sterile environment for mycelium growth.

Mycelium, after natural growth, is rich in water (over 60%) [41]. Most of the water must be removed to inactivate its growth and provide a high and reliable mechanical performance.

The existing literature does not mention the final percentage of residual moisture in MBF or

MBSC, but it needs to be dry enough to terminate the fungal growth [36]. The substrate and the species of fungi decided the final mycelium water content. For instance, a substrate made of hemp pulp absorbs more water than that made of cotton wool [105]. In addition, different coatings may affect moisture absorption. It is generally believed that the moisture before deactivation is about 59% [106] or 70–80% [107], but the residual percentage in the final material recognized by researchers is approximately 10–15% [107]. Therefore, the water content of the final mycelium-based bio-composites is the primary consideration for the mechanics of the mycelium samples.

Because of the lack of consistent results, here we perform our tests to understand the water loss of the pure mycelium network within the mushroom samples after baking for a certain amount of time, as shown in the **Figure 2-3**. We use king oyster (*Pleurotus eryngii*) mushrooms and prepare groups of samples with a total weight of  $M_0 \approx 100\text{g}$  for each group, keep the temperature at an elevated level of constant  $80\text{ }^\circ\text{C}$  in an oven and bake the samples for different amount of time ( $t$ ) before measuring and recording the weight of the residue materials ( $M(t)$ ). We intentionally take this temperature to avoid breaking the molecular structure of mycelium. The percentage of water loss is thereafter defined by  $P_{wat} = [M_0 - M(t)]/M_0$ . Every 15 minutes of baking, the two sets of samples (skin and core of the mushroom) were taken out and weighted. Repeat the measurement until baking for 4 hours, when the  $P_{wat}$  curve start to converge without further changing. The curve in the **Figure 2-3** shows that the total water loss of the samples near the skin of mushroom goes up to  $P_{wat} = 90\%$  after 4 hours of baking and the sample near the core has  $P_{wat} = 91\%$ , which is not so different

from the skin samples. Also, we notice that baking the samples for more than 4 hours will not generate more water loss, suggesting the water content in the natural mycelium of this king oyster mushroom is ~90%, which is even higher than many of the hydrogel [108], [109].

Using scanning electron microscope (SEM), it is shown that the natural mycelium within the mushroom is represented by a fully connected network of tubes partially filled by water, which become an array of flatten ribbons once lose water (inserted figures **in Figure 2-3**).

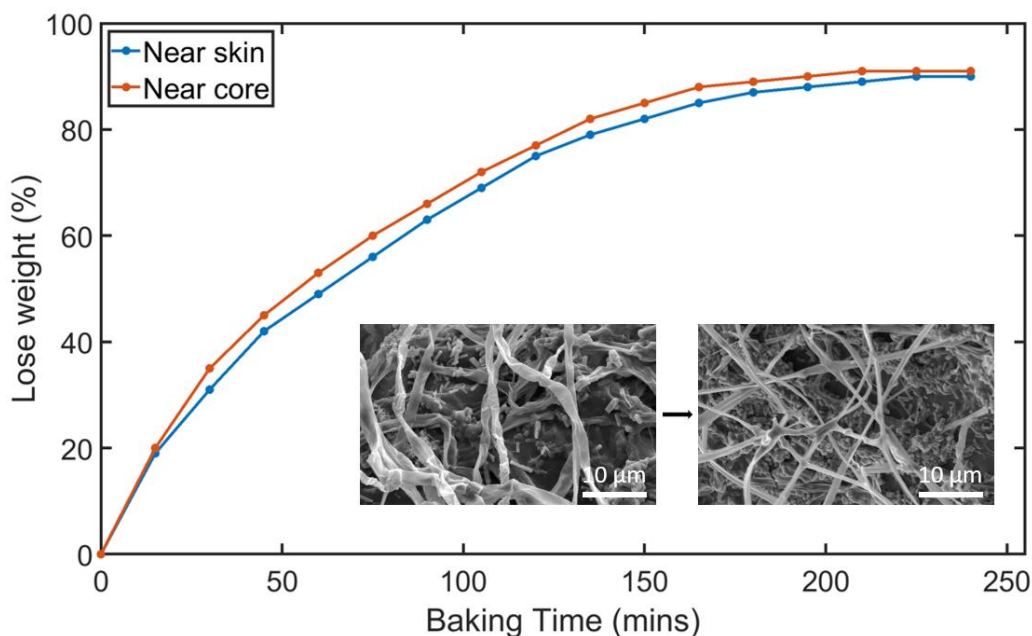


**Figure 2-3.** The amount of water loss percentage compared to the original weight. Inserted figure (LEFT): the natural mycelium fiber from the skin of king oyster mushroom. Inserted figure (RIGHT): baked 30 min of mycelium fiber from the skin of a king oyster mushroom. It is shown that the natural fibers represent tubes with naturally bent overall conformation. In contrast, the dry ones become a flat ribbon curved up in the radial direction with a straight overall conformation, suggesting the more significant bending stiffness of the fiber.

### 2.2.3 Fabrication Process

The different fabrication processes will create different functional mycelium bio-composites. The most common method is oven drying to remove the residue water within the mycelium and substrate, producing lightweight and high-strength foams [42], [78], [81], [85], [110]. It can be used as the core of sandwich MBSC structures by incorporating natural fiber fabrics on both sides. Besides forming foams, the mycelium plays the role of gluing the core material to the fiber fabrics (though the interface generates during the mycelium growth) to resist delamination at the material interface once the sandwich plate is subjected to shear force in loading, leading to a strong composite board with high bending stiffness [29]. Other natural glues (e.g., bioresin) can be added before combining the fabrics to the core part to increase the adhesion of the bio-composites together with mycelium foam. They do not hinder fungus growth through more layers of fiber fabrics, which is critical to forming a robust interface with a large cohesive zone in adhesion that prevents the fabric from easily separating from the foam part through a sharp single crack from defects [111].

The fabrication process that tunes the water content in the mycelium network can significantly affect its mechanics, as shown by former studies. Appels et al. show that pressing can substantially affect the water content and thus the mechanical properties of mycelium composites. This result is expected because pressing can squeeze water and air out of the porous mycelium network, reduces the porosity of the material, and increases the material density, leading to higher Young's modulus and strength [112], [113], [114]. Pressing also helps to reorientate fibers horizontally in the panel plane [115] and reduce plate

thickness during pressing, increasing fiber connection between the walls of the fibers at points of overlap [116]. Pressing may also help to reduce large voids as structural defects within the mycelium composite, preventing the crack from generating during a loading [36], [117]. In comparison to cold pressing, the hot pressing, with the pressure that comes from a pair of hot plates, can further improve the mechanical properties, as shown in an early study [50].

## **2.3 Multiscale Structure of Mycelium**

### **2.3.1 Fungal Species**

The mechanical properties of the mycelium bio-composite are determined mainly by species of fungus, which can be introduced by using different types of spores during the first stage of the incubation of mycelium. Based on the other species of fungus, its productivity, the thickness of mycelium fiber, the microstructure, and the surface topography are different [23], [29], [36], [50], [117]. Mycelium hyphae can be categorized in fungus taxonomy by generative, skeletal, and binding hyphae [11], [118]. Generative hyphae are relatively undifferentiated and can develop reproductive structures. They are typically thin-walled, with occasionally thickened walls, usually have frequent septa (i.e., cell walls that separate the cells), and may have clamp connections (i.e., the unique hook-like structure for hyphal cell growing). Skeletal hyphae are thicker, longer, and rarely branched. They have few septa and lack clamp connections. Binding hyphae are thick-walled, often solid, and usually branched [119], [120], [121]. Based on the three different hyphal types, the mycelium network can be divided into three categories which are monomitic, dimitic, and trimitic [120]. Monomitic

species comprise only generative hyphae, dimittic species form two hyphal types (usually generative and skeletal), and trimitic species contain all three principal hyphal types [122]. These mycelium networks have very different structures and mechanical properties, such as monomittic species, which are suggested to provide worse mechanical performance than dimittic and trimitic hyphal species [123], [124]. For example, trimitic species such as *T. Versicolor* exhibit higher tensile (0.04 MPa) and flexural strengths (0.22 MPa) than monomittic species, such as *P. Ostreatus* (0.01 MPa tensile strength, 0.06 MPa flexural strength), when grown on rapeseed straw [117].

Fungi represent a distinct kingdom of organisms, distinguished by several key attributes, including incorporating chitin within their cell walls, an inherent heterotrophic mode of nutrition, and a cosmopolitan distribution [122]. The full extent of fungal biodiversity remains elusive; while approximately 150,000 species have been cataloged, estimates suggest the existence of potentially 1.5 million to 5.1 million species in total [125], [126]. **Figure 2-4** shows the common fungal species reported in the literature as we reviewed here [42], [68], [69], [70], [71], [72], [73], [74], [75], [76], [77], [78], [79], [80], [81], [82], [83], [84], [85], [86]. *Pleurotus ostreatus* and *Ganoderma lucidum* are most frequently mentioned in scientific publications. Another commonly used species is *Trametes versicolor*. *P. ostreatus* and *G. lucidum* are the most frequently compared species. These fungi species cause white rot and are composed of trimitic and monomittic species [95]. There is tremendous scientific significance in these two species due to the essential chemicals they produced, including a variety of enzymes that can efficiently degrade plant components difficult to hydrolyze,

including lignin [21], [22], [23]. However, many publications do not reveal the species of fungus for the composite production (32%), making it hard to fully reproduce the work by overlooking the type of mycelium network, for example [29], [105], [127], [128].

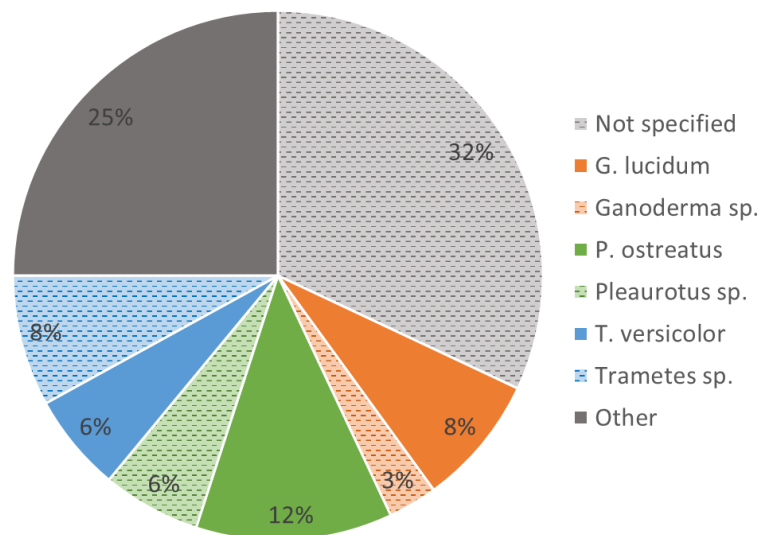


**Figure 2-4.** The main fungal species used for fabricating mycelium composites in the literature of the current review. Structural features of mycelium at different scales. (Not specified: the references do not state the fungi species they use. Other: the fungi species except than the other 6 species and occupy a small amount in the study)

### 2.3.2 Structural Features of Mycelium at Different Scales

The complex material functions of mycelium are attributed to its complex network structure at different scales. The mycelium mechanical properties are controlled by branched filaments and the topology of the network structures [17]. **Figure 2-5** shows the general structure of mycelium from the macroscale to the nanoscale. Since the mycelium has a symbiosis relationship with the substrate, it produces the branch fiber network structure, increasing the

contact area with the complex porous substrate. The mycelium network grows from a spore by extending through the cell membrane and cell wall at the tip of a mycelium fiber. Every single mycelium fiber comprises an array of slender cells separated by cross walls, so-called septum, and enclosed within the same cell wall. Tiny holes in the septum allow the rapid flow of nutrients, water, and other small molecules from cell to cell, along with the mycelium fiber. The cell wall protects the mycelium and provides mechanical strength, and is composed of a layer of chitin, a layer of glucans, and a layer of proteins (e.g., mannoproteins and hydrophobins) on the cell membrane [23]. Chitin is a complex polysaccharide, a polymer of N-acetylglucosamine located on the cell membrane and plays an essential role in giving structural strength to the cell walls of fungi. The mycelium network is cultured using an agar plate as the inoculated substrate for 7–14 days. It took a sample to show the pure mycelium network without other substrate fibers clearly. The SEM images show that the mycelium network comprises many fibers with a diameter of about 2  $\mu\text{m}$ . After that, the mycelium network is migrated to the substrate in the lab to generate the mycelium composite and mushrooms (e.g., the king oyster mushroom as shown in the image at the upper right of **Figure 2-5**), which allows the mechanical tests and microscopic images of the mycelium network at a large scale. The rectangular figure at the bottom shows the nanostructure of the  $\alpha$ -chitin. Two primary polymorphic forms of chitin exist,  $\alpha$  and  $\beta$ , with  $\alpha$ -chitin the most common polymorph for both crustacean and fungal chitin and  $\beta$ -chitin occurring only in squid pen, sea tube worms, and some algae (centric diatom) [129].

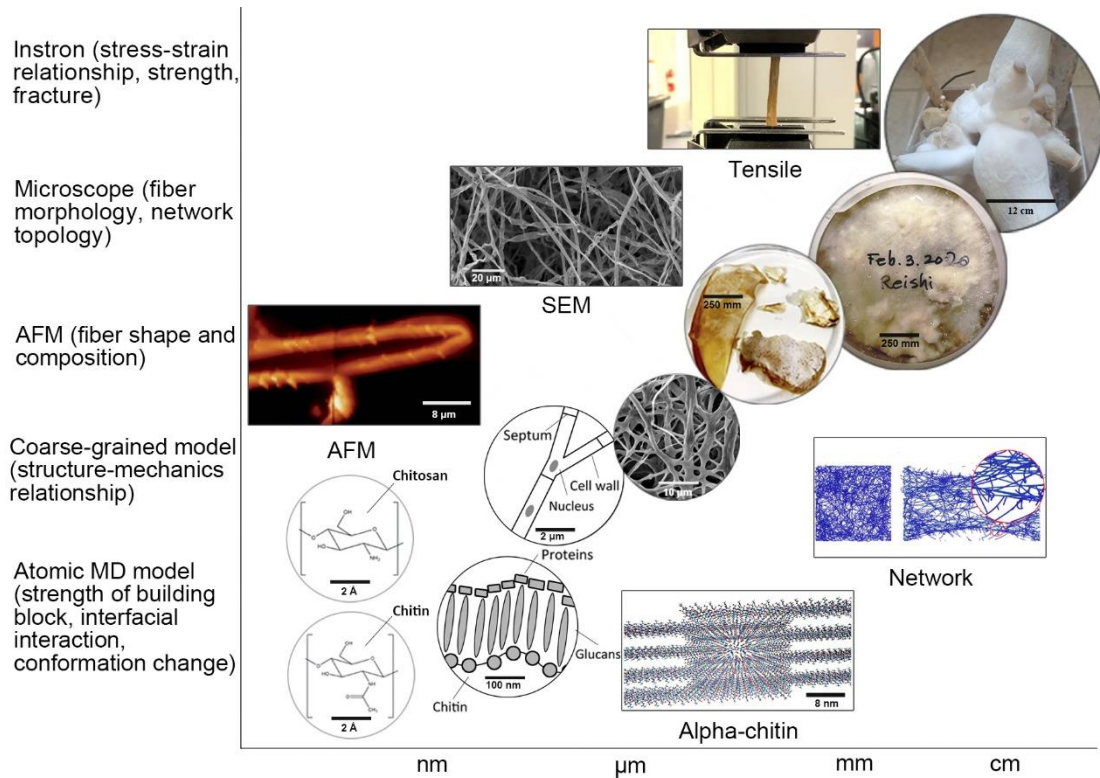


**Figure 2-5.** Multiscale structure of the mycelium. From the bottom left, the figure shows the molecular formula of chitin and chitosan, followed by two figures showing the structure of the single mycelium and mycelium cell wall and the SEM image of the mycelium network, as well as two figures showing the wet and dry mycelium samples in the culturing disk. The last figure at the right-up corner shows the cultured king oyster mushroom. We can use different research methods to study the structure-function relationship of the mycelium network at different scale levels, as noted at the axis of the plot (The AFM figure is reproduced under a creative commons attribution license) [23].

Mycelium-based biomaterials predominantly consist of intricate networks of hyphae. Each hyphal structure is tubular, characterized by elongated cellular constructs demarcated by septa (porous cross) walls, and its growth is predominantly facilitated by the extension of

cellular membranes from the apical regions of these cells [23]. Essential for fungal survival and interaction with external milieus, the cell wall is a complex construct. It typically integrates layers of chitin/chitosan,  $\beta(1-3)$  glucans, and other alkali-insoluble glucans, supplemented with various cell wall proteins and minor concentrations of lipids and pigments [130]. Chitin, a pivotal structural polysaccharide, comprises  $\beta(1-4)$ -linked N-acetyl-2-amino-2-deoxy-D-glucose monomers. Its structural rigidity arises from organizing contiguous chitin chains into hydrogen-bonded antiparallel microfibrils. However, glucans, the dominant cell wall polymers, connect through either  $\alpha$  or  $\beta$  linkages, providing the hyphae with flexibility [131]. The cell wall's external morphology is not uniform across fungal taxa and typically incorporates alkali-soluble glucans and proteins. These proteins, predominantly glycosylated with N- and O-linked carbohydrates, enhance the flexibility of the mycelial structure [23], [132], [133], [134]. They also play a vital role in the extracellular degradation of lignocellulosic substrates by secreting specialized enzymes, including laccases, peroxidases, oxidases, cellulases, and diverse glycosidases [135], [136].

### **2.3.2.1 Protein**

Although mushrooms are a rich source of many proteins, not many proteins have been identified. Enzymes involved in the degradation of lignocellulose are among the most investigated groups of proteins from fungi [137]. Laccases, peroxidases, oxidases, cellulases, and different glycosidases are content in other species of fungi to participate in degradation [134], [138]. The principle that enzymes degrade lignocellulose in fungi is the oxidative and hydrolytic enzymes cooperate. Fungi have two types of degradation systems: intracellular and

the outer cell envelope layer, which is essential for polysaccharide degradation. Moreover, in the extracellular, hydrolytic enzymes are responsible for polysaccharide degradation, and oxidative enzymes are responsible for degrading lignin and open phenyl rings [139], [140]. Mainly, there are three groups of fungi with different effects and degradation mechanisms of lignocellulose, as soft-rot, white-rot, and brown-rot fungi [139].

Soft-rot fungi can degrade surface polysaccharide layers of plants and mostly are ascomycete fungi. Peroxidases are involved in lignin modifications and laccases production, leading to the darkening and softening of the wood. These enzymes have limited degrading functions [141]. White-rot fungi can degrade lignin, cellulose, and hemicellulose. The degradation of lignin is more effective than brown-rot and soft-rot fungi. The wood changes its texture and becomes moist, soft, and silky. Its color becomes white or yellow [142]. Brown-rot fungi are basidiomycetes that have a different function from soft-rot fungi about degrading lignin. It can rapidly metabolize cellulose and hemicellulose and only slightly modify lignin. Due to the oxidizing reaction of lignin, the wood residue exhibits a cube shape and has a brown color [140]. The disruption of the lignocellulose matrix by brown-rot fungi can be demonstrated using iron-dependent Fenton chemistry known as the chelator-mediated Fenton system [143]. Hydrophobins are one of the other important groups of proteins unique to fungi.

Hydrophobins are localized on the outer surface of filamentous fungi cell walls [136]. They are essential to the growth of fungi and the interaction between fungi with their surrounding environment by facilitating aerial development (fungi prone to grow upwards) and contribute to the attachment of fungi to solid supports [135]. In addition, hydrophobins make fungi

hydrophobic by assembling into an amphipathic membrane, as the hydrophobic side is exposed to the exterior and the hydrophilic surface is combined with the cell wall polysaccharides [136].

### **2.3.2.2 Glucans**

The most abundant polysaccharides in the cell walls of fungi are glucans. They are essential to integrate functional proteins and skeletal chitin and form the most critical structural components of fungal cell walls. Glucans in the fungi are connected through alpha ( $\alpha$ ) or beta ( $\beta$ ) linkages. Alpha 1,3 are the most abundant alpha-glucans. They provide resistance to the large deformation of cell walls in the form of structural microfibrils. The structure of beta-glucans is more complex. They mainly contain  $\beta$  1,3 and  $\beta$  1,6 linkages, forming secondary microfibrils [131].

### **2.3.2.3 Chitin**

Chitin is the innermost layer of the fungi cell wall that can provide reinforcement and strength. Chitin is a biopolymer composed of [ $\beta$ (1–4) linked N-acetyl-2-amino-2-deoxy-d-glucose] units [144]. Chitin is a structural polymer made by the smaller monomers to form strong fibers. When secreted inside or outside of cells in an organized way, the fibers form weak bonds between each other, which increases the strength of the entire structure [52]. The development of the application for chitosan has expanded rapidly in recent years, especially in wound healing [53]. Even though chitin can be obtained from crustacean shells, the fungi still show many advantages [144], especially because they are not limited to season and

location. **Table 2-1** summarized the advantages and disadvantages of obtaining chitosan from crustacean shells and fungi.

**Table 2-1.** Advantages and disadvantages of chitosan from crustacean shells and fungi.

Source	Advantages	Disadvantages
Crustacean Shells	Well-established method for industrial production of chitosan [145], [146].	<p>Seasonal and limited supply, high cost and laborious process and not environmentally friendly [145], [147], [148].</p> <p>Large quantities of chemicals, such as alkali and acids, higher temperatures, and long processing time are required for extraction. Generally, alkali concentration of 30–50% w/v and temperature 100°C is required [146], [147], [148].</p> <p>Demineralization treatment is required to remove calcium carbonate, which accounts for 30–50% of crustacean shells [146], [147], [148].</p>

		It possesses high molecular weight and protein contamination, limiting its applications in biomedicines [147], [148].
Fungi	<p>The medium-low molecular weight is suitable for many biomedical applications [147].</p> <p>A higher degree of deacetylation can be achieved[147].</p> <p>Free of allergenic shrimp protein [147], [148].</p> <p>The molecular weight and degree of deacetylation of fungal chitosan can be controlled by varying the fermentation conditions [148].</p> <p>The supply of fungal biomass is infinite, mainly from the biotechnological and pharmaceutical industries [147], [148].</p>	Processes not scaled up to industrial level [145].

	<p>Cheap biowastes can be used as economic substrates for culturing fungi[147], [148].</p>	
--	--	--

Some evidence shows that the linkages between chitin and glucan in the fungi are covalent bonds [149], [150], [151]. The insoluble glucans in mushrooms, yeast, and hyphae have slight differences. However,  $\beta$ -glucans exhibiting a (1,3) or (1,6) branching for the backbone are associated with chitin in mycelium [152]. These are called  $\beta$ -(1-3)-(1-6)-glucans, which have chemical structures very similar to cellulose, which is  $\beta$ -(1-4)-glucan [153]. The location of chitin in different fungi is different; it is concentrated in the bud scar in yeast and the cell wall of most other fungi [154], [155]. Especially in the fungal species of Zygomycota, chitin and chitosan are simultaneously co-synthesized [154], [155]. Compared with fungal chitin, the crustacean chitin contains minerals that require an acidic extraction step for removal, thus degrading the chitin in the process. Crustacean chitin typically binds with sclerotized proteins and minerals and contains minimal residual protein. Such a difference makes the isolation procedure for fungal chitin nanofibers very simple, requiring just brief mechanical agitation in a kitchen blender after a mild alkaline treatment to remove proteins [14], [156]. However, the glucan associates with fungal chitin can occur in quantities exceeding the chitin content itself [64], [157], [158], [159], [160]. Moreover, the extracted chitin can be of different secondary structures (as  $\alpha$ ,  $\beta$ , and  $\gamma$  chitin), except for the most common polymorph  $\alpha$ -chitin, squid pen, sea tube worms, and some algae contain the  $\beta$ -chitin [129]. **Figure 2-6** shows the molecular structure of  $\alpha$  chitin and  $\beta$  chitin. The main difference between  $\alpha$  chitin and  $\beta$  chitin

is the secondary structure, as the neighboring chains of the  $\alpha$  chitin are in antiparallel directions. In contrast, the chains are parallel in the  $\beta$  chitin (**Figure 2-6**) [129]. Moreover, the  $\gamma$  chitin has chains both in parallel and antiparallel [129]. Such a structural difference causes the adjacent amide groups between the neighboring chains in parallel for the  $\alpha$  chitin, but they are not parallel for the  $\beta$  chitin, associating with the flexibility of the  $\beta$  chitin [161].

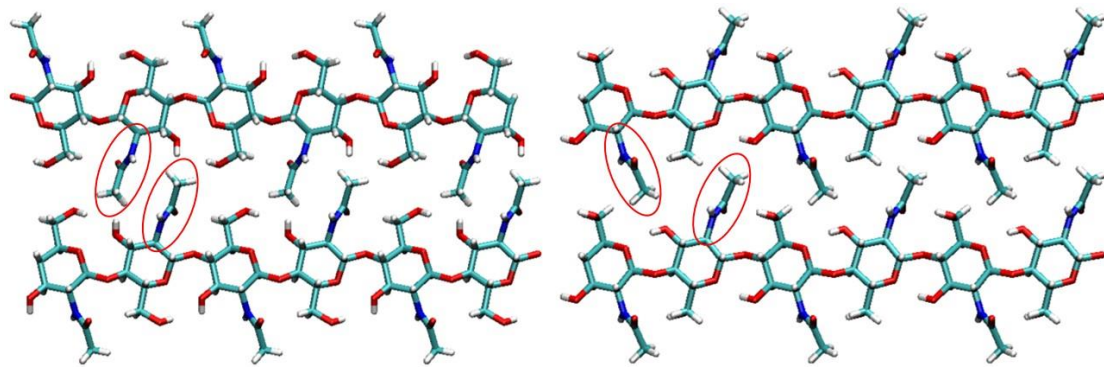


**Figure 2-6.** The molecular structure of  $\alpha$  chitin (left) and  $\beta$  chitin (right). Each atom is colored according to its type, with red for oxygen, cyan for carbon, blue for nitrogen, and white for hydrogen.

## 2.4 Material Functions

### 2.4.1 Mechanical Properties

The mechanical properties of mycelium-based bio-composites are crucial for their application to engineering fields. Since the network structure of mycelium within the composited is primarily determined by the species of the fungi and the substrate that are used to manufacture mycelium, it can be very different by comparing different studies. **Table 2-2** summarizes the test results for the MBF and MBSC in various studies. We can see the

material density significantly deviate from one test to another. Generally, the higher material density leads to a high Young's modulus and strength, as is shown in most cellular materials [162], while the mechanics of the mycelium composites seem to be very different once compared across various studies. The substrate is one of the important reasons that affects the density of the mycelium-based composite. Typically, the higher proportion of grain (fibers, husks, or wood pulp) contained in the substrate will lead to a higher density [144], [163]. Another reason is the different mycelium species used in various studies.

**Table 2-2.** The mechanical properties of mycelium-based composites. MBF = mycelium-based foam; MBSC = mycelium-based sandwich composite.

Density (g/cm <sup>3</sup> )	Young's Modulus (MPa)	Compressive Strength (kPa)	Flexural Strength (kPa)	Tensile Strength (kPa)	Material	References
0.10 - 0.14	66.14 - 71.77	670 - 1180	-	100 - 200	MBSC	[105]
0.183 ± 0.015	-	41.72 ± 13.49	10.91 ± 4.41	49.90 ± 20.00	MBF	[164]
0.29 - 0.35	-	156 - 340	-	-	MBF	[165]
0.18 - 0.36	-	105.85 - 233.62	-	-	MBF	[166]

0.029 - 0.045	0.6 - 2	40 - 83	-	180 - 300	MBF	[17]
0.24 ± 0.001	9 ± 1.2	-	210 ± 10	30 ± 0	MBF	[50]
0.39 ± 0.01	97 ± 9	-	870 ± 140	240 ± 30	MBF	[50]

Compressive strength is the capacity of a material or structure to withstand loads tending to compress the material, an essential feature for the mycelium-based composite that can be used as a package and construction material. López-Nava et al. focus on characterizing the mechanical property of MBF (substrate: common wheat stalks; fungi: *Pleurotus sp*) [164]. They stated that the compressive strength of MBFs is always lower than synthetic polymer foam of the same density as the water absorption, which can significantly affect the compressive strength, and both the substrate and mycelium absorb a large amount of water. In a study by Santos et al., the influence of water content on the mechanical properties of MBF (substrate: coconut powder; fungi: *Pycnoporus sanguineus*) materials was investigated [166]. Before compression testing, the samples are dehydrated at varying temperatures (50, 60, and 70°C) and durations (24, 48, and 72 hours.) They stated that there is no significant difference in compression strength by fixing the time and varying the temperature. However, a significant difference occurred when varying the drying time. The heat treatment connected the external mycelial network hyphae (mycelial film). However, as the drying time increased,

pores appeared in the network due to the disconnection of the hyphae, thereby reducing the mechanical properties. Moreover, Silverman stated that using the fiber (e.g., psyllium husk) in the substrate, MBF of higher compressive strength can be obtained from different species of mushrooms. Besides fabric, they also use chicken feathers in the substrate to increase the compressive strength. The feathers will not be degraded during mycelium growth since they are primarily composed of keratin protein of durability. Still, they are lightweight, hydrophobic, and can provide structural support for the composite and contribute to its mechanics. They reported that the compressive strength of the composite significantly increases with the same density [167].

Flexural strength is the stress at the fracture point for the sample in bending. It is also called modulus of rupture, bend strength, or transverse rupture strength. López-Nava et al. investigated that the range of the flexural strength of MBF is lower than the synthetic polymer foams with the same density, while the tensile strength is much larger than the synthetic ones [164]. However, Appels et al. get the opposite result. The authors test the mycelium-based bio-composite, created by *Trametes multicolor* and *Pleurotus ostreatus* grows on rapeseed straw and beech sawdust. The results show that its flexural strength is larger than the synthetic polymer foam [50]. The authors suggest that the contrasting mechanics between the substrate and the mycelium fibers cause the effect. The mycelium fibers are more elastic than the colonized substrate particles and, therefore, will contribute to the flexibility of the composite and may only rupture at high strain. Moreover, the authors think that the tensile strength is not significantly affected by the species of substrate and fungi

but can be affected by the pressing method, as heat pressing can substantially increase the tensile strength [50].

As mentioned, density is one of the essential factors that can affect mechanical properties. However, the density could be very different due to the different substrates used, sample shape, and treatment conditions, as shown in **Table 2-2**. Islam et al. test the mycelium samples by using tension and compression. In the tension test, the mycelium shows the linear elastic at the low strain and then yields and undergoes strain hardening before rupture. In the compression test, the mycelium shows behavior like the open-cell foam. The stress-strain curve shows the linear elastic initially, followed by a plateau with a softened response. The mycelium exhibits strain-related hysteresis and stress-softening effects between each cycle when subjected to continuous loading and unloading cycles (with their mechanical features summarized in **Table 2-2**) [17].

Ziegler et al. reported an MBSC with a core made of hemp pith and cotton mat. The surface binding fabric is made of a generic, natural fiber fabric such as burlap. As mentioned, the authors use the same approach that Jiang et al [29], [105]. They put the natural fiber fabric on both sides of the pre-inoculated active mycelium-based bio-composite foam. The mycelium as natural glue will continue growing to connect both sides of the natural fiber fabric. The fiber surface increases the compressive strength and gives a high tensile strength to MBSC. However, Young's modulus does not achieve the highest value of MBF [105] (**Table 2-2**). Jiang et al. discussed using different fibers as the MBF surface to make the MBSC. The

fungus could firmly cement the fabric layers by forming a tight mycelium net. The results show that flax, rather than jute or cellulose, is more efficient for colonization and yields higher mycelium production. The ultimate strength and yield stress of the samples produced with flax surface layers (35 kPa and 27 kPa, respectively) almost double that of the samples produced with jute (20 kPa and 12 kPa, respectively) or cellulose surface layers (16 kPa and 15 kPa, respectively) [29].

Researchers have tested the mechanical properties of the mycelium fibrous film. Haneef et al. used *Ganoderma lucidum* and *Pleurotus ostreatus* to grow on the pure cellulose and cellulose-potato dextrose broth (PDB), which can get four different combinations of mycelium [23]. Generally, *P. ostreatus* fibers are stiffer (i.e., higher Young's modulus as summarized in **Table 2-3**) than *G. lucidum* fibers, which have a lower critical strain, which refers to the elongation percentage of the material at the break. On the other hand, critical stress, which refers to the ultimate stress level at the break, is hardly affected by the mycelium species [23]. It is also noted that PDB can make the mycelium fibrous film softer but more stretchable (i.e., lower Young's modulus and higher critical strain). Moreover, César et al. tested 6 different mycelium films growing on the same substrate: Potato Dextrose Agar medium (PDA), as shown in **Table 2-4** [168]. They stated that due to the heterogeneous nature of the samples, the differences in mechanical properties are significant, demonstrating a wide variation in mechanical behavior between mycelium films obtained from the different species of fungi [168]. Compared with Haneef et al. results, the modulus values are registered between 4 and 28 MPa, higher for *P. ostreatus* growth in cellulose. The modulus value shown

by *P. ostreatus* is 44.4 MPa from César et al. It can be noticed that different substrates can lead to very different mechanical properties even by using the same species.

**Table 2-3.** Summary of main properties of mycelium film by Haneef et al [23].

4 Different Samples	<i>Ganoderma Lucidum on cellulose</i>	<i>Ganoderma Lucidum on cellulose-PDB</i>	<i>Pleurotus Ostreatus on cellulose</i>	<i>Pleurotus Ostreatus on cellulose-PDB</i>
Young's Modulus (MPa)	12	4	28	17
Critical strain (%)	14	33	4	9
Critical stress (MPa)	1.1	0.8	0.7	1.1

**Table 2-4.** Summary of main properties of mycelium film by César et al [168].

6 Different species	<i>Lentinus crinitus</i>	<i>Panus aff. conchatus</i>	<i>Ganoderma curtisii</i>	<i>Pleurotus ostreatus</i>	<i>Ganoderma mexicanum</i>	<i>Aurantiporus sp.</i>
Young's Modulus (MPa)	74 ± 48.6	3.5 ± 1.8	128.8 ± 49.6	44.4 ± 16.7	66.7 ± 11.8	112.5 ± 15.4
Critical strain (%)	2.56 ± 1.51	11.32 ± 6.23	1.55 ± 0.83	2.36 ± 1.19	4.09 ± 1.45	1.45 ± 0.39

Critical stress (MPa)	$0.87 \pm 0.49$	$0.27 \pm 0.12$	$0.84 \pm 0.12$	$0.61 \pm 0.14$	$1.5 \pm 0.48$	$0.91 \pm 0.41$
-----------------------	-----------------	-----------------	-----------------	-----------------	----------------	-----------------

We perform our mechanical test to samples taken from the skin and middle parts of *Pleurotus Eryngii* mushrooms (king oyster, as shown in **Figures 2-7A and B**) to better understand the mechanics of mycelium with different water content and thus material density. We use an Instron 5966 machine (10 KN static load cell, 1 KN pneumatic grips with 90 psi holding pressure) to stretch all the material samples to get their stress-strain curves in tension. We measure the initial sample length as the distance between the edges of the two grips as  $L_0$ , zero the force before clamping and zero the displacement before the test. The lower grips during the test are fixed by a pin and the upper grips move at a constant displacement speed of  $v = 2 \text{ mm/min}$ . The traveling distance of the upper grips is given by  $d = vt$  at any time  $t$  after the test starts, and the engineering strain is defined by  $\varepsilon = \frac{d}{L_0}$ . The load cell records the loading force  $f$  and computes the engineering stress with  $\sigma = \frac{f}{A_0}$ , where  $A_0$  is the initial cross-section area of the uniform testing region of the king oyster mushroom sample. The test automatically stops when the sample is broken. The software with the Instron machine returns the  $\sigma$ - $\varepsilon$  curve as well as Young's modulus, yield stress, and breaking strain during the test.

Our mechanical testing results, as shown in **Figure 2-7C-M** for the snapshot of the natural sample before and after tensile test, as well as the stress-strain curves of these samples after

baking with different amounts of time that correspond to a certain amount of water loss (**Fig. 2-3**). It is shown that the samples in tensile loading fail by generating zigzag surfaces at the breaking point after necking taking place, suggesting the ductile failure of the natural samples, govern by the sliding failure between mycelium fibers (**Fig. 2-7C**). The stress-strain curves of samples obtained after a certain amount of baking time are summarized in **Figure 2-7D-K**. We summarize all of the key mechanical features that can be learned from the stress-strain curves in **Figures 2-7L, M, and Table 2-5**. It is shown in **Figure 2-7L** that while the critical stress monotonically increases with the bake time, as well as the water loss (**Fig. 2-3**), of the skin and core samples, the critical strain of the mushroom sample after baking for 30 minutes with 31% and 35% of water loss is larger than the other samples (**Fig. 2-7M**). It is not clear why the critical stress keeps increasing for drier samples, but the critical strain increases up to 30% of water loss and then decrease afterward. The interaction between chitin and water may strongly attribute to this phenomenon, as water can play a key role to turn a biological interface from ductile to brittle in mechanical loading, as what have been observed in collagen and wood materials [169], [170].

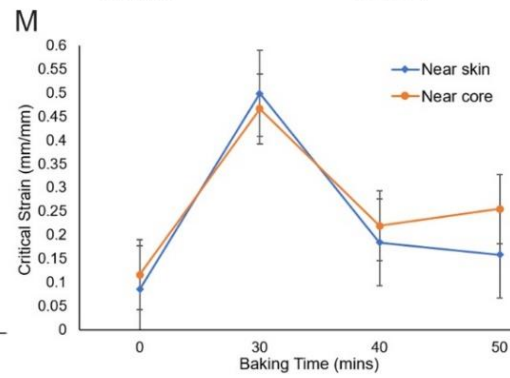
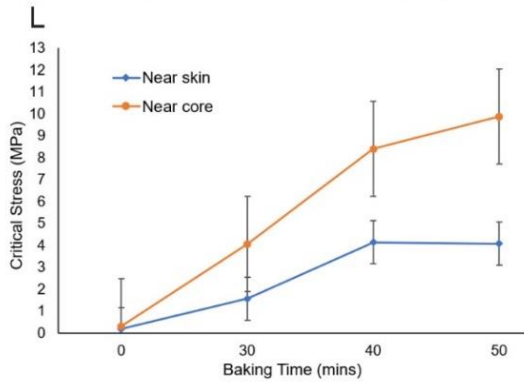
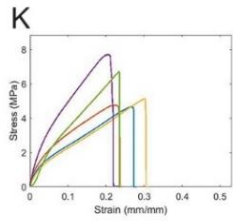
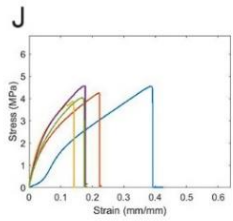
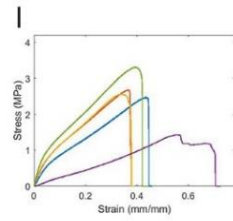
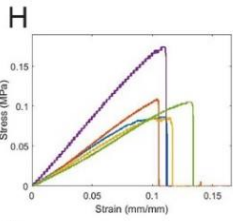
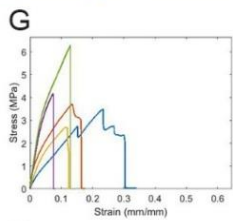
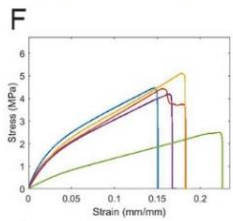
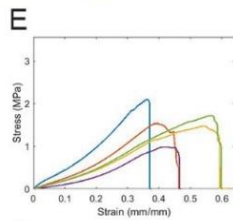
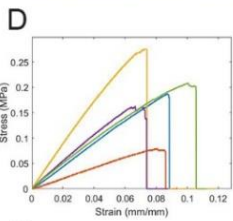
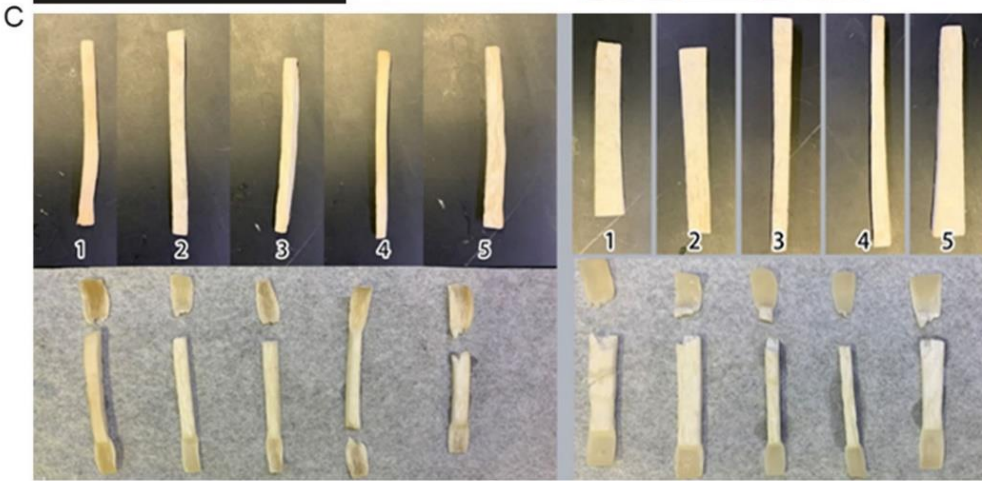


**Figure 2-7.** Tensile tests of *P. eryngii* samples after low-temperature baking (A). Snapshots of *P. eryngii* mushroom and the location where we obtain the skin and core samples (B). Snapshot of the Instron machine for tensile test (C). The natural *P. eryngii* (without baking and water loss) near the skin (LEFT) and core (RIGHT) samples before (UPPER) and after (lower) the tensile test (D–G). Stress-strain curve of different baking time of samples near the skin, with baking time of 0, 30, 40, and 50 min, respectively (H–K). Stress–strain curve of different baking times of samples near the core, with baking time of 0, 30, 40, and 50 min, respectively (L). Critical stress of *P. eryngii* mushrooms as a function of baking time for samples at skin and core (M). Critical strain of *P. eryngii* mushrooms as a function of baking time for samples at skin and core.

**Table 2- 5.** The main mechanical properties result of different conditions of *P. eryngii*.

Sample Conditions	Natural		Dry 30 minutes		Dry 40 minutes		Dry 50 minutes	
	skin	core	skin	core	skin	core	skin	core
Percentage of water loss (%)	0	0	31	35	38.4	42	45	47.5
Young's Modulus (MPa)	2.65	1.19	5.91	15.11	57.99	54.32	64.42	57.79
Critical strain (%)	8.55	11.65	49.88	46.60	18.41	21.94	15.84	25.48
Critical	0.18 ±	0.11 ±	1.56 ±	2.49 ±	4.14 ±	4.26 ±	4.07 ±	5.80 ±

stress (MPa)	0.07	0.04	0.41	0.68	0.98	0.30	1.35	1.36
--------------	------	------	------	------	------	------	------	------

### 2.4.2 Biomedical Application

Normally, the chitin can be obtained by the exoskeletons of crabs and prawns. However, the crustacean-derived chitin is limited by seasonal and regional variations and cannot be obtained anytime. In the meantime, the fungi-derived chitin academic and business interests are increasing. Even though the content of chitin is lower than the crustaceans, it provides a good alternative source. The fungi-derived chitin does not require strong acid to remove calcium carbonate and other minerals [65], [66]. Moreover, the fungi-derived chitin generates a natural nano-composite structure by branched  $\beta$ -glucan. It not only provided rigidity to the chitin but also can produce strong fiber networks when extracted [65], [156].

The biomedical properties of chitin and chitosan of their healing mechanisms and advanced wound-treatment methods have been proven through some research [53]. Jones stated how chitin and chitosan can improve wound healing. There are four stages of wound healing: hemostasis, inflammation, proliferation, and remodeling [171]. The first stage is called the blood clot. In this stage, chitosan forms a coagulum with red blood cells to improve the rate of clotting [172]. The second stage is called inflammatory. In this stage, the macrophage will consume dead cells, attract fibroblasts, and support skin and blood vessel replacement and synthesis of the extracellular matrix. Chitin and chitosan can attract macrophages to help the reaction in this stage [173]. The third stage is called proliferative, and in this stage, the function of fibroblasts is the reformation of the dermis and synthesis of the extracellular

matrix. Chitosan increases IL-8 production in fibroblasts, the IL-8 is an essential regulator of keratinocyte migration and proliferation [174]. The keratinocyte, an essential cell of the last stage for wound healing, can help the reformation of the epidermis [53].

### **2.4.3 Other Engineering Applications**

Pelletier et al. tested the mycelium-based foam with different substrates, and even under the worst-property samples, the acoustic absorption rate at 1,000 Hz exceeded 70–75% [10]. The comparison between the audio frequency spectrum shows that the absorption rate is highest when the substrate is composed of 50% switchgrass and 50% sorghum [10].

According to Jones et al., when the surface layer of MBF becomes carbon, the mycelium-based foam passivation occurs. Charcoal delays the generation and diffusion of smoke and reduces thermal conductivity. Especially the composite that contains the glass fines shows the best fire resistance because of its much higher silica concentration, making it less combustible [48]. Moreover, some authors discussed the thermal properties from the molecular scale. As a unique protein in fungi, hydrophobin associates with cell wall morphogenesis, hydrophobicity, and substrate adhesion in both water and air environments [175], [176]. Despite their small amounts, these proteins represent an important driver of the interfacial function of mycelium. It has been reported that hydrophobic is beneficial to the production of thermally stable carbonaceous structures when applied to cotton fabrics and has been used as a natural flame retardant for textile coatings [177]. The protein works by reducing the release of volatile substances that would hinder complete combustion but favor

carbonization [177], [178], [179].

For the materials applied to the construction industry, besides studying acoustic absorption and thermal insulation of mycelium bio-composite material, enhancing the resistance to pests in mycelium-based bio-composites is also crucial. The mycelium-based bio-composites are mainly used for substrate containing cellulose that is prone to termite attack. Bajwa et al. used four termiticides: vetiver oil, guayule resin, cedar oil, and borax [180]. The results showed that natural oils have a strong potential to act as effective termiticides in cellulosic fiber-based composites bonded with mycelium. Vetiver oil, cedar oil, and guayule resin exhibited variable repellency toward termite attack. Commercial termiticide borax at 10% concentration was the least effective, resulting in the highest weight loss. Corn stover fiber as a base material was preferred by termites than kenaf and hemp pith. The termites did not show any preference for fungus types. Overall, the lowest weight loss was recorded for guayule resin-treated kenaf pith-based bio composites [180].

## **2.5 Modeling and Simulation**

Further development of the mycelium composite materials requires modeling work that helps us to quantitatively understand the relationships between the environmental factors, multiscale structures, and the material functions of the mycelium composite materials. From the simple mechanical aspect, by taking the mycelium composite as a cellular material and studying its constitutive law as well as its mechanics as a function of density can be useful to guide the design and application of mycelium composite. A multiscale model of the

mycelium network is necessary. It is composed of specific chemical structures and microstructures of each fiber and the whole network that can predict the mechanical response of the mycelium composite in different loading conditions. Examples of mycelium models mainly focus on two scales: the mycelium network (microscale) and the stochastic continuum (macroscale).

Islam et al. state that the most appropriate model would be a random fiber network with stochastic fiber diameter and mechanical properties [17]. However, such a model includes many fibers, a complex problem requiring massive modeling and simulation effort. To solve this problem, the authors use a stochastic continuum with a finite element model to represent the macroscopic scale of the samples. The density and the mechanical behavior can change from sub-domain to sub-domain on this scale, with a characteristic length scale. A 3D stochastic continuum model they use contains 8,000 sub-domains and is based on the representative network configuration, which can obtain macroscopic mycelium mechanical behavior. Each subdomain is assigned a network density sampled from the distribution [17]. This finite element model can only represent the relationship between the change in density of the mycelium-based bio composite and the change in the strain-stress curve. Since this model focuses on the macroscale, it lacks the discussion of connection to the mesoscale structure and the molecular structure of the mycelium network. Shinde et al. use a different approach, which is intermediate scale, to model the mycelium growth [181]. They focus on the individual hypha modeled as a growing one-dimensional (1D) lattice and a single source of nutrients to generate a single-colony mycelium as a growing two-dimensional morphology.

They discussed a small-driven lattice gas model. This model generates the morphological characteristics associated with single-colony mycelium arising from fungal hyphae's growth and branching process, fed by a single source of nutrients. The 1D model defined the growth characteristics of the primary hypha, and the 2D model describes the single fungal hyphae elongation and branching to generate an entire single-colony mycelium [181].

Those two models help to understand the structure-function relationship of the mycelium network from two different scales. They provide valuable insights into the growth of the mycelium network and its mechanical properties. However, these models are limited to be applied to certain aspects of a mycelium study. In contrast, a comprehensive multiscale model should connect the molecular composition of mycelium fiber and its interaction with water and substrate particles to the mechanics of the mycelium network and its composite materials. It should also allow us to run simulations and see how the material responds to different external loading conditions and how the molecular interaction and environmental factors from one end may affect the material's function at the other end. To achieve these purposes, the following points need to be considered. We built a model of a mycelium-based composite based on accurate geometry and mechanical properties, allowing us to analyze density and mechanics' influence on the mechanical response of mycelium fiber. By varying mycelium fibers' number, type, and mechanical properties and performing tensile tests on the models, we determined the fiber failure and post-failure deformation for plastic deformation after yielding. Since the water content is also an important factor that can affect the mycelium-based bio-composite mechanical properties, the effect of water on the mechanics of fiber

(viscoelastic) and network (drag force from water in deformation) also needs to be considered. Moreover, the coarse-grained models composed of actual mycelium fibers can be used to simulate the mechanical behavior of the mycelium network. It provides a more accurate description of the network distortion in loading than a finite element model can do. The single fiber deformation may also connect to molecular simulation, which helps to understand the interfacial interaction between different material phases (e.g., chitin, glucan, protein, water, etc., **Figure 2-5.**)

## **2.6 Discussion and Conclusion**

Unlike protein or protein-based biological materials (e.g., silk, collagen, cytoskeleton, etc.), less attention is paid to microorganisms and their multiscale structures. Studying mycelium and their composite materials can help to understand the mechanics of the fungus network, its biological function, and its application to produce green composite materials with both good mechanics and lightweight, in both simulation and corresponding experiments for synthesis [9], [23], [28], [29], [36]. A method to grow and process mycelium-based composites can lead to a promising and innovative way to produce building materials from using the agricultural method [28]. The study of molecular composition and biological function in the mycelium network may facilitate the discovery of new drugs produced by a fungus with certain biological functions or inspire the design of the topology of the internet of things with low power consumption and the function of a fast response to pests and diseases [53], [57], [59], [60], [63].

As an alternative environmentally friendly material over synthetic foams, mycelium composite shows its advantage in several engineering applications (e.g., packaging materials, acoustic and thermal insulation boards) and is receiving more attention. Producing such material is still a pioneering field and the standardized process to yield optimized material property has yet to be identified. This bio-composite material has the ability to be widely used in furniture, agriculture, civil engineering, and the biomedical field. In general, in terms of mechanical properties, the mycelium composites show properties different from synthetic polymer foams or natural cellular materials. Their mechanics are not simply defined by the processing method at the end of its production but as the collective result of the fungi species, their substrate, and related environments during the growth. The properties of the substrate define the mechanics of the matrix material within the composite. The mycelium network itself is affected by the composition and structure of the substrate. Moreover, since both the mycelium and substrate can absorb water, the water content of the final composite is also crucial. Usually, a hot press process can help to remove the water and inactivate the mycelium, effectively preventing it from growing during application. However, due to the wide range of available parameters, results are often incomparable among different studies. For example, compared with the most important competitor traditional material (EPS), the mycelium-based bio-composite has not shown a lot of advantages.

In addition to be used as bio-composites because of its mechanics, mycelium is rich in chitin, which provides reinforcement and strength to cell walls. The interfacial interaction between chitin to other components, and how water plays an intermediate role, needs molecular

modeling and analysis at the fundamental length scale. Moreover, the chitin purified from crustacean shells has been widely used in biological applications, such as wound healing. Even though the mycelium cell wall contains a lot of chitins that can be gained without geographic and seasonal limitations, the applications of the chitin purified from mycelium is not as wildly used as that from crustacean shells, which requires more research and attention.

Even though the mycelium-based composites show advantages for their mechanics, lightweight, and many environmentally friendly features, they have limitations and challenges for their large-scale applications. For instance, as a biomaterial, its production is less standardized than conventional engineering materials such as steel, cement, and polymer, and it is not clear how to customize the types of substrates for the certain species of fungi to maximize the yield of mycelium and to optimize the composite mechanics. However, since there are over one million species [126] , testing the microstructure and mechanics for each of them is extremely difficult and we may need to investigate the structure-mechanics relationship of different classes of fungi (by type of rot, type of hyphae, gene, etc.) to identify the most promising species of yielding composite with the best mechanics. Moreover, unlike polymer foams, mycelium-based biocomposites cannot be massively produced within a short time by machines, as growing the mycelium needs about 2 weeks or more time. It is important to automatically control the growing factors, including temperature, humidity, supplied nutrition, and light within an incubating environment without direct usage of human labor during its growth. It is also not clear how each of its constituting building blocks contributes to its interface to wood fibers and thus affects the integrity of the fibrous network

of the composite. These limitations are crucial before supplying the material to the architect and there are broader industrial applications.

Studying mycelium can go broadly beyond material usage. As the vegetative part of a fungus, mycelium has the unique capability to utilize discrete agricultural wastes as substrates for the growth of its network, which integrates the wastes from pieces to continuous composites without energy input or generating extra waste [12], [36], [50]. Besides fixing pieces of the soil, mycelium in nature has a more important function as an information highway that speeds up interactions between a diverse population of plants [16], [182], [183]. It allows individual plants that are widely separated to effectively defend themselves against pests and diseases by communication and exchange matters [184]. The study of mycelium-based composite, as to how it integrates different discrete blocks and achieves material functions that none of the building blocks can achieve by themselves, goes beyond the mechanics of material study, and becomes the main reason we want to understand more about the mycelium network and its biological functions. The current point, the functions of the mycelium network are of the interest to primary ecologists, while how exactly the chemical signals are conducted in the hierarchical structure of the mycelium network and how its effectiveness relates to the geometry and topology of the network are still unknown, as well as how such knowledge may contribute knowledge to the topology of the Internet and the internet of things, or innovative Internet media with low energy consumption. Most of these questions need to be addressed with interdisciplinary efforts and some of them may be answered by developing a multiscale model of the mycelium network and use it in related

simulations. We will study its application to produce green composite materials but will also generate knowledge to design an information network system.

**CHAPTER 3. DESIGN AND BUILD A GREEN TENT ENVIRONMENT FOR  
GROWING AND CHARACTERIZING MYCELIUM GROWTH**

### **3.1 Introduction**

Mycelium has been recognized as an environmentally sustainable material with a great potential for various applications. Baked and pressed into a dense composite, mycelium has proved to be lightweight, fire-resistant, soundproof, and strong, which makes it highly sought-after in engineering, construction, packaging, and architecture [185]. These properties, combined with its biodegradability and customizability, have garnered a lot of interest in mycelium-based materials [9]. Mycelium plays a crucial role in soil health and plant growth. By secreting enzymes and acids, mycelium helps to break down organic matter and increase nutrient availability. Additionally, mycelium forms networks of hyphae that improve soil structure by binding soil particles together, resulting in better soil aeration, water retention, and nutrient availability [186]. As the main body of fungi, mycelium is growing in a dark and humid environment. It is a rapidly spreading network of thin hyphae tubular structures that absorb nutrients from the surrounding environment. The mycelium can continue to grow and spread, forming a dense and interwoven network of hyphae that can persist for years [187]. It is non-toxic, safe for use in human and animal contact, and a good insulator with thermal and acoustic properties [188].

The mycelium network is the vegetative part of a fungus, consisting of a mass of branching, thread-like hyphae [16], [17]. The topology of the mycelium network is complex and varies depending on the species of fungus and the environmental conditions. Mycelium networks typically consist of interconnected nodes, each representing a branching point where hyphae intersect. These nodes can be dense, with multiple hyphae crossing simultaneously. In some

species of fungi, the mycelium network can span great distances, with interconnected fibers extending for up to several kilometers [16], [182], [183]. This long-range connectivity is thought to be facilitated by specialized structures known as "rhizomorphs," which are bundles of hyphae that grow together in a linear, root-like form [189]. Rhizomorphs are thought to be vital in transporting nutrients and water over long distances, allowing the mycelium network to absorb resources from a wide area [189]. The mycelium network can also absorb nutrients from a wide area rather than being limited to the immediate vicinity of the growing mycelium. This is because the mycelium network can secrete enzymes and acids that break down organic matter in the soil, making nutrients available for absorption [190]. In addition, the mycelium network can form symbiotic relationships with other organisms, such as plants, exchanging nutrients in a mutually beneficial relationship [184]. Overall, the topology of the mycelium network is complex and dynamic, with a series of interconnected hubs and long-range fibers that allow for the absorption of nutrients from a wide area. The ability of the mycelium network to form symbiotic relationships and break down organic matter also makes it a key player in nutrient cycling and ecosystem functioning.

Mycelium growth in nature is always hidden underground or inside rotten woods, preventing direct observation and experimentation. It is crucial to develop lab facilities that enable the control of the conditions to mimic the natural environments and allow to directly observe the mycelium growth without damaging its structure. The most suitable environment for most mycelium to grow is a low-light environment with a temperature of 20-25 °C and a humidity level of 93-95 %RH [38], [191], [192]. At the same time, the incubation periods for the

fungus ranged from 12 to 32°C [193]. To build the environment and grow mycelium in the lab, a real-time climate control system is needed. Here, we design and build a fully customized green tent, meticulously designed to offer proper thermal and humidity in the tent for mycelium growth. Our goal for the green tent is to provide us with complete control over the temperature and humidity levels within the tent. We integrate an Arduino chip to monitor and regulate environmental data to achieve this effect. Moreover, the Arduino chip can help us to record the data for analysis.

## **3.2. Green Tent Design**

### **3.2.1 Circuit Design for Sensing, Storing Data and Device Control**

A small change in the environment will lead to mycelium growth failure. An Arduino Mega 2560 circuit with sensors is used to monitor the temperature, humidity, and CO<sub>2</sub> levels of mycelium growth to control the environment in the green tent. The scanning frequency during the operation is 115200 Hz. The accuracy of the sensors is the DHT22 Temperature-Humidity Sensor & DS18B20 Temperature Sensor (resolution of 0.1°C and 0.1%RH respectively), and Gravity Infrared CO<sub>2</sub> Sensor (resolution of 1PPM). All the data is written to a log file in a SD card for every 5 second through a data logger module (DS1307 V03 Real Time Clock Module and MicroSD Card Adapter) by using an Ethernet cable.

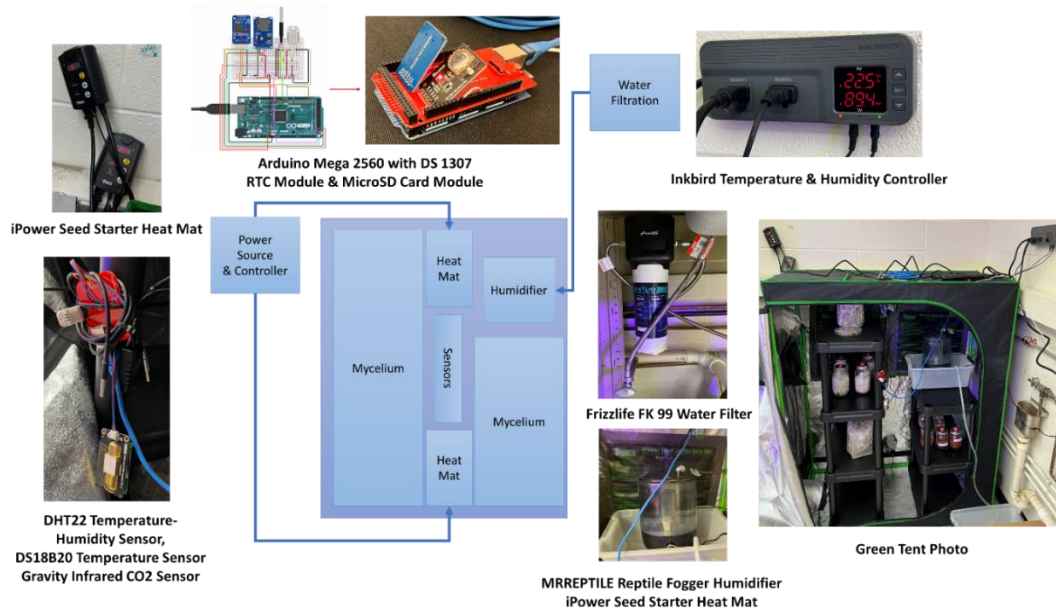


**Figure 3-1.** (A). Green tent appearance, a schematic of Arduino connection, a 3D circuit board, a placement chart of the system overview

### 3.2.2 Electric device for heat and humidity generation

Two of the heat mats provide enough heat in the green tent system. They are installed on the back wall center area. The iPower GLHTMTM Durable Waterproof Seedling Heat Mat has a size of 20 inch by 20 inch, and the temperature control range is 40-108 °F. The operating power is 96 W for two heat mats. We use an regular ultrasonic humidifier in the green tent to tune the humidity level inside. The humidifier has a 4 Liters water tank with 210 ml/h maximum mist output. It is controlled by the humidity sensor and only be turned on once the humidity level drops 90 %RH. The average water consumption is Approx. 1.5 Liter per Day. The water in the humidifier is filtered by an external water filter (Frizzlife FK99).

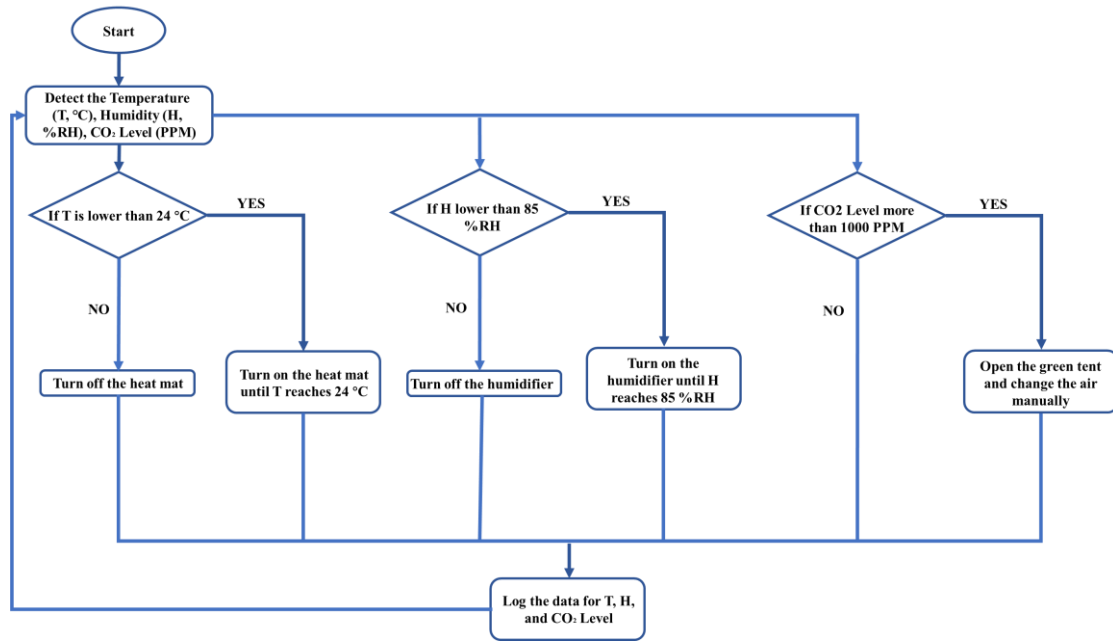


**Figure 3-2.** A schematic information flow chart from the sensor to Arduino and controllers.

### 3.3 Experimental Method and Procedures

#### 3.3.1 Preparation of Agar Plate for Mycelium Growth

We use the agar plate to culture the liquid *P. eryngii*, which is known as king oyster mushroom to better understand the mycelium microstructure. Moreover, we set an obstacle of a basal wood to observe the mycelium fiber growth behavior. Analysis of the SEM imaging results to recognize mycelium diameter in the different positions to understand how the basal wood can affect the mycelium microstructure.

To prepare the agar plate petri dish, we use 20 g of agar powder, 20 g of malt extract, 2 g of yeast, and 1000 g of water, as shown in the first step in **Figure 3-3**. We use malt extract and yeast because both can provide the nutrition for mycelium growth, and the agar as a substrate can allow the mycelium growth on the surface. To successfully get the agar plate, we boil the

water and put all the material into an Erlenmeyer flask, as shown in the second step in **Figure 3-3**. The thermal mixer keeps the mixture at a high temperature and solutes all the powder. Even though we boil all the mix in the water, some precipitate still cannot be solved. So, we use a funnel to filter the mixture into the other Erlenmeyer flask, as shown in the third step in **Figure 3-3**. Use aluminum foil to cover the Erlenmeyer flask and put it into an autoclave for high temperature (123 °C) and pressure (24 psi) sterilizing for 40 minutes. When the sterilizing is finished, take the Erlenmeyer flask to the clean room, and wait until the mixture temperature is cool down to around 45 °C. Use 75% alcohol wipes to clean the Petri dish and glass rod. We use a glass rod to guide the mixture into the Petri dish from the Erlenmeyer flask, as shown in step fifth in **Figure 3-3**. Wait until the mixture cools down to a solid, and then inoculate the liquid *P. eryngii* mushroom. Use the laboratory film to seal the Petri dish and put them into the green tent for 7 to 14 days; wait until the mycelium fully occupies the Petri dish and use it for the next step. Once the mycelium is fully occupied in the Petri dish, we cut a small piece, inoculate it into the new Petri dish, and put a long strip of balsa wood aside from it. Observer the mycelium growth state for 7 to 14 days and then use it for SEM imaging.

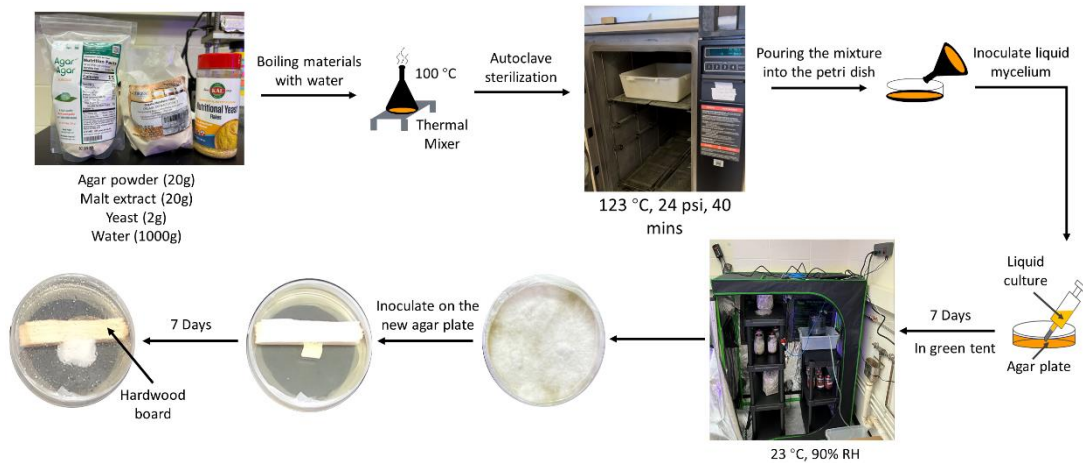


**Figure 3-3.** The general process of the agar substrate preparation and mycelium sample preparation.

### 3.4 Results and Discussion

After setting up the Arduino controller for the green tent, we test it for 8 hours to ensure it runs correctly. **Figure 3-4** shows that the log data results refer to 8 hours. The temperature and humidity are the correct results based on the setting. We set the target value of temperature as 23 °C and the tolerance range as 21.5 °C [6], as shown in **Figure 3-4A** (red and magenta horizontal line.) The reason that we set this range is that it is a relatively good temperature for mycelium growth. When the temperature sensor detects the temperature achieved at 23 °C, the controller will atomically turn off the heat mat. As the temperature decreases, when the temperature is lower than 21.5 °C, the controller will turn on the heat mat to allow the inside temperature of the green tent to increase to 23 °C. As with the temperature as shown in **Figure 3-4B**, the controller will turn on the humidifier when the humidity sensor detects the inside humidity of the green tent lower than 90% RH and turn off the humidifier when the humidity achieves 99% RH. Since the mycelium needs a relatively high-humidity

environment to grow [47]. The CO<sub>2</sub> sensor detects the CO<sub>2</sub> level in the green tent is around 400 to 500 PPM as shown in **Figure 3-4C**. We did not set a target value and tolerance range for the CO<sub>2</sub>. The only number we compared with is the average CO<sub>2</sub> in the air, around 420 PPM [195]. Since the mycelium is breathed when growing [196], the average value in the **Table 3-1** is higher than the CO<sub>2</sub> level in the air. Moreover, we calculate the mean value and standard deviation (SD) for the test results. To compare the results with the set value, our results can be acceptable. Using the Arduino controller, we can very well detect the environmental condition in the green tent.

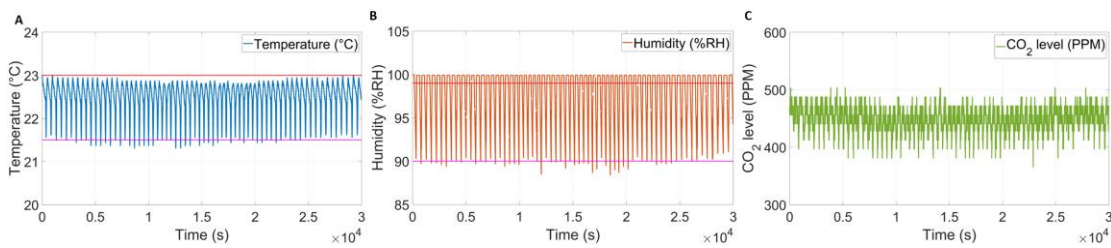


**Figure 3-4.** The plot of the **A. Temperature**, **B. Humidity**, and **C. CO<sub>2</sub>** history for the consequent 8 hours.

**Table 3- 1.** The mean value and standard deviation (SD) of the temperature, humidity, and CO<sub>2</sub>.

	<b>T (°C)</b>	<b>RH (%)</b>	<b>CO<sub>2</sub> (PPM)</b>
<b>Mean value (<math>\mu</math>)</b>	22.5	97.66	449.28
<b>Standard deviation (<math>\sigma</math>)</b>	0.37	3.05	19.95

We also calculated the thermal insulation (R value) for the green tent. The fluctuation is slight

due to the small range necessary to grow the mycelium. Given the DS18B20's accuracy of  $\pm 0.5$  °C, the max value peaked at 27 °C and remained above 25 °C. Using the data, we used thermodynamics principles to calculate the R-value of the green tent, which was 0.77  $\text{m}^2\cdot\text{K}/\text{W}$ . Though we do not have the actual product value, we compared our computed tent R-value to other materials and found that it is higher than drywall but lower than polystyrene. This means that the tent retained the heat inside of it better than any common wall material, at a caliber that was high, but not higher than one of the best insulating materials. From this test, we find that the data is representative of the experiment performed - the tent's purpose is to create a stable environment, retaining the heat, which is what the temperature data proved.

We use the equation:

$$R = \frac{t\Delta T}{Pt_{on}} \quad (3-1)$$

to estimate the thermal resistance R value of the green tent to understand its energy efficiency. Here,  $A = 7 \text{ m}^2$  is the surface exposed area of the green tent, °C is the temperature difference between the lab temperature and target temperature inside the tent,  $P = 96 \text{ W}$  is the total power of the heat mat,  $t = 28800 \text{ s}$  is total testing Time and  $t_{on} = 14400 \text{ s}$  is the total amount of time that the heat mat is on. Using the numerical values, we obtain the thermal resistance  $R=0.77 \text{ m}^2\cdot\text{K}/\text{W}$ , as R4.4 of an imperial unit. Considering the layer thickness of the tent is only 0.8 mm, this corresponds to the thermal conductivity of  $0.001038 \text{ W}\cdot\text{m}^{-1}\cdot\text{K}^{-1}$ , which is better than the stand air at the temperature of 300 K ( $0.02614 \text{ W}\cdot\text{m}^{-1}\cdot\text{K}^{-1}$ ), mainly because of the reflective inner layer that prevents the radiant heat given by the heat mat from escaping the tent.

We use the green tent to grow our *P. eryngii* samples. It is easy to grow, have high yield and is the same genus as the *Pleurotus ostreatus*, which is more widely used for material developments [23]. The mycelium is allowed to grow on the petri dish inside the tent for 14 days, and then put the petri dish into the freeze dryer for 48 hours to dry the sample for use in the SEM imaging. The sample is taken out of the freeze dryer after 48 hours, weighed it, and then put back to dry for three more hours to ensure that the model is completely dry. We marked six different positions on the Petri dish to analyze the diameter. The six positions mainly represent the mycelium growing on the wood and mycelium growing on the agar plate. The SEM imaging results of 6 positions are shown in **Figure 3-5A**. The results mainly show the unique structure of the mycelium fiber, which is the clamp connection. We chose 10 mycelium fibers for each position, randomly measured the fiber's diameter several times, and made the histogram, as shown in **Figure 3-5B**. Moreover, to better analyze the diameter distribution, we use normal distribution curve fitting to get the mean value of the diameter for each position, as shown in **Table 3-2**. It is shown that the average diameter value of mycelium from the wood and the agar plate is relatively the same. Apparently, the wood substrate reduces the growing speed of the mycelium network (**Figure 3-3**), making the growth slower than the network on agar substrate. However, such a reduction in the network growth seems not applicable to the fiber diameter, according to the many measurements (**Figure 3-5B**).

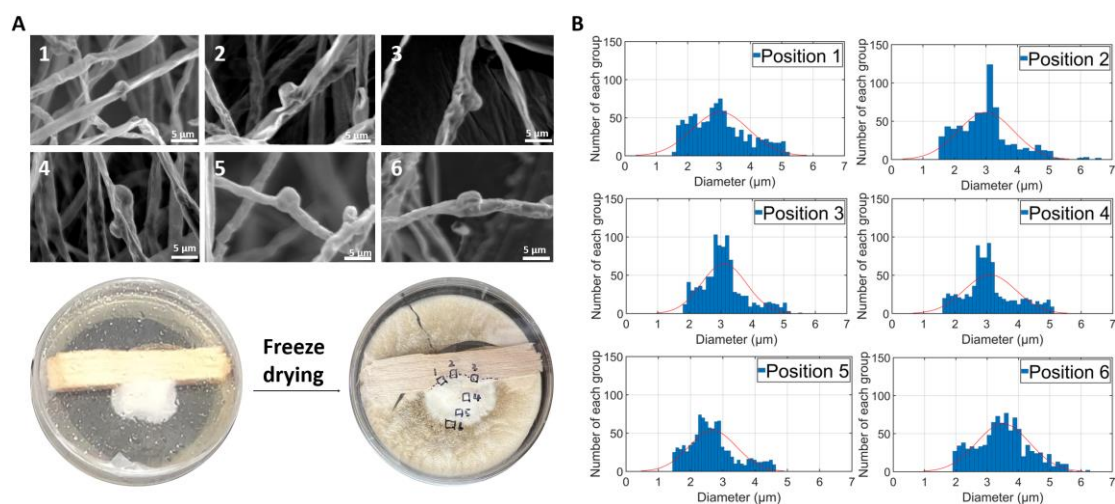


**Figure 3-5.** A. Picture of dried petri dish before and after taking the samples and SEM pictures for 6 different positions B. Diameter measurement histograms for each position.

**Table 3- 2.** The mean and standard deviation of the histogram curve fitting for 6 different positions.

Position number	$\mu$ ( $\mu\text{m}$ )	$\sigma$ ( $\mu\text{m}$ )
1 (wood)	3.05	0.90
2 (wood)	3.00	0.88
3 (wood)	3.1	0.71
4 (agar)	3.11	0.82
5 (agar)	2.68	0.74
6 (agar)	3.51	0.85

It is intriguing to discuss how the diameter of the mycelium fiber is affected by the substrate type. As the literature shows, some research chose cellulose-potato dextrose broth (PDB) as the substrate for growing *P. ostreatus*. The authors suggest that the failure of *P. ostreatus* filaments grown on PDB-cellulose substrate is likely due to a loss of internal hydrostatic

pressure, reflected in the filaments' reduced width [23]. Here we separate other diameter data into two groups; group 1 is the mycelium grown on the wood, and group 2 is the mycelium grown on the agar plate. We obtain the mean and standard deviation of the fiber diameter of the two groups as shown in **Figure 3-6**, which shows that the two groups' medians are almost identical, around 3  $\mu\text{m}$ . Since the normal distribution analysis results cannot distinguish the diameter difference between the mycelium growth on the wood and agar plate, we use Analysis of variance (ANOVA) to test the difference between two or more means which can let us know better how different substrates will affect the mycelium diameter [197]. We obtain a P value of 0.1301 by comparing the mean value of these two groups by performing multiple comparison tests to determine which group differs from the others in terms of mean diameter [198]. Based on our setup of the mycelium growth on the wood and agar plate, the two groups diameter are equivalent. To ensure this conclusion is applicable to other mycelium species, we perform test and measure the diameter of mycelium grown alone on agar plates and hardwood, as shown in **Figure 3-7**. We migrate the *Pleurotus eryngii* mycelium on the agar plate on a new agar plate and the hardwood separately. **Figure 3-7 A** shows the samples after the freeze drying for SEM imaging. Once we have the images, we use Image J to measure the diameter about 1000 times. **Figure 3-7 B** shows the diameter measurement histograms for the mycelium on the agar and hardwood. We used normal distribution curve fitting to determine the mean diameter value for the results to study the diameter distribution, as shown in **Table 3-3**. It is clearly shown that mycelium from the wood and the agar plate has a roughly similar average diameter value of about 3  $\mu\text{m}$ . We employed the ANOVA to compare two or more means to understand better how different

substrates may impact the mycelium diameter as shown in **Figure 3-7 C**. By comparing the means of these two groups on several occasions, we arrive at a P value of 0.266 Based on our setup of the mycelium growth on the wood and agar plate, the two groups' diameters are equivalent. So, to compare the results from the two experiments, the agar plate and hardwood we used cannot affect the mycelium fiber diameter. Moreover, even if we put the two substrates together to cultivate the mycelium, the substrates still do not affect the diameter.

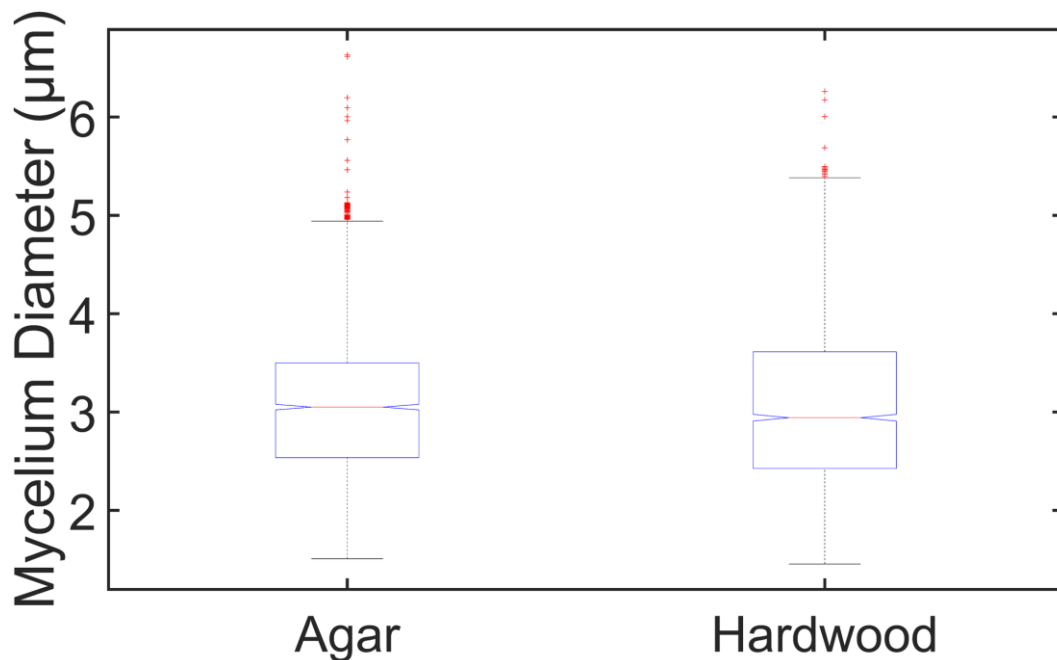


**Figure 3-6.** Distribution of two groups data (diameter of mycelium fiber on agar versus wood surface), the ANOVA test suggests that the mycelium diameters of the two groups are equivalent.

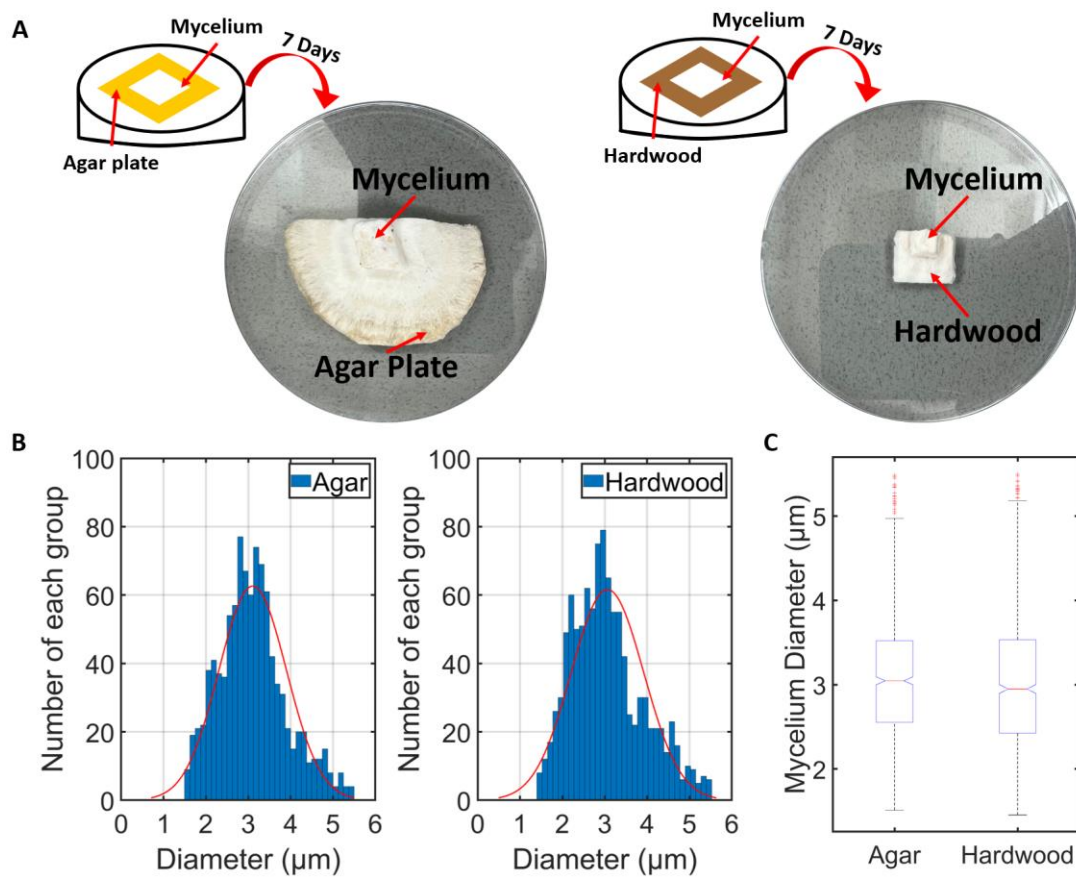


**Figure 3-7. A.** The freeze-dryer sample of mycelium grown alone on agar plates and hardwood. **B.** Diameter measurement histograms for each sample. **C.** Distribution of two groups of data (diameter of mycelium fiber on agar versus wood surface)

**Table 3- 3.** The mean and standard deviation of the histogram curve fitting for mycelium growth on the agar and hardwood.

	$\mu$ ( $\mu\text{m}$ )	$\sigma$ ( $\mu\text{m}$ )
<b>Agar</b>	3.11	0.79
<b>Hardwood</b>	3.06	0.86

**CHAPTER 4. EXPLORING THE RELATIONSHIP BETWEEN AGAR  
CONCENTRATION AND MYCELIUM GROWTH RATES IN FUNGI**

## 4.1 Introduction

Mycelium is the vegetative part of the fungus that consists of a network of thin branched filaments called hyphae [17], [23], [185], [199]. It is a fundamental building block of fungal organisms and is vital to ecosystem functions. Mycelium breaks down organic matter, recycles nutrients, and contributes to soil health [23], [44], [45]. It has recently received much attention for its potential applications in various industries, with one of the most notable uses in creating sustainable and environmentally friendly products [9], [10], [11], [14]. By harnessing mycelium's ability to grow on its own constantly, innovative companies have developed mycelium-based materials such as packaging, textiles, and construction materials [9], [10], [11], [17], [23], [52]. These products offer biodegradable alternatives to traditional materials and reduce the environmental impact of waste and pollution. The number of known fungal species exceeds 150,000, although scientists estimate millions of others are yet to be discovered [95], [125]. More than 80 species of basidiomycetes (a phylum under fungi) have been used as pure mycelium sheets or composites combined with bio-based matrices such as plant biomass [200], [201]. Due to the slow production of mycelial networks (typically only a few millimeters per day), mycelium-based products require more time than synthetic polymer materials [9], [13]. Therefore, there is a need to identify fungal species and growing conditions that can rapidly establish mycelial networks to reduce manufacturing time and cost. The substrate plays a crucial role in mycelium growth, alongside species considerations. Recent studies have used softwood substrates like pine wood [95], [202], but Hoa. H, et al. found that hardwood substrates, such as acacia wood, reduce colonization time to 30 days, compared to 40 days with softer substrates under the same conditions [203], [204]. Although

pine wood is commonly used for mycelium-based bio-composites, a comprehensive analysis of mycelium growth on different substrates is lacking. Mycelium growth depends on nutrient uptake, fiber extension, and branching at the substrate tips. The substrate's physical and chemical properties significantly affect the mycelium's morphology and physiology.

Growth occurs primarily at the mycelium apical, driven by cell wall synthesis and vesicle-facilitated enzyme and material transport [205], [206]. Hyphal branching enables extensive substrate exploration and nutrient utilization. New branches near the tips perpetuate growth and branching, forming a complex network that covers the substrate [207]. This network, as hyphae, secretes enzymes to break down complex molecules into simpler compounds for energy and growth [208], [209]. Hyphae also react to environmental factors including light, nutrients, moisture, temperature, and chemical signals, influencing growth direction and behavior. Mycelium hyphae can be categorized in fungus taxonomy by generative, skeletal, and binding hyphae [11], [118]. Based on the three different hyphal types, the mycelium network can be divided into three categories which are monomitic, dimitic, and trimitic [120]. Monomitic hyphal systems, which consists only of generative hyphae, tends to produce more uniform fibers. In contrast, trimitic systems, including also skeletal and binding hyphae, can result in a broader range of fiber diameters due to thicker and more rigid skeletal hyphae and flexible generative hyphae [210]. However, the intricate structural and chemical nature of natural wood substrates, as well as mycelium hyphae, makes it challenging to isolate these environmental effects [211], [212], and it is not clear if any effect is general to different mycelium species. Compared to wood, agar is a hydrogel with the polymer extracted from

seaweed, providing a growing substrate with ideal biocompatibility and tunable mechanical stiffness from a few kPa to several MPa, aligning with the stiffness of both soft and hardwood [213], [214]. It has been widely used to culture eukaryotic cells, bacterial biofilms, and slime molds [215], [216], [217]. Once the mycelium grows, the tips will continually extend and branch, as shown in **Figure 4-1**. To observe the mycelium growth condition during their lives, we use the blue color dye to clearly visualize the *G. lucidum* mycelium that grows on the agar plate for about three days. The digital microscope image shows the mycelium branch growth, and it usually branches near the clamp connection, which forms a septum to separate the two nuclei and process the mitotic division [218]. The mycelium growth on agar substrates of different stiffnesses will show different growing trajectories. By measuring the area ( $A$ ) occupied by the mycelium as a function of time ( $T$ ), we explore how the growing speed ( $dA/dT$ ) is affected by the substrate stiffness ( $E$ ).

The growth mechanisms of eukaryotic cells, bacterial biofilms, and slime molds [215], [216], [217] seem distinct from hyphae growth and subject to different biological imperatives.

Unlike hyphae, as a fully connected network composed of a collection of fungal cells confined by cell walls, eukaryotic cells attach to a substrate as individuals through integrins, which connect the cell's internal cytoskeleton to the extracellular matrix [219]. They sense substrate stiffness and grow via proliferation and migration, with varying responses based on cell type; for example, fibroblasts and cancer stem cells typically show increased growth rates on stiffer substrates [215], [220], [221]. Similarly, as individual amoeboid cells, the slime molds adapt their growth and foraging strategies based on the substrate stiffness [222]. Slime

mold creates a network-like structure with tubular channels, enabling the distribution of nutrients and chemical signals via cytoplasmic flow, which propels the cytoplasm movement and, thus, the growth [223]. A stiffer substrate has been shown to cause a slower growth rate in this process [216]. For bacteria biofilms, it is revealed that the growth of *Serratia marcescens* increases on softer substrates, which makes it easier for the biofilms to absorb nutrients [217].

Here, we aim to use a series of agar substrates to culture mycelium and increase substrate stiffness to study the mycelium growth rate. The dynamical growth of other biological tissues suggests that their growth rates are affected by the mechanical stiffness of their substrates. However, it is unclear whether the growing rate positively or negatively correlates to substrate stiffness, which is subjected to different mechanisms of different biological tissues. There is no clear clue how substrate mechanics affect mycelium growth, which is crucial for scaling up the mycelium-based composite material synthesis from lab to industrial production. Moreover, the substrate stiffness can also govern the propagation of mechanical waves that travel along the surface. For example, the Rayleigh wave is a surface acoustic wave with its speed determined by the stiffness of the material it travels through [224], [225]. In a recent paper, the authors compare the mycelium growth rate on agar and silicone-paper-coated agar substrates with a higher stiffness than pure agar [226]. The design of the study does not allow the evaluation of the stiffness effect, as the paper on the agar plate not only changes the substrate mechanics but also impedes the mycelium from absorbing the nutrition from the agar plate [226]. Another recent study indicates that mycelium has a higher growth rate on

hard agar than soft agar [227]. However, the mechanism is not clear, and it is illusive whether the growth rate preference is consistent for different mycelium species. The clear effects of the substrate stiffness on many biological tissues and wave propagation, in contrast to its illusive effect on mycelium growth, motivates us to perform our own tests to answer the question.

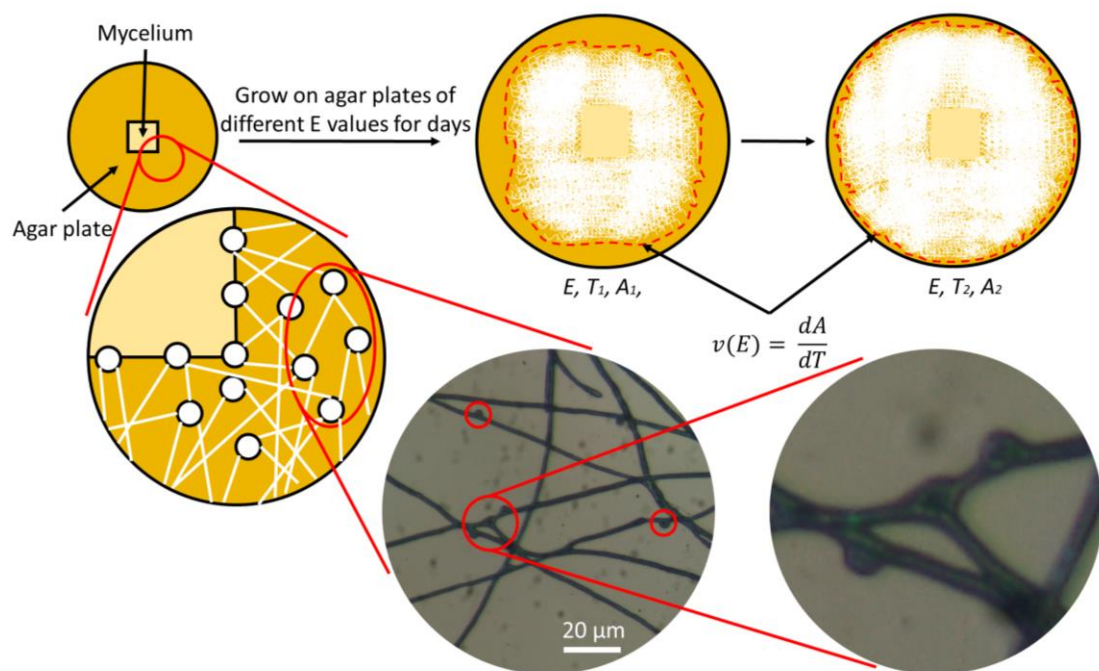


**Figure 4-1.** Mycelium growth schematic and digital microscope image. Agar substrate is prepared with different agar concentration to tune the substrate stiffness ( $E$ ). It fully covers the bottom of the petri dish. A small agar cube fully loaded with mycelium is placed at the center as the initiation point of the network. Timelapse images are taken during the growth of mycelium and analyzed to obtain the occupied area ( $A$ ) as a function of time ( $T$ ). We repeat the test on different substrates to investigate how substrate stiffness affects mycelium growth rate ( $v$ ). The right-down images are obtained from Hirox digital microscope. They show the

microstructure of *G. lucidum* mycelium after growing for three days and dyed (blue color dye) before taking the image. The clamp connection and the branching structures are circled and highlighted.

## **4.2 Experimental Method and Procedures**

### **4.2.1 Agar Plate Preparation**

To prepare the agar plate in a petri dish, we used the same nutrition concentration: 20 grams of malt extract and 2 g of yeast to combine with eight different agar concentrations of the agar powder (10, 20, 30, 32.5, 35, 37.5, 40, and 45g) mixed in 1000 ml of water. We used malt extract and yeast as both can provide nutrition, and we used agar hydrogel as a substrate because it is primarily composed of water with nutrition uniformly distributed inside, allowing the mycelium to grow on its surface. To begin making it, we boil water and add all the abovementioned ingredients into an Erlenmeyer flask. The thermal mixer keeps the mixture at a high temperature so the water can dissolve all its solutes. We then used aluminum foil to cover the Erlenmeyer flask and put it into an autoclave for sterilization at a high temperature (123 °C) and pressure (24 psi). The flask is left to sterilize for 40 minutes. When the sterilizing was finished, we took the Erlenmeyer flask to a cleanroom and waited until the temperature cooled to around 45 °C. After using 75% alcohol wipes to clean the Petri dish and glass rod, we stirred the contents of the liquid supernatant to keep the mixture liquid at the same nutrition and agar content we set for. The solution, now ready, is poured into Petri dishes and sealed with a laboratory film after cooling. At last, we put them into the refrigerator and waited to inoculate the substrate with mycelium.

#### 4.2.2 Mycelium Species and Sample Preparation

To ensure that our study is general for different mycelium species, we prepared the four species of mycelium, which are that of king oyster (*P. eryngii*), red reishi (*G. lucidum*), turkey tail (*T. versicolor*), and velvet shank (*F. velutipes*.) All the initial mycelium liquid cultures are brought from the online store, North Spore. These four species are usually used in experiments and belong to white-rot fungi [228], [229], [230], [231]. White-rot fungi are commonly used as a first choice because they degrade lignin in the cell walls of woody plants to a greater degree than they do with cellulose [95]. Another reason to select these four species is that they cover two out of the three hyphal categories: monomitic species (*P. eryngii* and *F. velutipes* [210], [232]) that is comprised of only generative hyphae and trimitic species (*G. lucidum* and *T. versicolor* [117], [233]) contain all three principal hyphae (generative, skeletal, and binding hyphae) [122]. We used the liquid culture of those four species in 20 g/L agar plates and settled them in a climate chamber, which is kept constant at 24°C and 90% humidity. Once the mycelium thoroughly colonized the Petri dish, we cut out 6 x 6 mm small samples. We put each on eight different Petri dishes of varying agar concentrations to monitor their growth.

#### 4.2.3 Time Lapse Photography Preparation

We set up a shelf in a dark room for a time-lapse and put the Petri dish on top of the rack, as shown in **Figure 4-2**. The dark space is created through light-tight curtains, which is crucial as the presence of light affects the growth of mycelium. We used transparent acrylic sheets as

the surface of the rack to allow the GoPro to take snapshots from below. The reason behind taking snapshots from below is that the top view is unclear due to the sealing films and condensation water on the lid over time. A timer controls the light and only turns on for 3 minutes in an hour to take the pictures. We set the room temperature to around 22 °C with the lab thermostat. The sealed petri dish will maintain the inner humidity to be ~100%. We used ImageJ to measure the area of the substrate occupied by the mycelium to get the growth curve. We summarized an example of the time-lapse photograph for all four species' growth on the 45g/L agar plate within 15 days, as shown in **Figure 4-3**. Generally, the *G. lucidum* and *T. versicolor* only need five to six days to occupy the petri dish fully. However, the *F. velutipes* cannot fully occupy the petri dish for fifteen days.

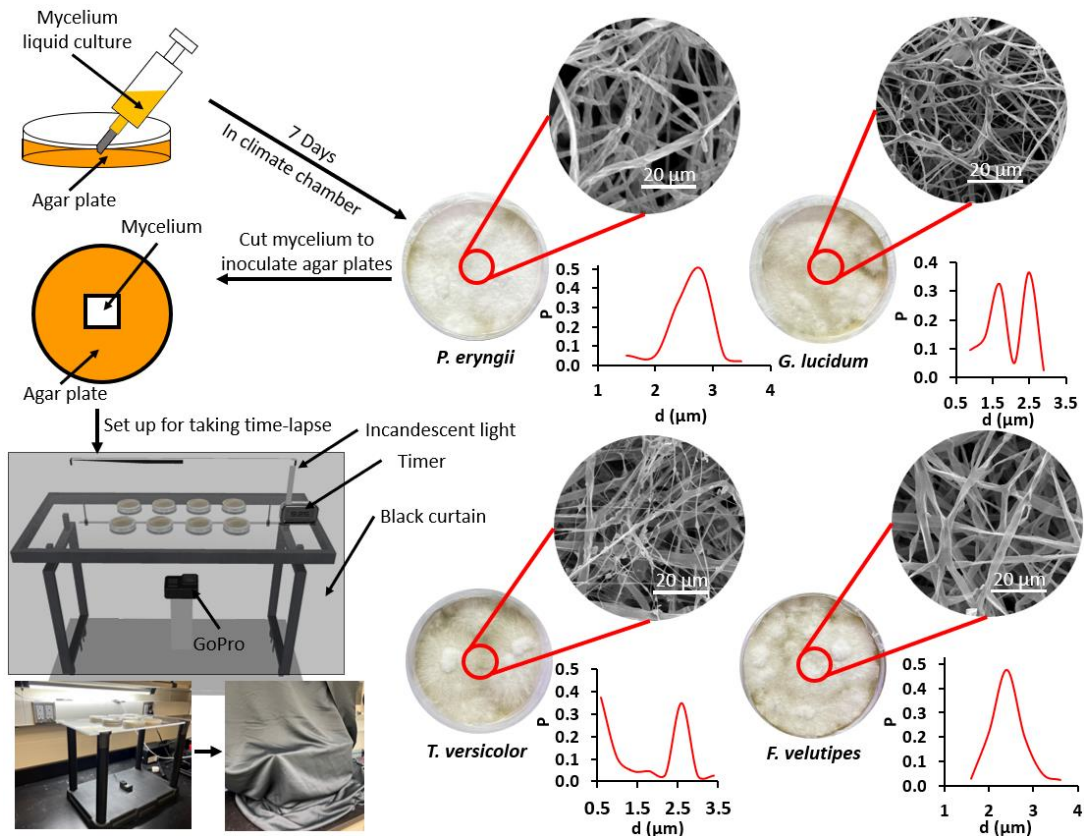


**Figure 4-2.** The general process of making the mycelium agar plate (SEM images and mycelium diameter distribution is next to each species) and setting the shelf for time-lapse photography.

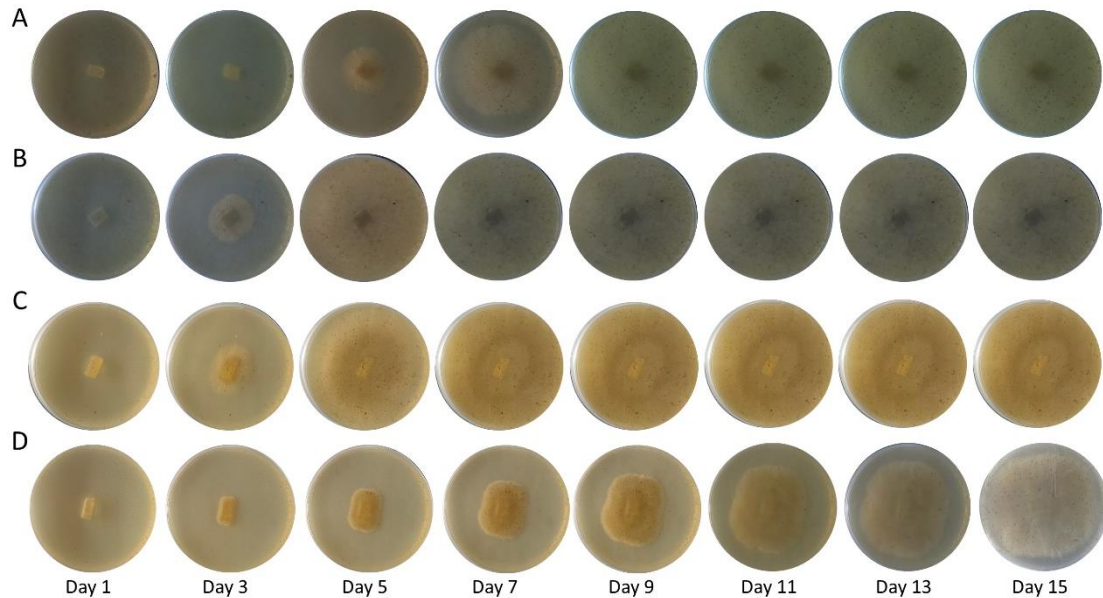


**Figure 4-3.** The time-lapse photograph for all four species' **A.** *P. eryngii* **B.** *G. lucidum* **C.** *T. versicolor* **D.** *F. velutipes* growth on the 45g/L agar plate within 15 days.

#### 4.2.4 Characterization of Agar Gel Stiffness

It is reported in the literature that the increase in agar from 10 g/L to 40 g/L increases Young's modulus by about 5 to 6 times [234]. To make the test result more reliable, we prepared 11 different types of pure agar plates of the concentration of agar, which are 10, 20, 22.5, 25, 27.5, 30, 32.5, 35, 37.5, 40, and 45 g/L. To test the material stiffness, we cut a 76.2 mm (3 inches) PVC pipe as a circular ring and stuck a same-sized round acrylic sheet on the bottom to make a 10 mm high container for the agar solution to be poured into. We created a 10 mm

diameter cylinder indenter that can be connected to the 50N load cell of the Instron 5966, as shown in **Figure 4-4A**. The agar deforms under the action of a rigid axisymmetric indenter pressed to the surface by an axial force through the indenter. Here, we use an indentation test based on a Hayes model to test the stiffness of the agar plate. We calculate the shear modulus [235] with the equation:

$$G = \frac{(1-\nu)}{4a\kappa(\nu \cdot a/h)} \cdot \frac{F}{\delta} \quad (4-1)$$

Where  $\nu$  is the Poisson ratio,  $F(N)$  is the indentation force,  $\delta(mm)$  is the indentation depth,  $a(mm)$  is the indenter radius,  $h(mm)$  is the material thickness, and  $\kappa$  is a geometry factor.

Values of  $\kappa$  for a range of  $a/h$  and  $\nu$  have been estimated by Hayes, et al [236]. In our case, we take the Poisson ratio as  $\nu=0.5$ , the same as that of incompressible water. We determined our  $\kappa$  value to be 1.947, based on Hayes's table [236]. Once we had the shear force for each sample, we can calculate the shear modulus and then use the following function to calculate Young's modulus, which is related by

$$E = 2G \cdot (1 + \nu) \quad (4-2)$$

We prepared samples and used the Instron machine to do the indentation test; the indentation test curves ( $F - \delta$ ) are summarized in **Figure 4-5**. Calculate the slope of each  $F - \delta$  curve and substitute it into **Eq. (4-1)** to get the shear modulus, then substitute the shear modulus into **Eq. (4-2)** to calculate Young's Modulus. All results are summarized in **Table 4-1** and include all the parameters used in **Eq. (4-1)** and **Eq. (4-2)**. Moreover, we summarized the average Young's modulus for 11 types of agar concentration results as shown in **Figure 4-4B**. Even though Young's modulus decreased with 35 and 37.5 g/L of the agar concentration, Young's modulus generally increased as the agar concentration increased.

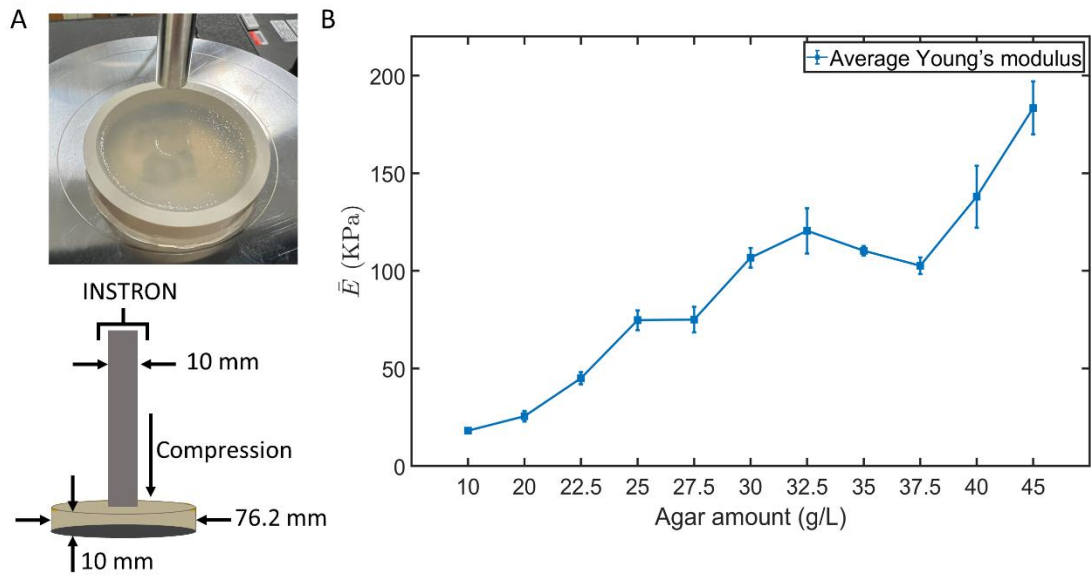


**Figure 4-4. A.** The indentation test of the agar plate is on the INSTRON machine, and the schematic drawing shows the details of the dimensions of the indenter and sample. **B.** The average Young's modulus for 11 types of agar concentration results.

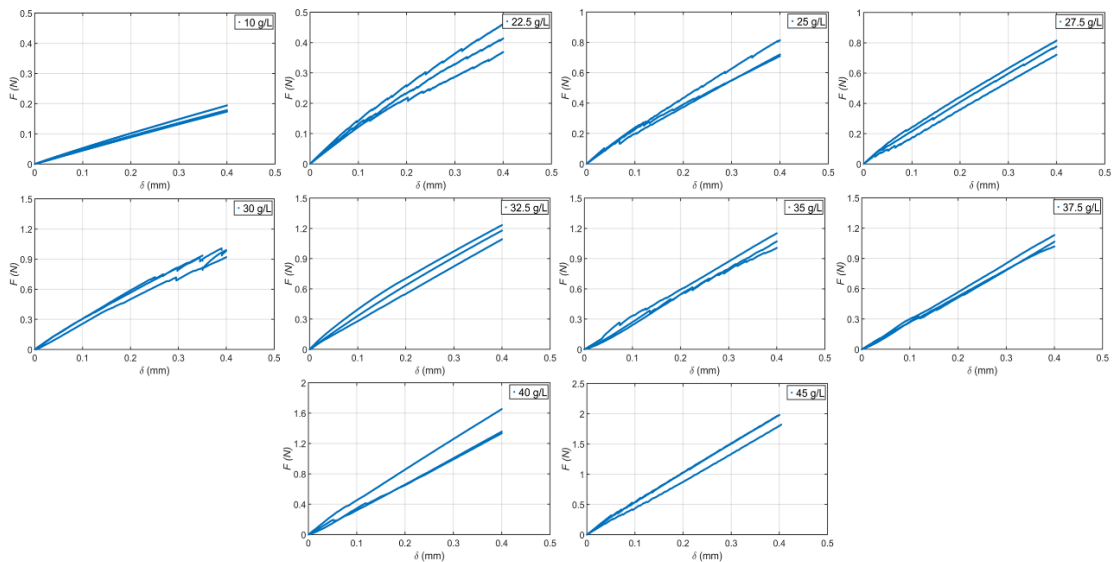


**Figure 4-5.** The indentation test curve ( $F - \delta$ ) for all the different agar concentration samples.

**Table 4- 1.** All the parameters for use to calculate the shear modulus and Young's Modulus, and the average Young's Modulus results for 11 agar concentration samples. These results were obtained by testing with a cylindrical indenter of 10 mm diameter, sample height of 10 mm and sample diameter of 76.2 mm, corresponding to the geometry factor  $\kappa=1.947$ . The Poisson's ratio of the hydrogel is assumed to be incompressible as  $\nu=0.5$ .

Agar amount (g/L)	Shear Modulus (KPa)	Young's Modulus (KPa)	Average Young's Modulus (KPa)
10	5.92	17.76	18.14
	6.50	19.50	
	5.72	17.16	
20	9.68	29.04	25.50
	7.50	22.51	
	8.31	24.93	
22.5	13.87	41.62	44.95
	14.70	44.09	
	16.38	49.14	
25	24.41	73.23	74.71
	23.12	69.37	
	27.18	81.53	
27.5	27.60	82.81	75.04
	22.27	66.82	
	25.16	75.48	

30	37.61	112.83	106.68
	35.59	106.77	
	33.48	100.44	
32.5	44.52	133.56	120.48
	40.83	122.48	
	35.13	105.39	
35	36.16	108.47	110.31
	37.89	113.67	
	36.26	108.78	
37.5	36.23	108.70	102.62
	33.27	99.82	
	33.11	99.33	
40	43.46	130.37	138.00
	41.18	123.54	
	53.36	160.09	
45	64.09	192.26	183.43
	64.59	193.77	
	54.76	164.27	

#### 4.2.5 Imaging with a Scanned Electronic Microscope (SEM)

All the samples must be dried before the coating and imaging. We use a freeze dryer and sublimate chills to -84 degrees Celsius. After freeze drying, the samples are placed on a 9 mm high and 10 mm diameter cylinder for further coating and imaging. Scanning electron

microscopy (SEM) measurements were performed using a field emission JEOL JSM-5600 (acceleration voltage, 10kV). Before imaging, the samples were coated with ca. 10 nm of gold via thermal evaporation to increase surface conductivity and, thus, image quality. To visualize the mycelium penetrating the agar substrate, we freeze-dried the sample piece before cutting through the middle of the sample. The mycelium sample is thoroughly dried to prevent it from attaching to the knife and mistakenly brought down to the interface between the agar and mycelium.

#### **4.2.6 Monte Carlo Simulation of Mycelium Growth**

Different environmental factors, such as temperature, pH, moisture, nutrient content, and concentration, can affect mycelium growth rate. Studying all the factors using the experiment is difficult since growing mycelium in laboratory conditions requires a relatively long time. Thus, developing a simulation method can be applied to run multiple repetitions and generate large amounts of data on varying input parameters that model the environment. The Monte Carlo (MC) algorithm simulates the mycelium growth on the agar plates in this study. The Monte Carlo method is a widely used computational algorithm that models the probability of different outcomes in processes involving random variables. It is a general-purpose technique applicable across various fields, including physics, engineering, and biology, and is not limited to simulating mycelium growth. **Figure 4-6** demonstrates the logic flow behind this algorithm. It simulates the random trial for the fiber extrusion and branching events, with its acceptance controlled by a Metropolis-Hastings criterion for each MC step. The simulation mimics the growth of mycelial networks and involves hyphal elongation and branching.

Apical branches, or leading hyphae, are typically responsible for colonization and nutrient acquisition, while lateral branching behind the growth front supports the exploitation of resources [237]. Input parameters of the simulation include nutrition range, nutrition amount, lattice length ( $l$ , which defines maximum extrusion length in each trial),  $k_B T$  (thermal fluctuation energy), linear stiffness  $K$  for fiber stretching, stiffness  $B$  for fiber bending, the energy given from each nutrition point  $\delta E$ , and total time steps. Before running the simulation, we initialized the conditions, including spore location and random distribution of nutrition points according to the range and density. Then, for every time step, we compute the driving energy for a fiber to grow,  $E_N = \delta E / (4\pi d^2)$  as the nutrition the fiber absorbs from the nearest nutrition point with a distance  $d$ . The nutrition of the fiber growth is given by  $E_d = \frac{1}{2} K l^2 + \frac{1}{2} B \theta^2$ , where  $\theta$  is the bending angle of the fiber during extrusion. We use **Eq. (4-3)** to determine the probability of accepting the extrusion attempt as  $p$ .

$$p = e^{-\frac{E_d(K,B,l,\theta) - E_N}{k_B T}} \quad (4-3)$$

After that, we need to determine if a fiber already takes the target spot by considering if there is an existing fiber within the cut-off distance  $d_{cut-off}$ . Having  $d_{cut-off} > l$  will prevent fibers from penetration, while  $d_{cut-off} = 0$  will allow the penetration. Moreover, for  $d < l$ , we consider that the fiber fully reaches a nutrition point and will branch at its growing point.

When we calculate the area of the growth area, first, we select the maximum and minimum point of the mycelium growth points and circle out a rectangular area for it. Then, we divided the rectangular area into 1000 rectangular regions along the x-axis to have a  $\delta x$ . To accurately calculate the whole area occupied by the mycelium, we select the maximum and minimum

points of the occupied points with each of the rectangular regions  $y_{i\_max} - y_{i\_min}$ . Then, we use  $A = \sum_{i=1}^{1000} (y_{i\_max} - y_{i\_min}) \delta x$  to compute the total mycelium growth area.

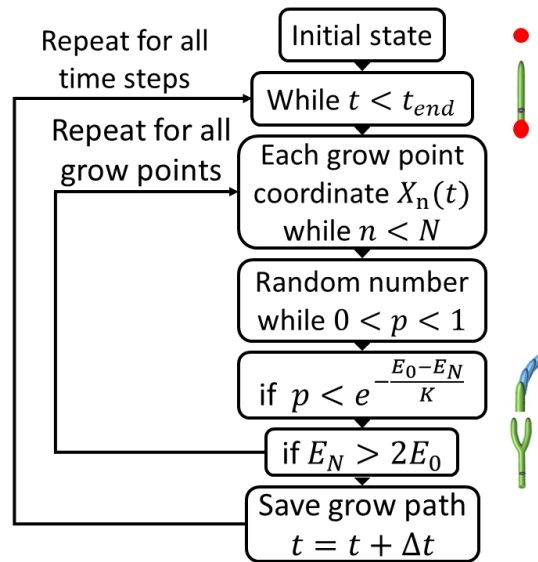


**Figure 4-6.** The flowchart of Metropolis-Hastings Monte Carlo algorithm for mycelium growth from a single point to a complex network.

### 4.3 Results and Discussion

We summarize our experimental setup as in **Figure 4-2**. Several trials have been performed before we identify the final setup of our time-lapse recording stage. We clamped the camera under the petri dish to get clear pictures despite the water condensed on the inner lid of the petri dish. We used a timer to control the light and made it only on during the picture-taking stage (1/20 of the total time) as we found that most mycelium stopped growing under the light. We used a black curtain to cover the entire experimental setup to prevent the other room light in the lab from affecting the mycelium growth. Using this general setup, we managed to monitor the growth of different mycelium species for up to 18 days, with a frame rate of 1/

hour. We found that other species exhibited different growth rates. Some fast-growing mycelium need only five days (*G. lucidum* and *T. versicolor*) to fully colonize a Petri dish, while *P. eryngii* needs ~10 days, and *F. velutipes* needs ~18 days to colonize fully. We took Scanned Electronic Microscope (SEM) images to understand if the microstructure correlates to the growth rates (**Fig. 4-2**). We find the monomitic hyphal (*P. eryngii* and *F. velutipes* [210], [232]) has a more uniform fiber diameter than the trimitic hyphal (*G. lucidum* and *T. versicolor* [117], [233]). Even though there is no direct conclusion in the literature telling which hyphal system grows faster, our results show that the trimitic hyphal grows faster than the monomitic hyphal. Different types of hyphae in trimitic systems may influence these growth processes, with generative hyphae promoting rapid growth and the addition of skeletal and binding hyphae for the resilience of the network [238].

To make the experiment more time efficient, we include multiple Petri dishes within the same batch for the growth test at the same time, as schematically shown in **Figure 4-7A**. The growth of *G. lucidum* on a substrate of 20 g/L agar concentration that corresponds to Young's modulus of  $25.5 \pm 2.7$  kPa, is given by the four representative time-lapse images as shown in **Figure 4-7B**. We can see that the mycelium fibers grow radially outwards from the initial inoculation square. For each of the time-lapse images, we measured the total area ( $A$ ) occupied by the mycelium network at different times ( $T$ ) by drawing a closed envelope curve around the agar substrate occupied by the mycelium and integrating the area of the envelope, as summarized in **Figure 4-7C**. The  $A-t$  function allows us to monitor their growth from the initial agar block until they fully colonize the Petri dish or stops growth. For this substrate, *G.*

*lucidum* requires only seven days to colonize the Petri dish fully. The growth rate is slow at the beginning, exponentially grows, hits its maximum value from Day 3 to 5, and then slows down from Day 5 to Day 7. It is reasonable as the initial growing curve is dominated by  $\frac{dA}{dt} \propto A$  as the growth rate of the mycelium is driven by the nutrition it absorbs from the occupied area, leading to an analytical exponential solution for the initial growth. At the end of the growth, the curve slows down because of the boundary confinement by the Petri dish of 80 mm diameter, which limits the maximum occupied area to 5026 mm<sup>2</sup>.

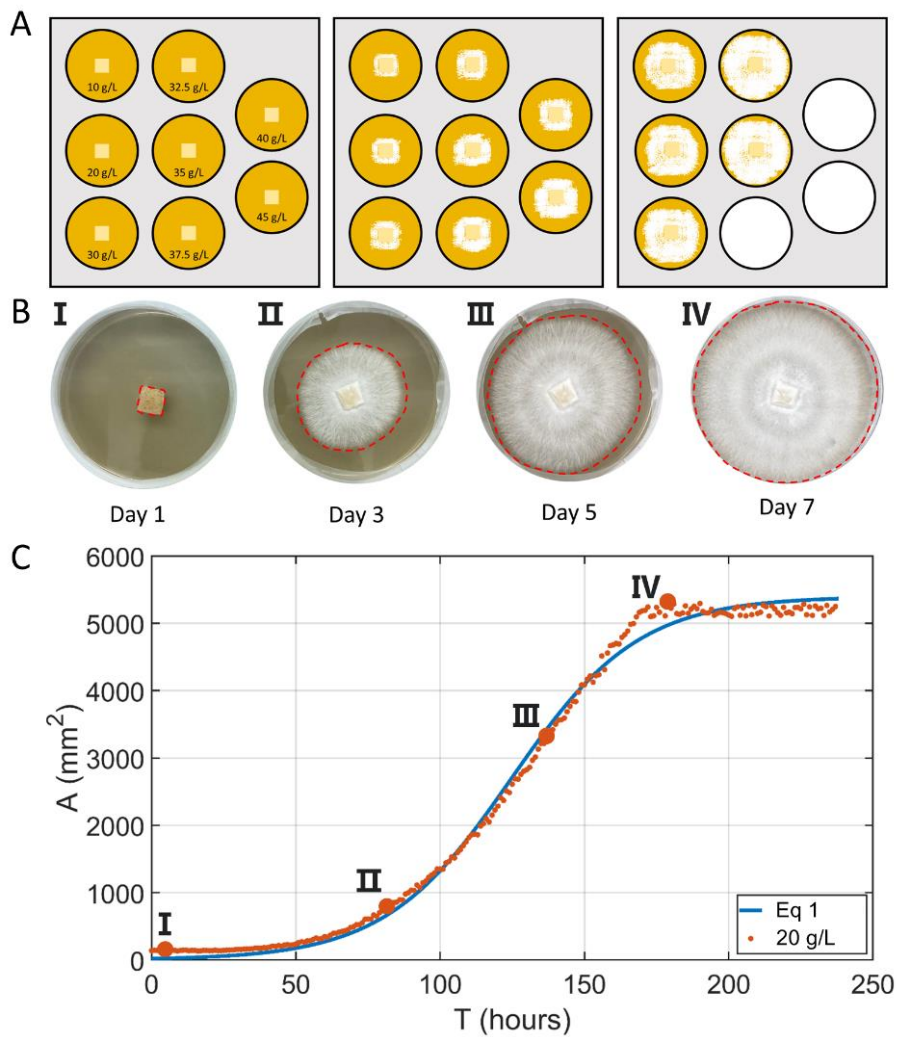


**Figure 4- 7. A.** The schematic figures of mycelium growth on different days, and the *G. lucidum* mycelium grows in the Petri dish until fully colonized. **B.** The images taken during the growth of *G. lucidum* at different time. The red dash lines are used to compute the occupied area. **C.** The growth curve (solid line) and exponential fitting curve (dotted line) of *P. eryngii* growth on the 20 g/L agar plate.

Considering both the exponential growth of  $A$  before the middle point of the curve, as well as its convergence to a limiting value for large  $T$ , we construct the following empirical function to simplify the  $A$ - $t$  relationship:

$$A = \left[ \frac{1}{e^{a\left(\frac{T-a}{T_a}\right)} + 1} \right] b \quad (4-4)$$

where  $T$ (hour) is the time of taking a frame,  $A$ (mm<sup>2</sup>) is the occupation area of the mycelium,  $T_a$ ,  $a$  and  $b$  are fitting parameters, with  $b$ (mm<sup>2</sup>) is the limiting occupation area ( $A = b$  for  $T = \infty$ ),  $T_a$ (hour) the approximate middle point of the curve ( $A = \frac{b}{2}$  when  $T = T_a$ ) and  $a$ (1/hour) the shape of the fitting curve. It is shown that **Eq. (4-4)** can be used to fit the growing curves of different species well (**Figure 4-7C** and **Figure 4-8**). Using the value of the fitted parameters, the mean growing speed is given by  $v = \frac{b}{2T_a}$  (mm<sup>2</sup>/hour).

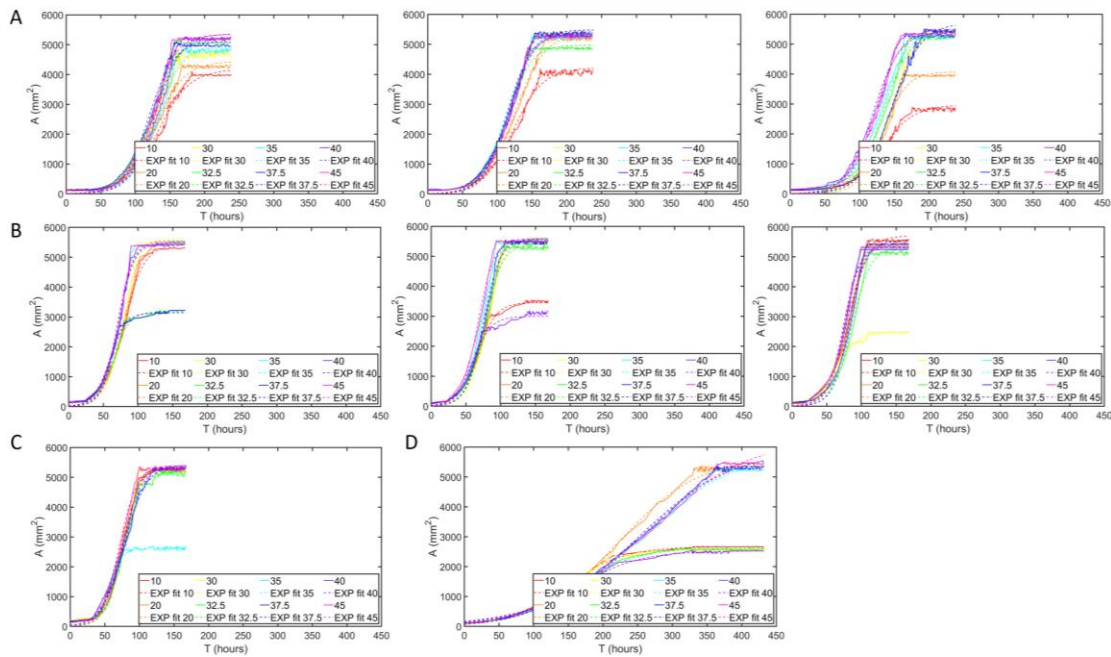


**Figure 4-8.** The growth curve (solid line) and exponential fitting curve (dotted line) of **A. *P. eryngii*** (repeating test #1, #2, #3), **B. *G. lucidum*** (repeating test #1, #2, #3), **C. *T. versicolor***, and **D. *F. velutipes***.

We repeated the tests for all the mycelium species for agar substrates of different Young's modulus ( $E$ ) that is realized by using different agar concentrations. *P. eryngii* (**Fig. 4-9A**) shows the monotonic  $\bar{v}$ - $E$  relationship, as increasing Young's modulus led to a higher mean growth rate. The other three species (*G. lucidum*, *T. versicolor*, *F. velutipes*) also showed that  $\bar{v}$  tended to increase for higher Young's modulus, but the relationship fluctuated for intermediate stiffness. For each of the four species we tested, the highest growth rate was also obtained for the substrate of the highest  $E$ . For example, the highest growth rate given by all four species is  $39.1 \pm 2.0$  mm<sup>2</sup>/hour, obtained from *G. lucidum* (**Fig.4-9B**) on the substrate of the highest  $E$ ,  $183.4 \pm 13.6$  kPa, for an agar concentration of 45 g/L. We analyze this  $\bar{v}$ - $\bar{E}$  relationship with an exponential function as

$$\bar{v} = v_{\infty} - (v_{\infty} - v_0)e^{-\frac{\bar{E}}{E_0}} \quad (4-5)$$

where  $v_{\infty}$  is the theoretical limiting growing speed at highest  $\bar{E}$  value ( $\bar{E} \rightarrow \infty$ ),  $v_0$  is the growing speed at lowest substrate stiffness  $\bar{E} = 0$ , and  $E_0$  is the critical substrate stiffness that yields 63% that of the growing speed increment from  $v_0$  to  $v_{\infty}$ . It is noted that the stiffness of an agar substrate cannot reach  $\bar{E} \rightarrow \infty$  and thus  $E_0$  provides a very useful practical value to choose optimal substrate stiffness. The fitting results, as summarized in **Figure 4-9**, show that both *P. eryngii* and *G. lucidum* faster on stiffer substrate. According to the fitting results, *P. eryngii*'s growth is greatly accelerated at  $E_0 = 11.2$  kPa, with the theoretical limiting rate of  $v_{\infty} = 21.61$  mm<sup>2</sup>/hour. *G. lucidum* is greatly accelerated at  $E_0 = 92$  MPa, with the theoretical limiting rate of  $v_{\infty} = 2045$  mm<sup>2</sup>/hour, which is two orders of magnitude higher than *P. eryngii*. Such a critical stiffness is like the stiffness of natural wood but is two orders of magnitude higher than that of our stiffest agar substrate. It needs to be cautious that such a high  $v_{\infty}$  is pure hypothetical prediction based on the low stiffness of agar substrate, as the maximum  $\bar{E}$  value in the experiments is  $183.4 \pm 13.6$  kPa. Preparing a uniform substrate on a Petri dish with a higher agar concentration was too difficult as the material becomes too thick to handle. The low  $R^2$  value of the *G. lucidum* fitting function also suggests that the stiffness given by the agar substrates for *G. lucidum* is probably far from the favorite stiffness to identify the exact fastest growth rate on surface.

Besides *G. lucidum*, *T. versicolor* (**Fig. 4-9C**) gives the second fastest growth rate for most of the samples. In contrast, the *F. velutipes* (**Fig.4-9D**) has the slowest growth rate. Moreover, to mimic the best environmental conditions for mycelium growth and observe the mycelium

growth rate, we culture the mycelium in the climate chamber (24 with 90% humidity), as shown in **Figure 4-10A**. We inoculated the *P. eryngii* and *G. lucidum* on the 20g/L agar plate in the climate chamber, which prevents us for taking the time-lapse photo and too frequent visiting. Instead, we took a daily picture to record the mycelium growth area, as shown in **Figure 4-10B**. Within seven days, two species fully occupied the petri dish and *G. lucidum* only needs five days to fully growth. Once we have all the pictures, we measure the growth area and use **Eq. (4-4)** to calculate the mycelium growth rate, as shown in **Figure 4-10C**. The results show that *G. lucidum* has a higher growth rate (36.6 mm<sup>2</sup>/hour) than that of *P. eryngii* (20.5 mm<sup>2</sup>/hour). These results obtain from well inoculation condition agree well with our results obtained from time-lapse bench tests, suggesting that our time-lapse setup provides a suitable growth environment compared to that within the climate chamber and the results are reliable.

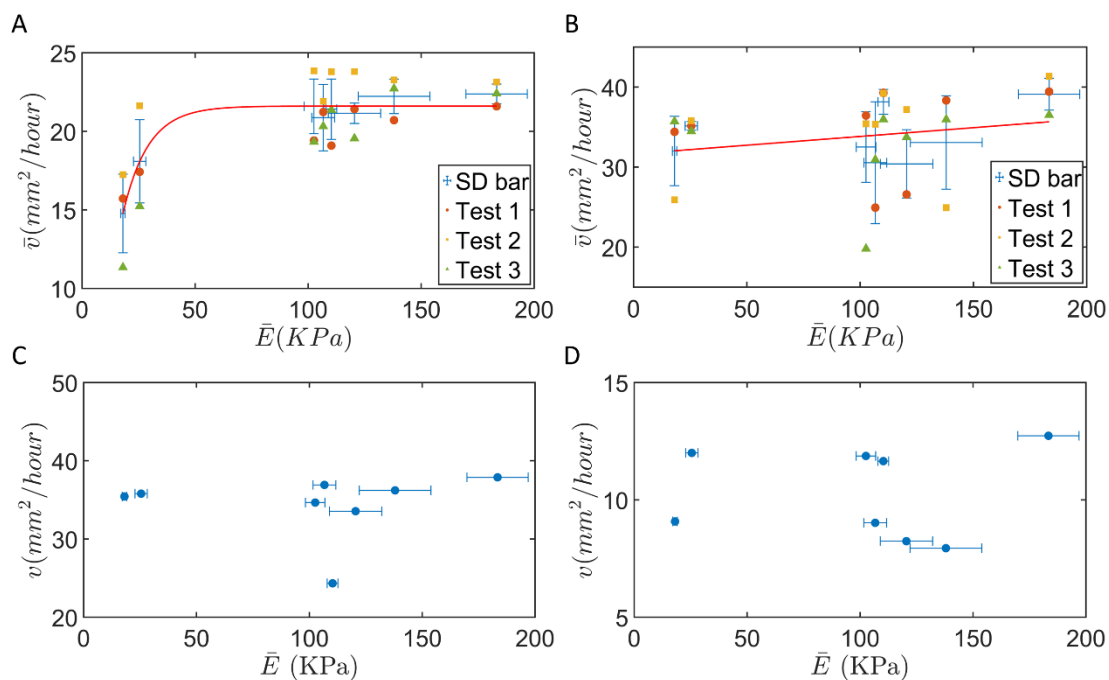


**Figure 4-9.**  $\bar{v}$ - $\bar{E}$  relationship obtained from three batches of experimental repeats for individual substrate stiffness and different mycelium species: **A.** *P. eryngii*, **B.** *G. lucidum*. Error bars are given for the standard deviation of the substrate stiffness with same agar concentration (horizontal) and the standard deviation of  $\bar{v}$  obtained from the repeating growing tests on the substrates of the same agar concentration (vertical). The exponential decaying curve fitting function is obtained for all the test results for *P. eryngii* is  $\bar{v} = 21.61 - 34.45e^{-\frac{E}{11.2}}$  ( $R^2 = 0.618$ ), and that for *G. lucidum* is  $\bar{v} = 2045 - 2013e^{-\frac{E}{92000}}$  ( $R^2 = 0.041$ ). It is noted that each data point in the plots is obtained from an individual growth experiment. (detailed growth and fitting curves are summarized in **Fig. 4-8**). The plot of the growth rate that based on the agar stiffness for the **C.** *T. versicolor* and **D.** *F. velutipes* as the comparison group.

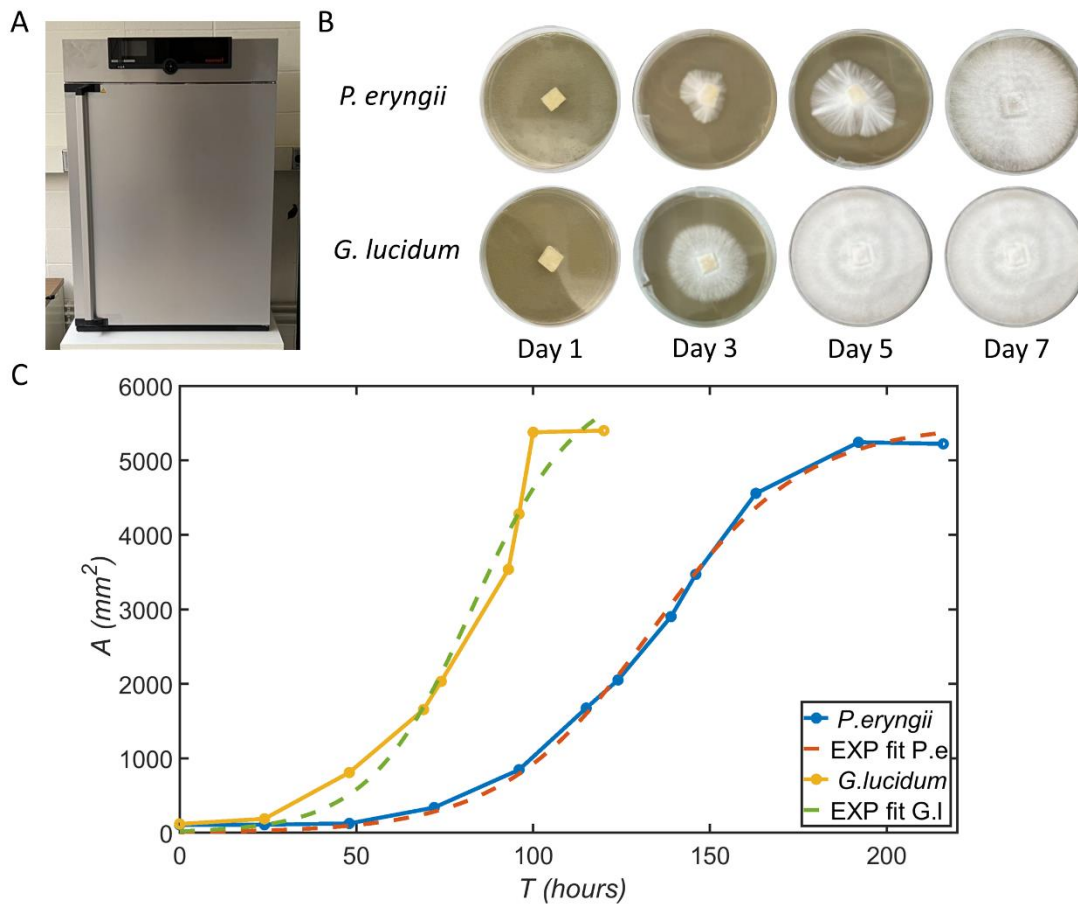


**Figure 4-10.** **A.** The HPP260ECO MEMMERT constant climate chamber is used to culture the mycelium. **B.** The *P. eryngii* and *G. lucidum* growth pictures within seven days. **C.** The growth curve (solid line) and exponential fitting curve (dotted line) of *P. eryngii* and *G. lucidum*.

Our results show that the mycelium grows faster on a stiffer substrate, which is the most important observation from our work. This observation is opposite to the growth of a biofilm by bacteria. Bacteria barely move or exhibit active movement on rigid agar plates, whereas, on soft agar plates, they actively move on their own [217], [239]. For example, *Bacillus subtilis* and *Escherichia coli* hardly move on a medium-hard substrate but quickly move on a soft one [240], [241], [242]. To investigate why mycelium grows faster on a stiffer substrate,

we cut out a small piece from the *P. eryngii* mycelium agar plate for both soft (10 g/L with  $E=18.1\pm 1.0$  Kpa) and rigid (45 g/L with  $E=183.4\pm 13.6$  kPa) agar plates. We freeze-dried these pieces for 48 hours, as shown in **Figure 4-11A**, before taking SEM images. Our SEM images show that for soft agar surfaces, the mycelium grows into the substrate by penetration from the mycelium-agar interface, which is demonstrated in **Figure 4-11B**, as the mycelium grows into the agar substrate and their fibers are identified with the unique clamp connection with the substrate. The images for growth on the rigid agar plate showed in **Figure 4-11C**, with no penetration into the substrate, and all the mycelium fibers were found to grow on the substrate surface. Therefore, on a rigid substrate, mycelium only tends to expand on the 2D plane with the growing edge defined by the periphery that is proportional to the radius ( $r$ ) of the occupied area, while the mycelium grown on the soft substrate, the growing edge is defined by the periphery of 3D semi-sphere that is proportional to  $r^2$  of the occupied area, causing the faster growth rate on the rigid substrate (**Figure 4-11D**).

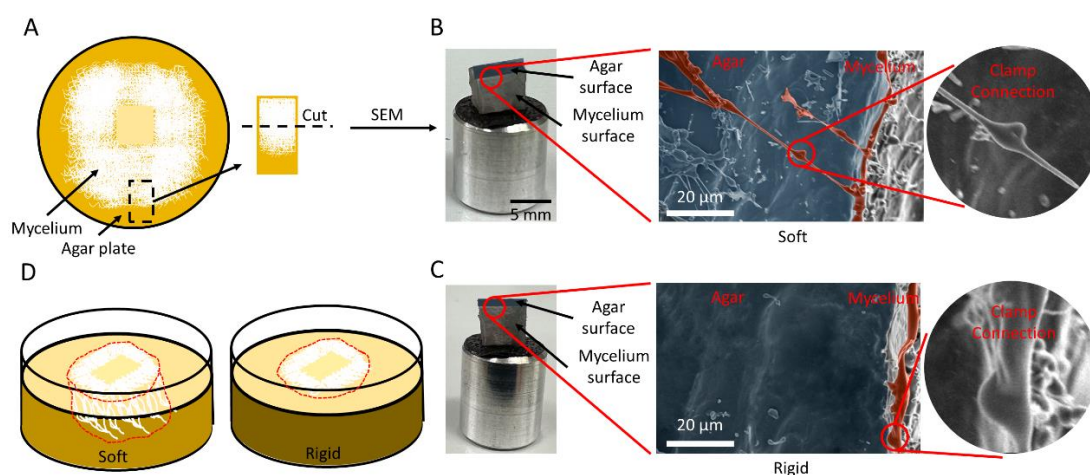


**Figure 4- 11. A.** The schematic of the sample for imaging the cross-section of the mycelium agar plate preparation for SEM. **B.** The sample of mycelium growth on the soft agar plate

with the sputter coating. The SEM shows the unique structure of the mycelium, which is a clamp connection, and the mycelium is growing vertically into the agar plate. **C.** The sample of mycelium growth on the rigid agar plate with the sputter coating. The SEM shows the unique structure of the mycelium, which is a clamp connection, and the mycelium only grows horizontally on the agar plate surface. **D.** The schematic of mycelium growth on the soft and rigid agar plate. On the soft agar plate, the mycelium growth shape is a 3D structure of a semicircle. On the rigid agar plate, the mycelium only grows a layer on the agar plate.

We develop and use a Monte Carlo (MC) algorithm on the 2D plane to simulate the mycelium growth on an agar plate, whose conditions depend on input parameters. MC simulations use random sampling and statistical modeling to estimate mathematical functions to mimic the operations of complex systems [243], [244]. It is especially suitable for simulating the mycelium growth pattern since its growth at every point is arbitrary, modeling the growth. The random growth of the mycelium network is summarized in **Figure 4-6** as the assembly of repeating hyphal elongation and branching from the initial growth point (details in the Method part). We repeat this simulation to compute the growth rate of the network by keeping all the parameters the same but adjusting the cut-off distance from lattice length ( $l$ ) to zero, tuning the random growth of the fibers from no penetration to penetration allowed between neighboring fibers. The cut-off distance within the MC simulation effectively models the stiffness of the agar. As for rigid substrates, penetration is not permitted, and all growth is restricted within the 2D surface. Still, for softer substrates, penetration of fibers is fully allowed as the fibers grow into the agar, as observed in SEM images. Using the

simulation, we find the same trend as in the experiment: when using a cut-off that prevents penetration for a rigid substrate, the growth rate is higher than the result for a soft substrate. We compute the occupied area ( $A$ ) without considering the fiber density, which is the exact definition for our experimental study. We summarize  $A$  as a function of MC step in **Figure 4-12A**. A consistently higher growth rate is seen when all movement is restricted to the substrate's surface, which prevents the fibers' penetration. Moreover, we select four representative stages of the mycelium growth of simulation and show these snapshots in **Figure 4-12B**. In the substrate with penetration, the mycelium will grow denser than the substrate without penetration, and the thicker part corresponds to the in-depth growth of the mycelium in the substrate. The inserted figures in **Figure 4-12B** clearly show how the cut-off distance significantly changes the local fiber interaction as well as the network geometry and causes the difference in  $A$  for the same number of MC steps.

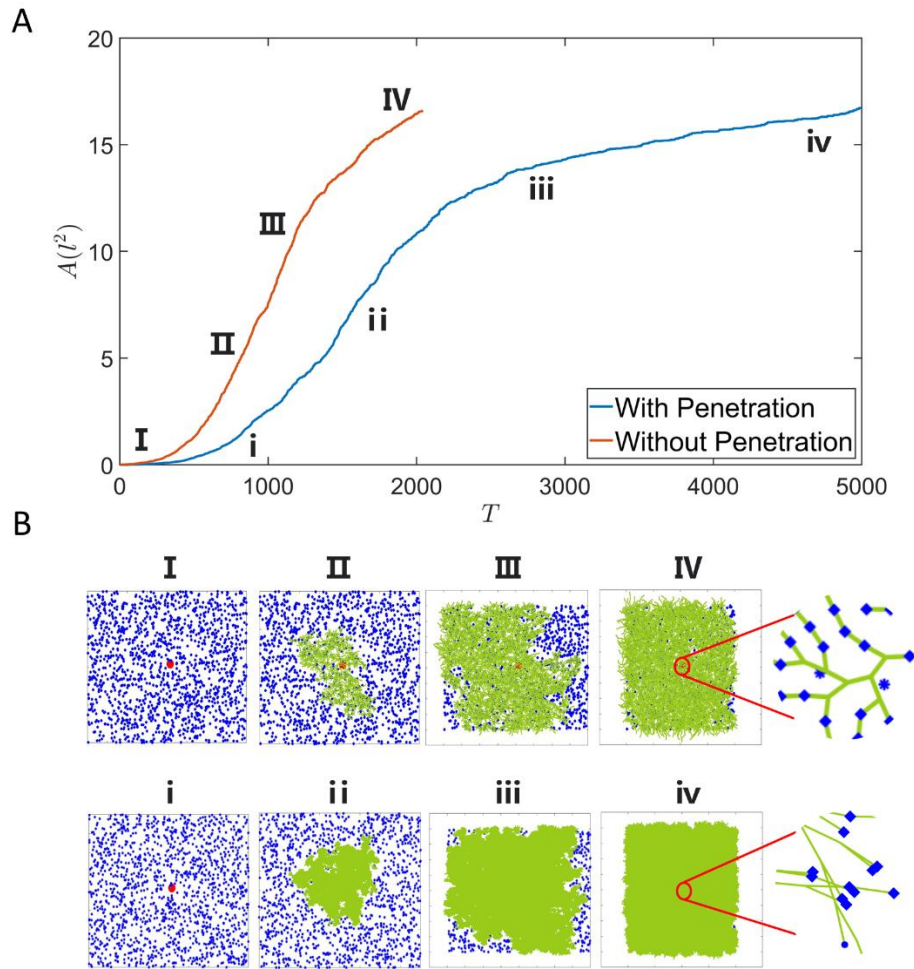


**Figure 4- 12. A.** The area-time relationship obtained from the Monte Carlo simulation of mycelium growth with (for soft substrate) and without (for rigid substrate) penetration. **B.** Simulation snapshots taken during the mycelium growth on without (I, II, III, and IV) and with (i, ii, iii, and iv) penetrating substrate as indicated on the  $A$ - $T$  curves as given in panel A. The inserted Figures show the structural difference of the mycelium grow on different substrates. The blue stars correspond to the initially randomly distributed nutrition points, the green network is for the mycelium, and the blue block is for the clamp connection within the mycelium fiber for the potential growth and branching point.

In summary, we try to keep all the other environmental factors and only vary the substrate

stiffness to investigate how it affects the mycelium growth rate. We consistently find that for all the species in our tests, mycelium grows faster on a rigid substrate than the soft one. We conclude that different mycelium species can yield very different growth rate and *G. lucidum* gives the highest growth rate out of all the test species. Moreover, *P. eryngii* exhibits the most consistent sensitivity about substrate stiffness. According to the fit curves in **Figure 4-9** and the physical meaning of the parameters as given by **Eq. (4-5)**, it is shown that the substrate stiffness above 11.2 kPa can significantly accelerate the growth of *P. eryngii*. In contrast, the growth rate of *F. velutipes* and *G. lucidum* does not significantly vary within the variation range of our agar substrates.

Using both SEM characterization and Monte Carlo simulations, we identify the mechanism behind fast growth of mycelium on a rigid substrate as it prevents the fiber from penetrating the substrate and confines the growth within a 2D surface, making the network only able to extrude from the periphery of the occupied area. Soft substrate cannot provide the necessary structural support, causing fiber penetration into the substrate and irregular growth patterns (other than radial expansion), which slow down the growth rate.

Mycelium has recently been shown to be a promising material for forming functional composites and surfaces by growing from biomass. It provides an economically efficient and environmentally friendly way to develop new materials. Its growing rate is an essential factor to consider as it can significantly accelerate composite production. Considering its geometry as a collection of branching, thread-like hyphae, its growth is complex and varies depending

on the species of fungus and the complex environmental conditions. For the millions of mycelium species in the natural world, it is challenging to determine which species of mycelium can be used to occupy a certain biomass rapidly and generate the composite material thereafter. It is, therefore, essential as we move forward to identify their growth rate in different mechanical environments. Our study of the different mycelium species, substrates, and their relationship with environmental factors can help quantify the genotype-phenotype relationship of the mycelium network, as well as the correlation between mycelium growth and composite properties within the limited amount of time, which will be essential to guarantee the scalable composite production.

**CHAPTER 5. MYCELIUM-BASED WOOD COMPOSITES FOR LIGHT WEIGHT  
AND HIGH STRENGTH BY EXPERIMENT AND MACHINE LEARNING**

## 5.1 Introduction

Wood composites are an ever-evolving product sector increasingly used in various engineering applications, and their demand has been on an upward trend for decades [245]. Wood composite is a broad term that encompasses a vast array of composites composed of wood sheets, fibers, and particles integrated via different adhesives (e.g., medium-density fiberboard [MDF] and particle board, plywood, oriented strand board, and wood polymer composites) [246], [247], [248], [249], [250]. They are often used as a substitute for natural wood for non-structural applications (e.g., fencing, decking, furniture, temporary construction, floorings, windows, and doors) [251]. The new generation of the wood composite can be multifunctional by incorporating fibers from different wood species with engineering fibers (e.g., glass, carbon, plastic) and adhesive resins [252], [253], [254], [255]. Functions beyond the natural wood can be realized during the manufacturing process by design (e.g., any thicknesses, grades, size, and exposure durability to UV, high temperature, etc.) [256], [257]. Wood fibers are the main component that contribute to the low cost of the composite material because most of them are conventionally treated as wastes, fuels, or landfills (e.g., cotton, flax, or hemp from crops, Christmas trees, landscaping, wastepaper, and agriculture byproducts or regenerated cellulose fiber [258]). These wood fibers lack intermolecular interactions that bind them to form a bulk material as hemicellulose and lignin do in natural wood [259]. Thus, the production of wood composites depends on the source and physical properties of these foreign adhesives that are added during manufacturing, which in turn affect the material functions (e.g., mechanical, thermal, chemical) and environmental impact (e.g., embodied carbon) of the composites [245], [260], [261], [262].

Synthetic wood adhesives are widely used in the wood composites industry. Still, they have disadvantages, including durability to humidity and aging in time, causing warping to wood structures, as well as long-term environmental effects, including carbon emission during material synthesis; the slow release of formaldehyde, which is hazardous to human health [263], [264], [265]; and a higher fire hazard than solid wood [256], [266]. Moreover, these synthetic adhesives are derived from non-renewable sources (e.g., petroleum and natural gas) [267], [268] that are limited by their storage. There is a growing interest in developing eco-friendly wood adhesives (e.g., lignin-, starch-, and protein-based adhesives) derived from renewable sources [262], [269]. They have a high molecular weight and are fully biocompatible and biodegradable.<sup>26</sup> Lignin is a suitable wood adhesive for its phenolic structures [269] and forms hydrogen bonds to cellulose and other desirable material features, including high hydrophobicity, a low glass transition temperature, and low polydispersity [270], [271], [272]. Its adhesion strongly depends on the molecular structure and, thus, the mechanics of the adhesive [273]. Starch is another natural adhesive that is available in most plants. It is cheap, easy to process, and forms an excellent thin film with strong adhesion. It was used for plywood manufacturing years ago [274], [275]. However, starch-based composites have poor water resistance and a slow drying rate [269]. Protein-based adhesives have high viscosity, short pot life, and high sensitivity to water, and their material functions are sensitive to the sequence. Although it is possible to predict the protein structure from its sequence with machine learning algorithms [276], its adhesion function at a large scale is still far from the molecular structure, making it elusive what key protein sequences are optimized

for wood adhesion [269], [277], [278].

Mycelium, another adhesive for wood composites, has attracted broad industrial interest in recent years [28], [279], [280], [281], [282]. Mycelium is the vegetative part of a fast-growing, regenerable fungus, consisting of a network of fine white filaments of 1–30  $\mu\text{m}$  diameter [185]. It grows in the form of numerous branching fibers, attaching itself to the medium in which it grows [283]. The medium can be agricultural waste or any other material capable of providing nutrients for growth, such as wood, straws, husks, chaws, and bagasse of the mycelium [29], [50], [117]. The mycelium multiplies and produces numerous self-assembled bonds in the form of tiny fibers called hyphae, which cover the entire loose substrate and digest the substrate during its growth, binding it into a strong and natural composite [23], [35], [39]. Mycelium-based biocomposites have similar strength to expanded polystyrene (EPS) and are biodegradable [33], [36]. Various properties of mycelium-based composites make it useful for different applications such as thermal and acoustic insulation [10], [12], [38].

Here, we explore an efficient way to produce a mycelium-based wood composite with outstanding mechanical properties. **Figure 5-1** shows the general structure of mycelium from microstructure to macroscale. Our results of the tensile test show that the mycelium-based sample has a higher ultimate strength. Moreover, our machine learning model provides a more reliable range of treatment conditions that can guide the wood composite synthesis for a specific mechanical function. Our study sheds light on developing new wood composites

made of mycelium instead of polymer adhesives, leading to environmentally friendly materials for wide engineering applications.

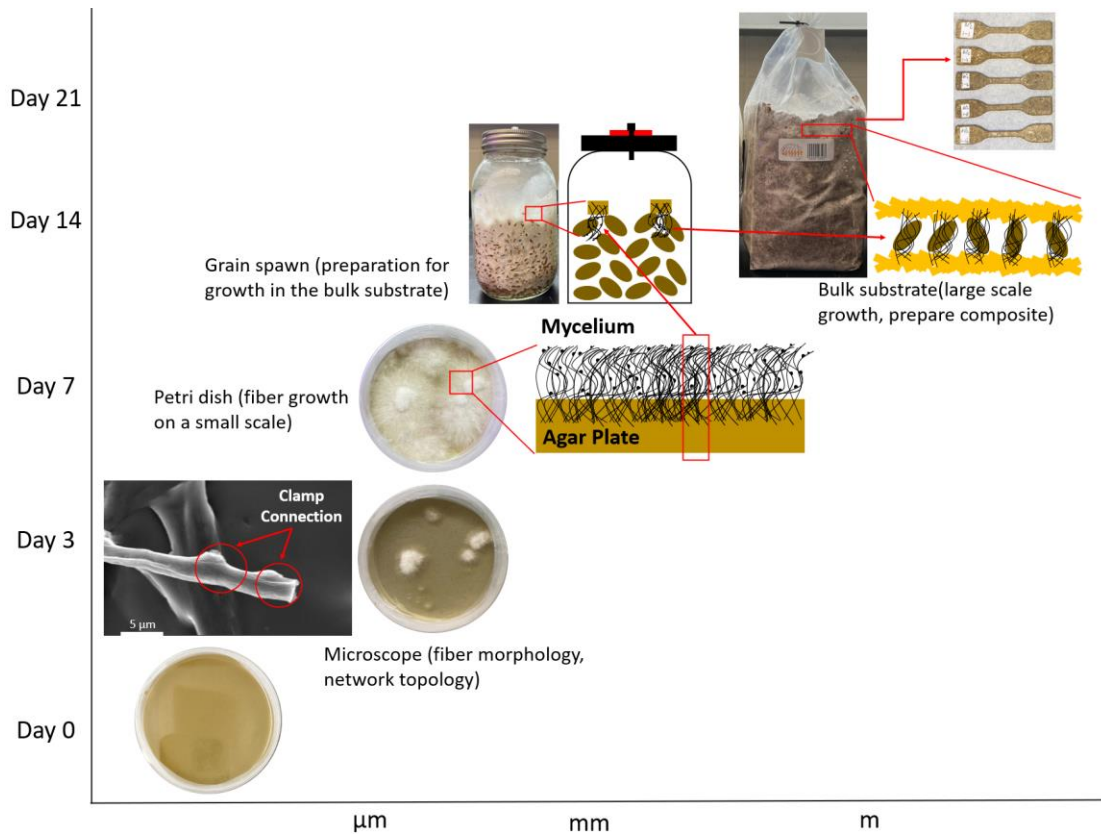


**Figure 5-1.** Multiscale structure of the mycelium in our study. From the bottom left, the figure shows the SEM image of the mycelium network and mycelium's unique structure (i.e., thin straight fiber with clamp connection), as well as the two figures of the wet mycelium sample's growth on day 3 and day 7 in the culturing disk. The schematics show the general process of preparation, including growth of mycelium in petri dish, jars, move the incubated mycelium on the rye from the jar to the larger substrate and heat press for samples for mechanical tests.

## 5.2 Experimental Method and Procedures

### 5.2.1 The General Information of Experiment

The general process of our experiment is that we grow the mycelium of *P. eryngii* on stalk (S) particles and fibers. We use a heat press to turn the mixture of the mycelium and growing medium into mechanical samples in different processing conditions and characterize their mechanical functions. We use machine learning, enabled by an artificial neural network, to build a model based on the experimental data that predicts the key mechanical features of the composite for different treatment conditions.

### 5.2.2 Preparation of Mechanical Samples

We first culture the spore on agar substrate for 7 days before cutting them into small pieces and mixing them with the grains in jars for another 7 days until the white fibers occupy most of the space in the jar. We then migrate the grains with the mycelium to the culture bag filled with the stalk (S) substrate (weight ratio 1:5; **Figure 5-2**). We keep the culture bag at room temperature (around 25°C) and use the ultrasonic humidifier to generate water mist to keep the growth environment at high humidity (relatively 98%) for 14 days (abbrev. SM). For control, we prepare a substrate material by mixing pure Ss with wet gains with the same weight ratio (5:1) and allow them to rest in the growing environment for 7 days to obtain the combination without mycelium fibers (abbrev. S). For the hardwood mixed with coffee grounds and mycelium (abbrev. HCM), we also culture the kit for 7 days in the same high humidity condition.

To ascertain whether mycelium can or cannot improve the material's mechanical properties, we prepare three different materials for the tensile test: S, SM, and HCM. **Figure 5-2 B** shows the three different materials. We use these three different raw materials for mechanical tests. We take ~200 g raw materials each time into a blender, add 200 g water, and blend the mixture until it becomes mushy. Next, we place a portion of the mixture in an aluminum dog bone-shaped mold and compress the upper layer of the mold against the bottom layer by using a 10-ton heat-press machine with the hydraulic hand pump, as shown in **Figure 5-3 A**, to perform the heat press and make the dog bone samples. The remaining mixture is stored in a sterilized plastic box in the refrigerator to keep it at a lower temperature before the heat press.



**Figure 5-2. A.** Mold design drawing (left) and model(right) **B.** Three different materials: stalk (S), stalk with mycelium (SM), and hardwood mixed with coffee grounds with mycelium (HCM) (from left to right.)

### 5.2.3 Mold Design

We design a two-part mold to make the mycelium-based bio composite sample of a type IV dog bone-shape according to the ASTM D638 standard. The sample has a shoulder at each end and a gauge section, which causes a stress concentration to occur in the middle when the sample is loaded with a tensile force. **Figure 5-2 A** shows the aluminum mold, including the top and bottom parts, which are all aluminum. For the top part, the length of the dog bone shape is 114 mm, the width at the two ends is 18 mm, and the width of the narrow part in the middle is 5 mm. The effective pressure area of the top part is  $1,370.11 \text{ mm}^2$ . We design the corners and the connecting parts into a curved transition because of the mechanical requirements. To make it easy to remove the upper part after heat press, the length and width of the bottom groove part are all longer than the top part, about 1.7 mm. We polish the side of the top of the dog bone-shaped mold about  $1^\circ$  from top to bottom. We also open four holes at the bottom part and make an aluminum plate that could be put into the bottom part. To prevent the mycelium-based material adhesive from sticking to the top part of the aluminum plate after the high-temperature baking, we cut aluminum foil in the dog bone shape and place it inside the mold before placing the materials.

## 5.2.4 Heat-Press Procedure

The press machine connected with the proportional-integral-derivative (PID) temperature controller box allows us to set different temperatures (**Figure 5-3 A**). We select three different temperatures for each material (i.e., 80°C, 90°C, and 100°C) and three different applied press forces, which are 1, 2, and 3 metric tons. We convert the applied force to the pressure on the sample with

$$\sigma_{press} = \frac{F_{plate}}{A} \quad (5-1)$$

Where  $\sigma_{press}$  and  $F_{plate}$  are the normal stress and force applied on the top surface of the sample, respectively,  $A = 13.68 \text{ cm}^2$  is the area of top surface of the dog-bone sample. The three applied pressure lead to pressure of 6.75, 13.51 and 20.27 MPa, respectively. For each sample, we set the targeting temperature first. When the temperature reaches the one designated, we put the mold with material on the bottom plate of the machine and begin to apply the pressure. We use the paper towel to wipe off excess water squeezed out after applying the target load. We allow the machine to bake the sample until the time that we are setting and then take the mold off the machine. Usually, the press machine will drop the pressure automatically, so we need to apply the pressure so that the machine will stay at the aim load that we set. For each material (i.e., S, SM and HCM), we have three different temperatures combined with three different pressures for each material. We set the five baking times for each combination: 1, 2, 4, 8, and 16 hours. We have prepared 45 samples for each material for mechanical tests.

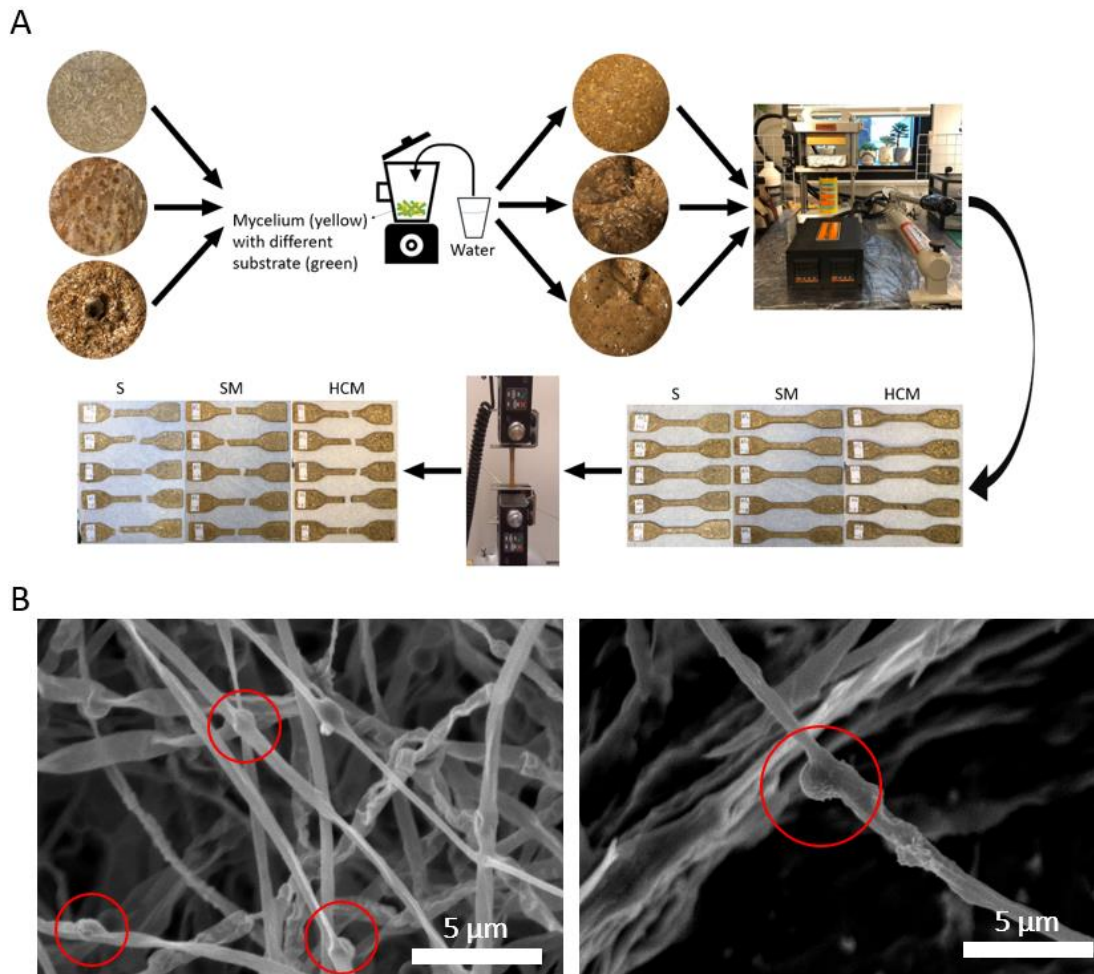


**Figure 5-3.** Processing of mycelium-based wood composites and their microstructural features. **A.** The general process of the experiment. The dog bone samples shown in the Figure are made with three different materials based on the 80 centigrade and 6.75 MPa pressure combined with five different baking times, which are 1 hour, 2 hours, 4 hours, 8 hours, and 16 hours. (material → mix with water → mushy material → heat press machine → test samples → Instron machine → broken samples) **B.** The SEM image of mycelium-based bio-composite material at room temperature dried for a month (left) and after the heat-pressing of 90 °C, baking time 16 hours, and 20.27 MPa pressure (right).

### 5.2.5 Tensile Test and Density Measurement

We perform the tensile tests on each dog-bone sample with an Instron 5966 machine (10 kN static load cell, 1 kN pneumatic grips with 90 psi (0.62MPa) holding pressure) to obtain its stress-strain curves in tension. We measure the initial sample length as the distance between the edges of the two grips as  $L_0$  before the test. The lower grips are fixed, and the upper grips move at a constant displacement speed of  $v = 0.5 \text{ mm/min}$  during our tests. The traveling distance of the upper grips is given by  $d$  at any time after the test starts, updated for every 0.02 seconds, and the engineering strain of the sample is defined by  $\varepsilon = \frac{d}{L_0}$ . The load cell records the loading force  $f$  and computes the engineering stress with  $\sigma = \frac{f}{A_0}$ , where  $A_0$  is the initial middle part cross-section area of the testing region of the dog bone sample. The test automatically stops when the sample is broken. We use the  $\varepsilon - \sigma$  data from  $\varepsilon = 0$  to  $\varepsilon = 0.001$  to perform the linear fitting and measure the slope of the fitting curve to calculate Young's modulus. We measure the maximum stress of the entire  $\varepsilon - \sigma$  curve as the ultimate stress. We measure the area under the entire stress-strain curve to obtain the toughness modulus. We measure the total weight of the sample  $m$  and use the equation  $\rho = \frac{m}{A\bar{t}}$  to calculate the sample density, where  $A$  is the area of each sample and  $\bar{t}$  is the average sample thickness which is taken by a micrometer for several times at different places for average.

### 5.2.6 K-means Clustering before Machine Learning

Due to the limited number of tests ( $N=135$ ) and randomness in the experiment, we could not directly predict the numeric values of all the specific mechanical properties with a high accuracy. We categorize the test samples for each of their material properties (i.e.,  $\rho$ ,  $\sigma_U$ ,  $E$ ,

$U_T$ ) into five levels (scale 0 to 4) by using K-means [284], [285], [286], [287]. K-means clustering is an algorithm to cluster objects based on certain attributes into a pre-determined number (K) of clusters. The grouping is done by minimizing the sum of squares of distances between individual data and the corresponding cluster center, calculated by averaging all the data within the cluster. It is an iterative procedure that refines the groupings in multiple steps, each improving the cluster quality [288]. We use the squared Euclidean distances to calculate the distance between each data point to the cluster center. By multiple iterative to get the relatively good cluster. Moreover, since the number of our experiment results is only 135, to avoid uneven grouping, we set a minimum of 25 data in a group, allowing each group to have the similar amount of data. We build a tri-layered neural network model with a uniform layer size for each layer, as the number of hidden neurons, to find the correlation between the processing conditions and a material property. Using 70% for training and 30% for testing, we adjust the layer size from 10 to 100 to obtain a highest testing accuracy without significantly overfitting. We end up with layer sizes of 100, 10, 40, 10 for models in predicting  $\sigma_U$ ,  $E$ ,  $U_T$ , respectively.

### **5.2.7 K-means Clustering for Scanning the Promising Processing Conditions**

After massively predicting and compute the  $\sigma_U/\rho$ ,  $E/\rho$ ,  $U_T/\rho$  values for the 100,000 sets of feasible processing conditions, we normalize the processing conditions and the predicted specific mechanical properties by computing the standardizing values (z-scores) for each dimension and use them to categorize the different processing conditions and a specific mechanical property (for same skewness and kurtosis [289], [290], [291]). We increase the

number of clusters ( $k$ ) to determine when the mean value of the cluster that correspond to the highest specific mechanical property converges to a constant level. It is shown in **Figure 5-4** that  $k = 49$  yields the convergence for all specific mechanical properties for different raw materials. We use  $k = 49$  to filter out the cluster of the highest specific mechanics values and highlight these data points.

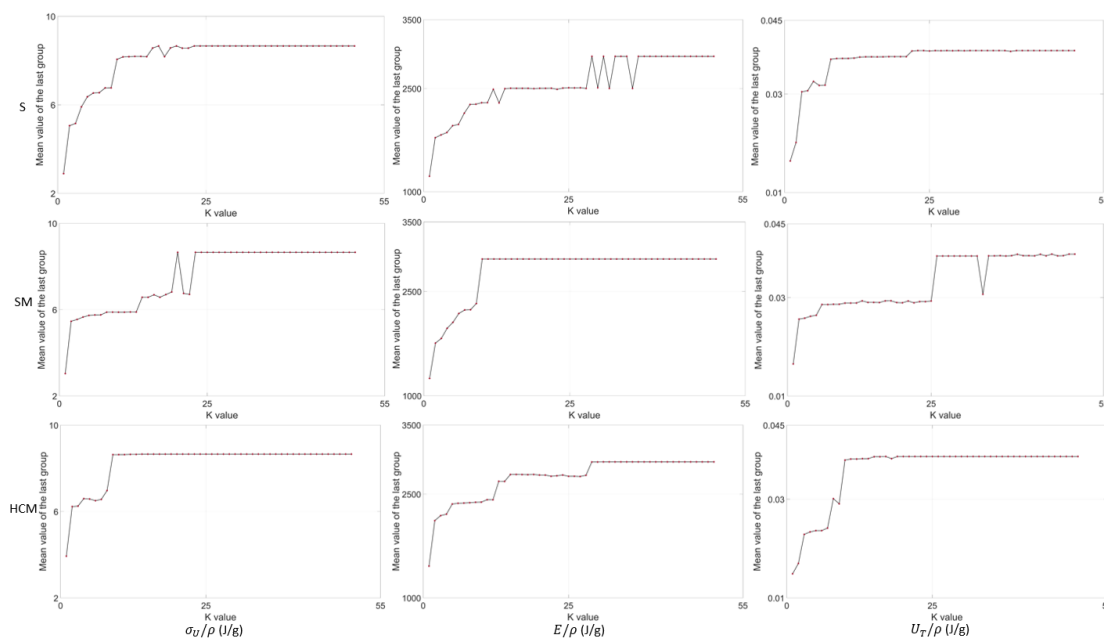


**Figure 5-4.** The last cluster's mean value which based on the different  $k$  values. Stalk (S); Stalk with mycelium (SM); Hardwood with coffee grounds with mycelium (HCM).

### 5.3 Result and Discussion

#### 5.3.1 Wood Composites Samples from Different Substrates

To investigate how mycelium can be used as a general adhesive for different wood-based substrates, we prepared three other substrate materials to make mechanical samples. To innovate the mushroom species that use in the existing experiment. We use *P. eryngii* known

as king oyster. It is not only because spores grow the mycelium, are easy to grow, and have high yield but also because it is the same genus as the *Pleurotus ostreatus* [185], [292]. The *P. ostreatus* is the most common species used in the experiment [95]. Ensuring the success of an experiment can be achieved by using fungi belonging to the same genus. The number of known fungal species alone exceeds 150,000, and scientists estimate that several million additional species could be yet to be discovered [125]. This vast diversity of fungi highlights the need for a systematic approach to experimental design, with careful consideration given to the selection of appropriate fungal strains. Choosing other species from the *Pleurotus* genus can avoid performing the same experiment with other researchers. Moreover, the *P. eryngii* has been used to develop fungus-based aerogels for green thermal insulation materials, thermal management materials for electrical devices, durable acoustic materials, pollution adsorption materials, etc [293]. Therefore, *P. eryngii* is a suitable undeveloped species that can be applied to our experiments. The S and SM are prepared by us. For comparison, we use the commercial mushroom grow kit [294], a mixture of wheat bran, hardwood saw dust (fruit wood), spent coffee grounds and other agriculture wastes for growing substrate and *P. eryngii* mycelium.

We used these three different raw materials and converted them into mechanical samples for testing. **Figure 5-3 A** summarizes the key steps: we mix each of the raw materials (i.e., S, SM, HCM) with water by using a blender until the material becomes uniform sludge, transferring the sludge to a dog-bone sample mold and turning the sludge to solid dog bone samples with a ten-ton heat-press machine. We vary the processing temperatures (i.e., 80, 90, 100 °C),

pressures (i.e., 6.7, 14.3, 20.3 MPa), and baking times (1, 2, 4, 8, and 16 hours) for producing the samples. We have 135 samples, with 45 samples for each raw material for mechanical tests, as illustrated by **Figure 5-3 A**. With this processing method, we obtained solid wood composite samples with densities varying 0.8587 to 1.55 g/cm<sup>3</sup>. It is noted that although the control group (S) lacks mycelium, the starch in the grains can still bind the stalk fibers together to form the solid material.

We compare the microscopic image of the mycelium sample in free air drying (~30 days) and heat-pressing conditions. All mycelium fibers become flat strips, and the clamp connection is buckled by losing its rounded shape in air drying. In contrast, the mycelium fibers are still cylindrical with the smoothly rounded clamp connection at the middle after heat-press (i.e., SM, 90 °C, 20.27 MPa, 16 hours), as shown in **Figure 5-3 B**. The flat fiber and the buckled clamp connection suggest that each mycelium fiber is a hollow tube filled with water with its cross-section profile supported by internal moisture. Losing the water leads to a mechanically buckled shape. The intact mycelium shape of the heat-press sample suggests that the tens of hours of baking at 90 °C is insufficient to empty the water within the mycelium fiber fully; therefore, its profile is intact even under much higher pressure than the atmosphere.

### **5.3.2 Mechanics of Mycelium-Based Composites**

We measure the bulk density and perform the tensile test on each sample with an Instron machine to understand the effects of mycelium and treatment conditions on the mechanical properties of the composite materials. **Figure 5-5** summarizes the stress-strain curves of

mechanical samples made of the three different raw materials, different pressure, and baking time under 90 °C (other loading curves for baking under 80 and 100 °C summarized in **Figure 5-6**). It is shown that all the mechanical samples reach the ultimate tensile strength ( $\sigma_U$ ), as the maximum stress, before the 1% strain, followed by a tail that accounts for energy dissipation during the failure. For SM samples, it is shown that most of the ultimate tensile strength increases with the baking time of up to 8 hours as more water is evaporated, leading to a more compact solid material in pressing. On the other hand, a baking time longer than 8 hours yield weaker samples, as the long heat press can break the mycelium fiber into small pieces, as shown by microscopic images in **Figure 5-7**.

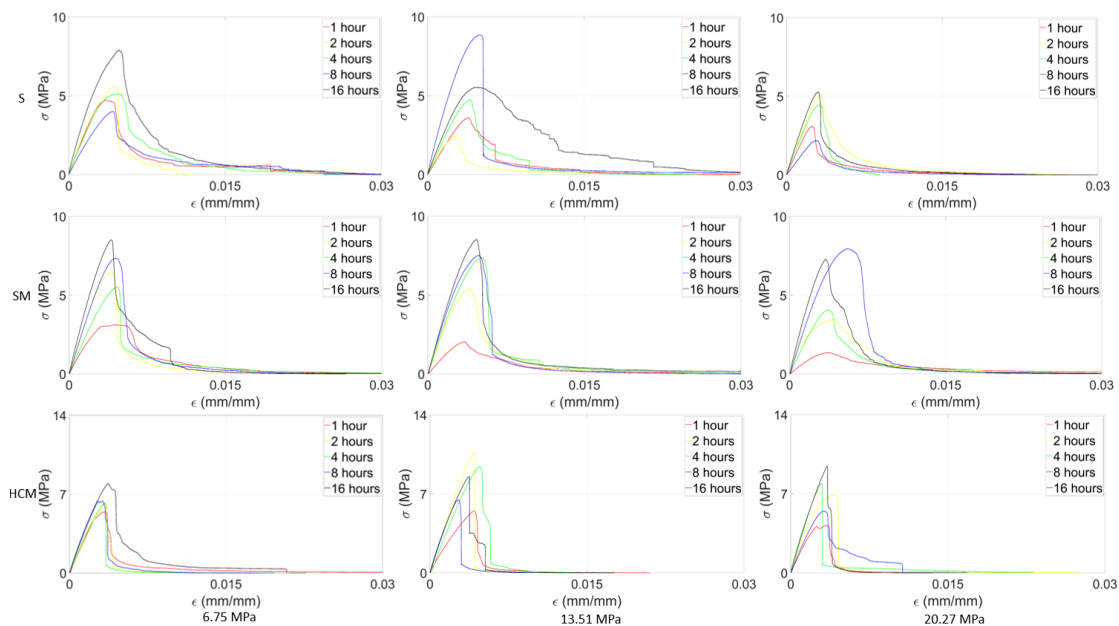


**Figure 5-5.** The stress-strain curve for dog bone samples tests the composites made of the pure stalk, stalk with mycelium, and hardwood mixed with coffee grounds and mycelium grown in it. Tests are based on samples prepared under 90 °C with different pressure (6.75, 13.51, and 20.27 MPa) and baking time (1, 2, 4, 8, 16 hours.)

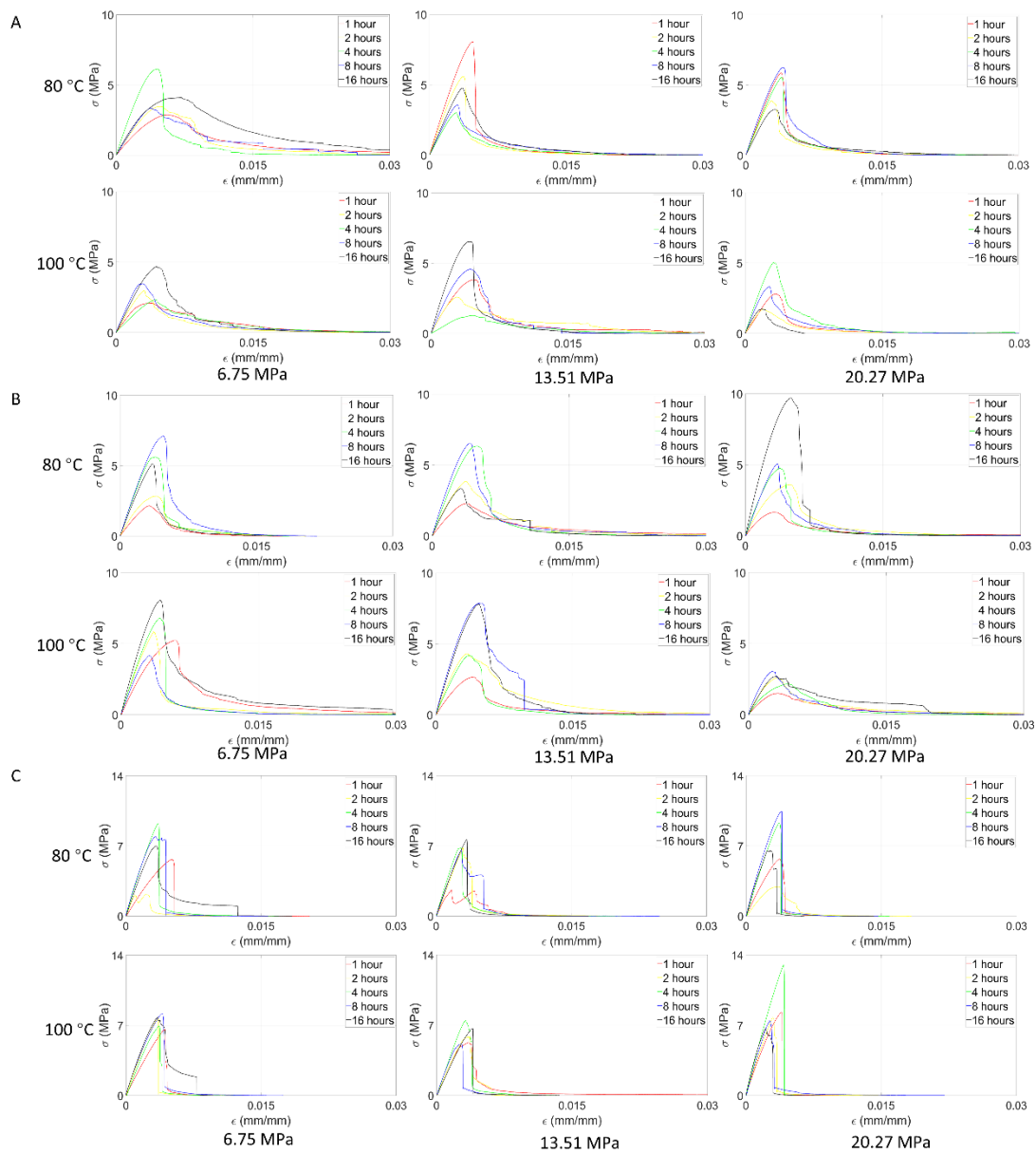


**Figure 5-6.** The stress-strain curve for dog bone samples tests the composites made of the **A.** Stalk (S) **B.** Stalk with mycelium (SM), and **C.** Hardwood, coffee grounds and mycelium grown. Tests are based on samples prepared under 80 and 100 °C with different pressure and baking time. (Different color in the stress-strain curve means the different baking times, which are 1 hour-red, 2 hours-yellow, 4 hours-green, 8 hours-blue, 16 hours-black.)

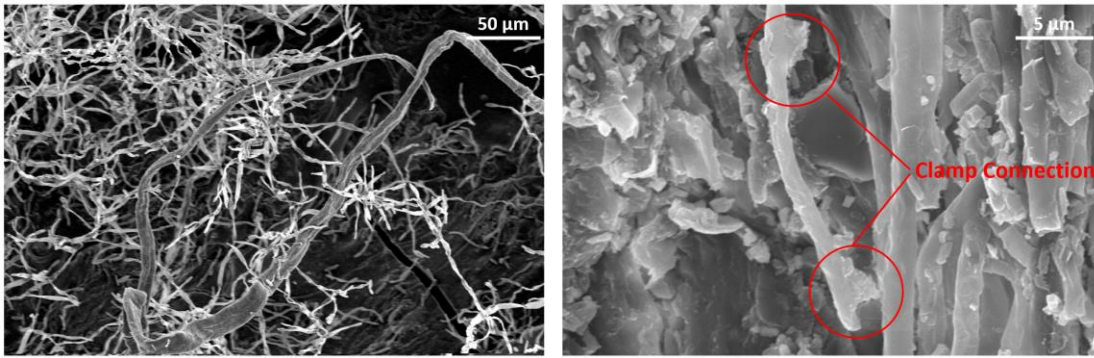


**Figure 5-7.** The SEM imaging of the mycelium (left: the mycelium-based bio-composite under 100 °C press for 16 hours, right: the unique structure, which is the clamp connection of mycelium fiber.)

We found that the different substrates can significantly affect the ultimate strength. We measure the density of each sample ( $\rho$ ) and compute Young's modulus ( $E$ ),  $\sigma_U$ , and modulus of toughness ( $U_T$ ) for each of the samples (raw data for all the samples in **Table 5-1 to 5-3**). **Table 5-4** summarizes all the physical properties of the samples of maximum  $\sigma_U$  given by different raw materials. It is shown that  $\sigma_U = 9.70$  MPa provided by SM is significantly larger than  $\sigma_U = 8.85$  MPa given by S without mycelium, suggesting that  $\sigma_U$  increases by 10% with density increased by 1.6% by adding mycelium. Furthermore, the SM sample of the highest  $\sigma_U$  shows an advantage over the S sample of the highest  $\sigma_U$  by having higher  $E$  by 6% and higher  $U_T$  by 16%, suggesting that the mycelium can also significantly increases the material stiffness and toughness. Moreover, the highest  $\sigma_U = 12.99$  MPa for all the samples is obtained from HCM, which is 19% higher than the 10.89 MPa as the strength of a corn-straw-based bio-composite in literature [295]. It is noted that the material density for the highest  $\sigma_U$  is much less than the highest  $\rho$  value ( $1.53$  g/cm<sup>3</sup> for SM and  $1.54$  g/cm<sup>3</sup> for HCM,

**Table 5-2 and 5-3**), indicating that the composite strength does not monotonically increase with the material density, making it different from ideal cellular materials (e.g., porous polystyrene) [296]. We also consider all 45 other processing conditions and compute the difference in  $\rho$ ,  $\sigma_U$ ,  $E$ , and  $U_T$  for samples made of S, SM, and HCM. It is shown that by using the same processing conditions,  $\rho$  of the samples made of SM and HCM increase by 11% by comparing to samples made of S on average, while  $\sigma_U$  increases by 35% and 96%,  $E$  increases by 14% and 76%,  $U_T$  increases by 47% and 7%, for SM and HCM, respectively. We excluded the calculation of Poisson's ratio for the samples, and the main reason is the challenges associated with accurately measuring the elongation along the y-axis. During the tensile tests, the elongation in the y-axis was minimal, typically around 1% to 2% for our samples. This slight elongation presents difficulty detecting the necking phenomenon, which is critical for precise strain measurements. Traditional methods of capturing elongation through imaging failed to provide reliable data due to the negligible deformation in the y-axis, making it impractical to obtain accurate measurements. Furthermore, calculating Poisson's ratio involves determining the ratio of lateral strain to axial strain. Given the minimal elongation in the y-axis, the resulting Poisson's ratio, calculated by dividing the lateral strain by the axial strain, would be exceedingly small. This disproportionate reduction further decreased the reliability and significance of the Poisson's ratio in this context. Consequently, focusing on other mechanical properties, such as tensile strength, Young's modulus, and toughness, provides a more accurate and meaningful assessment of the material's performance.

**Table 5-1.** Mechanical properties and density are obtained from each tested stalk (S) sample.

<b><i>T</i> (°C)</b>	<b><i>P</i> (MPa)</b>	<b><i>H</i> (hours)</b>	<b><math>\rho</math> (g/cm<sup>3</sup>)</b>	<b><math>\sigma_U</math> (MPa)</b>	<b><i>E</i> (MPa)</b>	<b><i>U<sub>T</sub></i> (J/m<sup>3</sup>)</b>
80	6.75	1	1.20	2.88	919.4	0.031
		2	1.25	3.47	1146.2	0.030
		4	0.95	6.13	2004.9	0.028
		8	0.86	3.34	1176.7	0.031
		16	0.93	4.11	1421.2	0.057
	13.51	1	1.16	8.06	2264.8	0.030
		2	1.30	5.57	1905.4	0.019
		4	1.32	3.02	1327.2	0.014
		8	1.34	3.57	1400.2	0.019
		16	1.32	4.77	1622.6	0.024
	20.27	1	1.26	5.89	1658.2	0.022
		2	1.33	3.89	1650.5	0.015
		4	1.35	5.55	1746.7	0.020
		8	1.34	6.25	2001.4	0.026
		16	1.33	3.27	1346.1	0.017
90	6.75	1	1.37	4.71	1913.6	0.028
		2	1.37	5.59	1756.9	0.013
		4	0.94	5.11	1822.7	0.033
		8	0.91	4.01	1425.5	0.026
		16	1.06	7.89	2464.5	0.049
	13.51	1	1.42	3.59	1186.1	0.020
		2	1.29	2.43	1148.5	0.008

		4	1.26	4.76	1589.9	0.022
		8	1.39	8.85	2669.5	0.038
		16	1.07	5.53	1824.8	0.059
	20.27	1	1.28	3.08	1525.9	0.011
		2	1.24	5.14	1937.4	0.023
		4	1.32	4.43	1735.3	0.009
		8	1.33	2.17	1005.6	0.008
		16	1.30	5.27	2199.2	0.018
		2	1.51	2.10	1047.6	0.020
		4	0.99	2.98	1224	0.016
		8	1.42	2.32	867.3	0.019
		16	1.47	3.47	1776.4	0.020
	13.51	1	0.93	4.68	1500.3	0.028
		2	0.90	3.82	1399.7	0.025
		4	1.16	2.60	1379.3	0.023
		8	1.04	1.28	827.7	0.011
		16	1.01	4.58	1726.2	0.025
	20.27	1	1.10	6.54	2273.4	0.027
		2	1.29	2.80	1071.6	0.011
		4	1.01	1.71	1158.3	0.008
		8	1.14	5.03	2071.3	0.022
		16	1.23	3.32	1810.5	0.014

**Table 5-2.** Mechanical properties and density are obtained from each tested stalk with mycelium (SM) sample.

$T$ (°C)	$P$ (MPa)	$H$ (hours)	$\rho$ (g/cm <sup>3</sup> )	$\sigma_U$ (MPa)	$E$ (MPa)	$U_T$ (J/m <sup>3</sup> )
80	6.75	1	1.18	2.15	922.8	0.009
		2	1.09	2.84	1236.3	0.014
		4	1.40	5.63	2011.4	0.022
		8	1.35	7.10	2091.9	0.031
		16	1.37	5.14	1777.5	0.017
	13.51	1	0.96	2.28	862.8	0.022
		2	1.11	3.86	1487.9	0.027
		4	1.37	6.33	1824.1	0.032
		8	1.52	6.51	2103	0.033
		16	1.53	3.35	1374.6	0.019
	20.27	1	1.06	1.65	855.6	0.012
		2	1.21	3.61	1308.8	0.023
		4	1.40	4.77	1831.7	0.020
		8	1.39	5.05	1816.3	0.022
		16	1.41	9.70	2841.4	0.044
90	6.75	1	1.05	3.13	1290.7	0.024
		2	1.40	6.46	2212.2	0.025
		4	1.36	5.53	1590.4	0.027
		8	1.32	7.35	2223.3	0.034
		16	1.38	8.51	2715.6	0.039
	13.51	1	1.15	2.02	773.1	0.014
		2	1.35	5.36	1932.3	0.027

		4	1.46	7.34	2042.6	0.037	
		8	1.47	7.51	2314.2	0.035	
		16	1.44	8.52	2521.6	0.041	
	20.27	1	1.12	1.34	546.3	0.015	
		2	1.48	3.46	1269.5	0.024	
		4	1.51	4.06	1451.2	0.021	
		8	1.07	7.94	2157.5	0.046	
		16	1.08	7.27	2726.3	0.033	
	100	6.75	1	1.25	5.24	1444.9	0.040
			2	1.28	5.85	2005.5	0.023
4			1.39	6.80	2096.3	0.025	
8			1.33	4.15	1757.7	0.017	
16			1.39	8.07	2511.7	0.053	
13.51		1	1.34	2.65	1009.9	0.016	
		2	1.40	4.31	1764.8	0.035	
		4	1.48	4.20	1502	0.018	
		8	1.50	7.88	2415.1	0.046	
		16	1.20	7.78	2243.1	0.040	
20.27		1	1.12	1.51	722.2	0.013	
		2	1.55	2.57	1256.8	0.019	
		4	1.07	2.15	945.2	0.014	
		8	1.54	3.06	1590.2	0.017	
		16	1.27	2.70	1245.7	0.025	

**Table 5-3.** Mechanical properties and density are obtained from each tested hardwood with coffee grounds with mycelium (HCM) sample.

$T$ (°C)	$P$ (MPa)	$H$ (hours)	$\rho$ (g/cm <sup>3</sup> )	$\sigma_U$ (MPa)	$E$ (MPa)	$U_T$ (J/m <sup>3</sup> )
80	6.75	1	1.03	5.65	1477.6	0.019
		2	1.30	2.18	2244.3	0.005
		4	1.51	9.24	3045.1	0.022
		8	1.51	7.93	3049.7	0.025
		16	1.08	7.01	2667.2	0.028
	13.51	1	1.29	2.61	1915.7	0.011
		2	1.35	6.80	2478.7	0.018
		4	1.54	6.77	3048.4	0.016
		8	1.16	6.59	2674.6	0.022
		16	1.24	7.66	2572.6	0.016
	20.27	1	1.49	5.69	1928.1	0.015
		2	1.41	2.91	1271.7	0.011
		4	1.48	9.27	3103.9	0.021
		8	1.54	10.44	3417.4	0.025
		16	1.16	6.57	3285.4	0.014
90	6.75	1	1.25	5.42	2235.6	0.021
		2	1.51	6.20	2092.1	0.016
		4	1.54	6.17	2295.2	0.014
		8	1.52	6.39	2708.5	0.017
		16	1.05	7.94	2733.2	0.036

	13.51	1	1.41	5.51	1624.4	0.017
		2	1.49	10.72	3025.1	0.026
		4	1.52	9.42	2573.3	0.033
		8	1.18	6.48	2951	0.013
		16	1.12	8.54	2931.3	0.024
	20.27	1	1.47	4.18	2032.6	0.012
		2	1.49	6.92	2692.3	0.023
		4	1.50	7.91	3145.8	0.019
		8	1.53	5.45	2311.2	0.023
		16	1.16	9.44	3261.7	0.022
100	6.75	1	1.49	6.60	1781.2	0.017
		2	1.14	7.67	2654.5	0.016
		4	1.12	6.93	2429.6	0.016
		8	1.20	8.20	2635.8	0.023
		16	1.26	7.80	2746.8	0.030
	13.51	1	1.41	5.28	2197.5	0.022
		2	1.40	5.82	2233.7	0.017
		4	1.35	7.44	2695.4	0.019
		8	1.40	5.13	2615.2	0.011
		16	1.54	6.67	1984.1	0.016
	20.27	1	1.53	8.27	2625.5	0.020
		2	1.24	7.78	2922.5	0.016
		4	1.26	12.99	3664.8	0.030
		8	1.36	7.46	3340.8	0.016

		16	1.35	6.63	3662	0.013
--	--	----	------	------	------	-------

**Table 5-4.** The maximum ultimate strength and other physical properties of a sample made of each raw material

Material properties	S	SM	HCM
$\sigma_U$ (MPa)	8.85	9.70	12.99
$E$ (MPa)	2669.5	2841.4	3664.8
$U_T$ (MJ/m <sup>3</sup> )	0.038	0.044	0.030
$\rho$ (g/cm <sup>3</sup> )	1.39	1.41	1.26

The results suggest that the mechanical advantage ( $\sigma_U$ ,  $E$ , and  $U_T$ ) of adding mycelium to wood composite is not limited to a specific processing condition but generally exists. These advantages in strength and modulus are very different from what is given by the scaling law of ideal cellular materials, as  $\frac{\sigma_{U1}}{\sigma_{U2}} = \left(\frac{\rho_1}{\rho_2}\right)^{1.5}$  and  $\frac{E_1}{E_2} = \left(\frac{\rho_1}{\rho_2}\right)^2$  [296], suggesting that adding the mycelium changes the interactions between the building blocks within the wood composite. We believe that HCM gives the highest strength mainly because of the higher content of mycelium, as the mycelium had already grown to fully occupy the substrate before our tests. In contrast, the total time for mycelium growth in SM is limited (14 days) in our lab. It is also noticed that in comparison to the significant increment in  $\sigma_U$  and  $E$ , HCM does not give much different  $U_T$  from S, indicating a negative effect on material toughness by having too much mycelium in the substrate. The unnecessary mycelium will reduce the flexibility of the composite and lead to brittle failure, which is shown again for different processing temperatures (80 and 100 °C) in **Figure 5-6**, as HCM reaches  $\sigma_U$  at a lower strain level

without ductile tail after  $\sigma_U$  and agree with the recent observation that a flexible mycelium composite has a higher toughness than the brittle one [166].

### 5.3.3 Design Toward the Specific Mechanics of Mycelium-Based Composites

We compute the specific mechanical properties  $\sigma_U/\rho$ ,  $E/\rho$ , and  $U_T/\rho$  based on values summarized in **Table 5-1 to 5-3**, which accounts for the effective material usage toward different mechanical functions, as shown by the Ashby plots in **Figure 5-8**. It is shown that the specific strength and modulus (**Figure 5-8 A**) are highly correlated that largely agree with the Ashby plot of the other cellular materials (e.g., foams, cork, bone, wood) [297], suggesting that even we have applied a heat-press treatment, the samples are largely similar to cellular materials, as both  $\sigma_U$  and  $E$  monotonically increases with  $\rho$ , and thus show overall agreement with the scaling laws of other cellular materials. However, neither  $U_T/\rho$  nor  $U_T$  shows a strong correlation with  $E/\rho$  or  $\rho$  of the composites, as shown in **Figure 5-8 B**, indicating that its optimization is more complex than  $\sigma_U$  and  $E$ .

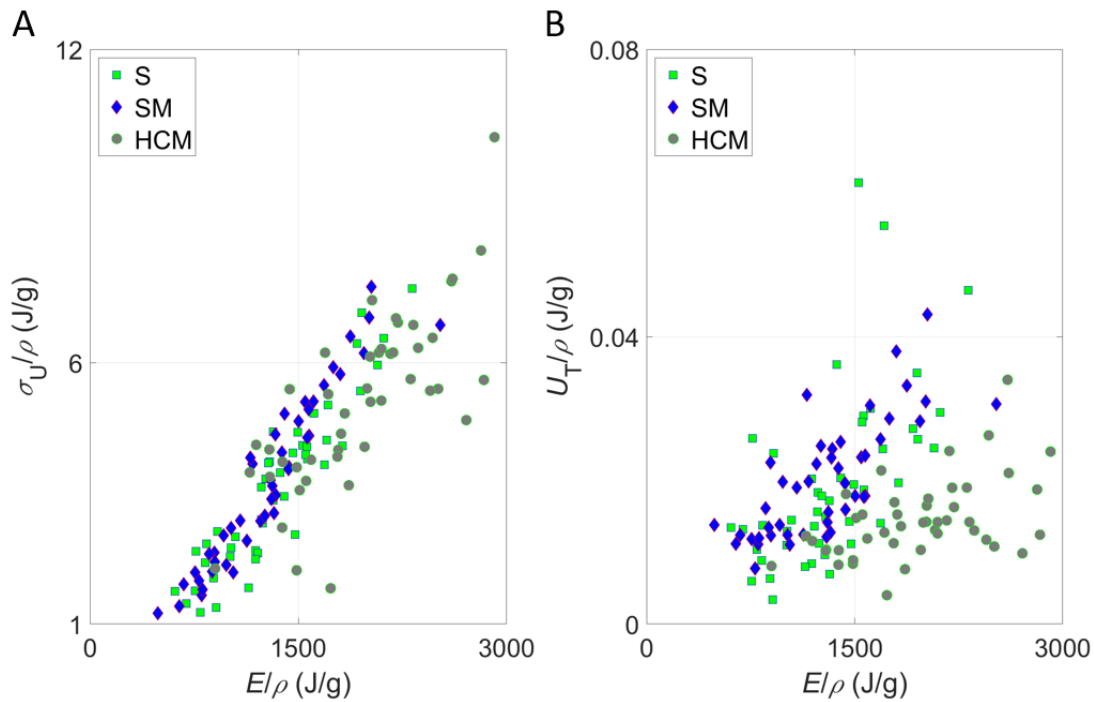


**Figure 5-8.** Ashby plots for specific mechanical properties of different wood composites. **A.** specific ultimate strength and Young's modulus normalized by density, showing these two mechanical properties of the wood composite are well aligned, that largely agrees with the other cellular materials (e.g., foams, cork, bone, wood) [297]; **B.** specific modulus of toughness and Young's modulus normalized by density, showing the toughness of the composites are highly dispersed and weakly determined by the Young's modulus.

**Table 5-5** summarizes the maximum specific mechanical properties with their corresponding processing conditions, which can help guide the treatment conditions for a specific optimized function. The temperature for yielding the best specific mechanical properties is from 90 to 100°C, which agrees with the water evaporation temperature, reducing the water volume and making the wood fibers more compact for a higher density. However, there is no other universal treatment condition that can lead to all the maximum mechanical properties. It is

shown that HCM gives the highest  $\frac{\sigma_U}{\rho} = 10.32 \text{ J/g}$  and  $\frac{E}{\rho} = 2912.3 \text{ J/g}$  with 4 hours of baking time, which is much shorter than S and SM, suggesting that more mycelium in the raw material enables a higher specific strength and modulus, as well as reduces the amount of baking time before reaching the optimal specific strength and modulus. Our samples have a similar  $\frac{\sigma_U}{\rho}$  in comparison to the corn-straw-based bio-composite in literature [295], while  $\frac{E}{\rho}$  of our samples is much larger than 1800 J/g as that of the literature value [295], suggesting that our samples are much stiffer with the same density. It is noted that the  $U_T/\rho$  values for all the S samples are smaller than 0.085 J/g as that of the literature value [295], and adding the mycelium (SM and HCM) further reduces the specific toughness value. This result agrees with the fact that adding mycelium reduces the flexibility of the composite, leading to higher modulus but lower toughness, because a strong interaction by mycelium prevents the wood fibers from sliding, which accounts for a portion of energy dissipation of a fibrous material [298], [299].

**Table 5-5.** The treatment conditions (i.e., Time ( $H$ ), Pressure ( $P$ ), Temperature( $T$ )) of each raw material to achieve the maximum specific mechanical properties

Material	Specific mechanical properties	Maximum values	$H$ (hours)	$P$ (MPa)	$T$ ( $^{\circ}\text{C}$ )
S	$\sigma_U/\rho$ (J/g)	7.42	16	6.75	90
	$E/\rho$ (J/g)	2481.9	16	6.75	90

	$U_T/\rho$ (J/g)	0.061	16	6.75	80
SM	$\sigma_U/\rho$ (J/g)	7.45	8	20.27	90
	$E/\rho$ (J/g)	2521.3	16	20.27	90
	$U_T/\rho$ (J/g)	0.043	8	20.27	90
HCM	$\sigma_U/\rho$ (J/g)	10.32	4	20.27	100
	$E/\rho$ (J/g)	2912.3	4	20.27	100
	$U_T/\rho$ (J/g)	0.034	16	6.75	90

#### 5.3.4 Supervised Machine Learning for Predicting the Specific Mechanics of Mycelium-Based Composites

We utilized all the experimental data by taking the processing conditions (i.e., time (H), pressure (P), temperature (T), material type (i.e., S, SM, and HCM)) as input predictors and the specific material properties (i.e.,  $\rho$ ,  $\sigma_U$ ,  $E$ ,  $U_T$ ) as outputs response of each mechanical sample and developed a neural network model as summarized in **Figure 5-9**. This model aims to map the output values from any given predictor values instead of running the specific

experimental test [300], [301]. Instead of directly predicting the mechanical properties, we use a k-means clustering method [284], [285], [286], [287] to divide the  $N$  tests into five levels for each of  $\sigma_U$ ,  $E$ ,  $U_T$  (see the detail of this clustering algorithm in the Method). Each sample is labeled by a 4-element vector  $\vec{V}$ , with each element  $V_i$  taking the response value from 0 to 4 for a specific material property. Hence, any samples with the same  $V_i$  value will have a similar corresponding material property compared to other samples. We build a tri-layered neural network model with a uniform layer size for each layer to find the correlation between the processing conditions and material property. **Figure 5-10** shows the confusion matrix for each model. It is shown that for training and testing data, the predicted response value  $V_{i\_pred}$  is largely aligned with the actual test result  $V_i$  for each material property, with over 70% of predictions being accurate or only one level different from the level of the test result, as  $|V_{i\_pred} - V_i| \leq 1$ .

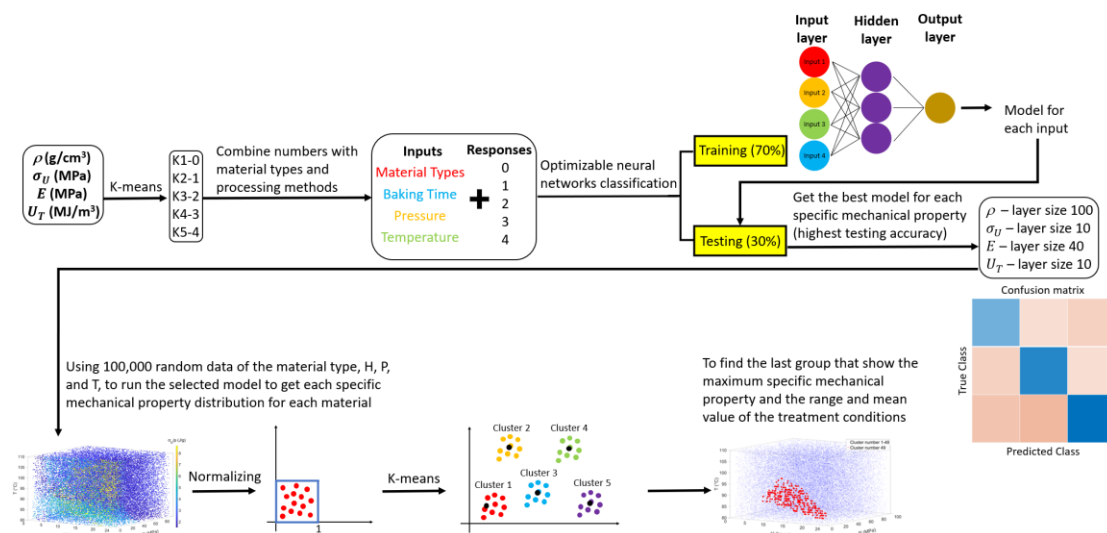


**Figure 5-9.** The general process of data clustering and the tri-layered neural networks classification method for making predictions beyond experimental tests.

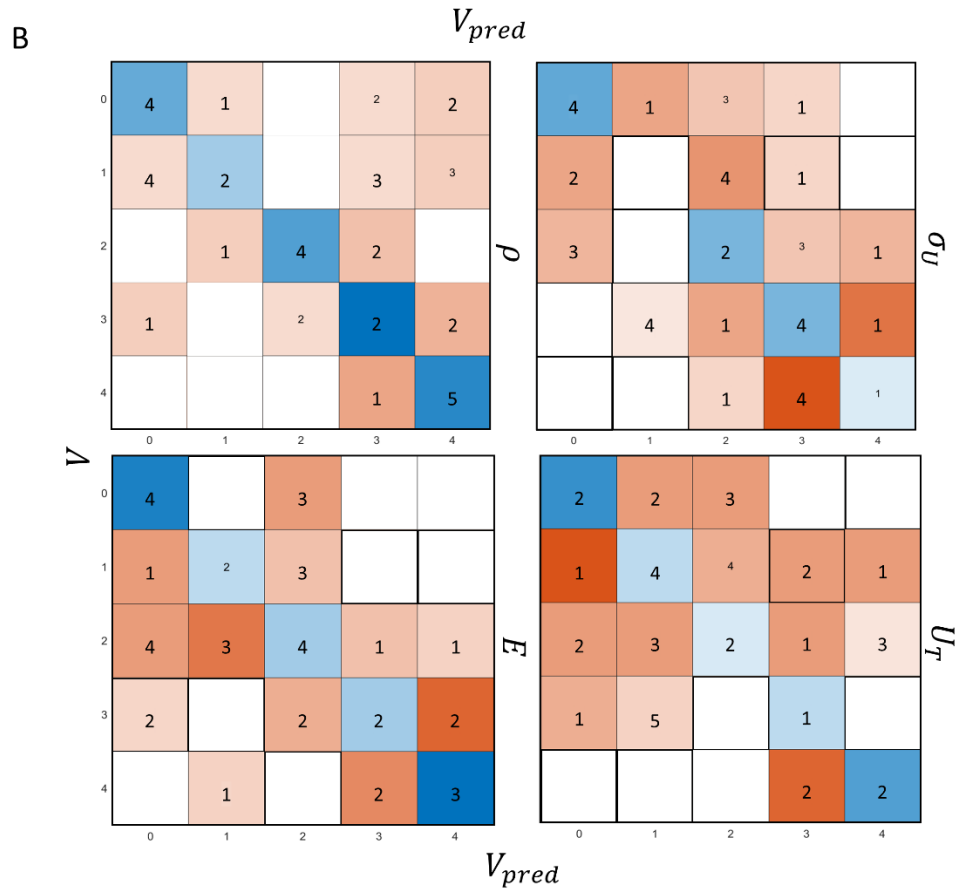
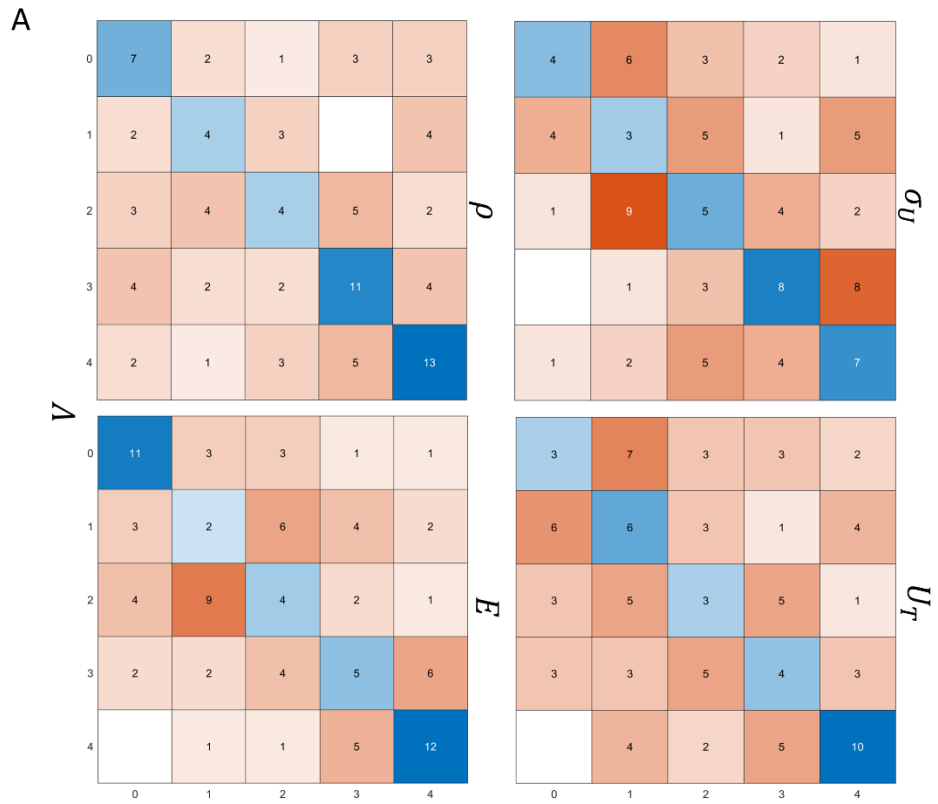


**Figure 5-10.** The confusion matrix of each response by the prediction (**A:** training, **B:** testing).

We use the neuron network models to predict the optimal processing condition that yields the highest specific mechanical properties. We randomly generate 100,000 sets of feasible processing conditions, as shown by points in **Figure 5-11**, and use the models to predict  $\rho$  and mechanical properties and further compute  $\sigma_U/\rho$ ,  $E/\rho$ ,  $U_T/\rho$  values that correspond to each feasible condition, as plotted in **Figure 5-12**. Then, we normalize each dimension of the different processing conditions and cluster them together with the predicted specific mechanical properties by k-means (see Method for details), which enables us to identify the cluster of processing conditions that yields the highest specific mechanical property. **Figure 5-11** highlights the location of all the points within the cluster of the highest  $\sigma_U/\rho$ ,  $E/\rho$  and  $U_T/\rho$  values, suggesting the range of the most favorable processing conditions for a particular specific mechanical property.

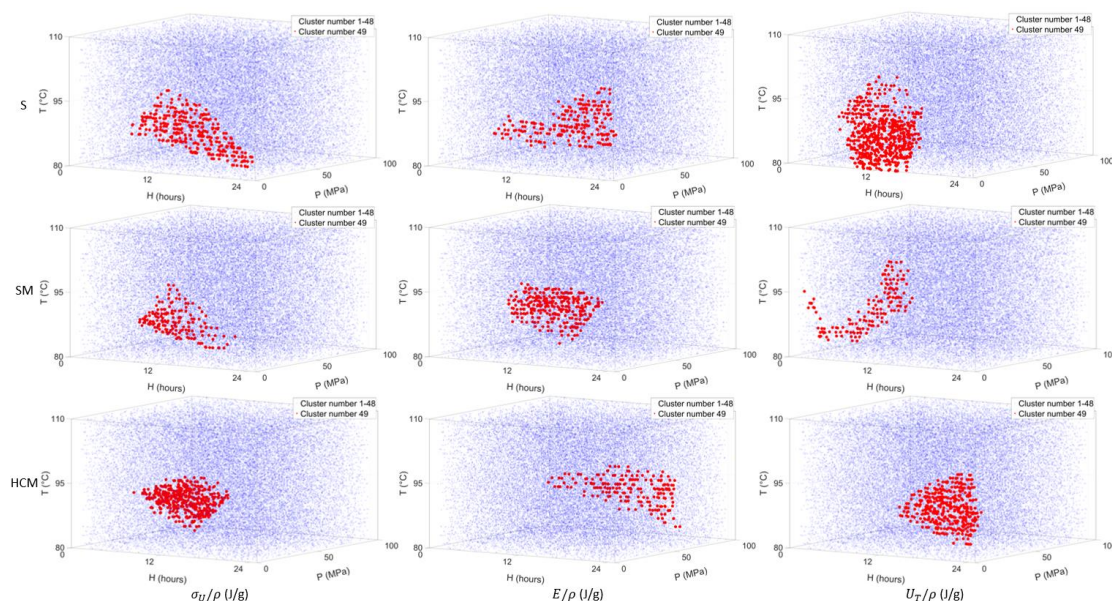


**Figure 5-11.** 3D scatter plots for the processing conditions of randomly generated 100,000 imaginary samples made of different raw materials (S, SM and HCM), with the points corresponding to the highest specific mechanical properties ( $\sigma_U/\rho$ ,  $E/\rho$  and  $U_T/\rho$ ) highlighted by a red color.

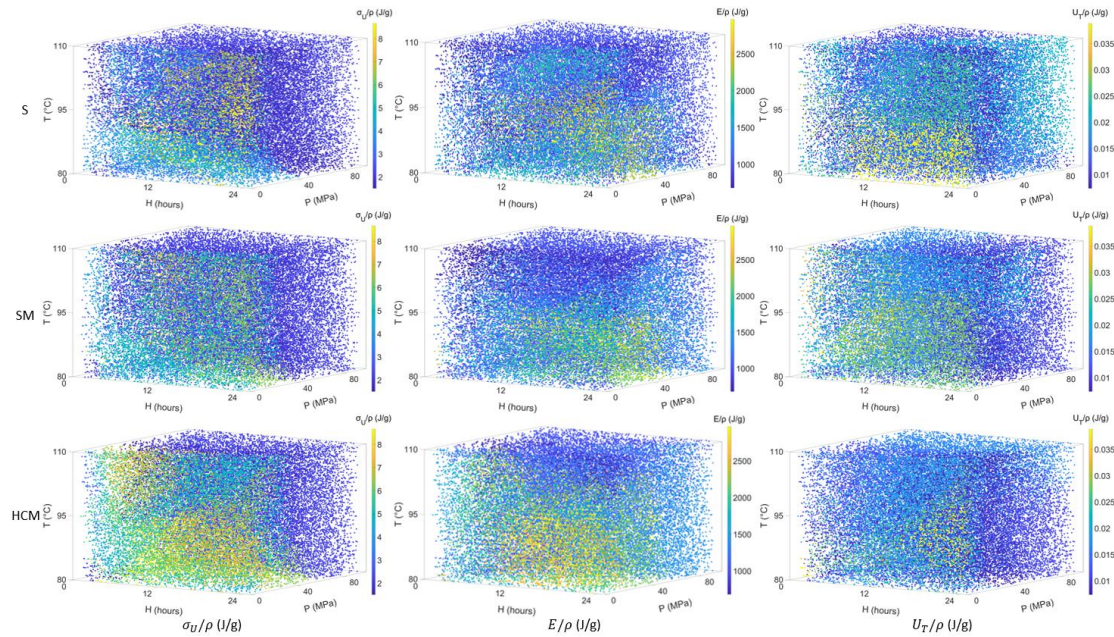


**Figure 5-12.** 3D scatter plots based on the treatment conditions and the color bar based on random 100,000 data specific mechanical properties. Stalk (S); Stalk with mycelium (SM); Hardwood with coffee grounds with mycelium (HCM).

We summarize the range of the data points of the last cluster by computing the mean values and the deviation for the processing conditions and the specific mechanical properties (**Table 5-6**). These predictions agree with the tensile test observations (**Table 5-5**), as shown in **Figure 5-13**. Furthermore, it is shown that the machine learning models predict some specific mechanical properties higher than the direct experimental observation, and the corresponding

processing conditions agree with the tensile tests. The learning model predicts according to the trend of all the testing results, while the direct observation is obtained from a single sample test that may be subjected to many random factors.

**Table 5-6.** The range and mean value of treatment conditions that shows the maximum mechanical properties of each material by the prediction

Material			s		
Specific mechanical properties (J/g)			$\sigma_U/\rho$	$E/\rho$	$U_T/\rho$
Mean results			8.6595	2966.7	0.0388
The range and mean value from predictions of treatment conditions	H (hours)	Min	6.9	7.1	5.2
		Mean	15.5	18.1	11.4
		Max	23.9	23.9	15.6
	P (MPa)	Min	1.02	1.05	1.03
		Mean	6.55	7.63	8.59
		Max	13.92	14.54	17.17
	T (°C)	Min	83	86	80
		Mean	90	92	88
		Max	99	101	101
Material			SM		
Specific mechanical properties (J/g)			$\sigma_U/\rho$	$E/\rho$	$U_T/\rho$
Mean results			8.6595	2966.7	0.0388
The range and mean value from predictions of treatment conditions	H (hours)	Min	4.1	6.9	1
		Mean	9.8	12.4	7.2
		Max	16.3	17.6	12.5
	P (MPa)	Min	19.09	19.09	6.06
		Mean	28.11	28.35	22.99
		Max	38.35	38.07	28.15
	T (°C)	Min	82	83	83
		Mean	88	92	91
		Max	97	97	102
Material			HCM		
Specific mechanical properties (J/g)			$\sigma_U/\rho$	$E/\rho$	$U_T/\rho$
Mean results			8.6595	2966.7	0.0388
The range and mean value from	H	Min	1.9	10.9	12.1

<b>predictions of treatment conditions</b>	<b>(hours)</b>	<b>Mean</b>	8.4	19.4	20.2
		<b>Max</b>	14.4	24	24
	<b>P (MPa)</b>	<b>Min</b>	32.54	34.67	1.04
		<b>Mean</b>	42.33	47.61	5.77
		<b>Max</b>	56.56	60.76	13.83
	<b>T (°C)</b>	<b>Min</b>	83	85	84
		<b>Mean</b>	90	94	92
		<b>Max</b>	96	99	100

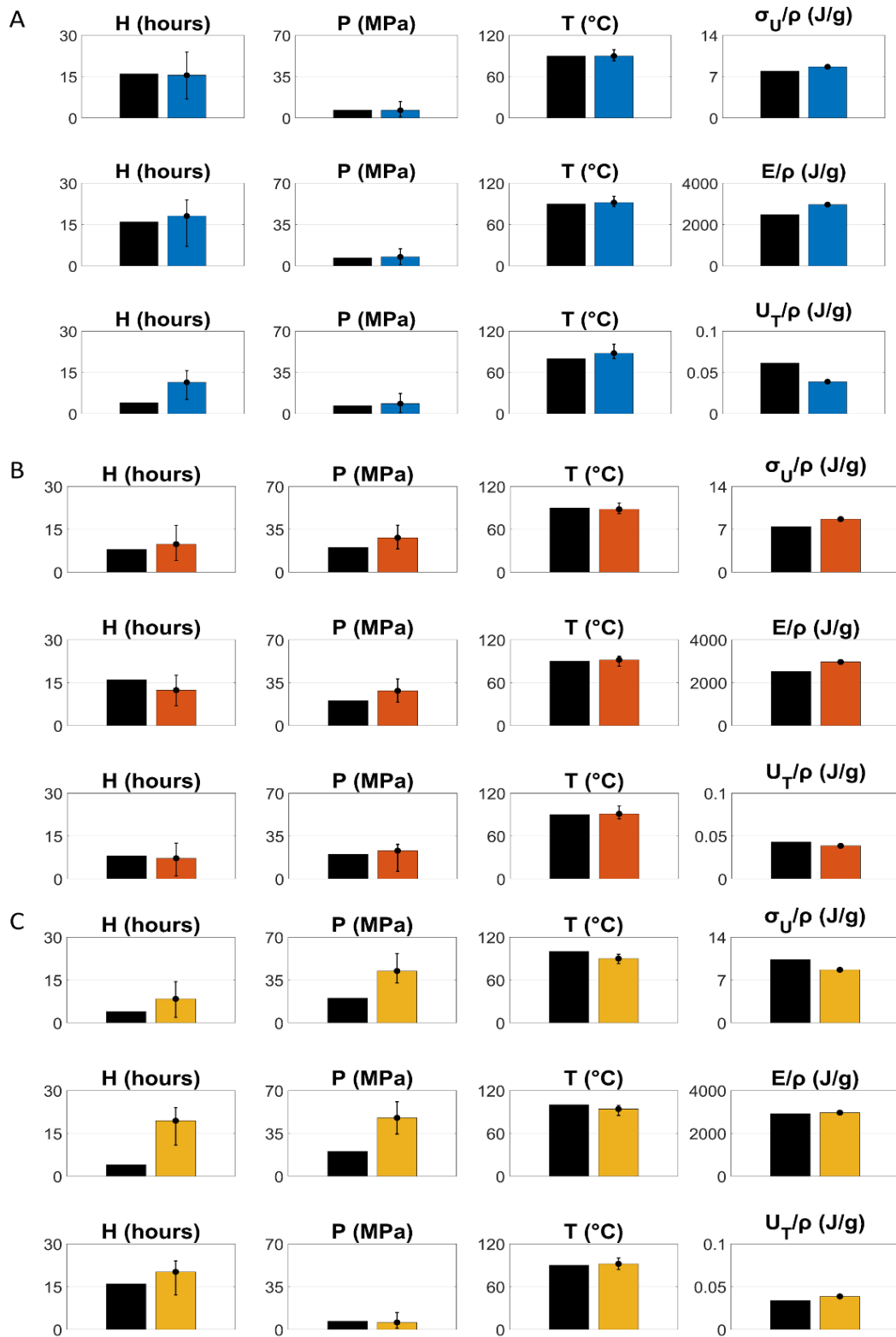


**Figure 5-13.** Histograms and the error bar for the treatment conditions of the cluster correspond to the high specific mechanical properties (colorful bars), in comparison to the

direct experimental observations (black bars) as summarized in **Table 5-6**. A. Stalk (S); B. Stalk with mycelium (SM); C. Hardwood with coffee grounds with mycelium (HCM).

The mycelium-based bio-composite as an environmentally friendly material shows more advantages in many applications (e.g., packaging materials, acoustic and thermal insulation boards) and is receiving more attention [95], [302]. However, the development of bio-composite materials is still in its infancy, and the standardized procedure that will result in optimum material properties has yet to be discovered. Therefore, a novel manufacturing method for producing mycelium-based bio-composite samples is developed in the current article. Compared to literature methods that directly inoculated mycelium in the substrate for manufacturing samples [29], [50], [52], we use the blender to mixing the mycelium with wood fibers and water before heat-pressing the composite that may enable to further dissolve chitin and enable it to expose and get more distributed to interact with cellulose fibers at their interfaces, which lead to reinforcement and strength [52]. Because of the promising applications [144], [200], [303], [304] and intrinsic environmentally friendly features over materials that requires the heavy involvement of synthetic chemistry, the development of mycelium-based wood composites will need to start from the lab by fully understand the mechanisms of the mycelium growth and the structure-mechanics relationship at the microscopic scale in our fundamental studies, but eventually aim to scale up to large-scale manufacturing for engineering applications including infrastructure and packaging. Indeed, its structural designs and applications to buildings for thermal insulation, fire resistance and acoustic absorption will be further explored, and complex structures and their related material functions will be evaluated [305]. For example, via 3D printing and foam forming. However,

it is crucial to identify a sustainable way that requires less energy consumption and carbon emission but yields material of higher specific mechanics during manufacturing [306]. This will give the large-scale manufacturing of the material commercial advantages over other conventional building and packaging materials. Compared to traditional engineering materials such as polymer matrix composites, mycelium-based wood composites have many limitations (e.g., shaping, time cost), motivating us to work with industrial units to understand the critical challenge for making the breakthrough that will lead to its mass production.

**CHAPTER 6. DEVELOPMENT AND EVALUATION OF MYCELIUM-BASED BIO-  
COMPOSITE INSULATION: A SUSTAINABLE ALTERNATIVE TO  
CONVENTIONAL BUILDING MATERIALS**

## 6.1 Introduction

The construction industry, particularly the production of building materials like insulation, significantly contributes to greenhouse gas (GHG) emissions globally. This contribution accounts for approximately 33% of all global emissions [307]. This environmental impact necessitates a shift towards sustainable practices and materials to reduce emissions without compromising on enhancing the energy efficiency of buildings. Among various sustainable materials, bio-based insulation composites, such as those derived from mycelium, present a promising alternative [185]. Mycelium, the vegetative part of fungi, can be cultivated on agricultural waste substrates like coconut coir, turning waste into valuable insulation materials [38], [48], [106], [308]. These mycelium-based composites offer several advantages, including biodegradability, low embodied energy, and the potential to reduce GHG emissions compared to conventional materials like blown-in cellulose and extruded polystyrene (XPS) [27], [309].

The building construction industry heavily relies on mineral wool, fiberglass, and synthetic foams for insulation [310]. While effective in thermal performance, these materials pose significant environmental challenges. They are often derived from non-renewable resources, involve high energy consumption during production, and are non-biodegradable, contributing to landfill waste at the end of their life cycle. Moreover, traditional insulation materials can release harmful substances during manufacturing and disposal, posing health risks to humans and ecosystems [311], [312]. The high carbon emissions associated with these materials also exacerbate climate change, underlining the urgent need for sustainable alternatives [313].

Mycelium-based composites represent a sustainable and innovative solution to these issues. Cultivated on substrates such as coconut coir, the mycelium grows into a dense network of hyphae, creating a solid, foam-like material that can be used for insulation. This process repurposes agricultural waste and sequesters carbon, contributing to a circular economy. In terms of performance, mycelium-based composites offer comparable thermal insulation properties to conventional materials. Ongoing research has highlighted their comparable thermal performance, making them suitable for building envelopes [48]. These materials are fire-resistant and have good moisture regulation capabilities, further enhancing their suitability for construction applications [12]. Mycelium-based composites have several advantages over traditional materials like blown-in cellulose and XPS. Blown-in cellulose, a bio-based material, involves energy-intensive production processes and chemical treatments to enhance fire resistance and durability [314]. XPS, a petroleum-based product, offers excellent insulation but is associated with high GHG emissions and environmental persistence due to its non-biodegradability [315], [316]. On the other hand, mycelium composites are produced through a low-energy process and are inherently biodegradable, reducing their environmental impact. Furthermore, mycelium-based insulation can be locally sourced and manufactured, supporting local economies, and reducing transportation emissions.

Integrating mycelium-based insulation into building envelopes makes it possible to achieve significant energy savings and contribute to global sustainability goals. Using such materials aligns with the need for innovative, eco-friendly solutions in the construction industry,

making mycelium-based composites a viable and advantageous option for future building projects. This study combined *Ganoderma Lucidum* with coconut coir to create a novel bio-based composite material. Comprehensive evaluations were conducted to assess its mechanical properties, thermal performance, fire resistance on the surface, and interactions with water. These tests aimed to determine its viability as a sustainable alternative to traditional building insulation materials. The results highlighted the composite's potential to provide adequate thermal and acoustic insulation while demonstrating good fire retardant and hydrophobic characteristics, essential for ensuring safety and durability in building applications.

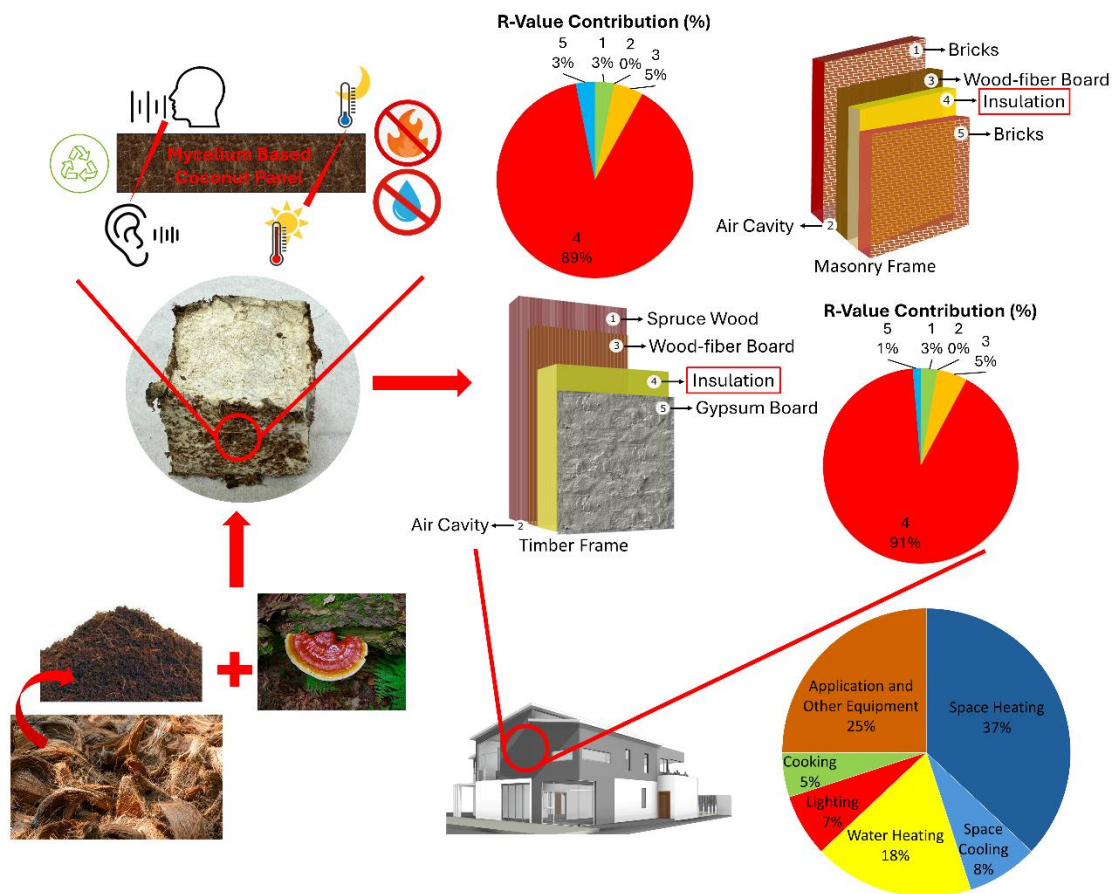


**Figure 6-1.** We illustrate the application and effectiveness of Mycelium-based coconut panels as sustainable insulation materials in building construction. The left part of the figure shows that using agricultural waste (coir) combined with mycelium (*Ganoderma Lucidum*) generates mycelium-based bio-composite materials. It can provide excellent thermal and acoustic insulation, water and fire resistance, and sustainability. The diagrams on the right compare the thermal resistance (R-value) contributions of various components within masonry and timber frame constructions, emphasizing the significant impact of the insulation layer. Additionally, the pie charts delineate energy consumption patterns in buildings, underscoring the potential of improved insulation for energy savings in areas like space heating and water heating.

## **6.2 Experimental Method and Procedures**

### **6.2.1 Flammability test**

A preliminary surface flammability test is conducted using a windproof butane fire source based on the DIN EN 13501–1 test standard [317]. Three samples of each material were tested. The fire source was positioned approximately 4 cm above the surface of each sample, and the surfaces are exposed to the flame for 40 seconds. After exposure, the fire source was removed, and the burned area and depth of penetration are measured. The penetration depth is assessed by cutting the samples along its depth in 0.5 cm increments. Additionally, surface ignition was recorded during the exposure to the fire source.

### **6.2.2 Surface flammability analysis**

This test aimed to analyze the surface flammability of the mycelium bio-composite and compare its performance with that of existing insulation materials. The area burnt and depth penetrated were measured to classify the material. Various flaming times are used according to EN standards to specify different flammability classes: B/C/D (low to medium flammable; 30 s) and E (highly flammable; 15 s). Non-flammable materials such as concrete, glass, or steel are classified as flammability class A. The SRLL samples are used to test the surface flammability of mycelium insulation materials. EPSFOAMULAR NGX F-250 2 in. x 4 ft. x 8 ft. SSE R-10 XPS Rigid Foam Board Insulation and Cellulose Blown-In Insulation by Greenfiber were selected for comparison. For each type of material, 5cm-by-5cm-by-5cm cube pieces are used. The SRLL pieces are dehydrated before testing. The Cellulose cubes are prepared by packing them layer by layer in a cubic mold. Water is added to bind the material together. The cubes are then dehydrated before testing. The XPS samples do not require any additional preparation.

### **6.2.3 Contact angle measurements**

A Rame-Hart Model 250 Standard Goniometer was used to determine the wettability of the prepared samples. The experiment is carried out at room temperature. Samples are taped to microscope glass slides, ensuring relative flatness, and 4 $\mu$ L deionized water droplets are dispensed on the sample surfaces. The contact angle is then measured using the Instrument DropImage Advanced software.

#### 6.2.4 Surface wettability analysis

This test aimed to assess the surface wettability of the mycelium bio-composite and compare its performance with that of existing insulation materials. The SRLI samples are used to test the wettability of mycelium insulation materials. EPSFOAMULAR NGX F-250 2 in. x 4 ft. x 8 ft. SSE R-10 XPS Rigid Foam Board Insulation and Cellulose Blown-In Insulation by Greenfiber are selected for comparison. For each type of material, thin 1.25cm by 0.75cm by 0.1cm pieces are cut. Sandpaper was used to ensure approximate uniformity of the thickness of each sample. For the SRLI and XPS samples, the pieces are taken from the top surface of the materials. A small sample of approximately similar size was selected for the cellulose insulation.

#### 6.2.5 Laser Flash Analysis

The laser flash Analysis via Linseis XFA 500 is used for thermal diffusivity measurements, as shown in **Figure 6-2A**. The Linseis XFA 500 uses a xenon flash to heat the sample from one end with a controlled energy pulse. A high-speed infrared detector measures the temperature increase at the opposite surface. We recorded the temperature rise curve over time, showing the sample temperature change caused by the xenon flash. By applying mathematical models and known parameters, this method calculates thermal diffusivity, providing essential information about the thermal properties of the materials over various temperature ranges. Here, we prepared 6 different mycelium species: *P. eryngii*, *G. lucidum*, *T. versicolor*, *F. velutipes*, *P. ostreatus*, and *G. resinaceum*. We inoculated the liquid mycelium on the agar plate and put them into the climate chamber for 7-14 days for growth. To get the dry

mycelium membrane, we used a dehydrator (60 °C and 4 hours) to remove the water from all the samples. The mycelium membrane can be easily torn off from the dry samples. All the samples are tailored in a 0.5-inch diameter disk shape—a graphite spray coated on both sides of the tailored samples to minimize pulse reflection. **Figure 6-2B** shows the sample after cutting and after spraying graphite. Then, the samples are mounted on the sample holder and measured thermal diffusivity at 20°C. The thermal diffusivity values are taken when the mathematical model and measured curves are fit. After the curves start fitting, the measurements are conducted 3 to 5 times per sample.

#### **6.2.6 Differential Scanning Calorimetry**

TA Instruments Differential Scanning Calorimeter (DSC) Auto 2500 is used for heat capacity measurements. DSC involves a single furnace where the sample and reference undergo a controlled heat-cool-heat cycle. Approximately 2-3 mg of the sample, placed in an aluminum pan, and an empty reference pan are positioned on a thermoelectric disk within the furnace. Heat is transferred to both the sample and the reference as the furnace temperature changes at a constant rate of 10°C per minute. Area thermocouples measure the differential heat flow. The heat flow amplitude comprises a heat capacity component and a kinetic component.

#### **6.2.7 Thermal Conductivity Calculation**

The sample's thermal conductivity was determined by multiplying thermal diffusivity, heat capacity, and density. To get a more accurate sample thickness, we place the mycelium vertically next to a stack of paper of similar height, and then we use the microscope to take

pictures to record the mycelium. We also drew a scale bar with 1 mm on the paper, which allowed us to use Image J to measure the thickness of the mycelium membrane, as shown in **Figure 6-2C**. We estimate that the area for all samples is the diameter of 12.7 mm round. The density is calculated through  $\rho_t = m/V$  by accurately measuring the mass ( $m$ ) and volume ( $V$ ) of the disk-shaped samples for the laser flash.

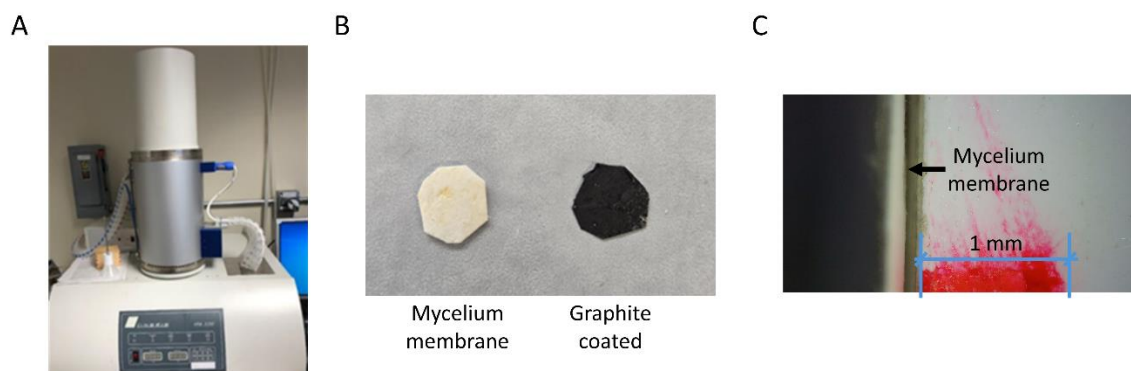


**Figure 6-2.** **A.** The experimental setup with the spectrometer is used for thermal conductivity measurements. **B.** Comparative visual of untreated mycelium membrane and graphite-coated mycelium membrane. **C.** Cross-sectional microscopy image of the mycelium membrane.

### 6.2.8 Dog bone samples preparation

There are three steps to prepare the mycelium-based bio-composite material. We first cultured the spore on agar substrate for 7 days before cutting them into small pieces. The second step is called grain spawn—the general process shown in **Figure 6-3**. We selected rye as the substrate to prepare the material since it has good water absorption capacity and nutritional benefits for mycelium growth. The rye is thoroughly washed and soaked in water for a specified period to hydrate, after which they are boiled and steamed to achieve sterilization,

eliminating unwanted microorganisms. Post-cooking, the grains are dried to remove excess moisture, a critical step to prevent the growth of contaminants. The sterilized grains are then evenly distributed into glass jars, leaving adequate space for mycelial expansion. We put one layer of rye and some small pieces of mycelium agar plate and repeated this operation several times. Each jar is fitted with a filter of polytetrafluoroethylene (PTFE) 0.22  $\mu\text{m}$  that allows for gas exchange while preventing the entry of contaminants. The inoculated jars are then stored in the green tent where temperature and humidity are 24°C and 98RH% by the mycelium to facilitate the colonization of the grains.

After 7 days, the mycelium is fully grown in the glass jar. We perform the last step, bulk substrate preparation; the detailed processes are shown in **Figure 6-3**. Here, we use the coco-coir, which is coconut fiber and oak wood chips, as the substrate and wheat bran as the nutrition. Coco-coir, a fibrous material derived from the outer husk of coconuts, is known for its water retention capabilities. The oak wood chips can provide additional nutrients and structural support for the developing mycelium. The coco-coir and oak wood chips are hydrated with boiling water and autoclaved, ensuring they are thoroughly soaked to achieve the desired moisture content and eliminate unwanted microorganisms. Then, the materials are allowed to cool to a safe handling temperature and mixed with the wheat bran to ensure an even distribution of moisture and nutrients. The mixed substrate is then loaded into sterilized bags, and here, we use the semi-permeable polypropylene bag with a microporous filter patch. The filter can allow mycelium to breathe when they are growing. We put one layer of the bulk substrate and some mycelium rye on it and repeated several times. Then, we used a zip

tie to seal the bags. The inoculated bags are then stored in the green tent where temperature and humidity are 24°C and 90RH% by the mycelium to facilitate the colonization of the grains for 14 days.

Once the mycelium fully occupied the culture bag, we use the same processing method in our previous publication to make the dog bone shape samples [318]. We take raw materials into a blender, add water, and blend the mixture until it becomes mushy. Next, we place a portion of the mixture in an aluminum dog-bone shape mold and compress the upper layer of the mold against the bottom layer by using a 10-ton heat press machine with the hydraulic hand pump, as shown in **Figure 6-3**, to perform the heat press and make the dog bone samples. The remaining mixture is stored in a sterilized plastic box in the refrigerator to keep it at a lower temperature before the heat press.

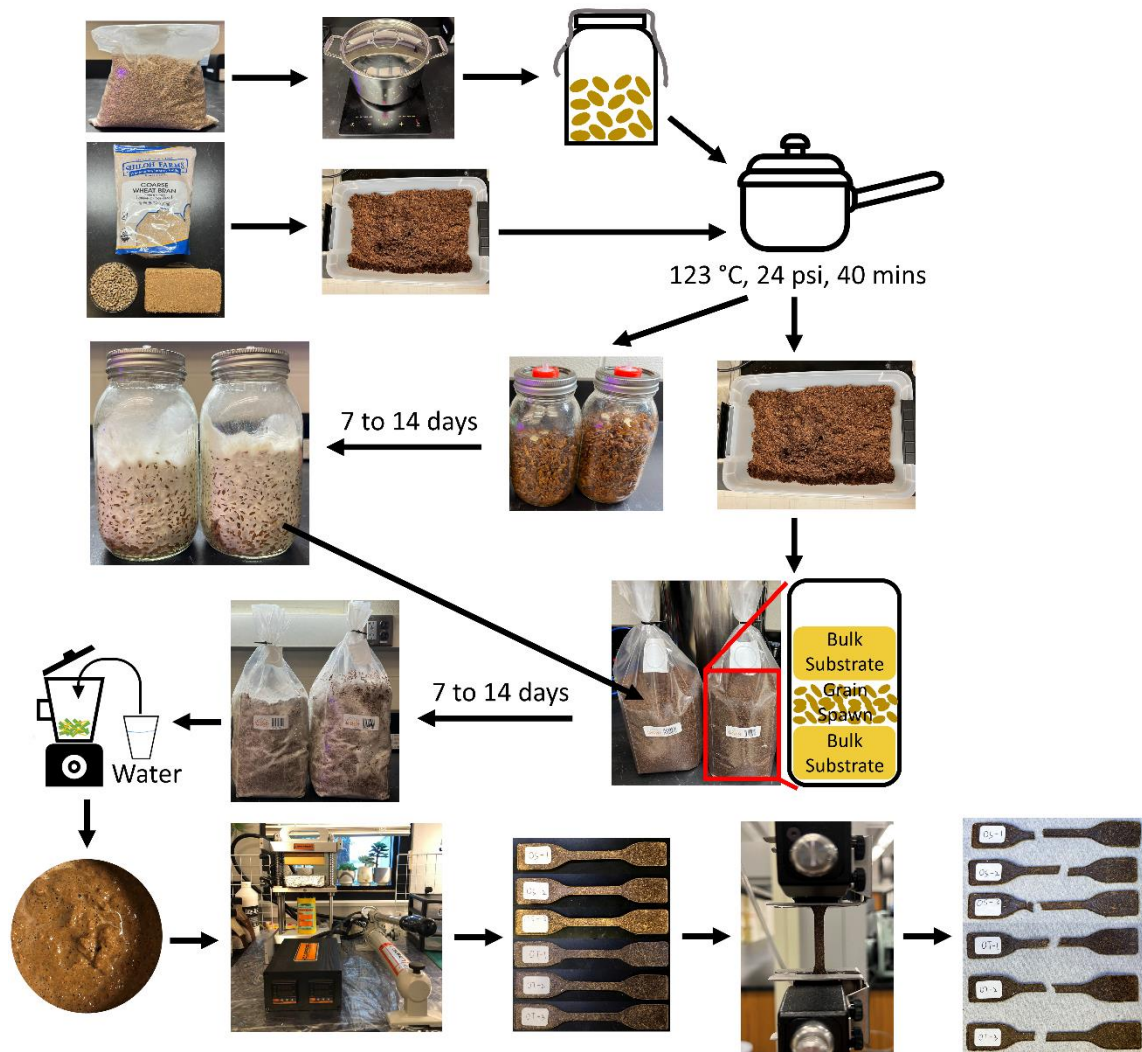


**Figure 6-3.** The general process of making the dog bone shape samples. Preparing the rye mycelium culture first, then inoculating it with the composite material to make the mycelium-based bio-composite bag for making the food bone shape samples. The dog bone samples shown in the figure are made with coir and oak wood with wheat as the nutrition based on different treatment conditions (material/mixed with water / mushy material / heat-press machine/test samples / Instron machine / broken samples).

### 6.2.9 Mycelium based bio composite bricks preparation

We use the coco-coir, which is coconut fiber, as the substrate and malt and yeast liquid

nutrition to support mycelium growth. The general process is shown in **Figure 6-4**. Coco-coir, a fibrous material derived from the outer husk of coconuts, is known for its water retention capabilities. The coco-coir is hydrated with boiling water and autoclaved, thoroughly soaked to achieve the desired moisture content and eliminate unwanted microorganisms. Then, the materials are allowed to cool to a safe handling temperature and mixed with liquid nutrition to ensure an even distribution of moisture and nutrients.

Here, we prepared two different amounts of liquid nutrients, which are 16 g malt with 8 g yeast with 100 ml water and 24 g malt with 12 g yeast with 100 ml water. To compare how different amounts of nutrition can affect the mycelium growth rate and mechanical properties. We use the acrylic sheet to make a model to prepare the mycelium-based bio-composite brick. Two different molds are prepared. The larger mold size is 15 mm in length by 15 mm in width and 5 mm in height. We cut 12 pieces of shapes 30 mm in length by 5 mm in width from the acrylic sheet to create the mold for preparing the small bricks. To connect each piece of acrylic sheet, we cut a groove 1.5 mm width by 2.5 mm length at 5 mm intervals for each piece. Once we connect each piece, we can get the mold's 5 x 5 cube shape. Each cube's length is 5 mm, width is 5 mm, and height is 5 mm. The mixed substrate is then loaded into each cube. We also prepared two different kinds of mycelium inoculation: rye mycelium culture and liquid mycelium culture. We first put one layer of the mixed substrate; for rye culture, we put 3 g cultured material; for liquid culture, we spray 3 ml cultured material. We repeat this processes three times to make the material fill a small cube. We use the semi-permeable polypropylene bag with a microporous filter patch. The filter can allow mycelium

to breathe when they are growing. Then, we used a zip tie to seal the bags. The inoculated bags are then stored in the green tent where temperature and humidity are 24°C and 90RH% by the mycelium to facilitate the colonization of the grains. We also set different growth periods to compare the different growth periods that can affect the mechanical properties of the bricks. Once the mycelium grows until the periods we set up, we use a dehydrator (60°C, 18 hours) to remove the water in the bricks.

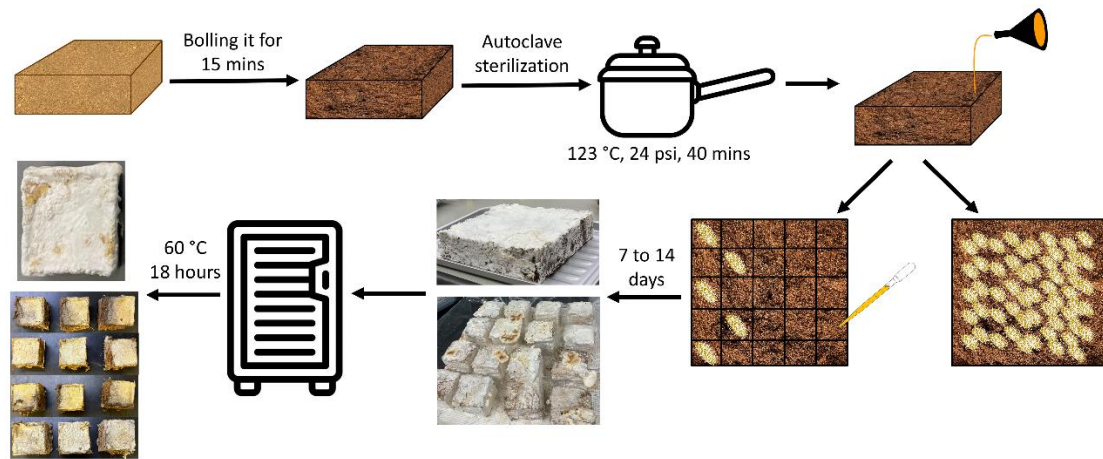


**Figure 6-4.** The general process of preparing the mycelium-based bio-composite brick. We use two different mycelia inoculated coir, rye mycelium culture and liquid mycelium culture, and two different molds, which are 1 larger square mold and a 5 X 5 small square mold.

### 6.2.10 Compression Test

We perform the compression tests on each brick sample with an Instron 5966 machine (10 kN static load cell) to obtain its stress-strain curves in tension. We measure the initial sample length as the distance between the edges of the two plates as  $L_0$  before the test. During our tests, the lower plate is fixed, and the upper plate moves at a constant displacement speed of

$v = -2 \text{ mm/min}$ . The traveling distance of the upper plate is given by  $d$  at any time after the test starts, updated every 0.02 seconds, and the engineering strain of the sample is defined by  $\varepsilon_c = d/L_0$ . The load cell records the loading force  $f_c$  and computes the engineering stress with  $\sigma_c = f_c/A_0$ , where  $A_0$  is the initial middle part cross-section area of the testing region of the brick sample. We use the  $\varepsilon_c - \sigma_c$  data from  $\varepsilon_c = 0$  to  $\varepsilon_c = 0.002$  to perform the linear fitting and measure the slope of the fitting curve to calculate elastic modulus ( $E_c$ ). We use the equation of  $\sigma_{c0.2\%} = (\varepsilon_c - 0.002)E_c$  to draw the linear function. The intersection between the linear function and the  $\varepsilon_c - \sigma_c$  curve is the 0.2% yield stress. We measure the area under the stress-strain curve to obtain the toughness modulus ( $U_c$ ).

## 6.3 Results and Discussion

### 6.3.1 Surface Flammability

A preliminary flammability test was performed on three materials to determine the surface flammability: SRLL (mycelium composite), cellulose, and EPS Foam (XPS). As can be seen in **Figure 6-5A**, the 3 SRLL samples exhibited burnt areas of 651.23 mm<sup>2</sup> (S1), 1052.66 mm<sup>2</sup> (S2), and 1054.30 mm<sup>2</sup> (S3), respectively. Notably, no depth penetration was recorded, and none of the samples ignited. This indicates a relatively good resistance to burning and limited damage to the material's integrity.

The 3 cellulose samples showed burnt areas of 1785.17 mm<sup>2</sup> (S1), 2095.93 mm<sup>2</sup> (S2), and 1258.93 mm<sup>2</sup> (S3) respectively. All samples showed a penetration depth of 5 mm and ignited upon exposure to the flame. This indicates a higher susceptibility to burning and deeper

damage penetration than the SRLl sample. The 3 XPS (EPS) samples had the largest burnt areas of 2769.45 mm<sup>2</sup> (S1), 2263.63 mm<sup>2</sup> (S2), and 2629.85 mm<sup>2</sup> (S3) respectively. Depths penetrated were 16.69 mm, 15.45 mm, and 18.1 mm, respectively. No ignition was observed. Despite the absence of ignition, the significant burnt area and depth penetration suggest that EPS Foam is highly flammable and sustains considerable damage.

The flammability test results highlight significant differences in the performance of the tested materials. The SRLl demonstrated superior fire resistance, with the most minor burnt areas, no depth penetration, and no ignition in any samples. The material should be classified as B1 according to EN 13501–1. This suggests that mycelium insulation materials can effectively limit the spread of flames and maintain structural integrity during fire exposure, making it a promising candidate for fire-resistant insulation. In contrast, although partially ignitable, cellulose exhibited more severe damage and larger burnt areas, indicating a higher risk of fire spread and damage. EPS displayed the poorest performance, with the largest burnt areas and substantial depth penetration, reflecting its high flammability and potential for severe fire damage. Overall, the mycelium bio-composite outperforms existing insulation materials like EPS and cellulose regarding fire resistance, making it a safer and more reliable choice for applications where fire safety is a critical concern.

### **6.3.2 Surface Wettability**

Water contact angle (WCA) measurements were taken to determine the surface wettability of the materials. As shown in **Figure 6-5B**, the WCA value for the SRLl sample was

approximately 133°, indicating a hydrophobic nature since values greater than 90° denote hydrophobicity. In contrast, the WCA for the XPS sample was 89.2°, aligning closely with literature values of 90-92°, suggesting a borderline hydrophobic/hydrophilic nature. The cellulose sample exhibited complete wetting, with a WCA of 0°, indicating the highest wettability among the tested materials. These results demonstrate that the SRLL (mycelium) sample possesses the lowest wettability, followed by XPS and cellulose. This is consistent with the expectation that lower WCA values correspond to higher wettability. The pronounced hydrophobicity of the SRLL sample could be advantageous in applications requiring moisture resistance. The XPS sample's near-neutral wettability can balance hydrophobic and hydrophilic properties that are suitable for various insulation contexts. The cellulose sample's complete wetting behavior confirms its hydrophilic nature, suggesting its suitability for applications where moisture absorption is beneficial. These findings highlight the distinct wettability characteristics of mycelium-based insulation compared to conventional materials, emphasizing its potential for specific environmental applications.

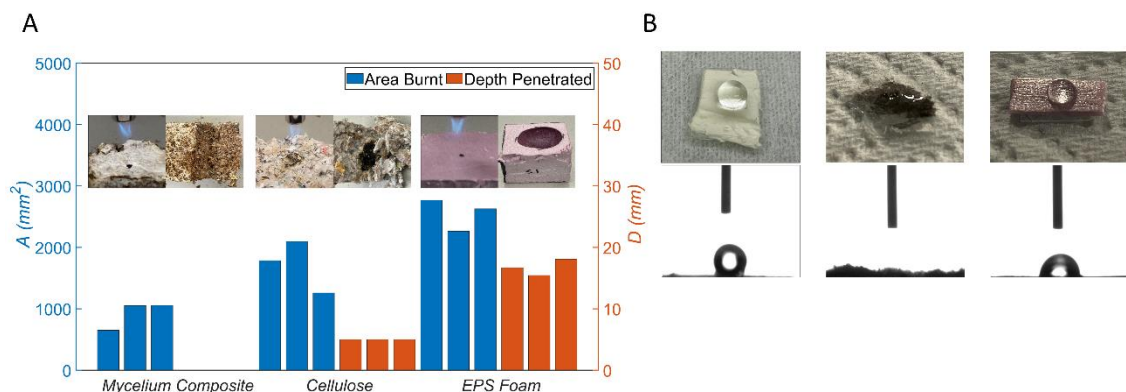


**Figure 6-5. A.** Comparative analysis of fire resistance properties among different materials, represented in terms of area burnt and depth penetrated. The graph illustrates experimental

results for three material categories: mycelium composite, cellulose, and EPS foam. The blue bars indicate the total area burnt during the test, while the orange bars represent the depth to which the fire penetrated each material. Insets show close-up images of each material post-burn, highlighting the physical impact of fire exposure. **B.** Contact angle tests on three different material samples. The top row displays the initial interaction of water droplets with each material—left to right: mycelium composite, cellulose, and EPS foam. The lower row images capture the droplet profiles at rest, demonstrating the contact angles of the surfaces. These images illustrate the varying hydrophobic properties of each material, with the mycelium composite and EPS foam showing significant water resistance compared to the more absorbent cellulose.

### 6.3.3 Mycelium membrane thermal conductivity

The thermal conductivity of the six different species of mycelium membranes at 20°C was calculated by multiplying three components: thermal diffusivity, heat capacity, and density. As shown in **Figure 6-6A**, most mycelium membranes exhibit a thermal diffusivity ( $\alpha$ ) of approximately  $2 \times 10^{-8} \text{ m}^2/\text{s}$ , significantly lower than typical polymers [319]. However, two species, *F. velutipes* and *G. resinaceum*, display a thermal diffusivity three times higher than the others, though still much lower than typical polymers [319]. The measured density ( $\rho_t$ ) of the mycelium membranes, depicted in **Figure 6-6B**, is generally less than  $1 \text{ g/cm}^3$ , which is substantially denser (by a factor of  $\approx 10$ ) than other insulation materials such as cellulose fiber and extruded polystyrene (XPS) [320]. The heat capacity ( $C$ ) of the mycelium membranes is around  $0.9 \text{ J} \cdot \text{g}^{-1} \cdot \text{K}^{-1}$  for all species, as illustrated in **Figure 6-6C**. This

value is comparable to the heat capacity of XPS but is half that of cellulose fiber [320]. By combining these three components, the thermal conductivity ( $K$ ) of the mycelium membranes was determined, as shown in **Figure 6-6D**. Most species exhibit a thermal conductivity of approximately  $0.02 \text{ W} \cdot \text{m}^{-1} \cdot \text{K}^{-1}$ , except for the *F. velutipes* species, which have a thermal conductivity of about  $0.06 \text{ W/m-K}$ . The reason for this difference in the thermal conductivity of F.V. species is the error in the thickness measurement. The method we used to measure the sample thickness can only measure the edge of the membrane. The central thickness of the sample may be very different from the edge. So, if the central part of the sample is thinner than the edge, it can cause the density calculation to become too small and affect the thermal conductivity results. Compared to typical insulation materials with thermal conductivities of  $0.04 \text{ W} \cdot \text{m}^{-1} \cdot \text{K}^{-1}$  for cellulose fiber and  $0.033 \text{ W} \cdot \text{m}^{-1} \cdot \text{K}^{-1}$  for XPS, most mycelium species demonstrate significantly lower thermal conductivity. Moreover, to compare our mycelium membrane thermal properties with the current insulation material, we calculate the specific thermal resistance, the R-value. **Table 6-1** summarizes the thermal resistance of various mycelium membranes (P.E., G.L., T.V., F.V., P.O., G.S.) alongside conventional construction materials such as Basswood, Plywood, Drywall, and EPS board. Notably, mycelium materials show 2 to 3 times the R-value of traditional insulation materials, which means they have good insulating properties. The species we use to prepare the mycelium composite brick, G.L., has the highest R-value of  $10.47 \text{ inch} \cdot \text{k/W}$ . The differences in specific thermal resistance show the potential of mycelium material to offer thermal insulation compared to many conventional materials. However, the relatively low thickness of the pure mycelium material compared to traditional materials suggests that, while they

provide good thermal resistance, their application may need to be optimized regarding material volume and layering techniques.

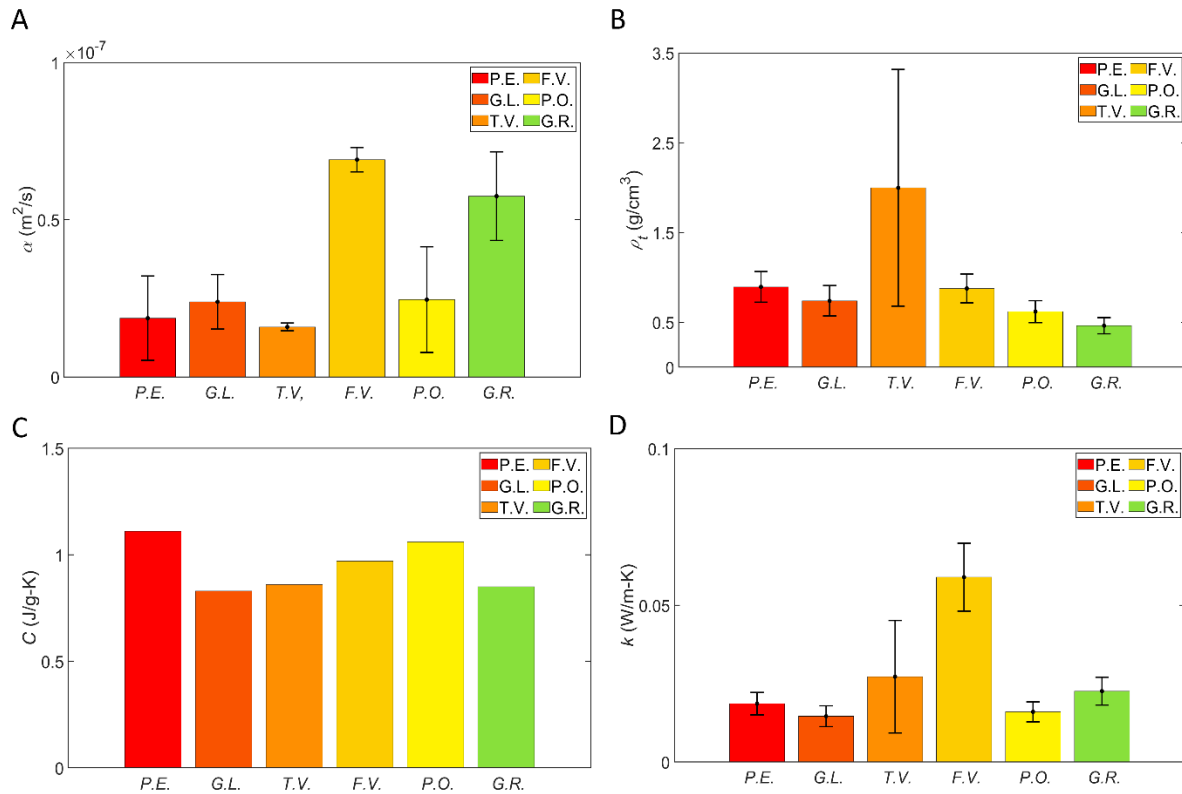


**Figure 6-6.** Graphical representation of the experimental data showing: **A.** thermal diffusivity ( $\alpha$ ), **B.** mycelium membranes density ( $\rho_t$ ), **C.** heat capacity ( $C$ ), and **D.** thermal conductivity ( $K$ ) of various mycelium species.

**Table 6-1.** Compares the thermal resistance (R-value), thickness, and specific thermal resistance of different pure mycelium materials (P.E., G.L., T.V., F.V., P.O., G.S.) and conventional construction materials (Basswood, Plywood, Drywall, EPS board). The R-value is presented in both metric ( $\text{m}^2\cdot\text{K}/\text{W}$ ) and imperial ( $\text{ft}^2\cdot^\circ\text{F}\cdot\text{h}/\text{BTU}$ ) units. Specific thermal

resistance is given in metric ( $m \cdot K/W$ ) and imperial ( $inch \cdot K/W$ ) units, demonstrating the effectiveness of each material in providing thermal insulation.

<b>Material type</b>	<b>R value (<math>m^2 \cdot k/W</math>)</b>	<b>R value (<math>ft^2 \cdot ^\circ F \cdot h/BTU</math>)</b>	<b>Thickness (<math>m</math>)</b>	<b>Specific thermal resistance (<math>m \cdot k/W</math>)</b>	<b>Specific thermal resistance (<math>R/inch</math>)</b>
<b>P.E.</b>	0.00270	0.01533	$5.02 \cdot 10^{-5}$ $\pm 0.008$	53.78	7.76
<b>GL</b>	0.00325	0.01848	$4.74 \cdot 10^{-5}$ $\pm 0.011$	68.66	9.91
<b>T.V</b>	0.00083	0.00474	$2.27 \cdot 10^{-5}$ $\pm 0.012$	36.75	5.30
<b>F.V</b>	0.00084	0.00475	$4.93 \cdot 10^{-5}$ $\pm 0.009$	16.96	2.45
<b>P.O</b>	0.00586	0.03327	$9.40 \cdot 10^{-5}$ $\pm 0.018$	62.33	8.99
<b>G.S</b>	0.00339	0.01924	$7.66 \cdot 10^{-5}$ $\pm 0.016$	44.23	6.38
<b>Basswood</b>	0.2934	1.6659	0.0127	23.10	3.33
<b>Plywood</b>	0.1682	0.9549	0.0064	26.49	3.82
<b>Drywall</b>	0.1450	0.8235	0.0064	22.84	3.29
<b>EPS board</b>	0.8806	5.0000	0.0254	34.67	5.00

Mycelium membranes consist of biopolymers from fungi, such as cellulose, lignin, and pectin [185]. They have inherently low thermal conductivity and do not conduct heat as efficiently as cellulose fiber and polystyrene. Furthermore, their lower density and porous structures (thread- and tube-like structures) create numerous tiny air pockets within the material [23], [321]. These air pockets reduce the ability of heat to pass through, similar to how the trapped air in materials like foam works as an insulator. These unique properties of mycelium membranes result in low thermal conductivity and can be used as potential insulation material. Mycelium membranes comprise biopolymers such as cellulose, lignin, and pectin derived from fungi. These biopolymers inherently possess low thermal conductivity and are less efficient at conducting heat than cellulose fiber and polystyrene. Additionally, mycelium

membranes have lower density and porous structures, characterized by thread- and tube-like formations, that create numerous tiny air pockets within the material [23], [321]. These air pockets function as insulators, impeding heat transfer like the trapped air in foam materials. These unique properties of mycelium membranes result in their low thermal conductivity, making them a promising candidate for insulation applications.

#### **6.3.4 Tensile test results**

To investigate the treatment conditions from our previous machine-learning results and whether they can make the mycelium-based bio-composite material achieve high mechanical properties, we chose the treatment conditions of specific ultimate stress and specific toughness from the ‘stalk with mycelium.’ The suffix of the original specific ultimate stress (OS) and original specific toughness (OT) shows that the baking time and pressure decreased and increased by 50 % ( $t \pm 50$  and  $p \pm 50$ ), as shown in the first column in **Table 6-1**, to make our validation more accurate. We do not change the baking temperature because the temperature prediction is always around 90. Following the previous method, we made the samples, measured the bulk density, and performed the tensile test on each sample with an Instron machine. **Figure 6-7A** summarizes the stress-strain curves of mechanical samples from different treatment conditions. It is shown that all the mechanical samples reach the ultimate tensile strength ( $\sigma_t$ ), as the maximum stress, before the 1% strain, followed by a tail that accounts for energy dissipation during the failure.

We discovered that changing the treatment conditions can significantly affect the ultimate strength. We measure the density of each sample ( $\rho$ ) and compute Young's modulus ( $E_t$ ) and modulus of toughness ( $U_t$ ) for each of the samples, as shown in **Table 6-1**. For each treatment condition, we have 3 samples to prove statistical reliability and reproducibility. It is shown that  $\sigma_t = 12.47 \text{ MPa}$  provided by OS is the largest ultimate strength, and  $U_t = 0.059 \text{ J/m}^3$  provided by OT is the largest toughness. However, our machine learning results suggested that the specific mechanical properties should achieve the maximum results.

**Figure 6-8 A** summarizes the specific mechanical properties of all the samples. The highlighted red sections show that OS gives the maximum average specific ultimate stress  $\frac{\sigma_t}{\rho} = 8.67 \pm 0.39 \text{ J/g}$  and OT gives the maximum average specific toughness  $\frac{U_t}{\rho} = 0.04 \pm 0.012 \text{ J/g}$ , conforming with machine learning results. With the OS treatment condition, the sample becomes more brittle. After the samples reached the ultimate stress, they all lost the ability to contain any force. Due to that, the OS treatment condition does not give in to high toughness, and the stress-strain curve shows a short tail, as shown in **Figure 6-7A**. For the samples made by the treatment condition that changes based on the OS, OSt+50 and OSp-50 give the lowest average specific ultimate stress. For the samples made by the treatment condition that changes based on the OT, OTt+50 and OTp-50 give the lowest average specific toughness. It is shown that an increase in time and a decrease in pressure can reduce mechanical properties. The baking time and pressure can relate to the fiber strength. The long baking time can break down the fiber, and the stiffness could decrease as the fibers become brittle. The short time press cannot align the fibers in one direction, which reduces the strength and stiffness in the tension direction.

**Table 6-2.** Mechanical properties and density are obtained from each tested sample.

Treatment Conditions	T (°C)	P (MPa)	H (hours)	$\rho$ (g/cm <sup>3</sup> )	$\sigma_{tu}$ (MPa)	$E_t$ (MPa)	$U_t$ (J/m <sup>3</sup> )
OS	88	28.11	9.8	1.42	12.47	3200.5	0.043
				1.37	12.45	2268.7	0.050
				1.35	10.99	2314.9	0.052
OT	91	22.69	7.5	1.48	10.60	2624.9	0.066
				1.50	10.63	2560.3	0.037
				1.42	10.93	2711.4	0.074
OSt-50	88	28.11	4.9	1.45	9.66	2685.4	0.032
				1.33	9.58	2335.3	0.036
				1.32	9.37	2114.0	0.062
OTt-50	91	22.69	3.75	1.31	6.24	1399.7	0.030
				1.32	6.36	1615.5	0.030
				1.27	6.90	1876.1	0.044
OSt+50	88	28.11	14.7	1.47	8.06	2189.7	0.039
				1.38	8.06	2062.0	0.030
				1.44	8.39	2345.5	0.024
OTt+50	91	22.69	11.25	1.40	4.40	1324.1	0.017
				1.47	4.73	1466.2	0.045
				1.42	4.31	1343.9	0.016
OSp-50	88	14.05	9.8	1.51	7.29	2699.1	0.015
				1.35	7.38	1782.5	0.043

				1.38	7.72	2117.0	0.037
OTp-50	91	11.35	7.5	1.21	3.61	1308.8	0.023
				1.11	3.86	1487.9	0.027
				1.38	3.76	1458.4	0.015
OSp+50	88	42.17	9.8	1.39	9.33	2164.5	0.049
				1.46	10.09	2346.4	0.042
				1.41	9.98	2553.9	0.029
OTp+50	91	34.04	7.5	1.40	5.61	1513.1	0.019
				1.46	5.82	1660.5	0.035
				1.38	5.84	1444.2	0.050

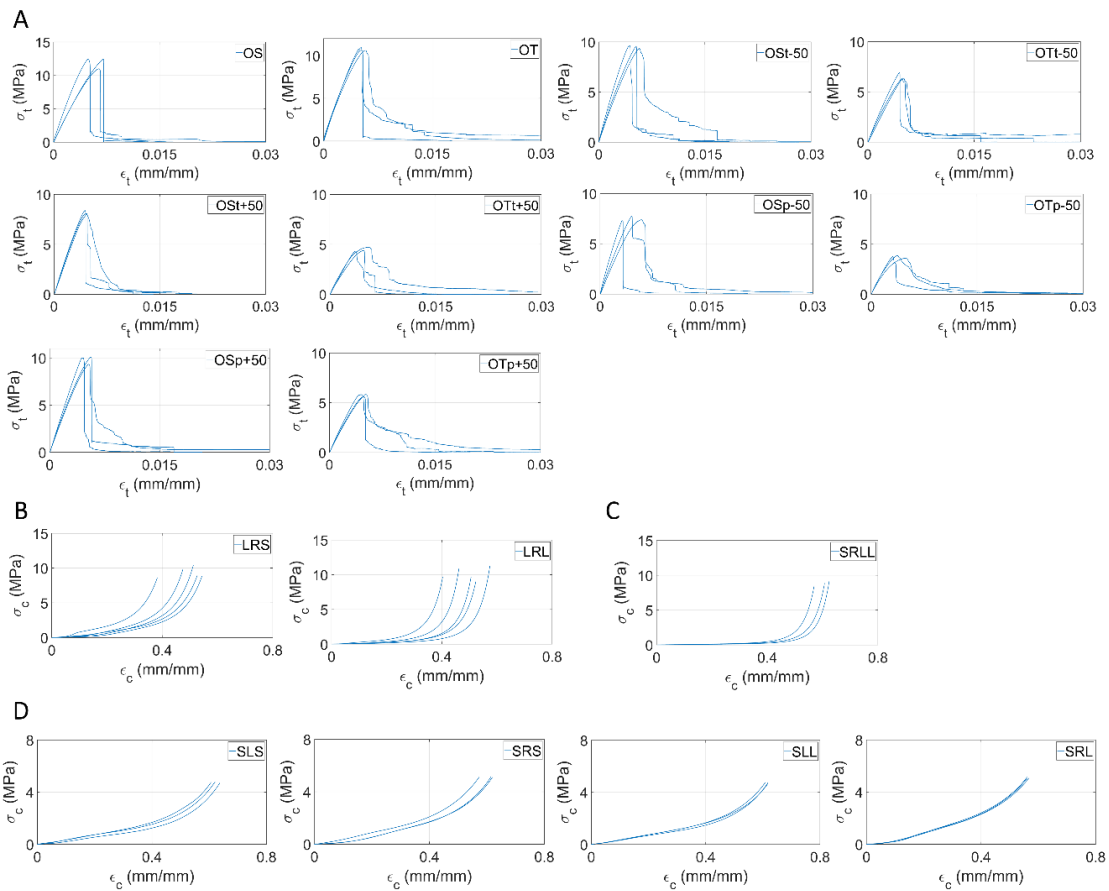


**Figure 6-7. A.** Stress-strain curves for various dog bone shape samples under different treatment conditions. The treatments include the original specific ultimate stress (OS), the original specific toughness (OT) with a baking time increase and decrease of 50% (t+50 and t-50), and pressure increase and decrease of 50% (p+50 and p-50). Showing how the different treatment conditions affect the mechanical behavior of the materials. **B.** Stress-strain curves for mycelium-based bio-composite bricks that are prepared by inoculating coir by using rye mycelium culture and 2 different amounts of nutrition concentrations in the larger square mold for 2 weeks. (L: larger mold, R: rye mycelium culture, S: low nutrition concentration, and L: high nutrition concentration). **C.** Stress-strain curves for mycelium-based bio-composite bricks that are prepared by inoculating coir using rye mycelium culture and a concentration of nutrition in the small square mold for 4 months. (S: small mold, R: rye mycelium culture, L: high nutrition concentration, and L: longest growth time). **D.** Stress-strain curves for mycelium-based bio-composite bricks that are prepared by inoculating coir by using 2 different mycelium cultures and 2 different amounts of nutrition concentrations in the small square mold for 1 week. (S: small mold, R: rye mycelium culture, L: liquid mycelium culture, S: low nutrition concentration, and L: high nutrition concentration). B, C, and D show how the different growth periods, forming mold shape, mycelium culture source, and nutrition concentration affect the mechanical behavior of the materials.

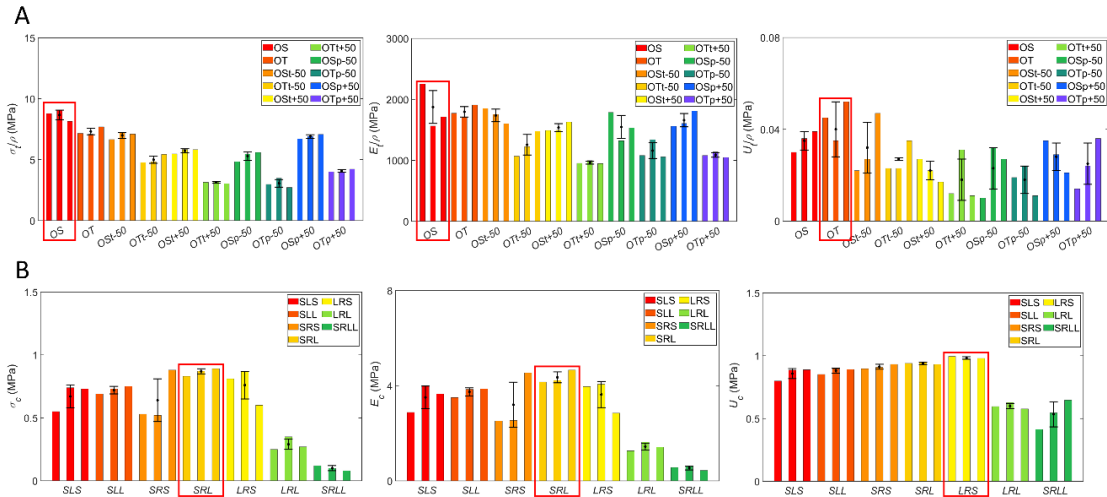


**Figure 6-8.** Comparison of mechanical properties under different treatment conditions. **A.** shows the specific ultimate strength ( $\sigma_t/\rho$ ), specific Young's modulus ( $E_t/\rho$ ), and specific toughness ( $U_t/\rho$ ) for dog bone shape samples based on various treatments labeled OS, OT, and combinations with  $t \pm 50$  and  $p \pm 50$  suffix. Error bars are given for the standard deviation of each mechanical property. The highlighted sections in red indicate the maximum average results. **B.** shows the 0.2% yield strength ( $\sigma_c$ ), elastic modulus ( $E_c$ ), and toughness ( $U_c$ ) for the mycelium-based bio-composite bricks based on different processing methods labeled SLS, SLL, SRS, SRL, LRS, LRL, and SRL. Error bars are given for the standard deviation of each mechanical property. The highlighted sections in red indicate the maximum average results.

### 6.3.5 Compression test results

We perform the compression test on each sample with an Instron machine to understand the effects of different preparations on the mechanical properties of the composite materials.

**Figures 6-7 B, C, and D** summarize the stress-strain curves of mechanical samples of

different growth periods, forming mold shape, mycelium culture source, and nutrition concentration (abbreviations of each sample are explained in the caption of **Figure 6-7**). It is shown that all the mechanical samples initially withstand increasing loads but rapidly lose strength upon reaching a critical stress level. For all samples, it is shown that most of the 0.2 yield strength increases with the growth periods of up to 1 week as more mycelium matures and combines with the substrate, leading to a more compact solid material. On the other hand, a culture longer than 1 or 2 weeks yields weaker samples, as the long-time growth, the mycelium can break the cellulose to reduce the strength of the whole composite sample.

We found that the different preparations can significantly affect the mechanical properties. We compute 0.2 % yield strength (0.2 %  $\sigma_c$ ), elastic modulus ( $E_c$ ), and modulus of toughness ( $U_c$ ) (see Method part) for each of the samples (raw data for all the samples in **Table 6-2** in the Supporting Material). **Figure 6-8 B** summarizes all the data and shows each mechanical property's average and standard deviation. Compared with the sample that grows in the same period, it is shown that  $0.2 \% \sigma_c = 0.87 \pm 0.02 \text{ MPa}$  and  $E_c = 4.66 \pm 0.23 \text{ MPa}$  provided by SRL is significantly larger than other samples in the 1-week growth period. We suggest using the mycelium rye culture and high nutrition concentration, which can lead to higher yield strength and elastic modulus. The mycelium growth from rye is more mature and more robust than the mycelium spor from liquid culture since the mycelium spor liquid culture needs more time to grow to the strong fibers. Moreover, the high nutrition concentration can accelerate mycelium growth and provide more nutrition to help mycelium form a strong fiber.

We believe that SRL gives the highest 0.2 %  $\sigma_c$  and  $E_c$  mainly because of the higher content of mycelium, as the mycelium had already grown to occupy the substrate before our tests fully. It is also noticed that compared to the 0.2 %  $\sigma_c$  and  $E_c$ , each sample does not differ much from  $U_c$ . Mycelium can alter the microstructure of the composite by creating a porous yet interconnected matrix. These structural features can contribute to toughness by allowing the material to deform under stress without losing coherence. Compared with the sample growth for 4 months with 1 week, all the mechanical properties significantly decreased. The long-time culture makes the mycelium digest the cellulose and lignin to weaken the mechanical properties of the composite.

**Table 6-3.** Mechanical properties are obtained from each tested sample.

<b>Growth Period</b>	<b>Forming Mold Shape</b>	<b>Mycelium Culture Source</b>	<b>Nutrition Concentration</b>	<b>Sample Name</b>	<b>0.2% <math>\sigma_{cy}</math> (MPa)</b>	<b><math>E_c</math> (MPa)</b>	<b><math>U_c</math> (J/m<sup>3</sup>)</b>
1 week	5 X 5 small square	liquid	16 g malt with 8 g yeast	SLS-1	0.55	2.88	0.799
				SLS-2	0.74	4.00	0.887
				SLS-3	0.73	3.66	0.888
			24 g malt with 12 g yeast	SLL-1	0.69	3.50	0.852
				SLL-2	0.73	3.85	0.895
				SLL-3	0.75	3.87	0.892
		rye	16 g malt with 8 g yeast	SRS-1	0.53	2.52	0.896
				SRS-2	0.52	2.54	0.908
				SRS-3	0.88	4.54	0.932

			24 g malt with 12 g yeast	SRL-1	0.83	4.16	0.940
				SRL-2	0.87	4.22	0.948
				SRL-3	0.89	4.66	0.931
2 weeks	1 X 1 large square	rye	16 g malt with 8 g yeast	LRS-1	0.81	3.96	0.995
				LRS-2	0.87	4.06	0.970
				LRS-3	0.60	2.85	0.980
			24 g malt with 12 g yeast	LRL-1	0.25	1.26	0.597
				LRL-2	0.35	1.63	0.627
				LRL-4	0.27	1.42	0.577
4 months	5 X 5 small square	rye	24 g malt with 12 g yeast	SROLL-1	0.12	0.56	0.413
				SROLL-2	0.10	0.62	0.545
				SROLL-3	0.08	0.44	0.646

## **CHAPTER 7. CONCLUSION AND RECOMMENDATIONS**

## 7.1 Summary and Conclusion

The thesis investigates the potential of mycelium-based bio-composites as sustainable materials within the construction industry. Traditional construction materials, such as steel and concrete, face energy-intensive production's environmental and economic challenges and contribute significantly to carbon emissions. Mycelium is known for its dense, thread-like structure and ecological benefits, including its role in decomposing organic matter, and facilitating plant communication through its networks. Mycelium-based materials leverage the natural growth processes of fungi to create strong, lightweight, and biodegradable composites. By integrating mycelium with organic waste, such as agricultural byproducts or sawdust, these materials offer a sustainable alternative to conventional building materials and help in waste management. The process, akin to natural 3D printing, results in materials that can be shaped into various forms, offering versatility in applications ranging from insulation and structural components to furniture and packaging.

Their resistance to fire and insulating properties of mycelium-based materials makes them an attractive option for building applications. Moreover, the environmental benefits, including their composability and the absence of toxic chemicals, align with the growing global emphasis on sustainability. The scalability and efficiency of producing mycelium-based composites are notable, as they require minimal energy input and can be cultivated quickly. This aspect is crucial for their adoption in mainstream industries, where the demand for eco-friendly materials is rising. Mycelium composites' versatility, which can be tailored to specific needs by manipulating growth conditions and substrates, further enhances their

appeal.

In conclusion, the potential of these materials to address environmental challenges, reduce waste, and offer sustainable alternatives in various industries is immense. Based on the results of this study, the following conclusions can be drawn:

1. The thesis investigates the impact of substrate stiffness on mycelium growth, revealing that mycelium tends to grow faster on stiffer substrates. Through experiments involving different mycelium species and substrates with varied stiffness, the research demonstrates that mycelium concentrates on the surface of rigid substrates. In contrast, it penetrates softer ones, affecting the overall growth rate. This finding suggests that the physical properties of substrates, specifically their stiffness, play a crucial role in mycelium growth dynamics, offering insights that could be pivotal for optimizing the production of sustainable mycelium-based composites by potentially reducing manufacturing times and costs.
2. The thesis focuses on enhancing their mechanical properties by integrating experiments and machine learning. By cultivating mycelium *P. eryngii* on stalk fibers, which acts as a natural adhesive, the study demonstrates that mycelium strengthens the composite materials and allows for a more energy-efficient production process. The findings reveal that these mycelium-enhanced composites exhibit superior mechanical strength compared to those without mycelium, achieving an ultimate strength of up to 12.99 MPa and a Young's modulus of 3.66 GPa. Furthermore, machine learning models derived from experimental data provide optimized treatment

conditions, suggesting that lower temperatures, higher pressures, and shorter pressing times are conducive to higher strength and modulus in the composites. This research underscores the potential of mycelium-based materials in engineering applications, offering a sustainable alternative to traditional synthetic adhesives in wood composites.

3. The thesis focuses on constructing a lab-scale green tent environment to closely monitor and analyze mycelium growth under controlled temperature and humidity conditions. The green tent, equipped with thermal and moisture insulation, utilizes an Arduino chip for precise environmental data monitoring. This setup aims to explore the influence of various substrates on the microscopic morphology of mycelium fibers during growth. Initial findings suggest that hydrogel substrates, rich in soluble nutrients, are more conducive to mycelium growth than hardwood boards, leading to faster growth rates. Despite the differences in substrates, the diameter of mycelium fibers remained consistent at approximately 3  $\mu\text{m}$ . This research lays the groundwork for further investigation into mycelium growth mechanisms and seeks to develop environmentally friendly and efficient methods for cultivating mycelium-based materials.
4. The thesis explores the development and evaluation of mycelium-based bio-composite insulation materials as a sustainable alternative to conventional building materials. By cultivating *G. Lucidum* on coconut coir, the study produces mycelium composites that exhibit biodegradability, low embodied energy, and comparable thermal performance. Experimental tests demonstrate the mycelium composite's

superior fire resistance, hydrophobic properties, and mechanical strength. Moreover, different substrates and mycelium species are used to make the mycelium-based bio-composite material, coconut fiber, and *G. lucidum* to verify the machine-learning results. Using the heat press processing method and the treatment conditions resulting from machine learning, the results show that the sample made by the machine learning treatment condition results show the maximum mechanical properties.

## **7.2 Recommendations for Further Study**

In this dissertation, I have explored mycelium-based bio-composites' multifaceted applications and benefits, particularly in the construction industry. However, the research on mycelium-based materials is far from complete. A vast landscape of uncharted territories in this field beckons further exploration. One notable area for future study is optimizing mycelium growth conditions. While I have delved into the effects of substrate stiffness on mycelium growth, the influence of other environmental factors such as light exposure, CO<sub>2</sub> levels, and the presence of specific nutrients in the substrate could offer deeper insights into maximizing the efficiency and quality of mycelium-based materials.

The scalability of mycelium-based material production is another critical area that warrants more in-depth investigation. My dissertation touches upon scalability from a theoretical standpoint. Still, practical challenges remain in large-scale production, including maintaining consistent quality, reducing production costs, and developing efficient harvesting and processing techniques. Future studies could address these challenges by exploring innovative

bioreactor designs or automated harvesting systems.

Furthermore, mycelium-based bio-composites face limitations such as variable mechanical properties, susceptibility to environmental conditions, and degradation over time. These shortcomings require further research to enhance their durability, stability, and performance. Addressing these limitations could involve developing new composite formulations or hybrid materials that combine mycelium with other sustainable components to improve their mechanical and functional properties.

A significant direction for enhancing the mechanical properties of mycelium-based bio-composites lies in the development of novel reinforcement strategies. This could include incorporating natural fibers, nanoparticles, or bio-based additives into the mycelium matrix. These reinforcements can potentially increase the composites' strength, toughness, and overall mechanical performance. Additionally, investigating advanced processing techniques, such as hot pressing or freeze-drying, could help achieve a more uniform and dense structure, further enhancing the mechanical properties. Future research is crucial for making mycelium-based materials more competitive with traditional materials, broadening their application scope in demanding engineering contexts.

Another intriguing direction for further study involves integrating mycelium-based materials with intelligent technologies to create living, responsive materials. Imagine a scenario where mycelium composites could adapt to environmental changes, such as altering their porosity in

response to humidity levels or healing cracks when damaged. This could be achieved by embedding sensors or incorporating self-healing mechanisms within the mycelium matrix. Research in this area could lead to the development of dynamic, sustainable materials that reduce the environmental impact of construction and enhance the functionality and longevity of buildings.

Additionally, applying mycelium-based materials in fields beyond construction, such as packaging, textiles, and filtration media, offers a broad spectrum for future research.

Investigating the suitability of mycelium materials in these diverse applications could open new markets and further enhance the sustainability of various industries. This could involve interdisciplinary research, combining insights from material science, biology, and industry-specific knowledge.

Lastly, the environmental impact of mycelium-based materials throughout their lifecycle, from production to disposal, is an area that deserves more attention. While mycelium is inherently sustainable, understanding the total environmental footprint, including any potential unintended consequences of large-scale adoption, is crucial. Future studies could employ lifecycle assessment (LCA) methodologies to provide a comprehensive view of the sustainability of mycelium-based materials.

In conclusion, while this dissertation lays the groundwork for understanding and utilizing mycelium-based bio-composites, the path forward is filled with opportunities for innovation

and discovery. Each of these recommended areas for further study promises to advance our knowledge and application of mycelium and contribute to the broader goal of sustainable development and environmental conservation.

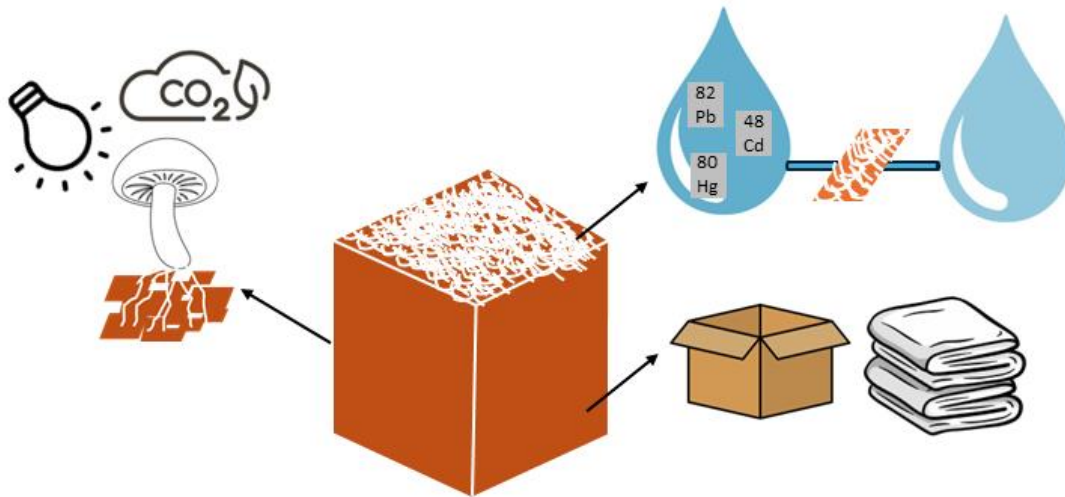


**Figure 7-1.** Future study directions for mycelium materials and mycelium-based bio-composites focus on their applications in packaging, textiles, and filtration media. It also highlights the importance of investigating the effects of light, CO<sub>2</sub> levels, different mycelium species, and substrate types on mycelium growth and its mechanical properties.

## References

- [1] Worldometers.info, “World Population Clock: 8.1 Billion People (2024) - Worldometers,” <https://www.worldometers.info/world-population/>.
- [2] M. V. Madurwar, R. V. Ralegaonkar, and S. A. Mandavgane, “Application of agro-waste for sustainable construction materials: A review,” *Construction and Building Materials*. pp. 872–878, 2013. doi: 10.1016/j.conbuildmat.2012.09.011.
- [3] L. S. Pheng and L. S. Hou, “The Economy and the Construction Industry BT - Construction Quality and the Economy: A Study at the Firm Level,” L. Sui Pheng and L. Shing Hou, Eds., Singapore: Springer Singapore, 2019, pp. 21–54. doi: 10.1007/978-981-13-5847-0\_2.
- [4] K. Wi, H. S. Lee, S. Lim, H. Song, M. W. Hussin, and M. A. Ismail, “Use of an agricultural by-product, nano sized Palm Oil Fuel Ash as a supplementary cementitious material,” *Constr Build Mater*, vol. 183, pp. 139–149, 2018, doi: 10.1016/j.conbuildmat.2018.06.156.
- [5] C. Maraveas, “Production of sustainable construction materials using agro-wastes,” *Materials*, vol. 13, no. 2, p. 262, 2020, doi: 10.3390/ma13020262.
- [6] Matt Jungclaus, Rebecca Esau, Victor Olgyay, and Audrey Rempher, “Reducing Embodied Carbon in Buildings: Low-Cost, High-Value Opportunities,” 2021.
- [7] S. Bhuvaneshwari, H. Hettiarachchi, and J. N. Meegoda, “Crop residue burning in India: Policy challenges and potential solutions,” *Int J Environ Res Public Health*, vol. 16, no. 5, p. 832, 2019, doi: 10.3390/ijerph16050832.
- [8] C. Defonseka, *Introduction to polymeric composites with rice hulls*. Smithers Rapra,

- 2014.
- [9] G. A. Holt, G. McIntyre, D. Flagg, E. Bayer, J. D. Wanjura, and M. G. Pelletier, “Fungal mycelium and cotton plant materials in the manufacture of biodegradable molded packaging material: Evaluation study of select blends of cotton byproducts,” *J Biobased Mater Bioenergy*, vol. 6, pp. 431–439, 2012, doi: 10.1166/jbmb.2012.1241.
- [10] M. G. Pelletier, G. A. Holt, J. D. Wanjura, E. Bayer, and G. McIntyre, “An evaluation study of mycelium based acoustic absorbers grown on agricultural by-product substrates,” *Ind Crops Prod*, vol. 51, pp. 480–485, 2013, doi: 10.1016/j.indcrop.2013.09.008.
- [11] M. Jones, T. Huynh, C. Dekiwadia, F. Daver, and S. John, “Mycelium composites: A review of engineering characteristics and growth kinetics,” *Journal of Bionanoscience*, vol. 11, no. 4, pp. 241–257, 2017, doi: 10.1166/jbns.2017.1440.
- [12] M. Jones *et al.*, “Waste-derived low-cost mycelium composite construction materials with improved fire safety,” *Fire Mater*, vol. 42, no. 7, pp. 816–825, 2018, doi: 10.1002/fam.2637.
- [13] M. Jones *et al.*, “Waste-Derived Low-Cost Mycelium Nanopapers with Tunable Mechanical and Surface Properties,” *Biomacromolecules*, vol. 20, no. 9, pp. 3513–3523, 2019, doi: 10.1021/acs.biomac.9b00791.
- [14] W. M. F. B. W. Nawawi, M. Jones, R. J. Murphy, K. Y. Lee, E. Kontturi, and A. Bismarck, “Nanomaterials Derived from Fungal Sources-Is It the New Hype?,” *Biomacromolecules*, vol. 21, no. 1, pp. 30–55, 2020, doi: 10.1021/acs.biomac.9b01141.
- [15] M. Fricker, L. Boddy, and D. Bebbler, “Network Organisation of Mycelial Fungi,” in

- Biology of the Fungal Cell*, 2007. doi: 10.1007/978-3-540-70618-2\_13.
- [16] M. D. Fricker, L. L. M. Heaton, N. S. Jones, and L. Boddy, “The mycelium as a network,” *The Fungal Kingdom*, pp. 335–367, 2017, doi: 10.1128/9781555819583.ch15.
- [17] M. R. Islam, G. Tudryn, R. Bucinell, L. Schadler, and R. C. Picu, “Morphology and mechanics of fungal mycelium,” *Sci Rep*, vol. 7, p. 13070, 2017, doi: 10.1038/s41598-017-13295-2.
- [18] K. Ritz and I. M. Young, “Interactions between soil structure and fungi,” *Mycologist*, vol. 18, no. 2, pp. 52–59, 2004, doi: 10.1017/S0269915X04002010.
- [19] L. L. Taylor, J. R. Leake, J. Quirk, K. Hardy, S. A. Banwart, and D. J. Beerling, “Biological weathering and the long-term carbon cycle: Integrating mycorrhizal evolution and function into the current paradigm,” *Geobiology*, vol. 7, no. 2, pp. 171–191, 2009, doi: 10.1111/j.1472-4669.2009.00194.x.
- [20] M. E. Benbow *et al.*, “Necrobiome framework for bridging decomposition ecology of autotrophically and heterotrophically derived organic matter,” *Ecol Monogr*, vol. 89, no. 1, pp. 0012–9615, 2019, doi: 10.1002/ecm.1331.
- [21] M. R. Islam, M. Omar, M. M. U. PK, and R. Mia, “Phytochemicals and antibacterial activity screening of three edible mushrooms *Pleurotus ostreatus*, *Ganoderma lucidum* and *Lentinula edodes* accessible in Bangladesh,” *American Journal of Biology and Life Sciences*, vol. 3, no. 2, pp. 31–35, 2015.
- [22] M. Petre, *Mushroom Biotechnology: Developments and Applications*. Cambridge, Massachusetts, United States: Academic Press, 2015.

- [23] M. Haneef, L. Ceseracciu, C. Canale, I. S. Bayer, J. A. Heredia-Guerrero, and A. Athanassiou, “Advanced Materials from Fungal Mycelium: Fabrication and Tuning of Physical Properties,” *Sci Rep*, vol. 7, p. 41292, 2017, doi: 10.1038/srep41292.
- [24] E. I. Newman and M. F. Allen, “Mycorrhizal Functioning. An Integrative Plant Fungal Process.,” *J Ecol*, vol. 82, no. 2, 1994, doi: 10.2307/2261311.
- [25] A. L. Castro-Delgado, S. Elizondo-Mesén, Y. Valladares-Cruz, and W. Rivera-Méndez, “Wood wide web: communication through the mycorrhizal network,” *Revista Tecnología en Marcha*, vol. 33, no. 4, pp. 114–125, 2020.
- [26] A. Ghazvinian, P. Farrokhsiar, F. Vieira, J. Pecchia, and B. Gursoy, “Mycelium-Based Bio-Composites For Architecture: Assessing the Effects of Cultivation Factors on Compressive Strength,” *Proceedings of the International Conference on Education and Research in Computer Aided Architectural Design in Europe*, vol. 2, pp. 505–514, 2019, doi: 10.5151/proceedings-ecaadesigradi2019\_465.
- [27] D. Alemu, M. Tafesse, and A. K. Mondal, “Mycelium-Based Composite: The Future Sustainable Biomaterial,” *International Journal of Biomaterials*, vol. 2022, no. 8401528, 2022, doi: 10.1155/2022/8401528.
- [28] N. Attias *et al.*, “Mycelium bio-composites in industrial design and architecture: Comparative review and experimental analysis,” *J Clean Prod*, vol. 246, no. 119037, 2020, doi: 10.1016/j.jclepro.2019.119037.
- [29] L. Jiang, D. Walczyk, G. McIntyre, R. Bucinell, and G. Tudryn, “Manufacturing of biocomposite sandwich structures using mycelium-bound cores and preforms,” *J Manuf Process*, vol. 28, pp. 50–59, 2017, doi: 10.1016/j.jmapro.2017.04.029.

- [30] J. Silverman, H. Cao, and K. Cobb, "Development of Mushroom Mycelium Composites for Footwear Products," *Clothing and Textiles Research Journal*, vol. 38, no. 2, pp. 119–133, 2020, doi: 10.1177/0887302X19890006.
- [31] A. Ghazvinian and B. Gursoy, "BASICS OF BUILDING WITH MYCELIUMBASED BIO-COMPOSITES:A REVIEW OF BUILT PROJECTS AND RELATED MATERIAL RESEARCH," *Journal of Green Building*, vol. 17, no. 1, pp. 37–69, 2022, doi: 10.3992/jgb.17.1.37.
- [32] Z. Zimele, I. Irbe, J. Grinins, O. Bikovens, A. Verovkins, and D. Bajare, "Novel mycelium-based biocomposites (Mbb) as building materials," *J Renew Mater*, vol. 8, no. 9, pp. 1067–1076, 2020, doi: 10.32604/jrm.2020.09646.
- [33] J. Jose, K. N. Uvais, T. S. Sreenadh, A. V. Deepak, and C. R. Rejeesh, "Investigations into the Development of a Mycelium Biocomposite to Substitute Polystyrene in Packaging Applications," *Arab J Sci Eng*, vol. 46, no. 3, pp. 2975–2984, 2021, doi: 10.1007/s13369-020-05247-2.
- [34] R. C. Rajendran, "Packaging Applications of Fungal Mycelium-Based Biodegradable Composites," in *Fungal Biopolymers and Biocomposites: Prospects and Avenues*, 2022, pp. 189–208. doi: 10.1007/978-981-19-1000-5\_11.
- [35] L. Jiang, D. Walczyk, G. McIntyre, and W. K. Chan, "Cost modeling and optimization of a manufacturing system for mycelium-based biocomposite parts," *J Manuf Syst*, vol. 41, pp. 8–20, 2016, doi: 10.1016/j.jmsy.2016.07.004.
- [36] C. Girometta *et al.*, "Physico-mechanical and thermodynamic properties of mycelium-based biocomposites: A review," *Sustainability (Switzerland)*, vol. 11, no. 1, p. 281,

- 2019, doi: 10.3390/su11010281.
- [37] H. Schritt, S. Vidi, and D. Pleissner, “Spent mushroom substrate and sawdust to produce mycelium-based thermal insulation composites,” *J Clean Prod*, vol. 313, no. 127910, 2021, doi: 10.1016/j.jclepro.2021.127910.
- [38] P. P. Dias, L. B. Jayasinghe, and D. Waldmann, “Investigation of Mycelium-Miscanthus composites as building insulation material,” *Results in Materials*, vol. 10, no. 100189, 2021, doi: 10.1016/j.rinma.2021.100189.
- [39] M. Sydor, A. Bonenberg, B. Doczekalska, and G. Cofta, “Mycelium-Based Composites in Art, Architecture, and Interior Design: A Review,” *Polymers*, vol. 14, no. 1, p. 145, 2022. doi: 10.3390/polym14010145.
- [40] T. Teeraphantuvat, K. Jatuwong, P. Jinanukul, W. Thamjaree, S. Lumyong, and W. Aiduang, “Improving the Physical and Mechanical Properties of Mycelium-Based Green Composites Using Paper Waste,” *Polymers (Basel)*, vol. 16, no. 2, 2024, doi: 10.3390/polym16020262.
- [41] E. Elsacker, S. Vandelook, J. Brancart, E. Peeters, and L. De Laet, “Mechanical, physical and chemical characterisation of mycelium-based composites with different types of lignocellulosic substrates,” *PLoS One*, vol. 14, no. 7, p. e0213954, 2019, doi: 10.1371/journal.pone.0213954.
- [42] A. Ghazvinian and B. Gürsoy, “Mycelium-Based Composite Graded Materials: Assessing the Effects of Time and Substrate Mixture on Mechanical Properties,” *Biomimetics*, vol. 7, no. 2, p. 48, 2022, doi: 10.3390/biomimetics7020048.
- [43] T. Balaş, B. M. Radu, and C. Tănase, “Mycelium-Composite Materials—A Promising

- Alternative to Plastics?,” *Journal of Fungi*, vol. 9, no. 2, 2023, doi: 10.3390/jof9020210.
- [44] B. Steigerwald, “NASA Goddard Instrument Makes First Detection of Organic Matter on Mars,” NASA. [Online]. Available: <https://www.nasa.gov/content/goddard/mars-organic-matter>
- [45] R. S. Swift, “Organic matter characterization,” *Methods of soil analysis: Part 3 chemical methods*, vol. 5, pp. 1011–1069, 1996.
- [46] V. Sejian, J. Gaughan, L. Baumgard, and C. Prasad, *Climate change impact on livestock: Adaptation and mitigation*. 2015. doi: 10.1007/978-81-322-2265-1.
- [47] H. T. Hoa and C. L. Wang, “The effects of temperature and nutritional conditions on mycelium growth of two oyster mushrooms (*Pleurotus ostreatus* and *Pleurotus cystidiosus*),” *Mycobiology*, vol. 43, no. 1, pp. 14–23, 2015, doi: 10.5941/MYCO.2015.43.1.14.
- [48] Y. Xing, M. Brewer, H. El-Gharabawy, G. Griffith, and P. Jones, “Growing and testing mycelium bricks as building insulation materials,” *IOP Conf Ser Earth Environ Sci*, vol. 121, no. 2, p. 022032, 2018, doi: 10.1088/1755-1315/121/2/022032.
- [49] V. Bansal, A. Ahmad, and M. Sastry, “Fungus-mediated biotransformation of amorphous silica in rice husk to nanocrystalline silica,” *J Am Chem Soc*, vol. 128, no. 43, pp. 14059–14066, 2006, doi: 10.1021/ja062113+.
- [50] F. V. W. Appels *et al.*, “Fabrication factors influencing mechanical, moisture- and water-related properties of mycelium-based composites,” *Mater Des*, vol. 161, pp. 64–71, 2019, doi: 10.1016/j.matdes.2018.11.027.

- [51] S. Bartnicki-Garcia, “Cell wall chemistry, morphogenesis, and taxonomy of fungi.,” *Annu Rev Microbiol*, vol. 22, pp. 87–108, 1968, doi: 10.1146/annurev.mi.22.100168.000511.
- [52] E. Karana, D. Blauwhoff, E. J. Hultink, and S. Camere, “When the material grows: A case study on designing (with) mycelium-based materials,” *International Journal of Design*, vol. 12, pp. 119–136, 2018.
- [53] M. Jones, M. Kujundzic, S. John, and A. Bismarck, “Crab vs. Mushroom: A review of crustacean and fungal chitin in wound treatment,” *Mar Drugs*, vol. 18, no. 1, p. 64, 2020, doi: 10.3390/md18010064.
- [54] P. Morganti and G. Morganti, “Chitin nanofibrils for advanced cosmeceuticals,” *Clin Dermatol*, vol. 26, no. 4, pp. 334–340, 2008, doi: 10.1016/j.clindermatol.2008.01.003.
- [55] S. Danti *et al.*, “Chitin nanofibrils and nanolignin as functional agents in skin regeneration,” *Int J Mol Sci*, vol. 20, no. 11, p. 2669, 2019, doi: 10.3390/ijms20112669.
- [56] B. Azimi *et al.*, “Electrosprayed chitin nanofibril/electrospun polyhydroxyalkanoate fiber mesh as functional nonwoven for skin application,” *J Funct Biomater*, vol. 11, no. 3, p. 62, 2020, doi: 10.3390/jfb11030062.
- [57] N. Naseri, C. Algan, V. Jacobs, M. John, K. Oksman, and A. P. Mathew, “Electrospun chitosan-based nanocomposite mats reinforced with chitin nanocrystals for wound dressing,” *Carbohydr Polym*, vol. 109, pp. 7–15, 2014, doi: 10.1016/j.carbpol.2014.03.031.
- [58] P. Morganti, G. Morganti, and M. B. Coltelli, “Chitin Nanomaterials and Nanocomposites for Tissue Repair BT - Marine-Derived Biomaterials for Tissue

- Engineering Applications,” A. H. Choi and B. Ben-Nissan, Eds., Singapore: Springer Singapore, 2019, pp. 523–544. doi: 10.1007/978-981-13-8855-2\_21.
- [59] C. Wang *et al.*, “Fabrication of electrospun polymer nanofibers with diverse morphologies,” *Molecules*, vol. 24, no. 5, p. 834, 2019, doi: 10.3390/molecules24050834.
- [60] R. A. A. Muzzarelli *et al.*, “Chitin nanofibrils/chitosan glycolate composites as wound medicaments,” *Carbohydr Polym*, vol. 70, no. 3, pp. 274–284, 2007, doi: 10.1016/j.carbpol.2007.04.008.
- [61] R. Jayakumar, M. Prabakaran, P. T. Sudheesh Kumar, S. V., T. Furuike, and H. Tamur, “Novel Chitin and Chitosan Materials in Wound Dressing,” in *Biomedical Engineering, Trends in Materials Science*, 2011, pp. 3–24. doi: 10.5772/13509.
- [62] R. A. A. Muzzarelli, “Nanochitins and Nanochitosans, Paving the Way to Eco-Friendly and Energy-Saving Exploitation of Marine Resources,” in *Polymer Science: A Comprehensive Reference, 10 Volume Set*, 2012, pp. 153–164. doi: 10.1016/B978-0-444-53349-4.00257-0.
- [63] N. Morin-Crini, E. Lichtfouse, G. Torri, and G. Crini, “Applications of chitosan in food, pharmaceuticals, medicine, cosmetics, agriculture, textiles, pulp and paper, biotechnology, and environmental chemistry,” *Environ Chem Lett*, vol. 17, pp. 1667–1692, 2019, doi: 10.1007/s10311-019-00904-x.
- [64] R. A. A. Muzzarelli, “Chitin Nanostructures in Living Organisms,” in *Chitin*, N. S. Gupta, Ed., Springer, Dordrecht, 2011, pp. 1–34. doi: 10.1007/978-90-481-9684-5\_1.
- [65] F. Di Mario, P. Rapanà, U. Tomati, and E. Galli, “Chitin and chitosan from

- Basidiomycetes,” *Int J Biol Macromol*, vol. 43, no. 1, pp. 8–12, 2008, doi: 10.1016/j.ijbiomac.2007.10.005.
- [66] A. Hassainia, H. Satha, and S. Boufi, “Chitin from *Agaricus bisporus*: Extraction and characterization,” *Int J Biol Macromol*, vol. 117, pp. 1334–1342, 2018, doi: 10.1016/j.ijbiomac.2017.11.172.
- [67] B. Azimi *et al.*, “Electrosprayed Shrimp and Mushroom Nanochitins on Cellulose Tissue for Skin Contact Application,” *Molecules*, vol. 26, no. 14, p. 4374, 2021, doi: 10.3390/molecules26144374.
- [68] E. Soh, Z. Y. Chew, N. Saeidi, A. Javadian, D. Hebel, and H. Le Ferrand, “Development of an extrudable paste to build mycelium-bound composites,” *Mater Des*, vol. 195, p. 109058, 2020, doi: 10.1016/j.matdes.2020.109058.
- [69] R. Liu, X. Li, L. Long, Y. Sheng, J. Xu, and Y. Wang, “Improvement of mechanical properties of mycelium/cotton stalk composites by water immersion,” *Compos Interfaces*, vol. 27, no. 10, pp. 953–966, 2020, doi: 10.1080/09276440.2020.1716573.
- [70] C. Müller, S. Klemm, and C. Fleck, “Bracket fungi, natural lightweight construction materials: hierarchical microstructure and compressive behavior of *Fomes fomentarius* fruit bodies,” *Appl Phys A Mater Sci Process*, vol. 127, p. 178, 2021, doi: 10.1007/s00339-020-04270-2.
- [71] I. Irbe, I. Filipova, M. Skute, A. Zajakina, K. Spunde, and T. Juhna, “Characterization of novel biopolymer blend mycocel from plant cellulose and fungal fibers,” *Polymers (Basel)*, vol. 13, no. 7, p. 1086, 2021, doi: 10.3390/polym13071086.
- [72] N. I. Nashiruddin *et al.*, “Effect of growth factors on the production of mycelium-

- based biofoam,” *Clean Technol Environ Policy*, vol. 24, pp. 351–361, 2022, doi: 10.1007/s10098-021-02146-4.
- [73] A. Adamatzky and A. Gandia, “Living mycelium composites discern weights via patterns of electrical activity,” *Journal of Bioresources and Bioproducts*, vol. 7, no. 1, pp. 26–32, 2022, doi: 10.1016/j.jobab.2021.09.003.
- [74] X. Zhang *et al.*, “Novel strategies to grow natural fibers with improved thermal stability and fire resistance,” *J Clean Prod*, vol. 320, p. 128729, 2021, doi: 10.1016/j.jclepro.2021.128729.
- [75] L. Gou, S. Li, J. Yin, T. Li, and X. Liu, “Morphological and physico-mechanical properties of mycelium biocomposites with natural reinforcement particles,” *Constr Build Mater*, vol. 304, p. 124656, 2021, doi: 10.1016/j.conbuildmat.2021.124656.
- [76] L. Stelzer *et al.*, “Life cycle assessment of fungal-based composite bricks,” *Sustainability (Switzerland)*, vol. 13, no. 21, p. 11573, 2021, doi: 10.3390/su132111573.
- [77] X. Y. Chan, N. Saeidi, A. Javadian, D. E. Hebel, and M. Gupta, “Mechanical properties of dense mycelium-bound composites under accelerated tropical weathering conditions,” *Sci Rep*, vol. 11, p. 22112, 2021, doi: 10.1038/s41598-021-01598-4.
- [78] T. Kuribayashi, P. Lankinen, S. Hietala, and K. S. Mikkonen, “Dense and continuous networks of aerial hyphae improve flexibility and shape retention of mycelium composite in the wet state,” *Compos Part A Appl Sci Manuf*, vol. 152, p. 106688, 2022, doi: 10.1016/j.compositesa.2021.106688.
- [79] A. Van Wylick, E. Elsacker, L. L. Yap, E. Peeters, and L. de Laet, “Mycelium

- Composites and their Biodegradability: An Exploration on the Disintegration of Mycelium-Based Materials in Soil,” *Bio-Based Building Materials*, vol. 1, pp. 652–659, 2022, doi: 10.4028/www.scientific.net/cta.1.652.
- [80] E. Özdemir *et al.*, “Wood-Veneer-Reinforced Mycelium Composites for Sustainable Building Components,” *Biomimetics*, vol. 7, no. 2, p. 39, 2022, doi: 10.3390/biomimetics7020039.
- [81] M. T. Nguyen, D. Solueva, E. Spyridonos, and H. Dahy, “Mycomerge: Fabrication of Mycelium-Based Natural Fiber Reinforced Composites on a Rattan Framework,” *Biomimetics*, vol. 7, no. 2, p. 42, 2022, doi: 10.3390/biomimetics7020042.
- [82] A. Sayfutdinova, I. Samofalova, A. Barkov, K. Cherednichenko, and D. Rimashevskiy, “Structure and Properties of Cellulose/Mycelium Biocomposites,” *Polymers (Basel)*, vol. 14, no. 1519, 2022, doi: 10.3390/polym14081519.
- [83] H. Vašatko, L. Gosch, J. Jauk, and M. Stavric, “Basic Research of Material Properties of Mycelium-Based Composites,” *Biomimetics*, vol. 7, no. 2, p. 51, 2022, doi: 10.3390/biomimetics7020051.
- [84] E. Elsacker, L. De Laet, and E. Peeters, “Functional Grading of Mycelium Materials with Inorganic Particles: The Effect of Nanoclay on the Biological, Chemical and Mechanical Properties,” *Biomimetics*, vol. 7, no. 2, p. 57, 2022, doi: 10.3390/biomimetics7020057.
- [85] C. Pohl *et al.*, “Establishment of the basidiomycete *Fomes fomentarius* for the production of composite materials,” *Fungal Biol Biotechnol*, vol. 9, no. 4, 2022, doi: 10.1186/s40694-022-00133-y.

- [86] E. Elsacker, E. Peeters, and L. De Laet, "Large-scale robotic extrusion-based additive manufacturing with living mycelium materials," *Sustainable Futures*, vol. 4, no. 100085, 2022, doi: 10.1016/j.sftr.2022.100085.
- [87] D. Tarasov, M. Leitch, and P. Fatehi, "Lignin-carbohydrate complexes: Properties, applications, analyses, and methods of extraction: A review," *Biotechnology for Biofuels*, vol. 11, no. 269. 2018. doi: 10.1186/s13068-018-1262-1.
- [88] R. H. Marchessault, "Wood chemistry, fundamentals and applications," *Carbohydr Res*, vol. 252, p. C1, 1994, doi: 10.1016/0008-6215(94)90030-2.
- [89] D. Nhuchhen, P. Basu, and B. Acharya, "A Comprehensive Review on Biomass Torrefaction," *International Journal of Renewable Energy & Biofuels*, vol. 2014, p. 506376, 2014, doi: 10.5171/2014.506376.
- [90] V. Menon and M. Rao, "Trends in bioconversion of lignocellulose: Biofuels, platform chemicals & biorefinery concept," *Progress in Energy and Combustion Science*, vol. 38, no. 4, pp. 522–550, 2012. doi: 10.1016/j.peccs.2012.02.002.
- [91] H. H. Nimz, *Wood-chemistry, ultrastructure, reactions*, vol. 42, no. 8. 1984. doi: 10.1007/bf02608943.
- [92] A. Komuraiah, N. S. Kumar, and B. D. Prasad, "Chemical Composition of Natural Fibers and its Influence on their Mechanical Properties," *Mechanics of Composite Materials*, vol. 50, no. 3, pp. 359–376, 2014, doi: 10.1007/s11029-014-9422-2.
- [93] M. Sydor, D. Kurasiak-Popowska, K. Stuper-Szablewska, and T. Rogoziński, "Camelina sativa. Status quo and future perspectives," *Industrial Crops and Products*, vol. 187, p. 115531, 2022. doi: 10.1016/j.indcrop.2022.115531.

- [94] B. Doczekalska and M. Zborowska, “Wood chemical composition of selected fast growing species treated with naoh part I: Structural substances,” *Wood Research*, vol. 55, no. 1, pp. 41–48, 2010.
- [95] M. Sydor, G. Cofta, B. Doczekalska, and A. Bonenberg, “Fungi in Mycelium-Based Composites: Usage and Recommendations,” *Materials*, vol. 15, no. 18. MDPI, Sep. 01, 2022. doi: 10.3390/ma15186283.
- [96] S. K. Ramamoorthy, D. Åkesson, R. Rajan, A. P. Periyasamy, and M. Skrifvars, “Mechanical performance of biofibers and their corresponding composites,” in *Mechanical and Physical Testing of Biocomposites, Fibre-Reinforced Composites and Hybrid Composites*, 2018, pp. 259–292. doi: 10.1016/B978-0-08-102292-4.00014-X.
- [97] I. Spiridon and V. I. Popa, “Hemicelluloses: Major sources, properties and applications,” in *Monomers, Polymers and Composites from Renewable Resources*, 2008, pp. 289–304. doi: 10.1016/B978-0-08-045316-3.00013-2.
- [98] “Hemicelluloses: Structure and Properties,” in *Polysaccharides*, 2020, pp. 475–489. doi: 10.1201/9781420030822-22.
- [99] F. J. Ruiz-Dueñas and Á. T. Martínez, “Microbial degradation of lignin: How a bulky recalcitrant polymer is efficiently recycled in nature and how we can take advantage of this,” *Microbial Biotechnology*, vol. 2, no. 2. pp. 164–177, 2009. doi: 10.1111/j.1751-7915.2008.00078.x.
- [100] S. A. N. Mohamed, E. S. Zainudin, S. M. Sapuan, M. D. Azaman, and A. M. T. Arifin, “Introduction to Natural Fiber Reinforced Vinyl Ester and Vinyl Polymer Composites,” in *Natural Fiber Reinforced Vinyl Ester and Vinyl Polymer Composites: Development*,

- Characterization and Applications*, 2018, pp. 1–25. doi: 10.1016/B978-0-08-102160-6.00001-9.
- [101] R. Vanholme, K. Morreel, J. Ralph, and W. Boerjan, “Lignin engineering,” *Current Opinion in Plant Biology*, vol. 11, no. 3. pp. 278–285, 2008. doi: 10.1016/j.pbi.2008.03.005.
- [102] J. C. Del Río, J. Rencoret, A. Gutiérrez, T. Elder, H. Kim, and J. Ralph, “Lignin Monomers from beyond the Canonical Monolignol Biosynthetic Pathway: Another Brick in the Wall,” *ACS Sustainable Chemistry and Engineering*, vol. 8, no. 13. pp. 4997–5012, 2020. doi: 10.1021/acssuschemeng.0c01109.
- [103] S. Shimizu, T. Yokoyama, T. Akiyama, and Y. Matsumoto, “Reactivity of lignin with different composition of aromatic syringyl/guaiacyl structures and Erythro/Threo side chain structures in  $\beta$ -O-4 type during alkaline delignification: As a basis for the different degradability of hardwood and softwood lignin,” *J Agric Food Chem*, vol. 60, no. 26, pp. 6471–6476, 2012, doi: 10.1021/jf301329v.
- [104] C. S. L. Christensen and S. K. Rasmussen, “Low lignin mutants and reduction of lignin content in grasses for increased utilisation of lignocellulose,” *Agronomy*, vol. 9, no. 5. p. 256, 2019. doi: 10.3390/agronomy9050256.
- [105] A. R. Ziegler, S. G. Bajwa, G. A. Holt, G. McIntyre, and D. S. Bajwa, “Evaluation of physico-mechanical properties of mycelium reinforced green biocomposites made from cellulosic fibers,” *Appl Eng Agric*, vol. 32, no. 6, pp. 931–938, 2016, doi: 10.13031/aea.32.11830.
- [106] P. M. Velasco, M. P. M. Ortiz, M. A. M. Giro, M. C. J. Castelló, and L. M. Velasco,

- “Development of better insulation bricks by adding mushroom compost wastes,” *Energy Build*, vol. 80, pp. 17–22, 2014, doi: 10.1016/j.enbuild.2014.05.005.
- [107] J. Deacon, *Fungal Biology: 4th Edition*. 2013. doi: 10.1002/9781118685068.
- [108] J. Wu, Z. Qin, L. Qu, H. Zhang, F. Deng, and M. Guo, “Natural hydrogel in American lobster: A soft armor with high toughness and strength,” *Acta Biomater*, vol. 88, pp. 102–110, 2019, doi: 10.1016/j.actbio.2019.01.067.
- [109] J. Liu *et al.*, “Fatigue-resistant adhesion of hydrogels,” *Nat Commun*, vol. 11, p. 1071, 2020, doi: 10.1038/s41467-020-14871-3.
- [110] A. Bhardwaj *et al.*, “3D Printing of Biomass-Fungi Composite Material: A Preliminary Study,” *Manuf Lett*, vol. 24, pp. 96–99, 2020, doi: 10.1016/j.mfglet.2020.04.005.
- [111] L. Jiang, D. Walczyk, G. McIntyre, R. Bucinell, and B. Li, “Bioresin infused then cured mycelium-based sandwich-structure biocomposites: Resin transfer molding (RTM) process, flexural properties, and simulation,” *J Clean Prod*, vol. 207, pp. 123–135, 2019, doi: 10.1016/j.jclepro.2018.09.255.
- [112] L. J. Gibson and M. F. Ashby, “The mechanics cellular materials of three-dimensional cellular materials,” *Proc. R. Soc. Lond*, vol. A382, pp. 43–59, 1982.
- [113] C. Dai, C. Yu, and X. Zhou, “Heat and mass transfer in wood composite panels during hot pressing. Part II. Modeling void formation and mat permeability,” *Wood and Fiber Science*, vol. 37, no. 2, pp. 242–257, 2007.
- [114] Z. Qin, G. S. Jung, M. J. Kang, and M. J. Buehler, “The mechanics and design of a lightweight three-dimensional graphene assembly,” *Sci Adv*, vol. 3, no. 1, p. e1601536, 2017, doi: UNSP e1601536 10.1126/sciadv.1601536.

- [115] B. Butterfield, K. Chapman, L. Christie, and A. Dickson, “Ultrastructural characteristics of failure surfaces in medium density fiberboard,” *Forest products journal (USA)*, vol. 42, no. 6, pp. 55–60, 1992.
- [116] L. M. H. CARVALHO and C. A. V COSTA, “Modeling and simulation of the hot-pressing process in the production of medium density fiberboard (MDF),” *Chem Eng Commun*, vol. 170, no. 1, pp. 1–21, 1998.
- [117] M. Jones, A. Mautner, S. Luenco, A. Bismarck, and S. John, “Engineered mycelium composite construction materials from fungal biorefineries: A critical review,” *Mater Des*, vol. 187, no. 108397, 2020, doi: 10.1016/j.matdes.2019.108397.
- [118] E. J. H. Corner, “THE CONSTRUCTION OF POLYPORES. 1. INTRODUCTION-POLYPORUS-SULPHUREUS, P-SQUAMOSUS, P-BETULINUS AND POLYSTICTUS-MICROCYCLUS,” *Phytomorphology*, vol. 3, no. 3, pp. 152–167, 1953.
- [119] L. Ryvardeen, “Genera of polypores: nomenclature and taxonomy,” *Synopsis fungi*, vol. 5, 1991.
- [120] D. N. Pegler, “Hyphal analysis of basidiomata,” *Mycol Res*, vol. 100, no. 2, pp. 129–142, 1996.
- [121] K. S. Ko and H. S. Jung, “Molecular phylogeny of *Trametes* and related genera,” *Antonie Van Leeuwenhoek*, vol. 75, no. 3, pp. 191–199, 1999.
- [122] J. Webster and R. Weber, *Introduction to fungi*. New York: Cambridge university press, 2007.
- [123] E. Bayer and G. McIntyre, “PATENT: Substrate Composition and Method for Growing

- Mycological Materials,” vol. 1, no. 19, p. 2, 2012, [Online]. Available: [https://patents.google.com/patent/US20120315687A1/en?assignee=Ecovative+Design+Llc&oq=assignee:\(Ecovative+Design+Llc\)](https://patents.google.com/patent/US20120315687A1/en?assignee=Ecovative+Design+Llc&oq=assignee:(Ecovative+Design+Llc))
- [124] E. Bayer and G. McIntyre, “METHOD FOR GROWING MYCOLOGICAL MATERIALS,” Jul. 2015 [Online]. Available: <https://patents.google.com/patent/US20150247115A1/en>
- [125] A. K. Gautam *et al.*, “Current Insight into Traditional and Modern Methods in Fungal Diversity Estimates,” *Journal of Fungi*, vol. 8, no. 3. 2022. doi: 10.3390/jof8030226.
- [126] M. Blackwell, “The fungi: 1, 2, 3 ... 5.1 million species?,” *Am J Bot*, vol. 98, no. 3, pp. 426–438, 2011, doi: 10.3732/ajb.1000298.
- [127] S. Parisi, V. Rognoli, and C. Ayala-Garcia, “Designing materials experiences through passing of time - Material driven design method applied to mycelium-based composites,” in *Proceedings - D and E 2016: 10th International Conference on Design and Emotion - Celebration and Contemplation*, Amsterdam, 2016, pp. 239–255.
- [128] J. Dahmen, “Soft futures: Mushrooms and regenerative design,” *Journal of Architectural Education*, vol. 71, no. 1, pp. 57–64, 2017, doi: 10.1080/10464883.2017.1260927.
- [129] M. Rinaudo, “Chitin and chitosan: Properties and applications,” *Progress in Polymer Science (Oxford)*, vol. 31, no. 7, pp. 603–632, 2006, doi: 10.1016/j.progpolymsci.2006.06.001.
- [130] N. P. Money, “Fungal Cell Biology and Development,” in *The Fungi: Third Edition*, 2016, pp. 37–66. doi: 10.1016/B978-0-12-382034-1.00002-5.

- [131] J. Ruiz-Herrera and L. Ortiz-Castellanos, “Cell wall glucans of fungi. A review,” *The Cell Surface*, vol. 5, p. 100022, 2019, doi: 10.1016/j.tcsw.2019.100022.
- [132] N. A. R. Gow, J.-P. Latge, and C. A. Munro, “The Fungal Cell Wall: Structure, Biosynthesis, and Function,” *Microbiol Spectr*, vol. 5, no. 3, 2017, doi: 10.1128/microbiolspec.funk-0035-2016.
- [133] J. P. Latgé and A. Beauvais, “Functional duality of the cell wall,” *Current Opinion in Microbiology*, vol. 20, pp. 111–117, 2014. doi: 10.1016/j.mib.2014.05.009.
- [134] A. Hatakka and K. E. Hammel, “Fungal Biodegradation of Lignocelluloses,” in *The Mycota*, 2011, pp. 319–340. doi: 10.1007/978-3-642-11458-8\_15.
- [135] M. B. Linder, G. R. Szilvay, T. Nakari-Setälä, and M. E. Penttilä, “Hydrophobins: The protein-amphiphiles of filamentous fungi,” *FEMS Microbiol Rev*, vol. 29, no. 5, pp. 877–896, 2005, doi: 10.1016/j.femsre.2005.01.004.
- [136] J. R. Whiteford and P. D. Spanu, “Hydrophobins and the interactions between fungi and plants,” *Mol Plant Pathol*, vol. 3, no. 5, pp. 391–400, 2002, doi: 10.1046/j.1364-3703.2002.00129.x.
- [137] J. Erjavec, J. Kos, M. Ravnikar, T. Dreo, and J. Sabotič, “Proteins of higher fungi - from forest to application,” *Trends Biotechnol*, vol. 30, no. 5, pp. 259–273, 2012, doi: 10.1016/j.tibtech.2012.01.004.
- [138] P. Baldrian and V. Valášková, “Degradation of cellulose by basidiomycetous fungi,” *FEMS Microbiol Rev*, vol. 32, no. 3, pp. 501–521, 2008, doi: 10.1111/j.1574-6976.2008.00106.x.
- [139] C. Sánchez, “Lignocellulosic residues: Biodegradation and bioconversion by fungi,”

- Biotechnol Adv*, vol. 27, no. 2, pp. 185–194, 2009, doi: 10.1016/j.biotechadv.2008.11.001.
- [140] M. Andlar, T. Rezić, N. Marđetko, D. Kracher, R. Ludwig, and B. Šantek, “Lignocellulose degradation: An overview of fungi and fungal enzymes involved in lignocellulose degradation,” *Eng Life Sci*, vol. 18, pp. 768–778, 2018, doi: 10.1002/elsc.201800039.
- [141] A. L. Woiciechowski *et al.*, “The pretreatment step in lignocellulosic biomass conversion: Current systems and new biological systems,” in *Lignocellulose Conversion: Enzymatic and Microbial Tools for Bioethanol Production*, 2013, pp. 39–64. doi: 10.1007/978-3-642-37861-4\_3.
- [142] M. Couturier and J. G. Berrin, “The saccharification step: The main enzymatic components,” in *Lignocellulose Conversion: Enzymatic and Microbial Tools for Bioethanol Production*, Berlin, Heidelberg: Springer, 2013, pp. 93–110. doi: 10.1007/978-3-642-37861-4\_5.
- [143] V. Arantes and B. Goodell, “Current understanding of brown-rot fungal biodegradation mechanisms: A review,” *ACS Symposium Series*, vol. 1158, pp. 3–21, 2014, doi: 10.1021/bk-2014-1158.ch001.
- [144] G. S. Dhillon, S. Kaur, S. K. Brar, and M. Verma, “Green synthesis approach: Extraction of chitosan from fungus mycelia,” *Crit Rev Biotechnol*, vol. 33, no. 4, pp. 379–403, 2013, doi: 10.3109/07388551.2012.717217.
- [145] K. Kilavan Packiam, T. S. George, S. Kulanthaivel, and N. S. Vasanthi, “Extraction, purification and characterization of chitosan from endophytic fungi isolated from

- medicinal plants,” *World J. Sci. Technol.*, vol. 1, no. 4, pp. 43–48, Jan. 2011.
- [146] I. Aranaz *et al.*, “Functional Characterization of Chitin and Chitosan,” *Curr Chem Biol*, vol. 3, no. 2, pp. 203-230(28), 2012, doi: 10.2174/2212796810903020203.
- [147] P. Pochanavanich and W. Suntornsuk, “Fungal chitosan production and its characterization,” *Lett Appl Microbiol*, vol. 35, no. 1, pp. 17–21, 2002, doi: 10.1046/j.1472-765X.2002.01118.x.
- [148] F. Streit, F. Koch, M. C. M. Laranjeira, and J. L. Ninow, “Production of fungal chitosan in liquid cultivation using apple pomace as substrate,” *Brazilian Journal of Microbiology*, vol. 40, no. 1, pp. 20–25, 2009, doi: 10.1590/S1517-83822009000100003.
- [149] J. H. Sietsma and J. G. H. Wessels, “Evidence for covalent linkages between chitin and  $\beta$ -glucan in a fungal wall,” *J Gen Microbiol*, vol. 114, no. 1, pp. 99–108, 1979, doi: 10.1099/00221287-114-1-99.
- [150] R. Kollár *et al.*, “Architecture of the yeast cell wall:  $\beta(1\rightarrow6)$ glucan interconnects mannoprotein,  $\beta(1\rightarrow3)$ -glucan, and chitin,” *Journal of Biological Chemistry*, vol. 272, no. 28, pp. 17762–17775, 1997, doi: 10.1074/jbc.272.28.17762.
- [151] L. Heux, J. Brugnerotto, J. Desbrières, M. F. Versali, and M. Rinaudo, “Solid state NMR for determination of degree of acetylation of chitin and chitosan,” *Biomacromolecules*, vol. 1, no. 4, pp. 746–751, 2000, doi: 10.1021/bm000070y.
- [152] J. P. Latgé, “The cell wall: A carbohydrate armour for the fungal cell,” *Molecular Microbiology*, vol. 66, no. 2, pp. 279–290, 2007. doi: 10.1111/j.1365-2958.2007.05872.x.

- [153] S. Zhou, K. Jin, and M. J. Buehler, "Understanding Plant Biomass via Computational Modeling," *Advanced Materials*, vol. 33, no. 28. p. 2003206, 2021. doi: 10.1002/adma.202003206.
- [154] S. Bartnicki-Garcia and W. J. Nickerson, "Isolation, composition, and structure of cell walls of filamentous and yeast-like forms of *Mucor rouxii*," *BBA - Biochimica et Biophysica Acta*, vol. 58, no. 1, pp. 102–119, 1962, doi: 10.1016/0006-3002(62)90822-3.
- [155] K. Karimi and A. Zamani, "Mucor indicus: Biology and industrial application perspectives: A review," *Biotechnology Advances*, vol. 31, no. 4. pp. 466–481, 2013. doi: 10.1016/j.biotechadv.2013.01.009.
- [156] W. M. Fazli Wan Nawawi, K. Y. Lee, E. Kontturi, R. J. Murphy, and A. Bismarck, "Chitin Nanopaper from Mushroom Extract: Natural Composite of Nanofibers and Glucan from a Single Biobased Source," *ACS Sustain Chem Eng*, vol. 7, no. 7, pp. 6492–6496, 2019, doi: 10.1021/acssuschemeng.9b00721.
- [157] R. Hackman, "Studies on Chitin IV. The Occurrence of Complexes in Which Chitin and Protein are Covalently Linked," *Aust J Biol Sci*, vol. 13, no. 4, pp. 568–577, 1960, doi: 10.1071/bi9600568.
- [158] M. M. Attwood and H. Zola, "The association between chitin and protein in some chitinous tissues," *Comp Biochem Physiol*, vol. 20, no. 3, pp. 993–998, 1967, doi: 10.1016/0010-406X(67)90069-2.
- [159] K. J. Kramer, T. L. Hopkins, and J. Schaefer, "Applications of solids NMR to the analysis of insect sclerotized structures," *Insect Biochemistry and Molecular Biology*,

- vol. 25, no. 10. pp. 1067–1080, 1995. doi: 10.1016/0965-1748(95)00053-4.
- [160] A. Percot, C. Viton, and A. Domard, “Characterization of shrimp shell deproteinization,” *Biomacromolecules*, vol. 4, no. 5, pp. 1380–1385, 2003, doi: 10.1021/bm034115h.
- [161] D. Elieh-Ali-Komi and M. R. Hamblin, “Chitin and Chitosan: Production and Application of Versatile Biomedical Nanomaterials.,” *Int J Adv Res (Indore)*, vol. 4, no. 3, pp. 411–427, 2016, [Online]. Available: <http://www.ncbi.nlm.nih.gov/pubmed/27819009><http://www.pubmedcentral.nih.gov/articlerender.fcgi?artid=PMC5094803>
- [162] L. J. Gibson, “The hierarchical structure and mechanics of plant materials,” *Journal of the Royal Society Interface*, vol. 9, no. 76. pp. 2749–2766, 2012. doi: 10.1098/rsif.2012.0341.
- [163] Y. H. Arifin and Y. Yusuf, “Mycelium fibers as new resource for environmental sustainability,” *Procedia Eng*, vol. 53, pp. 504–508, 2013, doi: 10.1016/j.proeng.2013.02.065.
- [164] J. A. López Nava, J. Méndez González, X. Ruelas Chacón, and J. A. Nájera Luna, “Assessment of Edible Fungi and Films Bio-Based Material Simulating Expanded Polystyrene,” *Materials and Manufacturing Processes*, vol. 31, no. 8, pp. 1085–1090, 2016, doi: 10.1080/10426914.2015.1070420.
- [165] A. G. Fallis, “Development and Testing of Mycelium-Based Composite Materials for Shoe Sole Applications,” *J Chem Inf Model*, 2013.
- [166] I. S. Santos, B. L. Nascimento, R. H. Marino, E. M. Sussuchi, M. P. Matos, and S.

- Griza, “Influence of drying heat treatments on the mechanical behavior and physico-chemical properties of mycelial biocomposite,” *Compos B Eng*, vol. 217, p. 108870, 2021, doi: 10.1016/j.compositesb.2021.108870.
- [167] J. Silverman, “Development and Testing of Mycelium-Based Composite Materials for Shoe Sole Applications,” Ann Arbor, 2018. [Online]. Available: <https://libezproxy.syr.edu/login?url=https://www.proquest.com/dissertations-theses/development-testing-mycelium-based-composite/docview/2088133051/se-2?accountid=14214>
- [168] E. César, G. Canche-Escamilla, L. Montoya, A. Ramos, S. Duarte-Aranda, and V. M. Bandala, “Characterization and Physical Properties of Mycelium Films Obtained from Wild Fungi: Natural Materials for Potential Biotechnological Applications,” *J Polym Environ*, vol. 29, pp. 4098–4105, 2021, doi: 10.1007/s10924-021-02178-3.
- [169] Z. Qin, A. Gautieri, A. K. Nair, H. Inbar, and M. J. Buehler, “Thickness of Hydroxyapatite Nanocrystal Controls Mechanical Properties of the Collagen-Hydroxyapatite Interface,” *Langmuir*, vol. 28, no. 4, pp. 1982–1992, 2012, doi: 10.1021/la204052a.
- [170] K. Jin, Z. Qin, and M. J. Buehler, “Molecular deformation mechanisms of the wood cell wall material,” *J Mech Behav Biomed Mater*, vol. 42, pp. 198–206, 2015, doi: 10.1016/j.jmbbm.2014.11.010.
- [171] R. W. WILLIAMS, L. B. MASON, and H. H. BRADSHAW, “Factors affecting wound healing,” *Surg Forum*, pp. 410–417, 1950, doi: 10.1177/0022034509359125.
- [172] W. G. Malette, H. J. Quigley, and E. D. Adickes, “Chitosan effect in vascular surgery,

- tissue culture and tissue regeneration,” in *Chitin in nature and technology*, Springer, 1986, pp. 435–442.
- [173] H. Ueno *et al.*, “Accelerating effects of chitosan for healing at early phase of experimental open wound in dogs,” *Biomaterials*, vol. 20, no. 15, pp. 1407–1414, 1999, doi: 10.1016/S0142-9612(99)00046-0.
- [174] H. Ueno, T. Mori, and T. Fujinaga, “Topical formulations and wound healing applications of chitosan,” *Adv Drug Deliv Rev*, vol. 52, no. 2, pp. 105–115, 2001, doi: 10.1016/S0169-409X(01)00189-2.
- [175] H. A. B. Wösten, “Hydrophobins: Multipurpose proteins,” *Annu Rev Microbiol*, vol. 55, no. 1, pp. 625–646, 2001, doi: 10.1146/annurev.micro.55.1.625.
- [176] F. Zampieri, H. A. B. Wösten, and K. Scholtmeijer, “Creating surface properties using a palette of hydrophobins,” *Materials*, vol. 3, no. 9, pp. 4607–4625, 2010, doi: 10.3390/ma3094607.
- [177] J. Alongi *et al.*, “Caseins and hydrophobins as novel green flame retardants for cotton fabrics,” *Polym Degrad Stab*, vol. 99, pp. 111–117, 2014, doi: 10.1016/j.polymdegradstab.2013.11.016.
- [178] F. V. W. Appels, J. Dijksterhuis, C. E. Lukasiewicz, K. M. B. Jansen, H. A. B. Wösten, and P. Krijgheld, “Hydrophobin gene deletion and environmental growth conditions impact mechanical properties of mycelium by affecting the density of the material,” *Sci Rep*, vol. 8, p. 4703, 2018, doi: 10.1038/s41598-018-23171-2.
- [179] A. M. Willsey, A. R. Hartwell, T. S. Welles, D. Park, P. D. Ronney, and J. Ahn, “Investigation of mycelium growth network as a thermal transpiration membrane for

- thermal transpiration based pumping and power generation,” in *American Society of Mechanical Engineers, Power Division (Publication) POWER*, 2020, p. V001T03A014. doi: 10.1115/POWER2020-16619.
- [180] D. S. Bajwa, G. A. Holt, S. G. Bajwa, S. E. Duke, and G. McIntyre, “Enhancement of termite (*Reticulitermes flavipes* L.) resistance in mycelium reinforced biofiber-composites,” *Ind Crops Prod*, vol. 107, pp. 420–426, 2017, doi: 10.1016/j.indcrop.2017.06.032.
- [181] B. Shinde, S. Khan, and S. Muhuri, “Model for growth and morphology of fungal mycelium,” *Phys Rev Res*, vol. 2, no. 2, p. 023111, 2020, doi: 10.1103/physrevresearch.2.023111.
- [182] S. W. Simard, K. J. Beiler, M. A. Bingham, J. R. Deslippe, L. J. Philip, and F. P. Teste, “Mycorrhizal networks: Mechanisms, ecology and modelling,” *Fungal Biol Rev*, vol. 26, no. 1, pp. 39–60, 2012, doi: 10.1016/j.fbr.2012.01.001.
- [183] M. A. Gorzelak, A. K. Asay, B. J. Pickles, and S. W. Simard, “Inter-plant communication through mycorrhizal networks mediates complex adaptive behaviour in plant communities,” *AoB Plants*, vol. 7, p. plv050, 2015, doi: 10.1093/aobpla/plv050.
- [184] Z. Babikova, D. Johnson, T. Bruce, J. Pickett, and L. Gilbert, “Underground allies: How and why do mycelial networks help plants defend themselves?: What are the fitness, regulatory, and practical implications of defence-related signaling between plants via common mycelial networks? Insights & Perspectives Z. Babikova,” *BioEssays*, vol. 36, no. 1, pp. 21–26, 2014, doi: 10.1002/bies.201300092.

- [185] L. Yang, D. Park, and Z. Qin, “Material Function of Mycelium-Based Bio-Composite: A Review,” *Front Mater*, vol. 8, pp. 1–17, 2021, doi: 10.3389/fmats.2021.737377.
- [186] P. Bhandana *et al.*, “Arbuscular mycorrhizal fungi and its major role in plant growth, zinc nutrition, phosphorous regulation and phytoremediation,” *Symbiosis*, vol. 84, no. 1, pp. 19–37, 2021. doi: 10.1007/s13199-021-00756-6.
- [187] E. Elsacker, A. Søndergaard, A. van Wylick, E. Peeters, and L. de Laet, “Growing living and multifunctional mycelium composites for large-scale formwork applications using robotic abrasive wire-cutting,” *Constr Build Mater*, vol. 283, no. 122732, 2021, doi: 10.1016/j.conbuildmat.2021.122732.
- [188] S. Manan, M. W. Ullah, M. Ul-Islam, O. M. Atta, and G. Yang, “Synthesis and applications of fungal mycelium-based advanced functional materials,” *Journal of Bioresources and Bioproducts*, vol. 6, no. 1, 2021, doi: 10.1016/j.jobab.2021.01.001.
- [189] M. Garbelotto, “PATHOLOGY | Root and Butt Rot Diseases,” in *Encyclopedia of Forest Sciences*, 2004, pp. 750–758. doi: 10.1016/b0-12-145160-7/00063-6.
- [190] S. D. Frey, “Mycorrhizal Fungi as Mediators of Soil Organic Matter Dynamics,” *Annual Review of Ecology, Evolution, and Systematics*, vol. 50, pp. 237–259, 2019. doi: 10.1146/annurev-ecolsys-110617-062331.
- [191] N. Attias, O. Danai, N. Ezov, E. Tarazi, and Y. J. Grobman, “Developing novel applications of mycelium-based bio-composite materials for design and architecture,” in *COST FP 1303: Building with Biobased Materials: Best practice and Performance Specification*, 2017.
- [192] L. van den Berg and C. P. Lentz, “The effect of relative humidity and temperature on

- survival and growth of *Botrytis cinerea* and *Sclerotinia sclerotiorum*,” *Canadian Journal of Botany*, vol. 46, no. 12, 1968, doi: 10.1139/b68-203.
- [193] R. Fu *et al.*, “The influence of nutrient and environmental factors on mycelium growth and conidium of false smut *Villosiclava virens*,” *Afr J Microbiol Res*, vol. 7, no. 9, 2013.
- [194] P. B. Flegg, “Response of the Cultivated Mushroom to Temperature at Various Stages of Crop Growth,” *Journal of Horticultural Science*, vol. 43, no. 4, pp. 441–452, 1968, doi: 10.1080/00221589.1968.11514272.
- [195] “GLOBAL CLIMATE CHANGE,” <https://climate.nasa.gov/vital-signs/carbon-dioxide/>.
- [196] E. S. Lazaro Vasquez and K. Vega, “Myco-accessories: Sustainable wearables with biodegradable materials,” in *Proceedings - International Symposium on Wearable Computers, ISWC*, 2019, pp. 306–311. doi: 10.1145/3341163.3346938.
- [197] L. Sthle and S. Wold, “Analysis of variance (ANOVA),” *Chemometrics and Intelligent Laboratory Systems*, vol. 6, no. 4, pp. 259–272, Nov. 1989, doi: 10.1016/0169-7439(89)80095-4.
- [198] J. Jaccard, M. A. Becker, and G. Wood, “Pairwise multiple comparison procedures: A review,” *Psychol Bull*, vol. 96, no. 3, pp. 589–596, 1984, doi: 10.1037/0033-2909.96.3.589.
- [199] M. Fricker, L. Boddy, and D. Bebbber, “Network Organisation of Mycelial Fungi BT - Biology of the Fungal Cell,” R. J. Howard and N. A. R. Gow, Eds., Berlin, Heidelberg: Springer Berlin Heidelberg, 2007, pp. 309–330. doi: 10.1007/978-3-540-70618-2\_13.

- [200] S. Vandeloos, E. Elsacker, A. van Wylick, L. de Laet, and E. Peeters, “Current state and future prospects of pure mycelium materials,” *Fungal Biology and Biotechnology*, vol. 8, no. 1. p. 20, 2021. doi: 10.1186/s40694-021-00128-1.
- [201] J. G. van den Brandhof and H. A. B. Wösten, “Risk assessment of fungal materials,” *Fungal Biology and Biotechnology*, vol. 9, no. 3. 2022. doi: 10.1186/s40694-022-00134-x.
- [202] X. Xu, R. Pan, and R. Chen, “Combustion Characteristics, Kinetics, and Thermodynamics of Pine Wood Through Thermogravimetric Analysis,” *Appl Biochem Biotechnol*, vol. 193, no. 5, pp. 1427–1446, 2021, doi: 10.1007/s12010-020-03480-x.
- [203] H. T. Hoa, C. L. Wang, and C. H. Wang, “The effects of different substrates on the growth, yield, and nutritional composition of two oyster mushrooms (*Pleurotus ostreatus* and *Pleurotus cystidiosus*),” *Mycobiology*, vol. 43, no. 4, pp. 423–434, 2015, doi: 10.5941/MYCO.2015.43.4.423.
- [204] S. H. Kim, H. M. Jeong, and G. S. Han, “Fuel characteristics of wood pellets fabricated with tropical acacia wood,” *Palpu Chongi Gisul/Journal of Korea Technical Association of the Pulp and Paper Industry*, vol. 52, no. 1, pp. 103–109, 2020, doi: 10.7584/jktappi.2020.02.52.1.103.
- [205] R. A. Zabel and J. J. Morrell, “The characteristics and classification of fungi and bacteria,” in *Wood Microbiology*, 2020. doi: 10.1016/b978-0-12-819465-2.00003-6.
- [206] S. Bartnicki-Garcia, C. E. Bracker, G. Gierz, R. López-Franco, and L. Haisheng, “Mapping the growth of fungal hyphae: Orthogonal cell wall expansion during tip growth and the role of turgor,” *Biophys J*, vol. 79, no. 5, pp. 2382–2390, 2000, doi:

- 10.1016/S0006-3495(00)76483-6.
- [207] N. L. Glass, C. Rasmussen, M. G. Roca, and N. D. Read, “Hyphal homing, fusion and mycelial interconnectedness,” *Trends in Microbiology*, vol. 12, no. 3. pp. 135–141, 2004. doi: 10.1016/j.tim.2004.01.007.
- [208] D. B. Archer and D. A. Wood, “Fungal Exoenzymes,” in *The Growing Fungus*, 1995, pp. 135–162. doi: 10.1007/978-0-585-27576-5\_7.
- [209] G. W. Gooday, “Cell Walls,” in *The Growing Fungus*, N. A. R. Gow and G. M. Gadd, Eds., Dordrecht: Springer Netherlands, 1995, pp. 41–62. doi: 10.1007/978-0-585-27576-5\_3.
- [210] E. Olivero *et al.*, “Gradient porous structures of mycelium: a quantitative structure–mechanical property analysis,” *Sci Rep*, vol. 13, no. 19285, 2023, doi: 10.1038/s41598-023-45842-5.
- [211] L. M. Corrochano, “Fungal photoreceptors: Sensory molecules for fungal development and behaviour,” *Photochemical and Photobiological Sciences*, vol. 6, no. 7. pp. 725–736, 2007. doi: 10.1039/b702155k.
- [212] A. Brand and N. A. Gow, “Mechanisms of hypha orientation of fungi,” *Current Opinion in Microbiology*, vol. 12, no. 4. pp. 350–357, 2009. doi: 10.1016/j.mib.2009.05.007.
- [213] Z. J. Meng *et al.*, “Viscoelastic Hydrogel Microfibers Exploiting Cucurbit[8]uril Host-Guest Chemistry and Microfluidics,” *ACS Appl Mater Interfaces*, vol. 12, no. 15, pp. 17929–17935, 2020, doi: 10.1021/acsami.9b21240.
- [214] M. Beaumont *et al.*, “Hydrogel-Forming Algae Polysaccharides: From Seaweed to

- Biomedical Applications,” *Biomacromolecules*, vol. 22, no. 3, pp. 1027–1052, 2021, doi: 10.1021/acs.biomac.0c01406.
- [215] M. Y. Ali, C. Y. Chuang, and M. T. A. Saif, “Reprogramming cellular phenotype by soft collagen gels,” *Soft Matter*, vol. 10, no. 44, pp. 8829–8837, 2014, doi: 10.1039/c4sm01602e.
- [216] Z. Sun, “The mechanics of flow, contractility and adhesion in soft-bodied locomotion,” UC San Diego, 2018. [Online]. Available: <https://escholarship.org/uc/item/72f214f9>
- [217] M. E. Asp *et al.*, “Spreading rates of bacterial colonies depend on substrate stiffness and permeability,” *PNAS Nexus*, vol. 1, no. 1, 2022, doi: 10.1093/pnasnexus/pgac025.
- [218] D. K. Aanen, A. van ’t Padje, and B. Auxier, “Longevity of Fungal Mycelia and Nuclear Quality Checks: a New Hypothesis for the Role of Clamp Connections in Dikaryons,” *Microbiology and Molecular Biology Reviews*, vol. 87, no. 3, 2023, doi: 10.1128/membr.00022-21.
- [219] S. Romero, C. Le Clainche, and A. M. Gautreau, “Actin polymerization downstream of integrins: Signaling pathways and mechanotransduction,” *Biochemical Journal*, vol. 477, no. 1, pp. 1–21, 2020. doi: 10.1042/BCJ20170719.
- [220] L. Benítez, L. Barberis, L. Vellón, and C. A. Condat, “Understanding the influence of substrate when growing tumorspheres,” *BMC Cancer*, vol. 21, no. 1, p. 276, 2021, doi: 10.1186/s12885-021-07918-1.
- [221] M. Guo *et al.*, “Cell volume change through water efflux impacts cell stiffness and stem cell fate,” *Proc Natl Acad Sci U S A*, vol. 114, no. 41, pp. E8618–E8627, 2017, doi: 10.1073/pnas.1705179114.

- [222] S. Zhang, J. C. Lasheras, and J. C. Del Alamo, “Symmetry breaking transition towards directional locomotion in *Physarum microplasmidia*,” *J Phys D Appl Phys*, vol. 52, no. 49, 2019, doi: 10.1088/1361-6463/ab3ec8.
- [223] K. Alim, G. Amselem, F. Peaudecerf, M. P. Brenner, and A. Pringle, “Random network peristalsis in *Physarum polycephalum* organizes fluid flows across an individual,” *Proc Natl Acad Sci U S A*, vol. 110, no. 33, pp. 13306–13311, 2013, doi: 10.1073/pnas.1305049110.
- [224] L. P. G. W.M. Telford and R. E. Sheriff, “Applied geophysics (second edition),” *Cambridge University Press*. 1991.
- [225] M. J. Buehler, F. F. Abraham, and H. Gao, “Hyperelasticity governs dynamic fracture at a critical length scale,” *Nature*, vol. 426, no. 6963, pp. 141–146, 2003, doi: 10.1038/nature02096.
- [226] T. Kuribayashi, P. Lankinen, and K. S. Mikkonen, “A layered solid-state culture system for investigating the fungal growth and decay behaviour on the cellulosic substrate,” *J Microbiol Methods*, vol. 212, no. 106794, 2023, doi: 10.1016/j.mimet.2023.106794.
- [227] E. C. Hotz, A. J. Bradshaw, C. Elliott, K. Carlson, B. T. M. Dentinger, and S. E. Naleway, “Effect of agar concentration on structure and physiology of fungal hyphal systems,” *Journal of Materials Research and Technology*, vol. 24, pp. 7614–7623, 2023, doi: 10.1016/j.jmrt.2023.05.013.
- [228] E. Rodríguez, F. J. Ruiz-Dueñas, R. Kooistra, A. Ram, Á. T. Martínez, and M. J. Martínez, “Isolation of two laccase genes from the white-rot fungus *Pleurotus eryngii*

- and heterologous expression of the pel3 encoded protein,” *J Biotechnol*, vol. 134, no. 1–2, pp. 9–19, 2008, doi: 10.1016/j.jbiotec.2007.12.008.
- [229] R. R. M. Paterson, “Ganoderma disease of oil palm-A white rot perspective necessary for integrated control,” *Crop Protection*, vol. 26, no. 9, pp. 1369–1376, 2007, doi: 10.1016/j.cropro.2006.11.009.
- [230] S. Montoya, A. Patiño, and Ó. J. Sánchez, “Production of lignocellulolytic enzymes and biomass of *trametes versicolor* from agro-industrial residues in a novel fixed-bed bioreactor with natural convection and forced aeration at pilot scale,” *Processes*, vol. 9, no. 2, p. 397, 2021, doi: 10.3390/pr9020397.
- [231] G. Janusz *et al.*, “Laccase production and metabolic diversity among *Flammulina velutipes* strains,” *World J Microbiol Biotechnol*, vol. 31, no. 1, pp. 121–133, 2015, doi: 10.1007/s11274-014-1769-y.
- [232] T. M. Roehl, *Examining the Genetics of Mushroom Development in the Cultivated Edible Mushroom Flammulina velutipes*. University of Wisconsin-La Crosse, 2022.
- [233] R. Singh, G. S. Dhingra, and R. Shri, “A comparative study of taxonomy, physicochemical parameters, and chemical constituents of *ganoderma lucidum* and *G. philippii* from Uttarakhand, India,” *Turk J Botany*, vol. 38, no. 1, 2014, doi: 10.3906/bot-1302-39.
- [234] H. Kaygusuz, G. A. Evingür, Ö. Pekcan, R. von Klitzing, and F. B. Erim, “Surfactant and metal ion effects on the mechanical properties of alginate hydrogels,” *Int J Biol Macromol*, vol. 92, pp. 220–224, 2016, doi: 10.1016/j.ijbiomac.2016.07.004.
- [235] C. Amador, M. W. Urban, S. Chen, Q. Chen, K. N. An, and J. F. Greenleaf, “Shear

- elastic modulus estimation from indentation and SDUV on gelatin phantoms,” *IEEE Trans Biomed Eng*, vol. 58, no. 6, pp. 1706–1714, 2011, doi: 10.1109/TBME.2011.2111419.
- [236] W. C. Hayes, L. M. Keer, G. Herrmann, and L. F. Mockros, “A mathematical analysis for indentation tests of articular cartilage,” *J Biomech*, vol. 5, no. 5, pp. 541–551, 1972, doi: 10.1016/0021-9290(72)90010-3.
- [237] A. Lehmann, W. Zheng, K. Soutschek, J. Roy, A. M. Yurkov, and M. C. Rillig, “Tradeoffs in hyphal traits determine mycelium architecture in saprobic fungi,” *Sci Rep*, vol. 9, no. 1, p. 14152, 2019, doi: 10.1038/s41598-019-50565-7.
- [238] K. Aleklett, P. Ohlsson, M. Bengtsson, and E. C. Hammer, “Fungal foraging behaviour and hyphal space exploration in micro-structured Soil Chips,” *ISME Journal*, vol. 15, no. 6, pp. 1782–1793, 2021, doi: 10.1038/s41396-020-00886-7.
- [239] M. Matsushita *et al.*, “Formation of colony patterns by a bacterial cell population,” *Physica A: Statistical Mechanics and its Applications*, vol. 274, no. 1–2, pp. 190–199, 1999, doi: 10.1016/S0378-4371(99)00328-3.
- [240] B. Bottura, L. M. Rooney, P. A. Hoskisson, and G. McConnell, “Intra-colony channel morphology in *Escherichia coli* biofilms is governed by nutrient availability and substrate stiffness,” *Biofilm*, vol. 4, p. 100084, 2022, doi: 10.1016/j.biofilm.2022.100084.
- [241] M. R. Warren, H. Sun, Y. Yan, J. Cremer, B. Li, and T. Hwa, “Spatiotemporal establishment of dense bacterial colonies growing on hard agar,” *Elife*, vol. 8:e41093, 2019, doi: 10.7554/eLife.41093.

- [242] D. Schwarcz, H. Levine, E. Ben-Jacob, and G. Ariel, “Uniform modeling of bacterial colony patterns with varying nutrient and substrate,” *Physica D*, vol. 318–319, pp. 91–99, 2016, doi: 10.1016/j.physd.2015.11.002.
- [243] K. R. Koch, “Monte Carlo methods,” *GEM*, vol. 9, no. 1, pp. 117–143, 2018, doi: 10.1007/s13137-017-0101-z.
- [244] R. L. Harrison, “Introduction to Monte Carlo simulation,” in *AIP Conference Proceedings*, 2010, pp. 17–21. doi: 10.1063/1.3295638.
- [245] A. Pizzi, A. N. Papadopoulos, and F. Policardi, “Wood composites and their polymer binders,” *Polymers*, vol. 12, no. 5. p. 48, 2020. doi: 10.3390/POLYM12051115.
- [246] D. J. Gardner, Y. Han, and L. Wang, “Wood–Plastic composite technology,” *Current Forestry Reports*, vol. 1, no. 3, pp. 139–150, 2015, doi: 10.1007/s40725-015-0016-6.
- [247] V. Mazzanti and F. Mollica, “A review of wood polymer composites rheology and its implications for processing,” *Polymers*, vol. 12, no. 10. p. 2304, 2020. doi: 10.3390/polym12102304.
- [248] M. H. Schneider, “Wood-Polymer Composites - Society of Wood Science and Technology State-of-the-Art Review Paper,” *Wood and Fiber Science*, vol. 26, no. 1, pp. 142–151, 1994.
- [249] M. Bazli, M. Heitzmann, and B. Villacorta Hernandez, “Durability of fibre-reinforced polymer-wood composite members: An overview,” *Compos Struct*, vol. 295, p. 115827, Sep. 2022, doi: 10.1016/J.COMPSTRUCT.2022.115827.
- [250] K. Oksman, “Improved interaction between wood and synthetic polymers in wood/polymer composites,” *Wood Sci Technol*, vol. 30, no. 3, pp. 179–205, 1996, doi:

10.1007/BF00231633.

- [251] L. Krišťák and R. Réh, “Application of wood composites,” *Applied Sciences (Switzerland)*, vol. 11, no. 8. p. 2479, 2021. doi: 10.3390/app11083479.
- [252] O. Adekomaya, T. Jamiru, R. Sadiku, and Z. Huan, “A review on the sustainability of natural fiber in matrix reinforcement – A practical perspective,” *Journal of Reinforced Plastics and Composites*, vol. 35, no. 1, pp. 3–7, Jan. 2016, doi: 10.1177/0731684415611974.
- [253] V. Kumar, L. Tyagi, and S. Sinha, “Wood flour-reinforced plastic composites: A review,” *Reviews in Chemical Engineering*, vol. 27, no. 5–6. pp. 253–264, 2011. doi: 10.1515/REVCE.2011.006.
- [254] B. V. Kokta, R. Chen, C. Daneault, and J. L. Valade, “Use of wood fibers in thermoplastic composites,” *Polym Compos*, vol. 4, no. 4, pp. 229–232, 1983, doi: 10.1002/pc.750040407.
- [255] G. A. Ormondroyd, “Adhesives for wood composites,” *Wood Composites*, pp. 47–66, Jan. 2015, doi: 10.1016/B978-1-78242-454-3.00003-2.
- [256] A. N. Papadopoulos, “Advances in wood composites,” *Polymers*, vol. 12, no. 1. p. 48, 2020. doi: 10.3390/polym12010048.
- [257] A. N. Papadopoulos, “Advances in wood composites II,” *Polymers*, vol. 12, no. 7. p. 1552, 2020. doi: 10.3390/polym12071552.
- [258] K. N. Bharath and S. Basavarajappa, “Applications of biocomposite materials based on natural fibers from renewable resources: A review,” *Science and Engineering of Composite Materials*, vol. 23, no. 2. pp. 123–133, 2016. doi: 10.1515/secm-2014-0088.

- [259] K. Jin, Z. Qin, and M. J. Buehler, “Molecular deformation mechanisms of the wood cell wall material,” *J Mech Behav Biomed Mater*, vol. 42, pp. 198–206, 2015, doi: 10.1016/j.jmbbm.2014.11.010.
- [260] Y. Sun, L. Guo, Y. Liu, W. Wang, and Y. Song, “Glue wood veneer to wood-fiber–high-density-polyethylene composite,” *Int J Adhes Adhes*, vol. 95, p. 102444, 2019, doi: 10.1016/j.ijadhadh.2019.102444.
- [261] H. Ye *et al.*, “Bio-based composites fabricated from wood fibers through self-bonding technology,” *Chemosphere*, vol. 287, no. 4, p. 132436, 2022, doi: 10.1016/j.chemosphere.2021.132436.
- [262] C. Xu, C. Sun, H. Wan, H. Tan, J. Zhao, and Y. Zhang, “Microstructure and physical properties of poly(lactic acid)/polycaprolactone/rice straw lightweight bio-composite foams for wall insulation,” *Constr Build Mater*, vol. 354, no. 129216, 2022, doi: 10.1016/j.conbuildmat.2022.129216.
- [263] B. Zhang, B. Fan, P. Huo, and Z. H. Gao, “Improvement of the water resistance of soybean protein-based wood adhesive by a thermo-chemical treatment approach,” *Int J Adhes Adhes*, vol. 78, pp. 222–226, 2017, doi: 10.1016/j.ijadhadh.2017.08.002.
- [264] C. Kumar and W. Leggate, “An overview of bio-adhesives for engineered wood products,” *Int J Adhes Adhes*, vol. 118, p. 103187, Oct. 2022, doi: 10.1016/J.IJADHADH.2022.103187.
- [265] W. Jiang, A. Kumar, and S. Adamopoulos, “Liquefaction of lignocellulosic materials and its applications in wood adhesives—A review,” *Industrial Crops and Products*, vol. 124, no. 15, pp. 325–342, 2018. doi: 10.1016/j.indcrop.2018.07.053.

- [266] M. Kaseem, K. Hamad, F. Deri, and Y. G. Ko, “Material properties of polyethylene/wood composites: A review of recent works,” *Polymer Science - Series A*, vol. 57, no. 6. pp. 689–703, 2015. doi: 10.1134/S0965545X15070068.
- [267] A. Hüttermann, C. Mai, and A. Kharazipour, “Modification of lignin for the production of new compounded materials,” *Appl Microbiol Biotechnol*, vol. 55, no. 4, pp. 387–394, 2001, doi: 10.1007/s002530000590.
- [268] J. A. Youngquist, “Wood-based composites and panel products,” in *Wood handbook : wood as an engineering material*, vol. 113, 1999, pp. 10.1-10.31.
- [269] F. Ferdosian, Z. Pan, G. Gao, and B. Zhao, “Bio-based adhesives and evaluation for wood composites application,” *Polymers*, vol. 9, no. 2. p. 70, 2017. doi: 10.3390/polym9020070.
- [270] J. F. Kadla, S. Kubo, R. A. Venditti, R. D. Gilbert, A. L. Compere, and W. Griffith, “Lignin-based carbon fibers for composite fiber applications,” *Carbon N Y*, vol. 40, no. 15, pp. 2913–2920, 2002, doi: 10.1016/S0008-6223(02)00248-8.
- [271] G. M. Irvine, “The significance of the glass transition of lignin in thermomechanical pulping,” *Wood Sci Technol*, vol. 19, no. 2, pp. 139–149, 1985, doi: 10.1007/BF00353074.
- [272] G. Vázquez, J. González, S. Freire, and G. Antorrena, “Effect of chemical modification of lignin on the gluebond performance of lignin-phenolic resins,” *Bioresour Technol*, vol. 60, no. 3, pp. 191–198, 1997, doi: 10.1016/S0960-8524(97)00030-8.
- [273] Z. ud Din *et al.*, “Starch: An Undisputed Potential Candidate and Sustainable Resource for the Development of Wood Adhesive,” *Starch/Staerke*, vol. 72, no. 3–4. p. 1900276,

2020. doi: 10.1002/star.201900276.
- [274] H. Tan, Y. Zhang, and X. Weng, "Preparation of the plywood using starch-based adhesives modified with blocked isocyanates," *Procedia Eng*, vol. 15, pp. 1171–1175, 2011, doi: 10.1016/j.proeng.2011.08.216.
- [275] H. Onusseit, "Starch in industrial adhesives: new developments," *Ind Crops Prod*, vol. 1, no. 2–4, pp. 141–146, 1992, doi: 10.1016/0926-6690(92)90012-K.
- [276] J. Jumper *et al.*, "Highly accurate protein structure prediction with AlphaFold," *Nature*, vol. 596, no. 7873, pp. 583–589, 2021, doi: 10.1038/s41586-021-03819-2.
- [277] N. Li, G. Qi, X. S. Sun, M. J. Stamm, and D. Wang, "Physicochemical properties and adhesion performance of canola protein modified with sodium bisulfite," *JAOCs, Journal of the American Oil Chemists' Society*, vol. 89, no. 5, pp. 897–908, 2012, doi: 10.1007/s11746-011-1977-7.
- [278] S. Pérez and E. Bertoft, "The molecular structures of starch components and their contribution to the architecture of starch granules: A comprehensive review," *Starch/Staerke*, vol. 62, no. 8, pp. 389–420, 2010. doi: 10.1002/star.201000013.
- [279] W. Sun, M. Tajvidi, C. Howell, and C. G. Hunt, "Functionality of Surface Mycelium Interfaces in Wood Bonding," *ACS Appl Mater Interfaces*, vol. 12, no. 51, pp. 57431–57440, 2020, doi: 10.1021/acsami.0c18165.
- [280] W. Sun, M. Tajvidi, C. G. Hunt, G. McIntyre, and D. J. Gardner, "Fully Bio-Based Hybrid Composites Made of Wood, Fungal Mycelium and Cellulose Nanofibrils," *Sci Rep*, vol. 9, no. 1, p. 3766, 2019, doi: 10.1038/s41598-019-40442-8.
- [281] D. Saez, D. Grizmann, M. Trautz, and A. Werner, "Exploring the Binding Capacity of

- Mycelium and Wood-Based Composites for Use in Construction,” *Biomimetics*, vol. 7, no. 2, p. 78, Jun. 2022, doi: 10.3390/biomimetics7020078.
- [282] O. Abdelhady, E. Spyridonos, and H. Dahy, “Bio-Modules: Mycelium-Based Composites Forming a Modular Interlocking System through a Computational Design towards Sustainable Architecture,” *Designs (Basel)*, vol. 7, no. 1, Feb. 2023, doi: 10.3390/designs7010020.
- [283] S. Sivaprasad, S. K. Byju, C. Prajith, J. Shaju, and C. R. Rejeesh, “Development of a novel mycelium bio-composite material to substitute for polystyrene in packaging applications,” *Mater Today Proc*, vol. 47, no. 15, pp. 5038–5044, 2021, doi: 10.1016/j.matpr.2021.04.622.
- [284] D. Arthur and S. Vassilvitskii, “K-means++: The advantages of careful seeding,” in *Proceedings of the Annual ACM-SIAM Symposium on Discrete Algorithms*, 2007, pp. 1027–1035.
- [285] S. P. Lloyd, “Least Squares Quantization in PCM,” *IEEE Trans Inf Theory*, vol. 28, no. 2, pp. 129–137, 1982, doi: 10.1109/TIT.1982.1056489.
- [286] M. Cooper and G. A. F. Seber, “Multivariate Observations,” *Journal of Marketing Research*, vol. 22, no. 2, 1985, doi: 10.2307/3151376.
- [287] B. Everitt and H. Spath, “Cluster Dissection and Analysis: Theory, Fortran Programs and Examples.,” *J R Stat Soc Ser A*, vol. 148, no. 3, 1985, doi: 10.2307/2981981.
- [288] T. Sterling, M. Anderson, and M. Brodowicz, “MapReduce,” in *High Performance Computing*, Elsevier, 2018, pp. 579–589. doi: 10.1016/b978-0-12-420158-3.00019-8.
- [289] S. Misra, O. Osogba, and M. Powers, “Unsupervised outlier detection techniques for

- well logs and geophysical data,” in *Machine Learning for Subsurface Characterization*, Elsevier, 2019, pp. 1–37. doi: 10.1016/B978-0-12-817736-5.00001-6.
- [290] K. Molugaram and G. S. Rao, “Random Variables,” in *Statistical Techniques for Transportation Engineering*, Elsevier, 2017, pp. 113–279. doi: 10.1016/B978-0-12-811555-8.00004-0.
- [291] U. Roessner, A. Nahid, B. Chapman, A. Hunter, and M. Bellgard, “Metabolomics - the combination of analytical biochemistry, biology, and informatics,” in *Comprehensive Biotechnology*, vol. 1, 2019, pp. 447–459. doi: 10.1016/B978-0-444-64046-8.00027-6.
- [292] P. Gonzalez and J. Labarère, “Phylogenetic relationships of *Pleurotus* species according to the sequence and secondary structure of the mitochondrial small-subunit rRNA V4, V6 and V9 domains The GenBank accession numbers for the sequences reported in this paper are given in Methods.,” *Microbiology (N Y)*, vol. 146, no. 1, pp. 209–221, 2000, doi: 10.1099/00221287-146-1-209.
- [293] J. Tong, H. Gao, Y. Weng, and Y. Wang, “Anisotropic Aerogels with Excellent Mechanical Resilience and Thermal Insulation from *Pleurotus eryngii* Fungus,” *Macromol Mater Eng*, p. 2200538, 2022, doi: 10.1002/mame.202200538.
- [294] “Back to the Roots (America’s Organic Gardening Company).” [Online]. Available: [https://backtotheroots.com/?gclid=CjwKCAiAnZCdBhBmEiwA8nDQxUPWX7l-Pxv41bRByR98Iw9VqyEDdwnUFkjhJg7XC19MD1I\\_t31ORBoCi1gQAvD\\_BwE](https://backtotheroots.com/?gclid=CjwKCAiAnZCdBhBmEiwA8nDQxUPWX7l-Pxv41bRByR98Iw9VqyEDdwnUFkjhJg7XC19MD1I_t31ORBoCi1gQAvD_BwE)
- [295] T. Wu, X. Wang, and K. Kito, “Effects of pressures on the mechanical properties of corn straw bio-board,” *Engineering in Agriculture, Environment and Food*, vol. 8, no. 3, pp. 123–129, 2015, doi: 10.1016/j.eaef.2015.07.003.

- [296] L. J. Gibson and M. F. Ashby, *Cellular solids: Structure and properties*. 1997.
- [297] U. G. K. Wegst, H. Bai, E. Saiz, A. P. Tomsia, and R. O. Ritchie, “Bioinspired structural materials,” *Nat Mater*, vol. 14, no. 1, pp. 23–36, 2015, doi: 10.1038/nmat4089.
- [298] F. Martínez-Hergueta, A. Ridruejo, C. González, and J. Llorca, “Deformation and energy dissipation mechanisms of needle-punched nonwoven fabrics: A multiscale experimental analysis,” *Int J Solids Struct*, vol. 64–65, pp. 120–131, 2015, doi: 10.1016/j.ijsolstr.2015.03.018.
- [299] C. R. Picu, “Constitutive models for random fiber network materials: A review of current status and challenges,” *Mech Res Commun*, vol. 114, p. 103605, 2021, doi: 10.1016/j.mechrescom.2020.103605.
- [300] D. R. Baughman and Y. A. Liu, “Classification: Fault Diagnosis and Feature Categorization,” in *Neural Networks in Bioprocessing and Chemical Engineering*, 1995, pp. 110–171. doi: 10.1016/b978-0-12-083030-5.50009-6.
- [301] H. Izadkhah, “Classification in bioinformatics,” in *Deep Learning in Bioinformatics*, Elsevier, 2022, pp. 113–130. doi: 10.1016/b978-0-12-823822-6.00013-5.
- [302] G. V. Angelova, M. S. Brazkova, and A. I. Krastanov, “Renewable mycelium based composite - Sustainable approach for lignocellulose waste recovery and alternative to synthetic materials - A review,” *Zeitschrift fur Naturforschung - Section C Journal of Biosciences*, vol. 76, no. 11–12. pp. 431–442, 2021. doi: 10.1515/znc-2021-0040.
- [303] L. Li, T. Liang, W. Liu, Y. Liu, and F. Ma, “A Comprehensive Review of the Mycelial Pellet: Research Status, Applications, and Future Prospects,” *Industrial and*

- Engineering Chemistry Research*, vol. 59, no. 39. pp. 16911–16922, 2020. doi: 10.1021/acs.iecr.0c01325.
- [304] E. Elsacker, S. Vandeloock, A. van Wylick, J. Ruytinx, L. de Laet, and E. Peeters, “A comprehensive framework for the production of mycelium-based lignocellulosic composites,” *Science of the Total Environment*, vol. 725, p. 138431, 2020, doi: 10.1016/j.scitotenv.2020.138431.
- [305] F. Gauvin, V. Tsao, J. Vette, and H. J. H. Brouwers, “Physical Properties and Hygrothermal Behavior of Mycelium-Based Composites as Foam-Like Wall Insulation Material,” in *Bio-Based Building Materials*, in *Construction Technologies and Architecture*, vol. 1. Trans Tech Publications Ltd, Apr. 2022, pp. 643–651. doi: 10.4028/www.scientific.net/CTA.1.643.
- [306] B. Ghazvinian Ali and Gürsoy, “Challenges and Advantages of Building with Mycelium-Based Composites: A Review of Growth Factors that Affect the Material Properties,” in *Fungal Biopolymers and Biocomposites: Prospects and Avenues*, M. V. and S. K. R. Deshmukh Sunil K. and Deshpande, Ed., Singapore: Springer Nature Singapore, 2022, pp. 131–145. doi: 10.1007/978-981-19-1000-5\_8.
- [307] B. Sizirici, Y. Fseha, C. S. Cho, I. Yildiz, and Y. J. Byon, “A review of carbon footprint reduction in construction industry, from design to operation,” *Materials*, vol. 14, no. 20 6094. 2021. doi: 10.3390/ma14206094.
- [308] X. Zhang, J. Hu, X. Fan, and X. Yu, “Naturally grown mycelium-composite as sustainable building insulation materials,” *J Clean Prod*, vol. 342, no. 130784, 2022, doi: 10.1016/j.jclepro.2022.130784.

- [309] E. D. Gezer and S. Kuştaş, “Acoustic and Thermal Properties of Mycelium-based Insulation Materials Produced from Desilicated Wheat Straw-Part B,” *Bioresources*, vol. 19, no. 1, pp. 1348–1364, 2024, doi: 10.15376/biores.19.1.1348-1364.
- [310] S. Schiavoni, F. D’Alessandro, F. Bianchi, and F. Asdrubali, “Insulation materials for the building sector: A review and comparative analysis,” *Renewable and Sustainable Energy Reviews*, vol. 62, pp. 988–1011, 2016. doi: 10.1016/j.rser.2016.05.045.
- [311] B. Abu-Jdayil, A. H. Mourad, W. Hittini, M. Hassan, and S. Hameedi, “Traditional, state-of-the-art and renewable thermal building insulation materials: An overview,” *Construction and Building Materials*, vol. 214, pp. 709–735, 2019. doi: 10.1016/j.conbuildmat.2019.04.102.
- [312] B. P. Jelle, “Traditional, state-of-the-art and future thermal building insulation materials and solutions - Properties, requirements and possibilities,” *Energy and Buildings*, vol. 43, no. 10, pp. 2549–2563, 2011. doi: 10.1016/j.enbuild.2011.05.015.
- [313] R. Kunič, “Carbon footprint of thermal insulation materials in building envelopes,” *Energy Effic*, vol. 10, no. 6, pp. 1511–1528, 2017, doi: 10.1007/s12053-017-9536-1.
- [314] E. Kosior, R. Bragança, and P. Fowler, “Lightweight compostable packaging: literature review,” *The Waste & Resource Action Program*, vol. 26, pp. 1–48, 2006.
- [315] T. Rasheed, S. Shafi, M. Bilal, T. Hussain, F. Sher, and K. Rizwan, “Surfactants-based remediation as an effective approach for removal of environmental pollutants—A review,” *Journal of Molecular Liquids*, vol. 318, no. 113960, 2020. doi: 10.1016/j.molliq.2020.113960.
- [316] N. H. Ramli Sulong, S. A. S. Mustapa, and M. K. Abdul Rashid, “Application of

- expanded polystyrene (EPS) in buildings and constructions: A review,” *Journal of Applied Polymer Science*, vol. 136, no. 20: 47529. 2019. doi: 10.1002/app.47529.
- [317] B. Schmidt *et al.*, “Mechanical, physical and thermal properties of composite materials produced with the basidiomycete *Fomes fomentarius*,” *Fungal Biol Biotechnol*, vol. 10, no. 1, 2023, doi: 10.1186/s40694-023-00169-8.
- [318] L. Yang and Z. Qin, “Mycelium-based wood composites for light weight and high strength by experiment and machine learning,” *Cell Rep Phys Sci*, vol. 4, no. 6, Jun. 2023, doi: 10.1016/j.xcrp.2023.101424.
- [319] I. H. Tavman, “Preparation and Characterization of Conductive Polymer Nanocomposites Based on Ethylene–Vinylacetate Copolymer (EVA) Reinforced with Expanded and Unexpanded Graphite,” *Adv Mat Res*, vol. 1114, pp. 92–99, 2015, doi: 10.4028/www.scientific.net/amr.1114.92.
- [320] Y. Yousefi and F. Tariku, “Thermal Conductivity and Specific Heat Capacity of Insulation materials at Different Mean Temperatures,” *J Phys Conf Ser*, vol. 2069, no. 1, p. 012090, Nov. 2021, doi: 10.1088/1742-6596/2069/1/012090.
- [321] S. Al-Qahtani, M. Koç, and R. J. Isaifan, “Mycelium-Based Thermal Insulation for Domestic Cooling Footprint Reduction: A Review,” *Sustainability (Switzerland)*, vol. 15, no. 17: 13217. 2023. doi: 10.3390/su151713217.

## **Current Vita**

**Libin Yang**

**Present Address:** 23 Presidential Court, Syracuse, NY, 13202

**Telephone:** 503-453-9138

**E-mail:** [lyang43@syr.edu](mailto:lyang43@syr.edu)

## *Academic Curriculum Vitae*

---

### *Education*

**2019-pres.** Ph.D. student, College of Engineering & Computer Science, Syracuse University

**2018-2019** Master of Sciences, Civil Engineering, College of Engineering & Computer Science, Syracuse University

**2011-2015** Bachelor of Sciences, Civil Engineering, Renai college of Tianjin University

### *Work Experience*

**Teaching Assistantship:** Awarded Graduate Teaching Assistantship in the Dept. of Civil and Environmental Engineering.

### **Fall Semester 2020**

- ECS 101: Introduction to Engineering and Computer Science: Holding office hours, making additional handouts, and grading. My very first role as a Teaching Assistant (TA)

was for ECS101 a course for freshmen, since it was a new experience for both the students and me, I tried my best to maintain an approachable demeanor. My primary responsibilities included handling and organizing the course's Blackboard platform, which enhanced my proficiency with the system. Additionally, I was tasked with establishing assignment portals, conducting regular office hours, instructing foundational Excel skills, and evaluating student submissions. This experience offered profound insights into the unique needs of first-year college students and shaped my understanding of how best to cater to their academic requirements as their TA.

- CEE 326: Engineering Materials: Leading lab sessions, holding office hours, and grading. In this course, I instructed lab sessions and aided students in optimizing their use of tools such as Structural Analysis 5.0 by Aslam Kassimail. My background in structural also proved useful to guide them on using useful tips and tricks to help them solve their problems faster. Additionally, I managed assignments and lab tasks and conducted office hours to support the students further.

### **Spring Semester 2021& Spring Semester 2022**

- CEE 325: Mechanics of Materials: Teaching recitation, holding office hours, making additional handouts, and grading. My responsibilities in this course included teaching recitations where I solve additional problems other than the ones solved in class and cleared doubts as they arose. I also tried to provide the concepts to the students in a way that it was easier for them to visualize and understand. I was also responsible for creating

a grading rubric and grading assignments and other course work, making solutions for assigned work as well as holding office hours to help students.

### **Fall Semester 2021**

- CEE 331: Analysis and Structure and Materials, holding office hours, making additional handouts, and grading. During office hours I tried my best to provide the concepts in a clear and concise manner for ease of understanding. I was also responsible for creating a grading rubric and grading assignments and as well as other course work. My responsibilities also included making solutions for all assignments.

### ***Research Assistant***

**2022- pres.** Lab of Multiscale Material Modeling and Simulation (LMMM), Syracuse University, Department of Civil and Environmental Engineering: Conducted various experiments related to mycelium growth over a range of species, characterization of fibers and their final use as bio-composites. Testing of bio-composites to understand suitability of applications. Also conducted tests for soft material characterization. (All the research work is funded by the National Science Foundation CAREER Grant (Award #: CMMI - 2145392).)

### ***Summer Research Positions***

**2019- pres. During Summer (June-Aug)** Lab of Multiscale Material Modeling and Simulation (LMMM), Syracuse University, Department of Civil and Environmental Engineering: Conducted experiments related to identifying suitable growth medium of

various mycelium species. Mentored K-12 students in a variety of these experiments and helped them develop a growing interest in the fields of science and engineering.

### ***Research Interests***

Biomaterials, alternative materials for construction, alternative sustainable materials, soft materials (hydrogels), bio-composites, alternative polymer research for substituting traditional construction materials.

***Technical skills:*** AUTOCAD 2D & 3D, MATLAB, Mathcad, VMD (Visual Molecular Dynamics), SAP2000, ABAQUS, ImageJ, SolidWorks, Microsoft office 365

***Instruments:*** Instron Tensile Machine, Stratasys 3D printer, SEM (Scanning Electron Microscope), Thermogravimetric Analyzer (TA Instruments Q500 TGA), Contact angle goniometer, Fourier-transform infrared spectroscopy (FTIR), Hirox 3D digital microscope.

### ***Additional Experience***

Helped train K-12 students from underrepresented minority groups from local high schools in various hands-on experiments during the summer of 2022. I was actively involved in engaging them to work alongside our team to build a customized green tent with an Arduino chip for environmental control for the growth of mycelium and mycelium-based bio-composites.

### ***Publications***

- Yang, L., Xu, R., Joardar, A., Amponsah, M., Sharifi, N., Dong, B., and Qin, Z. (2023). Design and build a green tent environment for growing and charactering mycelium growth in lab. *Lab Chip* 23, 4044–4051, DOI: 10.1039/D3LC00336A.
- Yang, L., and Qin, Z. (2023). Mycelium-based wood composites for light weight and high strength by experiment and machine learning. *Cell Rep Phys Sci* 4, DOI: 10.1016/j.xcrp.2023.101424.
- Xu, R., Yang, L., and Qin, Z. (2022). Journal of the Mechanical Behavior of Biomedical Materials Design, manufacture, and testing of customized sterilizable respirator. *J Mech Behav Biomed Mater* 131, 105248, DOI: 10.1016/j.jmbbm.2022.105248.
- Yang, L., Park, D., and Qin, Z. (2021). Material Function of Mycelium-Based Bio-Composite: A Review. *Front Mater* 8, 1–17, DOI: 10.3389/fmats.2021.737377.

### ***Book chapter***

- Yang, L., and Qin, Z. (2023). Experimental Analysis of the Mechanics of Mycelium-based Biocomposites. In *Bioprospects of Macrofungi*, K. R. S. H. A. E. E. Sunil Kumar Deshmukh, ed. (CRC Press), pp. 205–232.

### ***Conference & Workshop***

- **Oct 2023** Society of Engineering Science Technical Meeting (SES) at Minneapolis, Minnesota. Oral and poster presentation on “Exploring the Relationship between Agar Concentration and Mycelium Growth Rates in Fungi.”
- **June 2022** Biomechanics, Bioengineering, and Biotransport (SB3C) at

Cambridge, Maryland. Poster presentation on “ Multiscale Analysis of the Structure-Mechanics Relationship of Mycelium-Based Composites.”

- **June 2022** Attended MIT Professional Education Short Programs 'Predictive Multiscale Materials Design' course at Cambridge, Massachusetts.
- **Nov. – Dec. 2021** Attended Materials Research Society (MRS) at Boston, Massachusetts.

### ***AWARDS***

- **2021** Award for the Materials Research Society (MRS) Fall Meeting Science as Art second place.
- **2020** Award for the Syracuse University Engineering & Computer Science research day Civil and Environmental Engineering poster prize.